Characterization of the allowable operating region of a linear, supersonic MHD generator

by Donald James Hammerstrom

A thesis submitted in partial fulfillment of the requirements for the degree of Doctor of Philosophy in Electrical Engineering
Montana State University

Abstract:
Magnetohydrodynamic (MHD) power generation is the generation of electrical power from the flow of a conductive fluid through a magnetic field. The first commercial demonstration of coal-fired MHD power generation will likely be accomplished by retrofit of existing coal-fired steam generators. The combined MHD-steam generation plant must be controlled to supply its power demand. This thesis answers two questions: First, what is the size and shape of the allowable operating region of the linear, coal-fired, supersonic, diagonally-connected Proof of Concept (POC) MHD generator once operated for the U.S. Department of Energy by MSE, Inc. in Butte, Montana? Second, how much can the MHD generator contribute to load following? A quasi-one-dimensional FORTRAN computer model solves for steady-state MHD operation in few iterations. The MHD conservation equation set is discretized with Patankar's SIMPLER finite volume algorithm. The tridiagonal matrix algorithm (TDMA) then solves the resulting banded matrices. External and simple, equivalent internal electrical circuits are solved by relaxation. The separation of the electrical circuit into internal and external parts permits one to model various electrode configurations without changing the channel equivalent circuit model. Fully developed turbulent boundary and electrode voltage drop models are also incorporated.

Model results are compared to POC data. The model overestimates nominal electrical power extraction by 0.4 MW and underestimates channel cooling requirements by 25%. Mach behavior in the diffuser sections is questionable.

Eight parametric studies are then conducted using coal flow rate, oxidant preheat temperature, oxygen enrichment, stoichiometric ratio, seed fraction, load resistance, magnetic induction, and diagonal angle as independent variables. Indicators of imminent duct stress, electrical power and enthalpic efficiency are monitored. It is found that the operating region for the POC MHD generator is large. Shocks limit the allowable operating region at low flow and high magnetic induction. Combustor pressure limits the maximum allowable flow. Many of the parametric studies exhibit efficiency optima in their parametric domains. A strategy for efficient load following is suggested. In this strategy, coal flow rate and magnetic induction must be coordinated during off-nominal operation to maintain high efficiency.

CHARACTERIZATION OF THE ALLOWABLE OPERATING REGION OF A LINEAR, SUPERSONIC MHD GENERATOR

by

Donald James Hammerstrom

A thesis submitted in partial fulfillment
of the requirements for the degree

of

Doctor of Philosophy

in

Electrical Engineering

MONTANA STATE UNIVERSITY
Bozeman, Montana

May 1994

APPROVAL

of a thesis submitted by

Donald James Hammerstrom

This thesis has been read by each member of the thesis committee and has been found to be satisfactory regarding content, English usage, format, citations, bibliographic style, and consistency, and is ready for submission to the College of Graduate Studies.

4-21-94 — Roy M. Johnson

Date — Chairperson, Graduate Committee

Approved for the Major Department

4-21-94

Date — Head, Major Department

Approved for the College of Graduate Studies

5/1/94 — R L Brown

Date — Graduate Dean

STATEMENT OF PERMISSION TO USE

In presenting this thesis in partial fulfillment of the requirements for a doctoral degree at Montana State University, I agree that the Library shall make it available to borrowers under rules of the Library. I further agree that copying of this thesis is allowable only for scholarly purposes, consistent with "fair use" as prescribed in the U.S. Copyright Law. Requests for extensive copying or reproduction of this thesis should be referred to University Microfilms International, 300 North Zeeb Road, Ann Arbor, Michigan 48106, to whom I have granted "the exclusive right to reproduce and distribute my dissertation for sale in and from microform or electronic format, along with the right to reproduce and distribute my abstract in any format in whole or in part."

Signature Donald J. Hammerstrom

Date April 21, 1994

ACKNOWLEDGMENTS

The author thanks his wife and family. They have been very patient.

The author also thanks MSE, Inc. of Butte, Montana and its personnel who graciously made their MHD research data available. Special thanks are extended to David Lofftus for serving on a Montana State University academic graduate committee.

The author was able to attend graduate school at Montana State University thanks to a generous NASA Montana Space Grant Consortium fellowship.

TABLE OF CONTENTS

TABLE OF CONTENTS—Continued

LIST OF TABLES

LIST OF FIGURES

LIST OF FIGURES—Continued

LIST OF FIGURES—Continued

LIST OF FIGURES—Continued

LIST OF SYMBOLS

a_i equation coefficient at node i

A duct cross section area (m^2)

A_e electrode surface area (m^2)

A_w electrode wall area (m^2)

B magnetic scalar induction ($tesla$)

$\vec{B}$ vector magnetic induction ($tesla$)

c local velocity of sound (m/s)

C^i continuity class i (All i^{th} derivatives are continuous)

C_v constant volume specific heat (J/kgK)

C_p constant pressure specific heat (J/kgK)

D hydraulic pipe diameter (m)

$\vec{E}$ vector electric field (V/m)

E_x axial electric field (V/m)

E_y transverse electric field (V/m)

$\mathcal{E}_o$ stagnation (total) internal energy (J/kg)

$f_{friction}$ friction factor

F drag friction force per unit volume (Nt/m^3)

$\mathcal{F}^{\pm}$ monotone flux operator

G Rosa's nonuniformity factor

h channel height (m)

H specific enthalpy (J/kg)

LIST OF SYMBOLS—Continued

H_o stagnation (total) specific enthalpy (J/kg)

H_{o1} combustor stagnation (total) enthalpy (J/kg)

I_i current at iteration i $(amperes)$

I_{load} total MHD dc load current $(amperes)$

I_x equivalent circuit axial current $(amperes)$

I_y equivalent circuit transverse current $(amperes)$

$\vec{j}$ vector current density $(amperes/m^2)$

j_x axial current density $(amperes/m^2)$

j_y transverse current density $(amperes/m^2)$

M Mach number

N_{Pr} Prandtl number

N_{Re} Reynolds number

N_S the Stefan-Boltzmann constant (W/m^2K^4)

P static pressure (Pa)

P_o stagnation pressure (Pa)

P' pressure correction (Pa)

Q thermal power loss to wall per volume (W/m^3)

Q_c wall convection flux (W/m^2)

Q_r wall radiation flux (W/m^2)

$Q^{\pm}$ interpolated flux evaluation

R gas constant $(J/kmolK)$

R_{ccc} diagonal circuit resistance (Ω)

R_{drop} ohmic portion of voltage drop (Ω)

R_{invt} inverter, transformer or consolidation resistance (Ω)

R_{load} load resistance (Ω)

LIST OF SYMBOLS—Continued

R_s slag layer equivalent resistance (Ω)

$\mathcal{R}_{xx}, \mathcal{R}_{xy}, \mathcal{R}_{yx}$ and $\mathcal{R}_{yy}$ equivalent circuit "resistances"

s seed mass fraction

$\mathcal{S}$ source term

$\mathcal{S}_x$ x axis component of source term

t time (s)

T static temperature (K)

$T_\circ$ stagnation temperature (K)

$T_{\circ w}$ temperature of an adiabatic wall (K)

T_p oxidant preheat temperature (K)

T_s slag wall temperature (K)

T_w duct wall temperature (K)

v velocity (m/s)

v_x axial velocity component (m/s)

$\hat{v}$ velocity less pressure gradient effects (m/s)

$v^\star$ an improved velocity (m/s)

V_{back} inverter back voltage (V)

V_{DR} non-ohmic voltage drop (V)

V_i source voltage at iteration i (V)

V_{load} total MHD load voltage (V)

V_x control volume axial voltage (V)

V_y control volume transverse voltage (V)

w duct width in z direction (m)

W mass flow rate (kg/s)

x axis direction

LIST OF SYMBOLS—Continued

y axis direction

z axis direction

Z average molecular mass ($kg/kmol$)

Z_L load impedance (Ω)

Z_S source impedance (Ω)

α electrode segmentation ratio

β Hall parameter

β_{eff} effective Hall parameter

γ specific heat ratio

Γ diffusion coefficient

δ_i insulator separation of adjacent electrodes (m)

δ_s slag thickness (m)

Δx control volume axial dimension (m)

Δt discrete time step (s)

ε gas emissivity

ε_w duct wall emissivity

ζ a numerical relaxation factor

θ diagonal configuration diagonal angle

Θ oxygen enrichment ratio

κ fluid thermal conductivity (W/mK)

μ electron mobility ($1/tesla$)

ν_c viscosity of the core flow (Nts/m^2)

ν_W viscosity at the duct wall (Nts/m^2)

ρ static density (kg/m^3)

ρ' density correction (kg/m^3)

LIST OF SYMBOLS—Continued

σ conductivity\(℧/m)

σ_{eff} effective conductivity (℧/m)

σ_s slag conductivity (℧/m)

ϕ spline basis function, generalized dependent variable

ϕ_i dependent variable evaluation at node i

ϕ_x axial component of independent variable ϕ

$\phi^\star$ dependent variable from previous iteration

Φ stoichiometric combustion ratio

ABSTRACT

Magnetohydrodynamic (MHD) power generation is the generation of electrical power from the flow of a conductive fluid through a magnetic field. The first commercial demonstration of coal-fired MHD power generation will likely be accomplished by retrofit of existing coal-fired steam generators. The combined MHD-steam generation plant must be controlled to supply its power demand. This thesis answers two questions: First, what is the size and shape of the allowable operating region of the linear, coal-fired, supersonic, diagonally-connected Proof of Concept (POC) MHD generator once operated for the U.S. Department of Energy by MSE, Inc. in Butte, Montana? Second, how much can the MHD generator contribute to load following?

A quasi-one-dimensional FORTRAN computer model solves for steady-state MHD operation in few iterations. The MHD conservation equation set is discretized with Patankar's SIMPLER finite volume algorithm. The tridiagonal matrix algorithm (TDMA) then solves the resulting banded matrices. External and simple, equivalent internal electrical circuits are solved by relaxation. The separation of the electrical circuit into internal and external parts permits one to model various electrode configurations without changing the channel equivalent circuit model. Fully developed turbulent boundary and electrode voltage drop models are also incorporated.

Model results are compared to POC data. The model overestimates nominal electrical power extraction by 0.4 MW and underestimates channel cooling requirements by 25%. Mach behavior in the diffuser sections is questionable.

Eight parametric studies are then conducted using coal flow rate, oxidant preheat temperature, oxygen enrichment, stoichiometric ratio, seed fraction, load resistance, magnetic induction, and diagonal angle as independent variables. Indicators of imminent duct stress, electrical power and enthalpic efficiency are monitored. It is found that the operating region for the POC MHD generator is large. Shocks limit the allowable operating region at low flow and high magnetic induction. Combustor pressure limits the maximum allowable flow. Many of the parametric studies exhibit efficiency optima in their parametric domains. A strategy for efficient load following is suggested. In this strategy, coal flow rate and magnetic induction must be coordinated during off-nominal operation to maintain high efficiency.

CHAPTER 1

INTRODUCTION

Magnetohydrodynamic (MHD) power generation is the generation of direct current (dc) electrical power from a conducting fluid's motion through a magnetic field. Although continued MHD power research in the United States is at this time uncertain, MHD power generation may provide the key to improved electric energy production efficiencies for the next century. Of particular interest is the combination of an MHD generator with a conventional steam plant. In this MHD-steam generator combination, the exit flow from the MHD generator enters the steam generator boilers. The MHD generator is called a *topping cycle*, and the steam generator is called a *bottoming cycle*. The MHD topping cycle in a combined MHD-steam generation plant has a less demanding efficiency criterion than that for a stand-alone MHD generator. Furthermore, retrofit of existing steam generators with MHD topping cycles may provide a cost effective alternative to developing new generation sites. Coal-fired plants of this MHD-steam combination are the focus of this thesis.

It will be assumed throughout this thesis that the reader has some knowledge of MHD theory. One can access a number of good sources for information about MHD [1, 2, 3, 4] and recent international MHD efforts [5].

This thesis addresses two questions necessary for the eventual commercial development of MHD power. First, what is the nature of the allowable steady-state operating region for a given supersonic MHD generator? Second, to what extent is an MHD generator capable of contributing to load following? While a great deal of technical work went into the preparation of this thesis, the purpose of the thesis is to simply begin a dialog concerning the flexibility one has in changing MHD operation to supply a range of loads. Load demands may change instantaneously, or they may change with a daily, weekly or seasonal cycle. A *load following* generator is one which can supply those varying load demands and, as such, is a flexible and valuable addition to the power grid. In contrast, a *base load* generator is one for which the quantity of generated power is largely immutable. MHD base load generators could still find favor with utilities if their energy generation efficiencies were demonstrated to be high.

The question of MHD plant flexibility is important to the future of MHD power generation at this stage of development. Predicted MHD generation efficiencies continue to rise with increasing plant size. Competing power generation technologies have relatively flat economies of scale. The first commercial MHD combined cycle demonstration plants will be of the 25 MW_e to 50 MW_e size, not large enough to fully demonstrate the predicted efficiencies of large MHD generators. Therefore, the first demonstrated MHD generator efficiencies will at best match competing technology efficiencies, and the MHD generator may be required to demonstrate additional benefits. These benefits could be in the areas of pollution control, power grid stabilization, maintainability, trouble-free operation, load flexibility and, of course, economic operation. Without one or more of these demonstrated benefits, power utilities may not be willing to risk building still larger commercial MHD generators.

Background Information

This section provides the context in which the thesis should be read. The amount of background introduced here is intended only as a review of those concepts necessary for understanding the computer model and any resulting discussion. This thesis addresses only the MHD topping cycle, but the operating region of the topping cycle must be understood in relation to entire plant operation.

The linear geometry, open cycle MHD generator has five sections: (1) The *combustor* mixes the combustion components and seed. The ratio of oxygen and fuel within the combustor determines the combustion temperature and controls nitrogen oxide emissions. Metallic seed is introduced in the combustor. The metallic seed, usually an alkali metal salt mixture, readily ionizes to increase the conductivity of the working fluid. (2) The *nozzle* accelerates the fluid. The load voltage in an MHD generator is strongly influenced by the fluid velocity. Therefore, it is prudent to maintain a high velocity throughout the MHD channel. (3) The *channel* is the power generator from which energy is extracted. The power from the interaction of magnetic field and moving charged particles is extracted at electrodes along the channel walls. (4) Some linear ducts have a constant cross section exit region called the *transition section*. This duct section is designed to slow the fluid gradually from supersonic to subsonic flow without a strong shock. (5) The *diffuser* is the section in which pressure and temperature are recovered. The diffuser exit poses an important junction between topping and bottoming cycles.

The coordinate system used throughout this thesis gives fluid flow primarily in the x direction, magnetic induction in the z direction and induced electrical currents in the x-y plane. See figure 1.

Words used to describe the MHD generator studied in this thesis include *supersonic*, *linear*, *open cycle*, *coal-fired*, *segmented electrode* and *diagonally connected*. The fluid flow in a *supersonic* MHD duct exceeds the velocity of sound in the nozzle and maintains a weak shock in the transition section under nominal operating conditions. The condition described as a *shock* is characterized by a discontinuity in certain state variables. While physical states may be discontinuous across a shock, mass flow

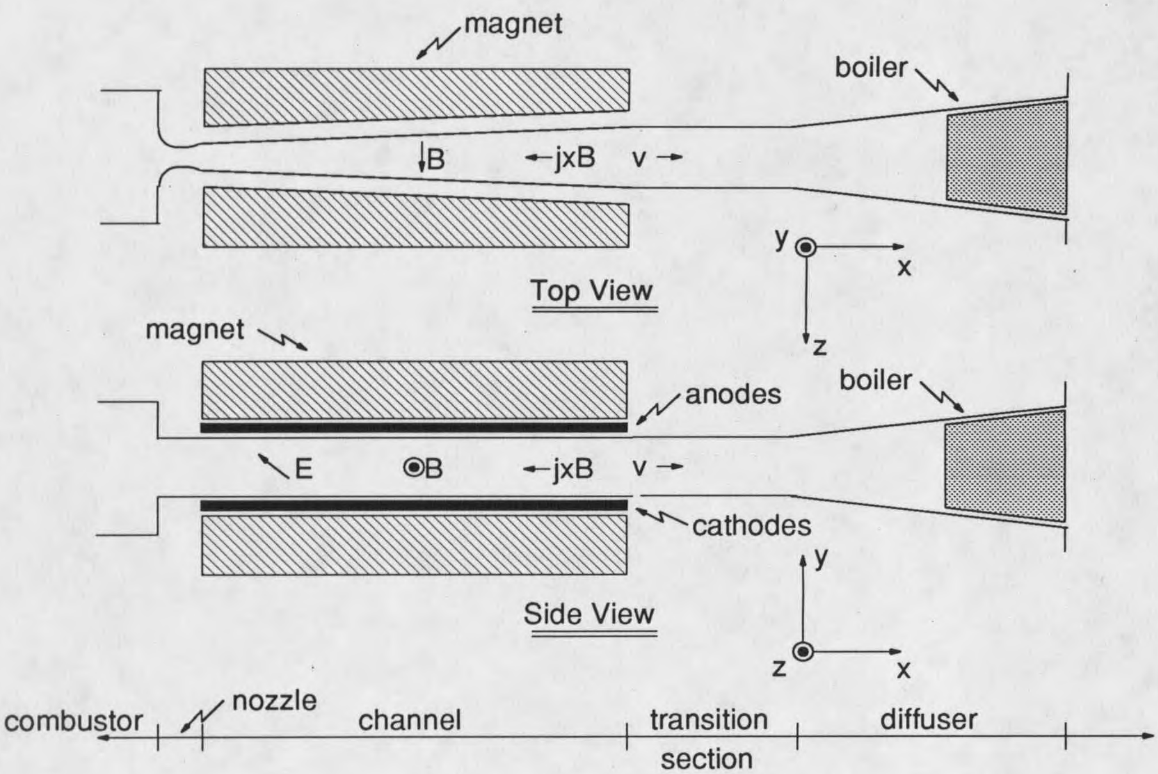

Figure 1: Duct Sections and Axis Convention

continuity, momentum conservation and stagnation enthalpy conservation cannot be violated. The words *linear geometry* differentiate the generator from disk geometry MHD generators. The plasma in a linear geometry MHD generator flows through the duct in a roughly linear path. An *open cycle* MHD generator does not recycle its working fluid. In contrast, *closed cycle* generators recycle their working fluids, usually liquid metals or noble gases. Many possible electrode configurations exist, but the *diagonal* electrode configuration is one which shorts most anodes and cathodes diagonally throughout the channel along equipotentials. The diagonal connection external circuit imposes an electric field angle and consolidates the many segmented electrodes into a lesser number of power electrodes at the channel extremities. The diagonal electrode configuration is a compromise between the Hall and Faraday electrode configurations and, as such, utilizes both the Hall and Faraday electrical fields in generating its terminal voltage. MHD generator electrodes are *segmented*, divided into numerous insulated electrodes in the axial direction, in order to prevent shorting the axial electric circuit within the channel.

Coal is an abundant fuel in the United States. MHD may be an environmentally advantageous method for coal-fired power generation. The efficient MHD generator produces less carbon dioxide, and the alkali seed efficiently removes any sulfur coal pollutant. One enriches the fuel mixture in a coal-fired MHD generator with oxygen to attain very high combustion temperatures. The coal may be burned at very high temperatures because the MHD generator has no moving parts in contact with the flowing combustion mixture. The higher combustion temperatures mean higher Carnot efficiencies may be obtained for the combined cycles. The MHD duct effluents flow into the bottoming cycle at about the same temperature as the combustion temperatures for a stand-alone coal steam plant. Therefore, any net energy produced in the MHD topping cycle improves the efficiency over that of the stand-alone, conventional steam plant. Unfortunately, coal slag, glass-like coal components, create difficult corrosion problems within the duct.

A number of studies have been completed during development of linear geometry, open cycle MHD generator theory, and these studies explain specifics of the issues introduced above. Two such texts are a 1978 joint U. S. A. and U. S. S. R. study [6] and a 1969 British study [7].

Of particular interest is the question of how one might eventually control the combined MHD-steam plant conditions to supply a large range of load demands. The solution could require modification of topping cycle operation, modification of the bottoming cycle operation, or a combination of both. The MHD generator is often considered a constant load device, but early commercial developers may ask that the MHD generator contribute to load following. Indeed, it was proposed that the 28 MW_e Billings demonstration plant design [8], which unsuccessfully competed for a United States DOE Clean Coal Technology grant in 1993, have the capability to vary its electrical power output from 40% to 105% of the nominal load. A number of papers have claimed to address parts of this problem, but because of the problem's complexity, each uses simplifications, and the results have been largely anecdotal.

One simplification required for this and most other combined MHD-steam plant system studies is the separation of MHD dynamics and steam plant dynamics. The MHD topping cycle responds almost immediately to fuel and load changes while the steam plant may take over one hundred seconds [9]. This assumption allows the MHD topping cycle to be treated as an algebraic input-output model for the dynamic responses of the steam bottoming plant. From the combined cycle control standpoint, only the steady-state behaviors of the MHD generator need to be addressed in this thesis.

Some of the more significant, previous system studies of MHD-steam plant behaviors will now be cited. These studies and the methods used in these studies lay the groundwork for the computer experiment and computer model used in this thesis.

Trung [10] and Matair [11] simulated the connection of MHD generators to commercial power grids in their PhD theses. Each used time-dependent computer models which couple the electrical and fluid interactions within the MHD channel. The models were built upon a complete formulation of the MHD conservation equations, which have become the standard for computer MHD simulations. These theses are noteworthy for having integrated the MHD model and external power grid through multi-pulse bulk inverters. Combined cycle operation was not studied.

Ishikawa [9] combined a similar computer model with that for a rotating generator at the same power bus. The rotating machine represents steam boiler turbine generation using a synchronous machine. The synchronous machine was modeled by Park's equations. The MHD inverter and synchronous generator of a combined cycle plant necessarily share the same bus. He observed that the MHD topping cycle can have a great effect on the steam turbine system, but the feedback from the steam plant to the MHD topping cycle is rather small. This observation is partly explained by the relatively small proportion of MHD topping cycle power extraction in the combined MHD-steam plant power production. Ishikawa concluded that stability of the overall system should not be a troublesome issue because of the lack of feedback and the fast MHD dynamics.

Boulay [12] concluded that the MHD portion of the combined MHD-steam plant must be controlled by the electrical power take-off of the channel. The other inputs have response rates in the range of 1% per minute, and the coal feed system may take an hour to fully respond to requested changes. Only the electrical power take-off (PTO) has response times on the same order as MHD dynamics.

Jackson [13, 14] suggests that the MHD topping cycle power extraction might be shut down during fault transients. This control could be accomplished very quickly by introducing electrical short or open conditions across the MHD channel. However, one must then ask if the bottoming cycle is able to handle the excess heat during such a transient. Any such control strategy must be faster than the fastest response time of the bottoming cycle.

A number of papers demonstrate the MHD plant control experience developed at MSU. Rudberg [15] has shown considerable expertise in boiler dynamics. Aspnes, Pierre and Johnson [16, 17, 18, 19] have completed a study similar to the present one, in which they investigated the effect of coal feed and oxygen preheat on combined plant dynamics. This early study utilized only two independent input variables and modeled a Faraday electrode configuration channel.

Statement of Problem

Not one of the cited studies adequately addresses the range of operation available from a given combined MHD-steam plant design or the ramifications of modifying MHD generator operation within that range to supply different steady-state loads. The problem may be divided into three parts: What is the available range of operation for the topping cycle? What is the available range of operation for the bottoming cycle? And what is the range of operation for a combined cycle plant? Of these questions, the question of steam plant capability is fairly well understood after years of steam plant operation. The question of combined plant operation requires the answer to the first question. Therefore, this thesis will address only the topping cycle portion of the problem.

The logical procedure used to address the thesis question is as follows: A steady-state computer MHD duct model is developed. This model relies on first principles physical theory and experiences reported in the literature. The computer model is then used to model the nominal operation of an existing and operating MHD generator for which steady-state data exists. The accuracy with which the computer model predicts the steady-state condition of the physical MHD generator is critiqued. At this point, one knows the strengths and weaknesses of the computer model. The computer model is then used in a series of parametric studies spanning as large a domain as possible. Relying on a number of criteria cited in the literature as causing or predicting harmful MHD generator stresses, one can then characterize an allowable operating region for the investigated MHD generator.

Load capabilities and efficient operation can also be discussed from the parametric study results. However, any results must be discussed from the perspective of the MHD generator apart from any system considerations. For example, it may be economical at some reduced load to turn off MHD interaction altogether and use only the thermal flow from the MHD generator in a bottoming cycle. This systems solution cannot be predicted from this study, but the results of this study could help the system controller decide when it is best to turn off the MHD interaction.

One hopes that the results of this study may be extrapolated or scaled to other and possibly larger MHD generators. Great care must be used in making any such conjecture. Any limitations found for topping cycle operation may affect the ability of a combined cycle plant to supply a wide load range. It is hoped that this thesis will be helpful in eventually investigating the capabilities of the combined cycle plant.

Thesis Overview

The first four chapters discuss portions of the thesis computer model. The next two present experimental results. The final chapter summarizes results, offers conclusions and suggests areas for possible further study.

In chapter 2 the real gas model is described. The model consists of a number of lookup tables representing the equilibrium properties of a Montana Rosebud coal combustion mixture. These tables are interpolated using a multidimensional Hermitian spline FORTRAN computer program set. The program set allows up to five independent variables and is one of the factors which allow such a broad set of parametric studies to be undertaken.

Chapter 3 describes the computer electrical model, which consists of internal and external circuit portions. The internal model is of the equivalent circuit type and models electrical-fluid interactions using electrical circuit elements. The internal and external circuits must be solved by relaxation.

Chapter 4 describes solution of the quasi-one-dimensional flow problem by a modified finite volume method. The method was adopted for this study because it solves the steady-state duct flow without numerical marching in time. Pressure, velocity and stagnation internal energy are chosen as the fluid states.

In chapter 5, nominal steady-state behavior of the thesis computer model is compared to nominal data from the POC channel operated for the United States Department of Energy by MSE, Inc. in Butte, Montana. It is found that electrical power extraction is overestimated, and channel thermal power loss to the walls is underestimated. Otherwise, modeled behaviors are acceptable.

Chapter 6 presents and discusses the results of a series of parametric studies using the POC channel model. A total of seven possible control variables and diagonal angle are used as independent variables. The results are discussed and summarized using five basic criteria related to identified channel stresses or generator efficiency. The computer model allows investigation of operating conditions which have not yet been tried or cannot be tried on research generators.

Finally, the results are summarized, and conclusions are offered in the last chapter. It is concluded that the allowable operating region for the Butte POC channel is large, but efficient operation of the POC channel demands a much smaller operating region. These results may be extended to larger channels, but it must be understood that the Mach behavior of high interaction channels may dominate all other effects.

The appendix to this thesis contains all FORTRAN program listings used in this study. Any symbols not explicitly defined in the text may be found in the List of Symbols within the front sections of this thesis.

CHAPTER 2

MODELED FLUID PROPERTIES

Modeling Combustion Product Flows

This chapter chronicles how fluid properties were modeled in this thesis. The modeling of combustion product fluid flows is a complex art due to the inhomogeneity of the combustion mixture, the extreme temperatures and pressures within an MHD duct, and the fact that the combustion mixture changes as it traverses the duct length. The ideal gas law

$$P = \rho RT \tag{1}$$

holds well for only simple, pure, monatomic gases at moderate temperatures and pressures. Pure, real gases like carbon dioxide and water vapor exhibit more complex behaviors as they expand, condense and possibly dissociate at temperature and pressure extremes. Combustion gas mixtures are even more complex because the mixture continues to react and changes numbers and identities of mixture components.

To make the modeling of the combustion mixture tractable, it is assumed that all components instantaneously attain their equilibrium composition and equilibrium properties at every location along the duct. This assumption allows equilibrium conditions—measured, or simulated—to be compiled throughout the domains of reactant composition, temperature and pressure. For this study, such a compilation of equilibrium conditions was prepared by MSE, Inc. in Butte, Montana, and the resulting tables were interpolated by a cubic Hermitian spline FORTRAN program set. The program set and interpolation procedure are described in the first part of this chapter.

The MHD combustor section is not modeled as part of the flow train in this thesis computer model. Combustor behavior is described instead by a set of interpolated tables again prepared by MSE. The interpolated tables introduce the total flow rate and specific stagnation enthalpy at the combustor-nozzle interface, where the computer flow model begins. Another table helps predict combustor thermal cooling requirements. All the MSE combustor data was prepared at MSE, Inc. using a plug flow, equilibrium energy balance combustion computer model. The equilibrium combustion product code used by MSE is similar to the NASA-SP-273 code used in Chandra [20] and a number of others. Slag retention of 30 % was assumed. The enthalpies introduced in these MSE data tables are calculated for the true combustion mixture. Many combustion studies use instead the enthalpy of fully combusted products. This difference must be remembered during any data comparisons.

The high velocities (approaching Mach 1.5) within a supersonic MHD duct also complicate the modeling of fluid properties. A flowing fluid has a set of *stagnation* properties, which correspond to a stationary reference point, and a set of *static* properties, which correspond to a reference frame moving at the fluid's velocity [21]. Translating a static property into its related stagnation property requires proper accounting of the transformation of kinetic energy into internal and expansion energies.

Cubic Hermitian Splines

A FORTRAN program set was developed to read a number of combustor and equilibrium combustion product property tables (F1), create an indexed spline data file (SPLINER), and later interpret that data file using cubic Hermitian interpolation (SR). See the appendix for these FORTRAN program listings. This program set creates and interpolates splines in up to five independent variables.

The mathematical formulation of the spline algorithm is an extension of the one- and two-dimensional cubic Hermitian spline formulations found in texts like Prenter's *Splines and Variational Methods* [22]. The cubic spline of a given function in domain $\underline{x}$ may be carried out in any dimension as a weighted sum of products of the two basis functions shown in Figure 2. Let the first basis function ϕ_1 at a node in dimension x be weighted by a magnitude at that node. The second, ϕ_2, will be weighted by a gradient at that node. A function may be approximated in a single dimension having N nodes by

$$f(x) \cong \sum_{k=1}^{N} f(x_k)\phi_{1,k} + \left.\frac{df}{dx}\right|_{x_k} \phi_{2,k}. \tag{2}$$

In a second dimension,

$$\begin{aligned} f(x_1, x_2) \cong \sum_{k=1}^{N_1}\sum_{l=1}^{N_2} f(x_{1,k}, x_{2,l})\phi_{1,k}\phi_{1,l} + f(x_{1,k}, x_{2,l})\left.\frac{\partial f}{\partial x_2}\right|_{x_{k,l}} \phi_{1,k}\phi_{2,l} \\ + f(x_{1,k}, x_{2,l})\left.\frac{\partial f}{\partial x_1}\right|_{x_{k,l}} \phi_{2,k}\phi_{1,l} + \left.\frac{\partial^2 f}{\partial x_1 \partial x_2}\right|_{x_{k,l}} \phi_{2,k}\phi_{2,l}, \end{aligned} \tag{3}$$

and so on for higher dimensions.

The spline calculation becomes inefficient for high dimensionality. In fact, the calculation effort increases by at least 2^{n-1}, where n is the dimensionality. This means that working with more than about five dimensions becomes impractical. Although the multidimensional cubic Hermitian splines are computationally costly, they create accurate interpolations for which all gradients are continuous.

An option in the SPLINER, SR program set allows one to drop to quadratic interpolation near function boundaries. This option was used for all interpolations in this study, and it is a wise option whenever gradient data at function boundaries is of questionable accuracy. The program linearly extrapolates beyond function boundaries

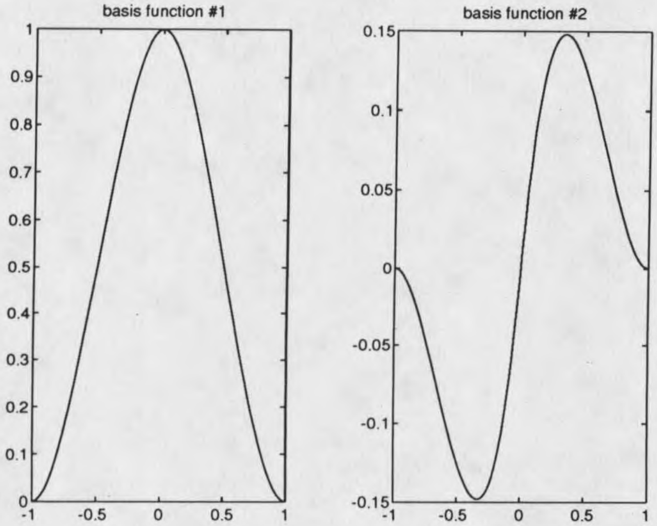

Figure 2: Cubic Hermitian Spline Basis Functions

if it is necessary to do so. A warning may be implemented in SR to warn the user when an extrapolation beyond the original function domain is being performed.

Real Gas Data

It is appropriate to demonstrate some of the real gas property spline interpolations at this time. Not only will these examples demonstrate the spline capabilities, but they also should be referred to when reviewing later parametric studies. For example, the dependency of equilibrium temperature upon stoichiometry may be instrumental in later interpreting the parametric study using stoichiometry as an independent variable. Table 1 lists the real gas and combustor state interpolations used in this study. Table 2 gives the domains for the independent variables in each of the splines.

Figure 3 shows the dependence of combustor stagnation enthalpy upon its five independent variables. Since it is hard to visualize multidimensional surfaces, the plot shows variation in combustor stagnation enthalpy while four independent variables remain fixed at their nominal values (shown in the key), and the remaining variable

spline	description
$H_{o,1}(\Theta, \Phi, s, P_{o,1}, T_p)$	combustor stagnation enthalpy
$W(\Theta, \Phi, s, P_{o,1}, T_p)$	total flow rate
$\sigma(\Theta, \Phi, s, P, T)$	equilibrium conductivity
$\mu(\Theta, \Phi, s, P, T)$	equilibrium electron mobility
$T_o(\Theta, \Phi, s, P_o, H_o)$	equilibrium stagnation temperature
$T(\Theta, \Phi, s, P, H)$	equilibrium static temperature
$\varepsilon(\Theta, \Phi, s, P, T)$	equilibrium gas emissivity
$Z(\Theta, \Phi, s, P, T)$	equilibrium molecular mass

Table 1: Equilibrium Real Gas and Combustor State Spline Functions

Combustor Splines

symbol	definition	range	units
Θ	oxygen enrichment	[0.2099 : 0.425]	mole fraction O_2
Φ	stoichiometric ratio	[0.85 : 0.95]	mole fraction
s	seed ratio	[0.0 : 0.025]	mass fraction K
P_o	combustor stagnation pressure	[3.0 : 6.0]	atm
T_p	oxidant preheat temperature	[922.2 : 1089.]	K

Equilibrium Splines

symbol	definition	range	units
Θ	oxygen enrichment	[0.2099 : 0.425]	mole fraction O_2
Φ	stoichiometric ratio	[0.8 : 1.0]	mole fraction
s	seed ratio	[0.0 : 0.025]	mass fraction K
P	pressure	[0.25 : 7.0]	atm
T	temperature	[1300 : 2800]	K
H	specific enthalpy	[1.5 : 5.5]	MJ/kg

Table 2: Independent Variable Domain Summary

is varied throughout its domain. Each independent variable has been normalized by dividing it by its nominal value. There exist strong dependencies upon oxygen enrichment and upon stoichiometric ratio. Combustor temperature, and consequently combustor enthalpy, rise as more and purer oxidant is added to the combustion mixture.

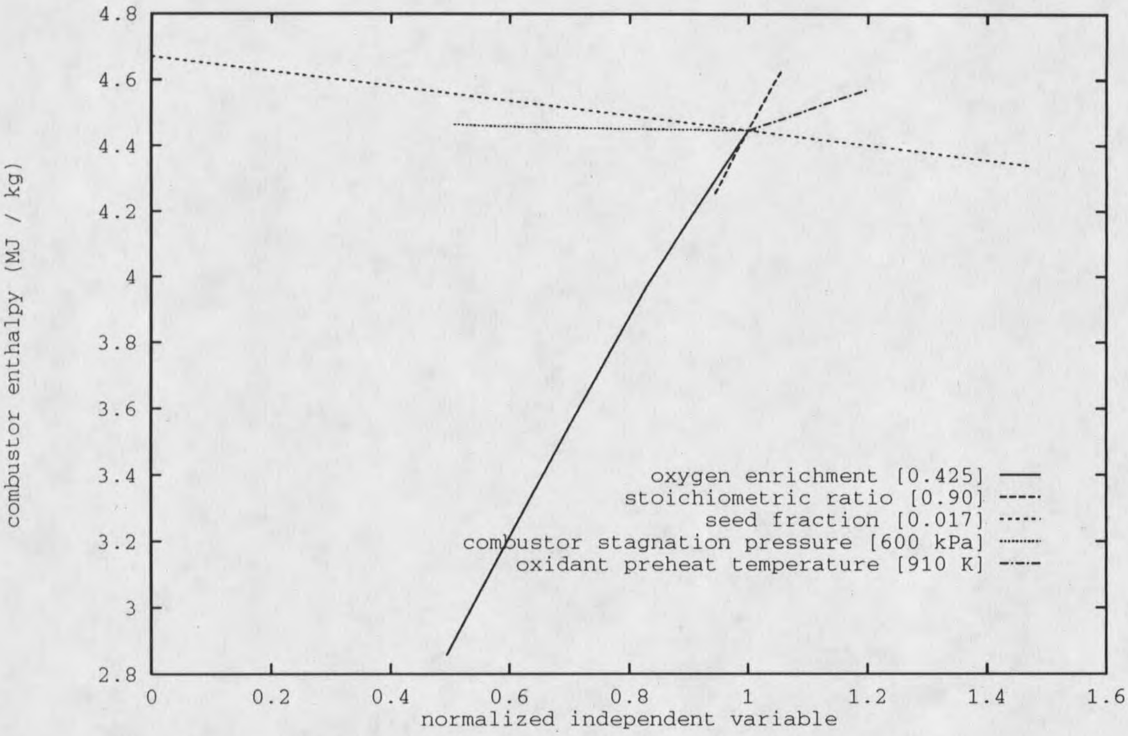

Figure 3: Combustor Stagnation Enthalpy Dependencies

Similar figures are included for equilibrium conductivity and temperature. Figure 4 for conductivity shows that the first one-half percent of metallic seed significantly increases conductivity. Additional seed does so at a lesser rate. The conductivity of unseeded fluid is negligible. Equilibrium temperature (Figure 5) at a given pressure and enthalpy is a strong function of both oxygen enrichment and stoichiometric ratio. Again, coal burns hotter with more and purer oxidant.

Figure 6 shows that conductivity is a strong function of both temperature and

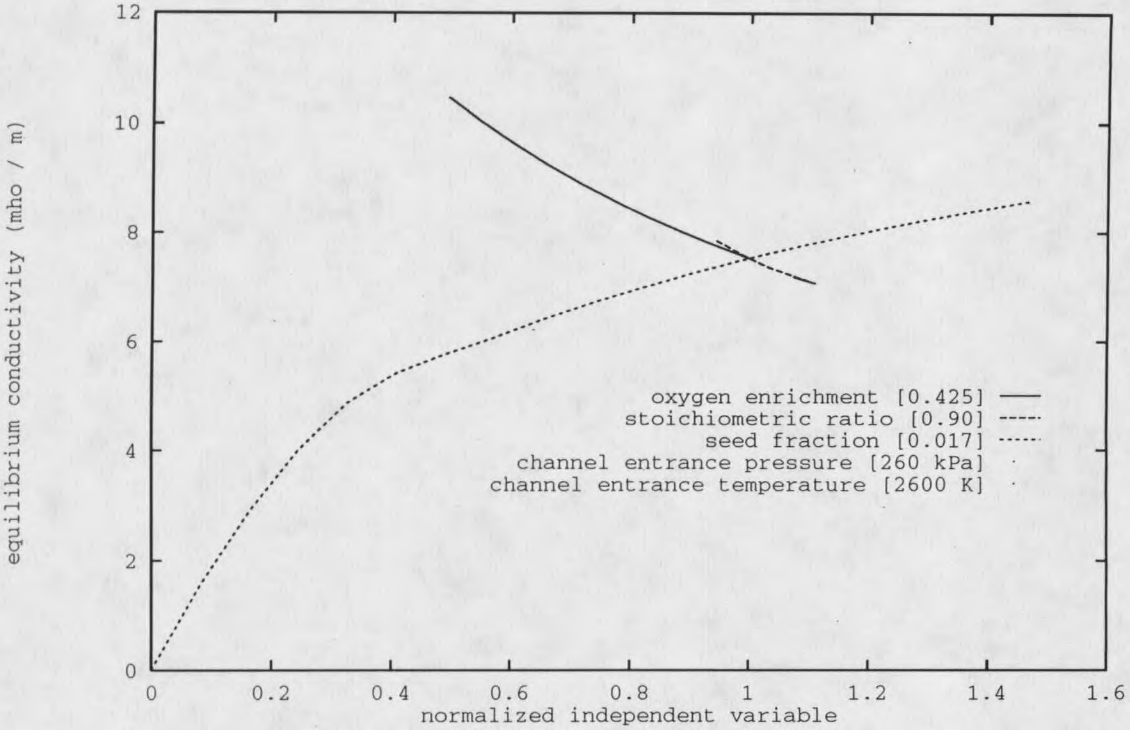

Figure 4: Equilibrium Conductivity Dependence upon Three Independent Variables

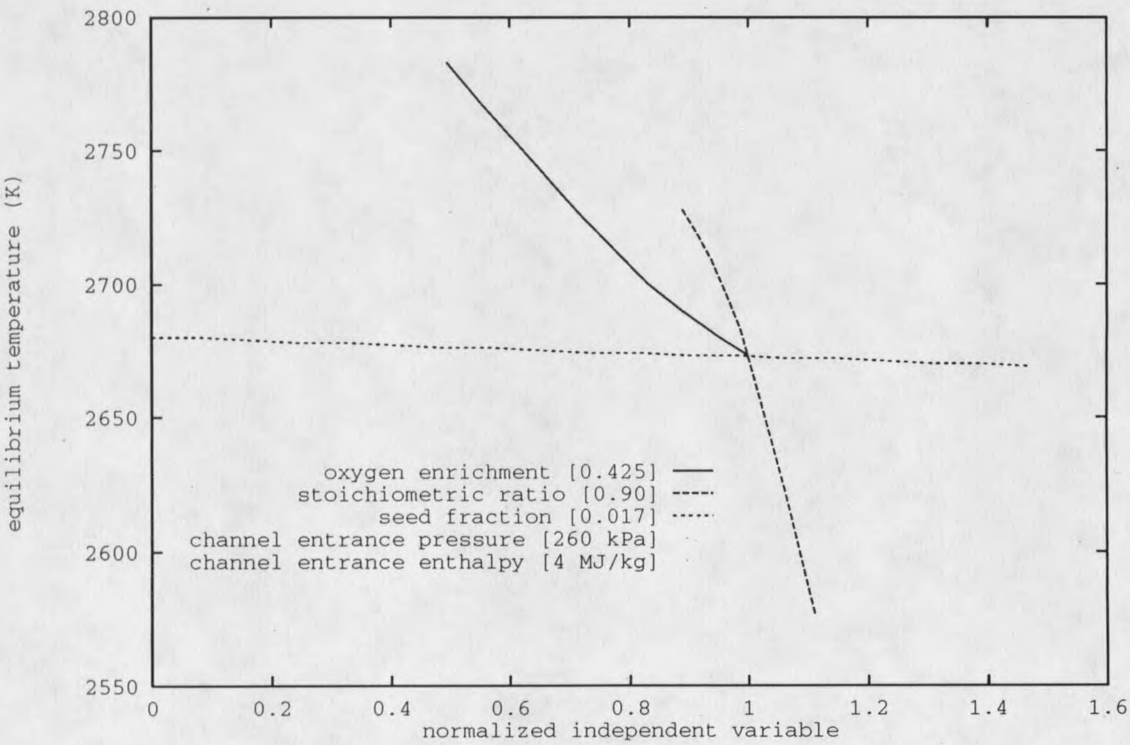

Figure 5: Equilibrium Temperature Dependence upon Three Independent Variables

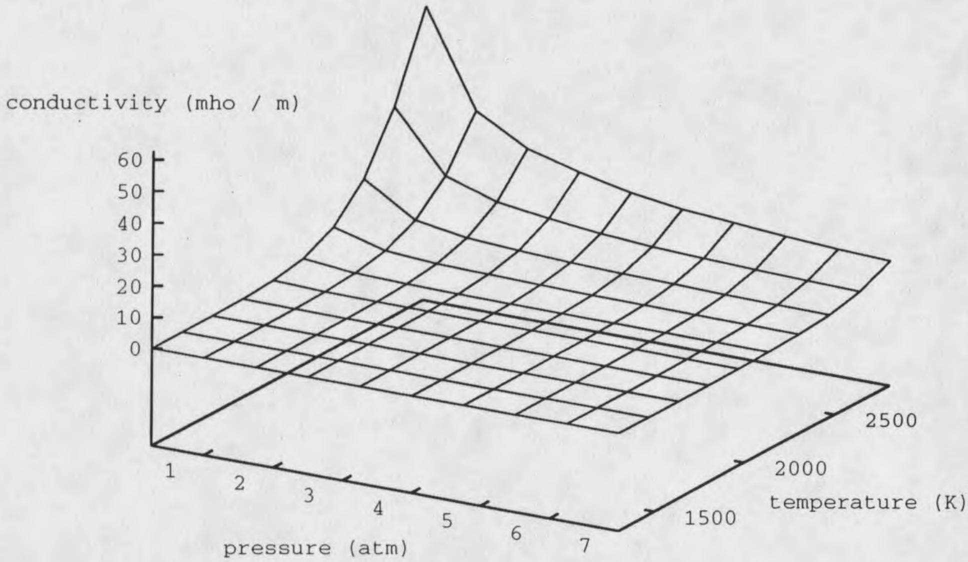

Figure 6: Equilibrium Conductivity as a Function of Temperature and Pressure

pressure. Other independent variables are held at their nominal values for this figure. Higher temperatures encourage ionization, but high pressures increase ion collision frequency and reduce the likelihood of free ions. Only a small region of Figure 6—that with temperatures between 2000 and 2600 K and with pressures between 0.5 and 2.0 atm—are significant to the operation of an MHD generator. Conductivity is unlikely to exceed 12 mho/m.

Figure 7 gives fluid temperature as a function of enthalpy and pressure. Temperature does not change greatly with pressure, but it changes rapidly with enthalpy. The same spline is used for evaluation of both static and stagnation temperatures. Static temperature is evaluated from local static pressure and specific enthalpy; stagnation temperature is evaluated using stagnation pressure and stagnation specific enthalpy.

Other real gas functions are not shown in this thesis, but it is worthy of note that electron mobility is a strong function of pressure. As pressure is lowered, the mean time between electron-particle collisions increases, and electron mobility

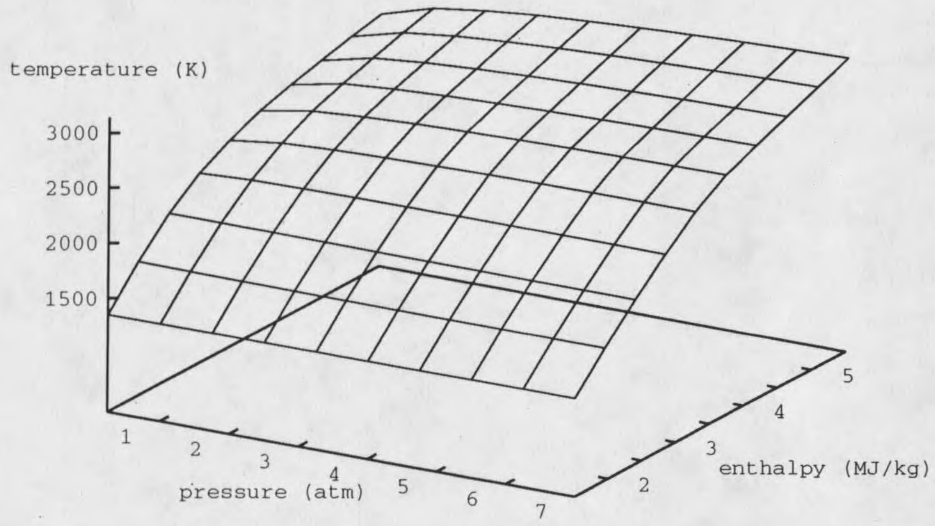

Figure 7: Equilibrium Temperature as a Function of Pressure and Enthalpy

improves. The effect of pressure on electron mobility also affects the Hall parameter β since

$$\beta = \mu B$$

for electron mobility μ and magnetic induction B.

Other Fluid Properties and Relations

The states of the numerical solution equation set are P, the static pressure, v, the velocity, and $\mathcal{E}_\circ$, the stagnation internal energy. The reasons for the choice of these state variables will be discussed in chapter 4. Most other fluid variables are updated in module NONLIN as now described.

Stagnation and static enthalpies are calculated from the states.

$$H_\circ = \mathcal{E}_\circ + \frac{P}{\rho} \tag{4}$$

and

$$H = H_\circ - \frac{v^2}{2}. \tag{5}$$

Once T and $T_\circ$ have been interpolated, the constant pressure specific heat may be deduced

$$C_p = \frac{v^2}{2(T_\circ - T)}, \tag{6}$$

and the ratio of specific heats is

$$\gamma = \frac{C_p}{C_p - \frac{R}{Z}}. \tag{7}$$

In this equation the ratio $\frac{R}{Z}$, a gas "constant," varies with average molecular mass Z.

Then the stagnation pressure may be calculated.

$$P_\circ = P(\frac{T_\circ}{T})^{\frac{\gamma}{\gamma-1}} \tag{8}$$

A modified ideal gas law couples static pressure P and density ρ.

$$\rho = \frac{PZ}{RT} \tag{9}$$

All of these are standard thermodynamic gas relations. However, deducing specific heat C_p as shown in equation 6 is unique. This technique was found to be better than direct implementation of the specific heat definition

$$C_p = (\frac{\partial H}{\partial T})_p \tag{10}$$

in this formulation.

CHAPTER 3

ELECTRICAL MODEL

The MHD computer model used in this thesis simulation consists of a fluid model and an electrical model. The fluid model is integrated to update the state, from which all fluid properties can be derived. The electrical model equations, along with those fluid property evaluations described in chapter 2, are solved as side equations. The calculated electrical properties, in turn, affect the next iteration of the fluid state. Electrical power extraction interacts with fluid flow by producing a retarding body force ($\vec{j} \times \vec{B}$) and a power extraction ($\vec{j} \cdot \vec{E}$). The body force retards flow and generates back pressure. The power extraction reduces stagnation enthalpy and stagnation temperature throughout the channel.

The electrical model has been separated into an internal electrical model and an external electrical model. This separation allows great flexibility in the types of external electrode configurations which can be investigated. The internal and external electrical models must be simultaneously iterated. A criterion for the stability of this method shall be proposed based on an analogy to a simple series source and load circuit. An integral voltage drop model is also introduced. The voltage drop is divided between internal and external models in a way which stabilizes numerical solution of the overall electrical circuit.

The MHD Channel Internal Electrical Model

The formulation of the internal electrical model begins with Ohm's law [3].

$$\vec{j} = \sigma(\vec{E} + \vec{v} \times \vec{B}) - \frac{\beta}{|\vec{B}|}\vec{j} \times \vec{B} \tag{11}$$

Finite segmentation of electrodes reduces the conductivity σ and the Hall parameter β to σ_{eff} and β_{eff} [3], where

$$\sigma_{eff} = \frac{\sigma}{1 + \alpha(\beta - 0.44)}, \tag{12}$$

and

$$\beta_{eff} = \frac{\beta}{1 + \alpha(\beta - 0.44)}. \tag{13}$$

The electrode segmentation ratio α is defined as the ratio of electrode pitch to the separation between anode and cathode. The anode and cathode electrode separation is a constant, the channel height h, in many Z-bar sidewall MHD channels and shall be assumed constant in this thesis channel model.

A number of assumptions are necessary before proceeding. First, assume that only the axial velocity component v_x is significant, and properties like conductivity σ, induction $\vec{B}$, Hall parameter β, electric field $\vec{E}$, and current density $\vec{j}$ vary only in the axial direction. This assumption is inherent in a quasi-one-dimensional fluid model. The great axial currents in some diagonal or Hall generator channels result in significant transverse pressure gradients and transverse velocity components. These transverse nonuniformities violate the above assumption. However, the quasi-one-dimensional model remains useful if one works with quantities averaged across the transverse directions. Second, one assumes that the only channel electric field and current components are in the x-y plane. This assumption is somewhat violated in channels with conducting Z-bar [23] sidewalls. The z tensor conductivity is greater than that in the x-y plane [7]. Therefore, there will be currents in the z direction near the conducting sidewalls.

Nonetheless, the increased complexity of a higher dimension model is not justifiable at this point. Hence the simplified two-dimensional components of Ohm's law may be written as

$$j_x = \sigma_{eff} E_x - \beta_{eff} j_y \tag{14}$$

$$j_y = \sigma_{eff}(E_y - v_x B_z) + \beta_{eff} j_x. \tag{15}$$

After rearranging these two equations and integrating over the discretized control volume, one can write

$$\begin{bmatrix} V_x \\ V_y + hvB \end{bmatrix} = \begin{bmatrix} -\frac{\Delta x}{\sigma_{eff} wh} & -\frac{\beta}{\sigma w} \\ \frac{\beta}{\sigma w} & -\frac{h}{\sigma_{eff} \Delta x w} \end{bmatrix} \begin{bmatrix} I_x \\ I_y \end{bmatrix}. \tag{16}$$

The symbols Δx, h and w represent control volume dimensions in the x, y and z axis directions, respectively. Figure 8 shows the equivalent internal channel circuit for equation 16. The simpler notation $\mathcal{R}$ has been introduced in Figure 8 by rewriting equation 16 as

$$\begin{bmatrix} V_x \\ V_y + hvB \end{bmatrix} = - \begin{bmatrix} \mathcal{R}_{xx} & \mathcal{R}_{xy} \\ \mathcal{R}_{yx} & \mathcal{R}_{yy} \end{bmatrix} \begin{bmatrix} I_x \\ I_y \end{bmatrix}. \tag{17}$$

The matrix diagonal members in equation 17 are represented in the equivalent circuit as resistances, and the off-diagonal matrix members are represented as dependent voltage sources. The terms V_{DR} in Figure 8 represent the non-ohmic portion of the total voltage drop at the electrode surfaces. The voltage drop, not shown in equation 16, is treated as a necessary correction to the total transverse voltage V_y.

A two-dimensional equivalent circuit technique for modeling channel electrical interactions was first introduced by Yoshida and Umoto in 1980 [24]. The method has been more recently been used by Hammerstrom [25, 26, 27], Inui [28],

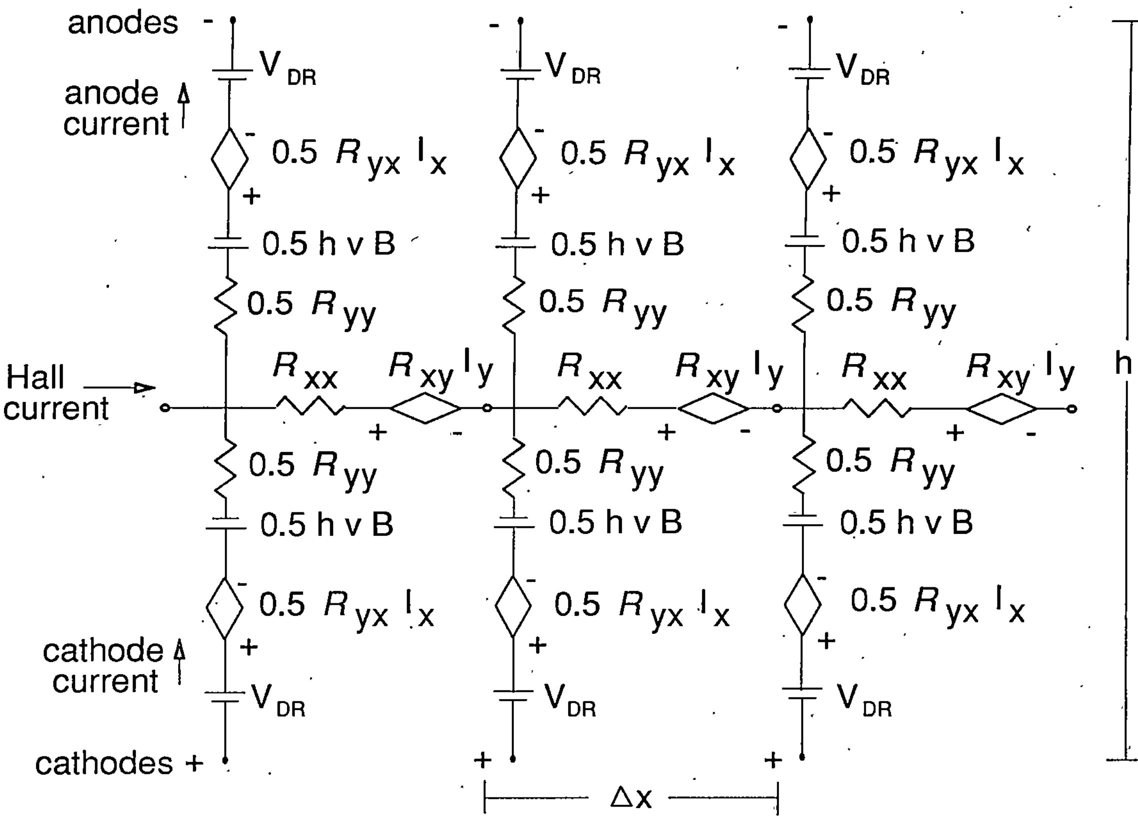

Figure 8: Internal Circuit Model

Ishikawa [29, 30, 31], Martinez-Tamayo, Hruby and Pote [32], Yoshida [33], and others. Some researchers, most notably Ishikawa and Yoshida, have successfully used greater transverse discretization of the equivalent circuit. However, the added complexity of greater transverse discretization may not be justifiable for use with a quasi-one-dimensional flow model, and the correct method for distributing currents throughout a complex equivalent circuit mesh with body forces is not clear. Yoshida [24] introduced a rotation of the equivalent circuit to make the transverse circuit axis parallel to the diagonal configuration diagonal angle θ. The benefit of this rotation is unclear. The rotation may, in fact, complicate representation of channel current paths. Other investigators have introduced Rosa's nonuniformity factor G into the two-dimensional equivalent circuit formulation [33]. The effect of fluid nonuniformity in reducing electrical parameters may be significant and real, but inclusion of this factor into a first principles model does not appear to be warranted.

The great advantage of the two-dimensional equivalent circuit model is that terminals of the internal circuit model correspond immediately to multiples (or fractions) of electrodes, depending on the fineness of discretization. Therefore, the external circuit may be modeled with as great complexity as necessary. The average axial and transverse current densities, j_x and j_y, are readily approximated from axial equivalent circuit current I_x and the averaged transverse equivalent circuit current I_y. Averaged electric fields E_x and E_y may be approximated from the total voltages between nodes, V_x and V_y, where V_y is reduced by any electrode voltage drops V_{DR}.

The External Circuit Model

The external electrical circuit models one's choice of electrode configuration. Three possible and common electrode configurations are shown in Figure 9. The simple segmented Faraday configuration allows no axial channel currents, and transverse currents are proportional to channel loading. On the other extreme, the loaded, segmented Hall generator must allow axial channel currents. The open circuit Hall generator is equivalent to the fully short circuited Faraday generator, and great transverse currents flow. Therefore, the currents in a Hall generator do not directly correspond to channel loading. The segmented diagonal generator channel should be expected to behave much like a Hall generator. However, a diagonal MHD generator can, in theory, be designed to minimize axial currents at its nominal operating condition.

The diagonal configuration is of primary concern in this thesis. Module EXTCIRC is a flexible subroutine in which one calculates electrode currents given the solved electrode voltage profile from the internal electric circuit model. Any electrode configuration may be modeled. The version of EXTCIRC presented in the

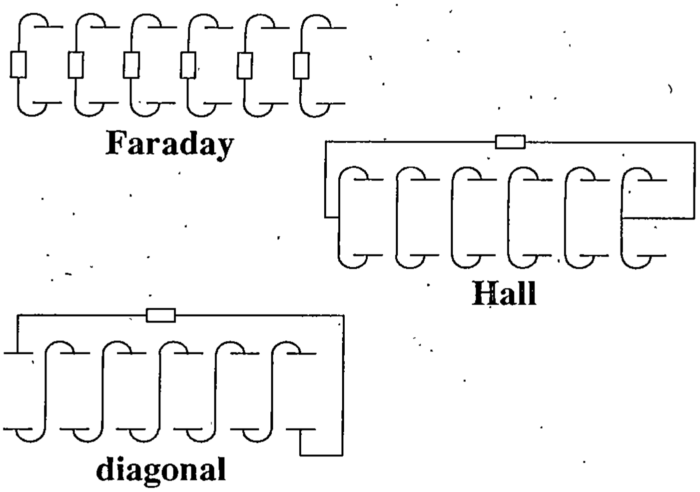

Figure 9: Faraday, Hall and Diagonal Electrode Configurations

appendix models a diagonal electrode configuration as shown in Figure 10. In this diagram, R_{ccc} (0.05Ω) represents diagonal connection losses nominally chosen to give 3% electrical losses. R_{load} represents generated load power; R_{invt} ($0.03R_{load}$), inverter, consolidation and transformer losses of 3%; V_{back} (not implemented), inverter back voltage; and R_{drop}, the calculated resistive portion of the electrode voltage drop. One electrode from each PTO region is selected as a master, and it is assumed that lossless consolidation occurs [34]. The master electrodes are used to calculate the load voltage and load current. The load current is shared equally among PTO electrodes.

The alternatives to the paired equivalent internal circuit and external circuit models for modeling diagonal electrode configurations are a discretized field solution [35, 36] or a load current conservation equation [7]. The field solution formulation is initiated by differentiating equations 14 and 15 with respect to their axis variables. The results are $\frac{\partial j_x}{\partial x}$ and $\frac{\partial j_y}{\partial y}$. If one assumes that the current density field is sourceless, the divergence of $\vec{j}$ is zero.

$$\frac{\partial j_x}{\partial x} + \frac{\partial j_y}{\partial y} = 0 \tag{18}$$

The method has been used with success, but the interaction between internal and

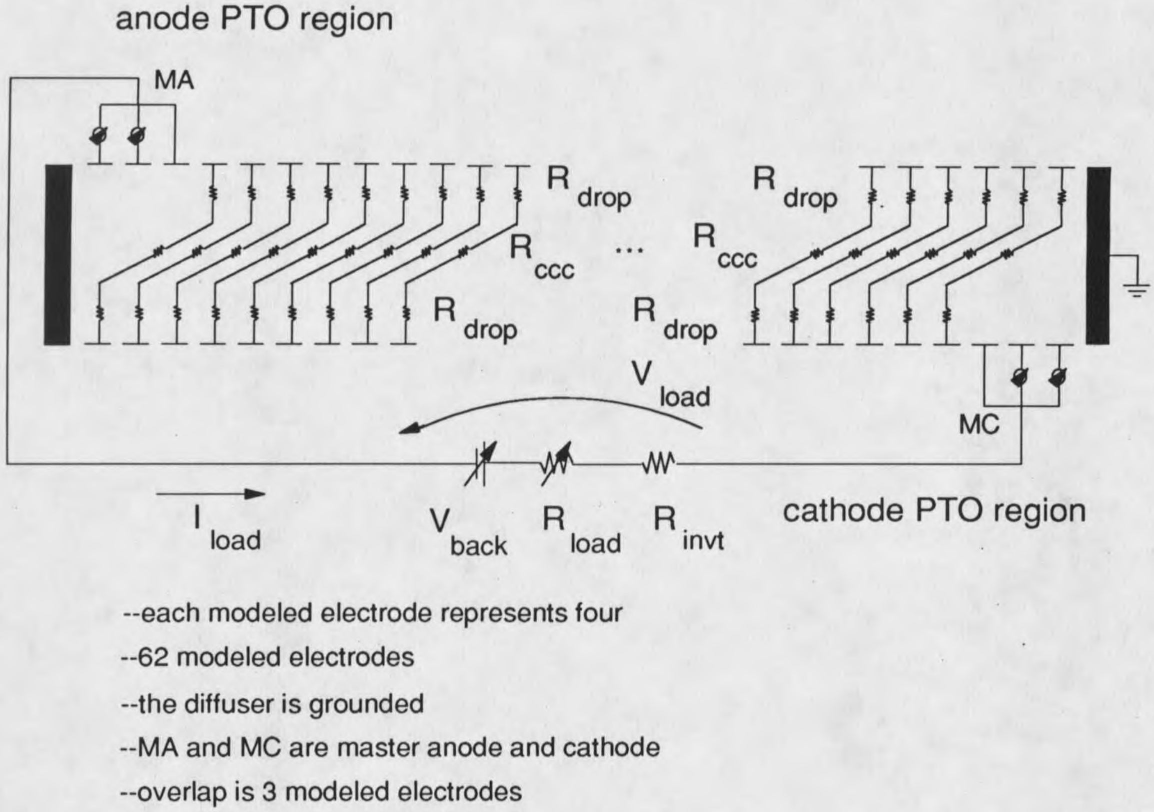

Figure 10: Diagonal Electrode Configuration Modeled by EXTCIRC Module

external circuits is not easily implemented. Also note that integration of equation 18 over a control volume simply yields a statement of charge conservation. The equivalent circuit method is, therefore, similar to an integrated form of the field solution.

The second alternative is the equation

$$(j_x - j_y \cot\theta)A = I_{load}. \tag{19}$$

This equation in concert with the relation

$$\cot\theta = -\frac{E_y}{E_x} \tag{20}$$

and the two Ohm's law equations 14 and 15 may be used to fully define the diagonal electrode configuration. This alternative has the advantage of allowing one-pass spatial marching solutions (*ie.* Runge-Kutta) to the steady-state equation set. It has disadvantages of requiring *a priori* knowledge of the load current, incorrectly calculating PTO regions, and averaging out effects of rapid axial changes within the channel. The method proposed for this thesis requires no prior knowledge of load current and properly relays information both up and down the channel via the diagonal angle.

Boundary Layer Voltage Drop Model

The theoretical voltage developed in an MHD channel must be reduced by a voltage drop near the electrode surfaces. This voltage drop is attributable to ohmic losses through the slag, the mechanics of charge transfer to the electrodes, and nonuniformities in the thermal and velocity boundary layers near the electrodes. The voltage drop model incorporated into this thesis computer model is of the integral approach type [37]. In this approach, one calculates bulk boundary layer properties like thermal loss and total voltage drop by integrating through the depth of the boundary layers and slag. Reasonable temperature and velocity profiles must be assumed.

Gupta and Rohatgi [38] proposed a voltage drop model having three parts in their 1982 paper. The model is specific to slagging MHD generators. The first part of the model consists of the ohmic drop through the slag. A linear temperature profile through the slag is assumed, and the slag depth is integrated between T_s at the slag-fluid interface and T_w at the duct wall. The simulations in this thesis assume a duct wall temperature of 1400 K and a slag wall temperature of 1750 K.

A second component to the voltage drop model is called an electrical sheath voltage drop. It is caused by the assumed diffuse charge transfer mechanism at electrode surfaces. The term generally contributes little to the the overall voltage drop. The assumption of diffuse charge transfer will be in error for high electrode current densities, for which the arc mode of charge transfer becomes important [63].

The last component of the voltage drop model comes from integration of electrical parameters through the nonuniform thermal boundary layers. A $\frac{1}{7}^{th}$ power law boundary profile for velocity and temperature is assumed. The sum of the three voltage drop components gives the total voltage drop at an electrode surface.

The majority of the total voltage drop is proportional to electrode current. Figure 11 shows that the total voltage drop may be modeled by resistors (ohmic components) and voltage sources (non-ohmic components). Module VDROPR calculates an equivalent resistivity for the ohmic components, and VDROPP calculates a voltage drop for the non-ohmic components of Gupta and Rohatgi's model. The resistive component is used in the definition of the external circuit in module EXTCIRC, and the other modifies the internal circuit in module SOLVELEC. The electrode voltages used in the computer simulations are not the true electrode voltages, but they are instead voltages located within the thermal boundary layer. This artificial location of electrode voltages stabilizes numerical solution of the electrical model for reasons to be described later in this chapter.

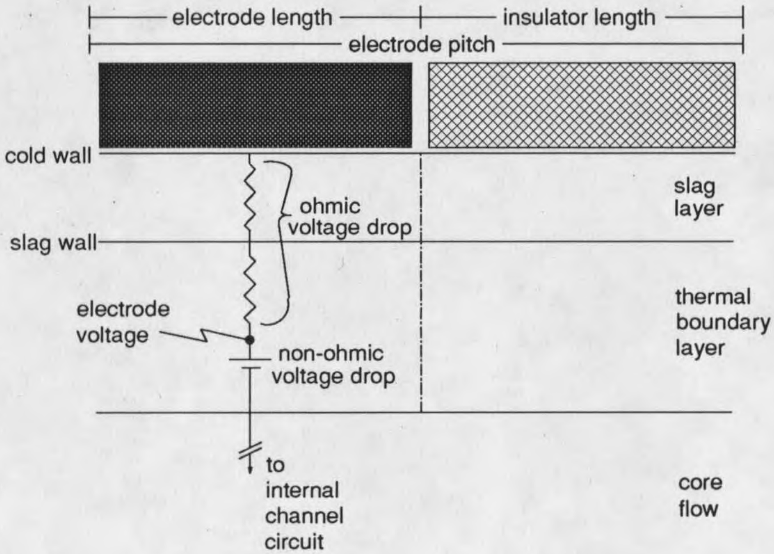

Figure 11: Voltage Drop Components Near the Electrode Surface

The resistivity calculated in VDROPR must be increased to reflect the fact that the electrode surface is less than the electrode duct wall surface. In other words, j_y is greater near the electrode surface than it is in the core flow. A factor of $\frac{A_w}{A_e}$ is used to reflect the fraction of electrode wall area to the lesser electrode surface area. This factor is assigned the value 1.4286 for all simulations in this thesis based upon descriptions of the $1A_4$ channel [39].

Numerical Scheme

An iterative solution to the internal and external electrical circuits is necessary for flexibility in modeling varied external electrode configurations. A non-iterative matrix solution would have to be reposed for every change in external electrode configuration. Simple relaxation of the internal and external circuits is utilized.

Suppose the system could be treated as a voltage source V_o in series with its internal impedance Z_s and a passive load Z_L as shown in Figure 12. First calculate a voltage across the load given initial current I_i.

$$V_i = V_o - I_i Z_s \tag{21}$$

Then use this voltage to calculate a revised current.

$$I_{i+1} = \frac{V_i}{Z_L} \tag{22}$$

A few iterations of this scheme very quickly show that convergence is guaranteed only if the load impedance is greater than that of the source. Providing this criterion is met, one may iteratively solve the series circuit by first treating the source as a constant voltage source and calculating current, followed by treating the load as a constant current source to recalculate the source voltage.

It is proposed that the criterion for successful relaxation of the electrical model internal and external parts is like that for this simple series source and load example.

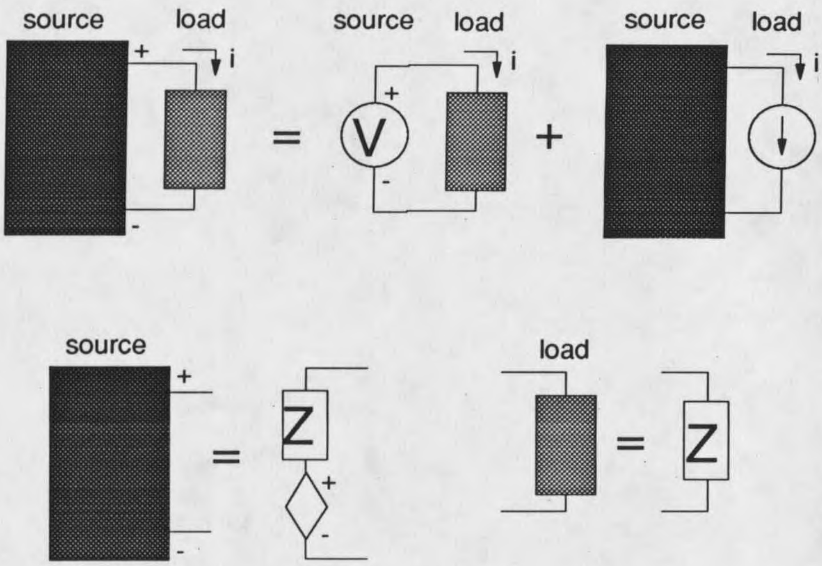

Figure 12: Simple Series Source and Load Analogy for Numerical Convergence

Relaxation will be successful only if the load impedance provided by the load R_{load}, inverters and consolidators R_{invt} or diagonal connection circuit R_{ccc} exceeds the internal channel resistance. The internal channel resistance is difficult to quantify exactly, but the above analogy proved useful in choosing iteration strategies which promote convergence. Two modifications were implemented in light of this simple analogy. First, the electrode current calculated in module EXTCIRC is underrelaxed.

$$I_{i+1} = (1 - \zeta)I_i + \zeta \frac{V_i}{Z_L} \tag{23}$$

An underrelaxation factor ζ conservatively less than $\frac{2Z_L}{Z_s+Z_L}$ in magnitude should guarantee convergence. Second, the location of the electrical model electrodes is moved inside the resistive portion of the voltage drop. This location of the electrode voltage increases the effective external circuit impedance and promotes numerical relaxation success. If needed, the true electrode potentials may be calculated from V_{DR}, the modeled electrode voltage and the electrode current.

CHAPTER 4

MHD DUCT FLOW MODEL

This chapter presents the numerical method used to solve the MHD flow problem in this thesis and discusses the reasons for which this numerical scheme was chosen.

Equation Set

The one-dimensional MHD equation set consists of three equations in conservation form. These three equations represent conservation of mass (continuity)

$$\frac{\partial \rho}{\partial t} + \frac{\partial \rho v_x}{\partial x} + \frac{\rho v_x}{A}\frac{\partial A}{\partial x} = 0, \tag{24}$$

momentum

$$\frac{\partial \rho v_x}{\partial t} + \frac{\partial \rho v_x^2}{\partial x} + \frac{\rho v_x^2}{A}\frac{\partial A}{\partial x} = -\frac{\partial P}{\partial x} - F + j_y B_z, \tag{25}$$

and energy

$$\frac{\partial \rho \mathcal{E}_\circ}{\partial t} + \frac{\partial \rho v_x H_\circ}{\partial x} + \frac{\rho v_x H_\circ}{A}\frac{\partial A}{\partial x} = -Q + j_x E_x + j_y E_y. \tag{26}$$

F and Q represent wall drag force per unit volume and thermal power loss to walls per unit volume, respectively. The terms with cross sectional area A account for duct divergence. Although this thesis addresses only steady-state solution of MHD flow, the above equation set is presented in time-dependent form. Many steady-state Euler equation solution methods march forward in time at the greatest stable time step until convergence occurs. Steady-state and transient solution methods do not differ greatly.

The Euler equation set is formally described as hyperbolic [40], meaning it has a set of real eigenvalues, v and $v \pm c$, where c is the local sonic velocity. Patankar [41] defines equation types which correspond to flow types: *Parabolic* flows are those for which the state at a location in the duct depends upon only upstream states. *Elliptic* flows are those for which the state at a location depends upon both the upstream and downstream states. *Hyperbolic* flows are a special case of elliptic flow for which the state at a duct location depends upon state information transported upstream or downstream along characteristic lines. Considerable numerical simplicity can be gained if flows can be treated as parabolic or elliptic rather than elliptic or hyperbolic. In this thesis, the one-dimensional MHD flow will be treated as elliptic since flow is parabolic in the supersonic channel and at least elliptic in subsonic portions of the nozzle and diffuser.

What does this categorization imply for boundary conditions? In the subsonic combustor, flow is elliptic. Two of the three eigenvalues are positive, and two of the three states must be defined as inlet boundary conditions. Flow accelerates through the nozzle to the choke point, where flow becomes supersonic and all three eigenvalues become positive. At the choke point of the nozzle, any two states may be used to calculate the third. At the shock location in the transition section, one eigenvalue again becomes negative, so one state at the diffuser exit must be specified.

In the model used here, input stagnation enthalpy, input flow rate and exit stagnation pressure are specified as boundary conditions. The input flow rate, $\rho v A$, is not a state, but it specifies one state in respect to another. The given choice of input boundary conditions allows combustor pressure to vary naturally with flow rate. Once the nozzle has choked, flow increases cause combustor pressure increases regardless of channel behavior. The exit pressure boundary condition corresponds to a controlled pressure at the diffuser exit. This exit pressure is often slightly above the ambient pressure, but it may be less than or equal to the ambient pressure if fans are used to lower pressures beyond the diffuser. See Messerle [42] for a discussion about the advantages and disadvantages of operating with a sub-atmospheric exit pressure.

Equations 24–26 suggest the choice of states ρ, v and $\mathcal{E}_\circ$, but there are numerous other options. The most freedom of state variable choice exists for the energy equation 26, for which $\mathcal{E}_\circ$, $H_\circ$ and $T_\circ$ are equally good choices. One's selection from these three options, however, is influenced by his confidence in the specific heats C_p and C_v which interrelate them. For high temperature combustion product flows like the one in this study, the calculation of specific heats may be one of the weakest parts of the simulation. Rigorous calculation of stagnation state from the static state requires an integration between the two state conditions. In practice, an "averaged" specific heat, a good representative specific heat for the transition range, is used to reduce computation.

In this case, stagnation internal energy $\mathcal{E}_\circ$ or stagnation enthalpy $H_\circ$ are better choices than either stagnation or static temperature. Of all the primitive variables, only stagnation enthalpy $H_\circ$ is fully C^0 continuous throughout the length of the transonic duct. Velocity v_x, pressure P and stagnation enthalpy $H_\circ$ were chosen as the states in this fluid flow model. The choice of velocity and pressure as states was advocated in Patankar's SIMPLER algorithm [41].

Methods which have successfully integrated the Euler equation set include Runge-Kutta [19, 18], MacCormack's, Godunov's and Casulli's schemes [43], Lax-Wendroff [25, 44], variational methods [45], and Patankar's parabolic flow methods [46, 35]. Finite differences, finite elements [45] and finite volume [46, 35] discretizations have all been utilized. Of these methods, Runge-Kutta methods and similar spatial marching methods are best suited to fully sub- or supersonic flows. The method should be halted at shock locations and restarted on the other side.

Spatial marching methods calculate a steady-state solution in one pass.

The MacCormack and Lax-Wendroff explicit methods may require artificial viscosity [40] to stabilize solutions near discontinuities. Even then, the methods are prone to overshoot and may exhibit ringing phenomena [40]. Both methods are limited by the Courant-Friedrichs-Lewy (CFL) condition [40], which assures that the domain of dependence of the discretized equation set is the same as the domain of dependence for the physical system. The specific form of the CFL stability condition depends upon the formulation. MacCormack's method [43], for example, has the CFL stability criterion

$$\Delta t \leq \frac{\Delta x}{(|v_i| + c_i)_{max}}, \tag{27}$$

where Δt is the maximum stable time step. CFL imposes a great restriction on solution time step size—on the order of tens of microseconds for moderate spatial discretization. The CFL condition restricts both transient and steady-state solutions equally when explicit methods are used. The Gudunov method is of the Riemann solver type. As such it nicely captures discontinuities like shocks, but the CFL condition must be met [43].

Patankar's SIMPLER [41] method was chosen for this study. SIMPLER is a finite volume method which staggers the location of nodes. Velocity nodes are located between the nodes at which other states are defined. The mass and momentum equations are coupled in such a way that each iterative solution for the pressure profile and the velocity profile adheres to mass conservation equation 24. It is a fully implicit method. Fully implicit methods are those methods which use no data from a previous time step in calculating the present state. The domain of influence in the time dimension loses its numerical significance, and a problem can be formulated to be stable without adhering to a CFL condition. Therefore, a steady-state solution can be obtained in few iterations. This point is important because the spline interpolations introduced in chapter 2 are numerically inefficient, and the number of computer iterations should be minimized. Van Leer flux splitting [47, 48], a monotonicity-preserving, non-centered difference discretization scheme, was used for the spatial derivative in the momentum equation. Flux splitting improves stability better than simple upwind differencing, and it more correctly reflects the parabolic and elliptic natures of flow in supersonic and subsonic duct regions.

Effects of Boundaries

The variables F and Q, the viscous wall drag force per unit volume and the thermal power loss to walls per unit volume, are calculated in module FG. The module FG was originally developed by Pierre, Dudding and Miller to model parametric effects on a 1976 Faraday channel design [19, 18]. Numerous modifications to the code occurred since that study, and it was once again modified for this thesis.

Fully developed turbulent flow is assumed. There are two important parts to this assumption. The first part to be addressed is *turbulent flow*, and the second part is the meaning of *fully developed.*

Turbulent flow rather than laminar flow occurs in flow with high Reynolds numbers [49]. MHD flows usually fall in this category [3, 7]. The Reynolds numbers for the supersonic MHD flows modeled in this thesis are approximately one million. This thesis model uses one of the many available empirical equations [50] to approximate drag force and heat transfer. These equations are based upon Reynolds number and a number of other common heat transfer coefficients. Some researchers have incorporated more complex, two parameter turbulent boundary models into their MHD flow models [35, 36], but good turbulent flow models add at least two more equation sets which must be simultaneously integrated.

As flow strikes an obstacle or flows past a wall, velocity and thermal boundary layers develop. The turbulent layer develops until it reaches some constant thickness at a downstream location. A starting length of 25 to 40 pipe diameters may be necessary before the fully developed turbulent boundary layer has formed [49]. Friction decreases, and thermal exchange to the wall increases as the flow is developing. It is difficult, however, to simply determine the degree of boundary layer development in a duct which has changing cross sectional area. Therefore, a fully developed turbulent flow model is used in this thesis, and moderate errors are accepted in the first half of the channel, where flow has most likely not yet fully developed.

MHD interactions have been claimed to affect boundary layer interaction. Satyamurthy [51] states that the effects of joule heating and Hall interaction near electrode surfaces are significant. The coefficient of friction may be increased in an MHD channel by 30% or more by MHD effects [3]. None of these effects were incorporated into this thesis model. Less than a 10% channel pressure drop may be attributed to friction in an MHD generator [3]. Therefore, MHD effects in the channel, if significant, will account for less than a 3% pressure drop over and above that calculated without the MHD effects.

The frictional drag force is characterized by a friction factor $f_{friction}$. The term F is calculated as

$$F = \frac{2 f_{friction} \rho v_x^2}{D}, \tag{28}$$

where the friction factor comes from an equation attributed to Knudsen and Katz in the Rohsenow and Hartnett *Handbook of Heat Transfer* [50]. D is the hydraulic diameter. A sand roughness e of 3 mm is assumed for this calculation.

$$f_{friction} = (1.74 \ln\left(\frac{D}{e}\right) + 2.28)^{-2} \tag{29}$$

The thermal wall loss term Q has both a radiation component Q_r and a convection component Q_c.

$$Q = \frac{4(Q_c + Q_r)}{D} \tag{30}$$

The radiation term is calculated from an equation on page 447 of Chapman [49]. Radiation flux is a function of the temperature across the thermal boundary layer, an assumed emissivity ($\varepsilon_w = 0.6$) for the duct walls, and a gas emissivity ε calculated from equilibrium combustion product properties (chapter 2). N_s is the Stefan-Boltzmann constant.

$$Q_r = N_s \frac{T^4 - T_w^4}{\left(\frac{1}{\varepsilon}\right) + \left(\frac{1}{\varepsilon_w}\right) - 1} \tag{31}$$

The convection term is calculated from an equation attributed to Sieder and Tate on page 341 of Chapman [49]. In this equation, the values of N are the dimensionless Reynolds and Prandtl fluid parameters, the ν are viscosities for the core and wall flows, and κ is the thermal conductivity of the fluid.

$$Q_c = 0.027 N_{Re}^{0.80} N_{Pr}^{0.33} \left(\frac{\nu_c}{\nu_W}\right)^{0.14} \left(\frac{\kappa}{D}\right) (T_{\circ W} - T_s) \tag{32}$$

The convection term is seen to be a largely empirical function proportional to the difference between the adiabatic wall temperature $T_{\circ W}$ and the temperature of the slag wall T_s.

Numerical Solution

Patankar's Semi-Implicit Method for Pressure-Linked Equations, Revised (SIMPLER) [41] was originally formulated for solution of the transverse axis elliptic flows in three-dimensional parabolic flows. Patankar and Spalding point out that the algorithm is not necessary for one- and two-dimensional parabolic flow [52]. The method's capability to stably solve elliptic flow in one dimension was recognized and utilized in this thesis. The scheme described in the next paragraphs is implemented in module SIMPLER, which can be found in the appendix.

First, Patankar points out that all differential flow and diffusion equations are of the general equation type

$$\frac{\partial \rho \phi}{\partial t} + \nabla \cdot \rho v \phi = \nabla \cdot \Gamma \nabla \phi + \mathcal{S} \tag{33}$$

for dependent variable ϕ, diffusion coefficient Γ and source function $\mathcal{S}$. Viscosity and thermal conductivity are two examples of possible diffusion coefficients.

In open cycle MHD combustion flows, one should expect the effect of the diffusion terms in the axial direction to be much smaller than the effect of convection terms. This statement cannot be made for two-dimensional flow problems, for which the transverse gradient of the dependent variable near walls is significant. In the two-dimensional case, stress tensors replace the viscous drag term F in equation 25. The general equation may be written in one-dimensional form without time dependence or diffusion terms.

$$\frac{\partial \rho v_x \phi_x}{\partial x} + \frac{\rho v_x \phi_x}{A}\frac{\partial A}{\partial x} = \mathcal{S}_x \tag{34}$$

Note that the effect of duct divergence must be shown in equation 34. From this point on, the term representing duct divergence will be included in the source term $\mathcal{S}_x$. Patankar suggests some strategies to improve convergence. First, if possible, source terms should be linearized in the dependent variable in such a way that the variable's coefficient is negative. This strategy was used on the viscous drag term F and the area dependence term in the momentum equation. These two terms have squared dependence on velocity.

$$\mathcal{S}_x = \mathcal{S}_x|_{\phi_x^\star} + \left.\frac{\partial \mathcal{S}_x}{\partial \phi_x}\right|_{\phi_x^\star} (\phi_x - \phi_x^\star) \tag{35}$$

The starred dependent variable is the value of the dependent variable from the previous iteration. The linearized term coefficient becomes part of the dependent variable coefficient. For variables like pressure and temperature, which must remain positive

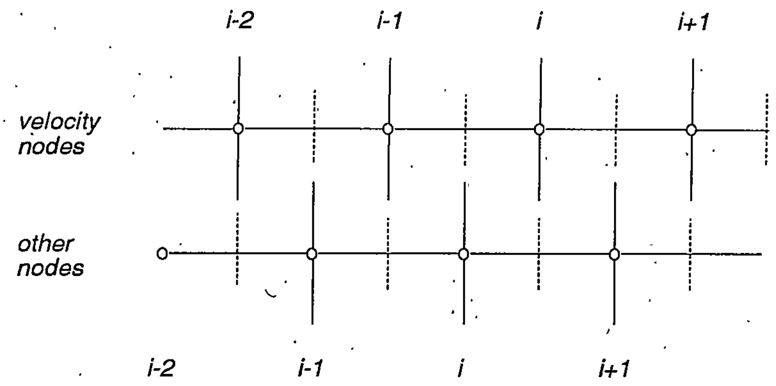

Figure 13: Staggered Node Spacing

at all times and for all iterations, the negative components of the source terms may be used to stabilize the solution. This is true even if the dependencies of the source term are not obvious. For example, many source terms $\mathcal{S}_x$ can be separated into positive and negative parts $\mathcal{S}_x^+$ and $\mathcal{S}_x^-$. A stabilizing dependence upon the dependent variable ϕ_x can then be introduced into the formulation as

$$\mathcal{S}_x = \mathcal{S}_x^+ - \frac{\mathcal{S}_x^-}{\phi_x^*}\phi_x. \tag{36}$$

Discretization is performed as suggested in Figure 13. Note that the velocity nodes are half way between those major nodes at which all other variables are defined. The staggering of the grid dampens the spatial oscillations which often occur in calculations of pressure and velocity, which appear in the conservation equations only in differentiated form. Velocity node enumeration precedes other variable node enumeration in space by one half of the cell length Δx.

The simplified and discretized version of equation 34 is

$$\mathcal{F}(\phi_{i-1}, \phi_i, \phi_{i+1}) = \mathcal{S}_x, \tag{37}$$

where $\mathcal{F}$ is a suitable monotone difference operator. A difference operator is monotone if the partial differential of the dependent variable in respect to the neighbor variables within the discretization method's domain of dependence is positive [40]. Simple upwind differencing and Van Leer flux splitting are the two monotone difference operators used in this thesis. Van Leer flux splitting [48] appropriates flux coefficients in a way which correctly reflects the relay of information up or down the duct. State information is transferred both up and down the duct for subsonic flow and only downstream for supersonic flow.

Let the upwind differencing scheme be demonstrated. The centered difference representation of a flux term is modified in the next equation by replacing averaged node values of the dependent variable by those displaced one-half node upstream.

$$\begin{aligned}\frac{\partial \rho v_x \phi}{\partial x} &\cong \frac{1}{\Delta x}\left[\left.\frac{\rho v_x}{2}\right|_{i+\frac{1}{2}}(\phi_{i+1}+\phi_i) - \left.\frac{\rho v_x}{2}\right|_{i-\frac{1}{2}}(\phi_i+\phi_{i-1})\right] \\ &\equiv \frac{1}{\Delta x}\left[\left.\rho v_x\right|_{i+\frac{1}{2}}\phi_i - \left.\rho v_x\right|_{i-\frac{1}{2}}\phi_{i-1}\right] \qquad (38)\end{aligned}$$

The flux splitting operator is given by

$$\mathcal{F} = \frac{1}{\Delta x}\left[\mathcal{F}^+(\mathcal{Q}^-)_{i+\frac{1}{2}} - \mathcal{F}^+(\mathcal{Q}^-)_{i-\frac{1}{2}} + \mathcal{F}^-(\mathcal{Q}^+)_{i+\frac{1}{2}} - \mathcal{F}^-(\mathcal{Q}^+)_{i-\frac{1}{2}}\right]. \qquad (39)$$

The notations $\mathcal{F}^+$ and $\mathcal{F}^-$ stand for downstream and upstream advection operators, respectively. The notations $\mathcal{Q}^-$ and $\mathcal{Q}^+$ stand for flux variable evaluations approximated from the upstream and downstream sides, respectively. The particular interpolation using evaluations $\mathcal{Q}$ as shown above is called the monotone upstream-centered scheme for conservation laws (MUSCL) [48] and is usually performed with second order accuracy. In this thesis, first order accuracy will be used so that the resulting banded matrices have only three diagonals. Therefore, $\mathcal{Q}^{\pm}$ refer simply to flux evaluations at the nearest major node locations upstream or downstream.

Liou and Steffen [47] present a particularly readable formulation of flux splitting in primitive variables. In their paper, it is explained that the state at any node is *advected* by the fluid velocity at that node $v = Mc$, where c is the local sonic velocity, and M is the Mach number. With this understanding, the Van Leer flux splitting operator is shown here for the momentum flux.

$$\mathcal{F}_i^{\pm} \equiv \begin{cases} \pm\frac{1}{4}(M_i \pm 1)^2 c\rho v_x, & |M_i| \leq 1 \\ \frac{1}{2}(M_i \pm |M_i|)c\rho v_x, & |M_i| \geq 1 \end{cases} \tag{40}$$

Now the steps of the SIMPLER algorithm can be examined. Equations 24–26 are rewritten here in the steady-state form used as the starting place for the SIMPLER formulation.

$$\frac{\partial \rho v_x}{\partial x} = -\frac{\rho v_x}{A}\frac{\partial A}{\partial x} \tag{41}$$

$$\frac{\partial \rho v_x^2}{\partial x} = -\frac{\rho v_x^2}{A}\frac{\partial A}{\partial x} - \frac{\partial P}{\partial x} - F + j_y B_z \tag{42}$$

$$\rho v_x \frac{\partial \left(\mathcal{E}_\circ + \frac{P}{\rho}\right)}{\partial x} = -Q + j_x E_x + j_y E_y \tag{43}$$

Note that the chosen form of the energy conservation equation assumes continuity. This assumption simplifies the equation and speeds convergence.

The discretized and integrated form of the momentum equation can be arranged to give

$$a_i v_i = a_{i-1} v_{i-1} + a_{i+1} v_{i+1} - (P_{i+1} - P_i) + \mathcal{S}_x \Delta x, \tag{44}$$

where a_i is the coefficient for the dependent variable at node i.

Define $\hat{v}$ using equation 44 such that

$$v_i = \hat{v}_i - \frac{1}{a_i}(P_{i+1} - P_i). \tag{45}$$

The variable $\hat{v}$ may be thought of as a velocity calculated without the effect of pressure gradient. This new "velocity" $\hat{v}$ will be used in the integrated continuity equation,

$$\rho v_x A|_{i+\frac{1}{2}} - \rho v_x A|_{i-\frac{1}{2}} = 0, \tag{46}$$

to calculate pressure.

By substitution of equation 45 into equation 46, Patankar's pressure equation can be derived.

$$\rho_{i+\frac{1}{2}}(\hat{v}_i - (P_{i+1} - P_i))A_{i+\frac{1}{2}} - \rho_{i-\frac{1}{2}}(\hat{v}_{i-1} - (P_i - P_{i-1}))A_{i-\frac{1}{2}} = 0 \tag{47}$$

Note that both the pressure equation 47 and a later pressure correction equation use a suggestion from Patankar's *Numerical Heat Transfer and Fluid Flow* [41] practice problem 6.6. This important modification corrects for fluid compressibility by replacing ρ with $\rho^\star + \rho'$, where $\rho^\star$ is the best estimate of density from the last iteration, and ρ' is the density correction due to the present calculation. Not all the details of this fluid compressibility correction will be shown in this text. One may refer to Module SIMPLER for details. The pressure equation 47 is rearranged to the form

$$a_i P_i = a_{i-1} P_{i-1} + a_{i+1} P_{i+1}, \tag{48}$$

which can be efficiently solved using the tridiagonal matrix algorithm (TDMA) [53]. See module TRIDIAG.

This updated pressure is used in the momentum equation to define an improved velocity $v^\star$, which better conserves momentum.

$$a_i v_i^\star = a_{i-1} v_{i-1}^\star + a_{i+1} v_{i+1}^\star - (P_{i+1} - P_i) + \mathcal{S}_x \Delta x \tag{49}$$

This equation is again efficiently solved by the TDMA.

The improved velocity $v^\star$ is once more inserted into the continuity equation,

$$\rho_{i+\frac{1}{2}}(v_i^\star - (P'_{i+1} - P'_i))A_{i+\frac{1}{2}} - \rho_{i-\frac{1}{2}}(v_{i-1}^\star - (P'_i - P'_{i-1}))A_{i-\frac{1}{2}} = 0, \tag{50}$$

where P' represents a pressure correction needed to conserve mass with the choice of velocity $v^\star$.

Equation 50 is then rearranged into tridiagonal form to be solved for pressure correction P' by the TDMA.

$$a_i P'_i = a_{i-1} P'_{i-1} + a_{i+1} P'_{i+1} + \rho v_x^\star A|_{i-\frac{1}{2}} - \rho v_x^\star A|_{i+\frac{1}{2}} \tag{51}$$

Finally, the velocity can be updated.

$$v_i = v_i^\star - \frac{1}{a_i}(P'_{i+1} - P'_i) \tag{52}$$

At this point, both the pressure and velocity profiles have been corrected in such a way that mass conservation is assured. Before the next SIMPLER iteration, the energy equation must be solved for the stagnation enthalpy profile, all fluid side equations must be solved, and the electrical state must be corrected.

Normally the complete SIMPLER algorithm would be considered computationally expensive for solution of a one-dimensional flow problem. However, the algorithm has a remarkable ability to stabilize and solve the Euler equation set in relatively few iterations. The magnitudes of the flow rate errors

$$\left| \rho v_x^\star A|_{i-\frac{1}{2}} - \rho v_x^\star A|_{i+\frac{1}{2}} \right| \tag{53}$$

from equation 51 can be summed along the duct length to monitor convergence progress. From 10 to 50 iterations were necessary to reduce the summed magnitudes of convergence criterion to about 2 in this thesis model, depending on the accuracy of the initial conditions.

CHAPTER 5

THE NOMINAL POC GENERATOR

The POC Generator

The 50 MW_{th} $1A_4$ supersonic, coal-fired MHD generator was the most recent in a series of MHD generators tested for the Department of Energy (DOE) by MSE, Inc. in Butte, Montana. MHD generator tests at this facility began in 1980. The purpose of the research was to prove the viability of sustained, large scale, coal-fired MHD generation. MHD generator research at the Butte facility was discontinued in 1993.

The $1A_4$ channel will be referred to throughout this thesis as the proof of concept (POC) channel. MSE collected much data during operation of the POC channel, and that data is compared in this thesis to results from the thesis computer model. Results are reported in the next two chapters. The present chapter compares the modeled nominal operation predicted for the POC with existing data. The next chapter evaluates behavior of the modeled channel through a series of parametric studies.

Table 3 summarizes important nominal operating parameters and compares them to MSE data. The test conditions referred to in the table are MSE condition data summaries from April 1, 1993 (test #2) and September 28, 1993 (test #7). Any discrepancies from Table 3 will be discussed. Where appropriate, the table refers the reader to relevant figures and citations.

parameter	model	MSE data	references	figure
maximum β	2.31			23
maximum B (tesla)	2.50	2.50,2.93	tests #7,2	15
electric power (MW)	1.37	0.926,1.21	tests #7,2	
seed fraction (%)	1.70	1.68,1.74	tests #7,2	
inlet σ (℧/m)	8.2	7.0–9.0	[54]	22
maximum j_y (a/cm^2)	-1.01			20
diagonal angle (°)	54.1	53.8		
load voltage (kV)	6.21	4.98,5.55	tests #7,2	19
load current (a)	230	186,218	tests #7,2	19
load resistance (Ω)	26.0	26.8,25.5	tests #7,2	
thermal input (MW)	43.8	50.1,51.0	tests #7,2	
combustor P_o (kPa)	603	566,598	tests #7,2	17
coal flow rate (kg/s)	1.85	1.85,1.90	tests #7,2	
combustor loss (MW)	3.94	4.09,3.41	tests #7,2	
nozzle loss (MW)	0.668	0.541,0.510	tests #7,2	
channel loss (MW)	3.42	4.93,4.61	tests #7,2	
diffuser loss (MW)	1.54	2.57,2.41	tests #7,2	
mass flow (kg/s)	8.81	8.05,8.51	tests #7,2	
preheat T (K)	910	915,901	tests #7,2	
slag rejection (%)	70	67	[54]	
combustor T_o (K)	2840			
oxygen enrichment	0.425	0.438,0.405	tests #7,2	
stoichiometric ratio	0.90,0.98	0.95,0.94	tests #7,2	
enthalpy extraction (%)	3.65			

Table 3: Comparison of Important Nominal Operation Parameters

The definition of stoichiometric ratio used in this thesis differs from that used in the MSE data. Stoichiometric ratio is the molar ratio of molecular oxygen and carbon reactants in the reaction mixture entering the channel. Combustion tables (chapter 2) used for calculation of combustor stagnation state and duct equilibrium states in this thesis assume that only the oxygen within the enriched air mixture affects the stoichiometric ratio [55]. The MSE stoichiometric ratio calculation includes both the oxygen in the enriched air mixture and any oxidizing agents present in the coal [56]. The second stoichiometric ratio in the "model" column was corrected for an assumed 14% oxygen content [18] by mass in the coal. This modified stoichiometric ratio is comparable to the POC data and is shown to be 3% higher than MSE nominal conditions. The discrepancy will also affect the total flow rate.

It is not as easy to compare the oxygen enrichment numbers, which suffer from the same type of discrepancy.

Total thermal power calculations also differ for the model and MSE data. Thermal power is the product of specific stagnation enthalpy and mass flow rate. The equilibrium and combustor combustion tables (chapter 2) use actual combustion gas composition to calculate the stagnation enthalpy. The MSE thermal power data is found by summing heats of combustion for all combustible component quantities whether they have reacted or not. Both methods of calculation are defensible.

The POC channel is a relatively small channel as shown in Figure 14. The duct section boundaries have been located on the figure. The short combustor section eliminates the effects of channel area variations at the inlet boundary. No thermal losses or frictional losses are modeled in the short combustor section. Some liberties were taken in the subsonic portion of the nozzle. In this region, channel area converges very rapidly. The quasi-one-dimensional numerical model is not valid for very rapid cross sectional area changes, so the inlet area in the subsonic nozzle and combustor exit are modeled with smaller than correct dimensions.

The POC channel is a low interaction channel. It was built as a research generator and was never intended to generate surplus power. Figure 15 shows the assumed magnetic induction profile for the POC generator. Fringing, the gradual decrease in induction at the ends of the magnet, is accurately modeled at the extremes

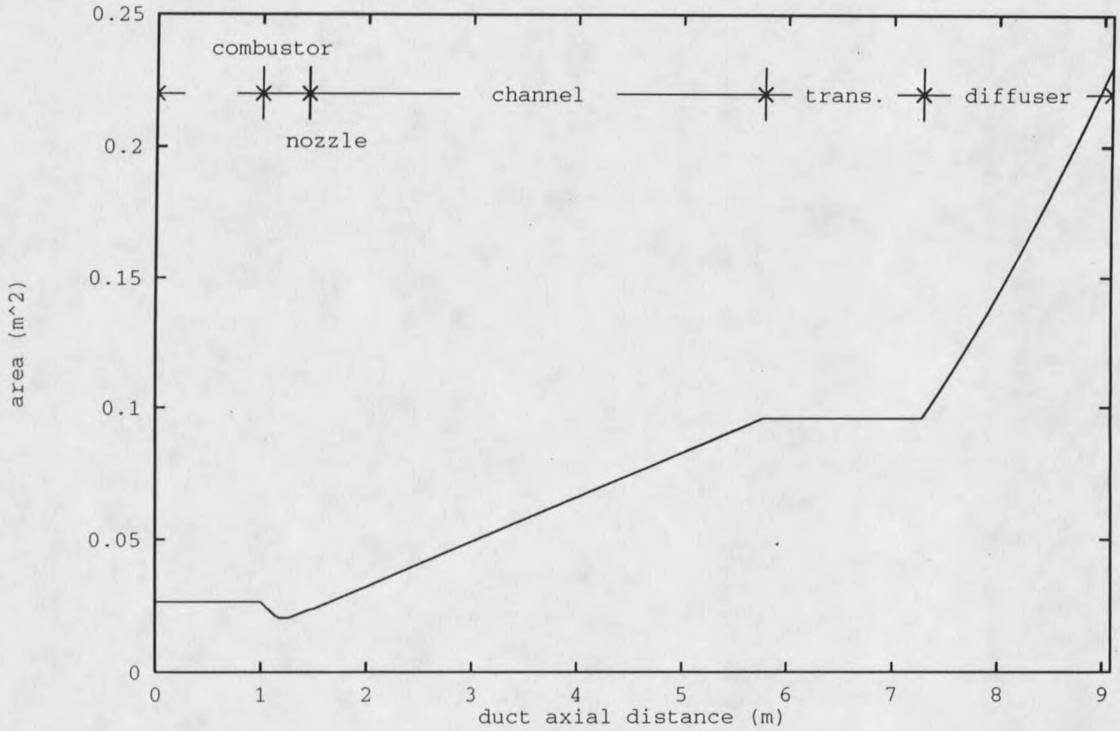

Figure 14: POC Channel Cross Sectional Area Profile

of the generator. Because of fringing effects, there will be some MHD interaction in the nozzle and beginning of the transition section [57, 58]. The POC nozzle and transition section were designed to mitigate the effects of the fringing, but these effects are not included in the computer electrical or fluid models. See Martinez-Tamayo, Hruby and Pote [32] for a description of an MHD electrical model which incorporates these fringing effects.

Fluid Property Nominal Profiles

This section displays the fluid state profiles which result from steady-state simulation of the POC channel at nominal conditions. The profiles for velocity, pressures and temperatures were chosen since these three profiles sufficiently describe the fluid state.

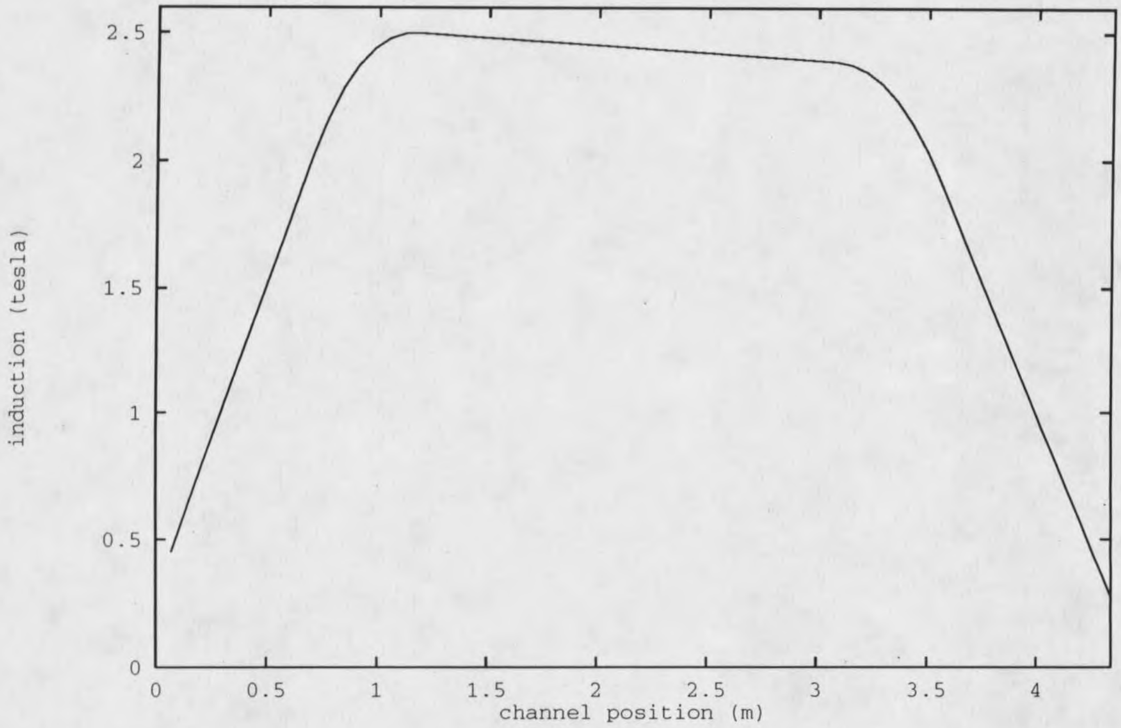

Figure 15: Modeled POC Channel Induction Profile

Figure 16 shows the steady-state velocity profile for the modeled POC MHD duct. Velocity remains constant in the short combustor starting section, where no area variation occurs and where no thermal or frictional losses are modeled. Flow then accelerates and becomes supersonic through the nozzle. The deceleration caused by electrical power extraction and friction through the channel is roughly equal to the acceleration caused by the channel divergence. The net effect is a slowly decelerating flow through the channel. Flow more rapidly decelerates in the transition section. However, this model suggests that the flow either fails to become subsonic or becomes supersonic again toward the end of the transition section. The supersonic flow accelerates quickly through the diverging diffuser, and a strong shock occurs within the diffuser. This questionable Mach behavior may result from the particular equilibrium state description, insufficient thermal or frictional extraction in the diffuser or channel, a numerical method weakness, or a combination of any of these possible reasons. Regardless, modeling the elliptic nature of flow through the diffuser is very difficult, and very few examples of duct behavior in these regions are found in literature. Instead, the diffuser is often addressed with bulk behavior parameters like recovery factors and diffuser efficiencies [7, 59].

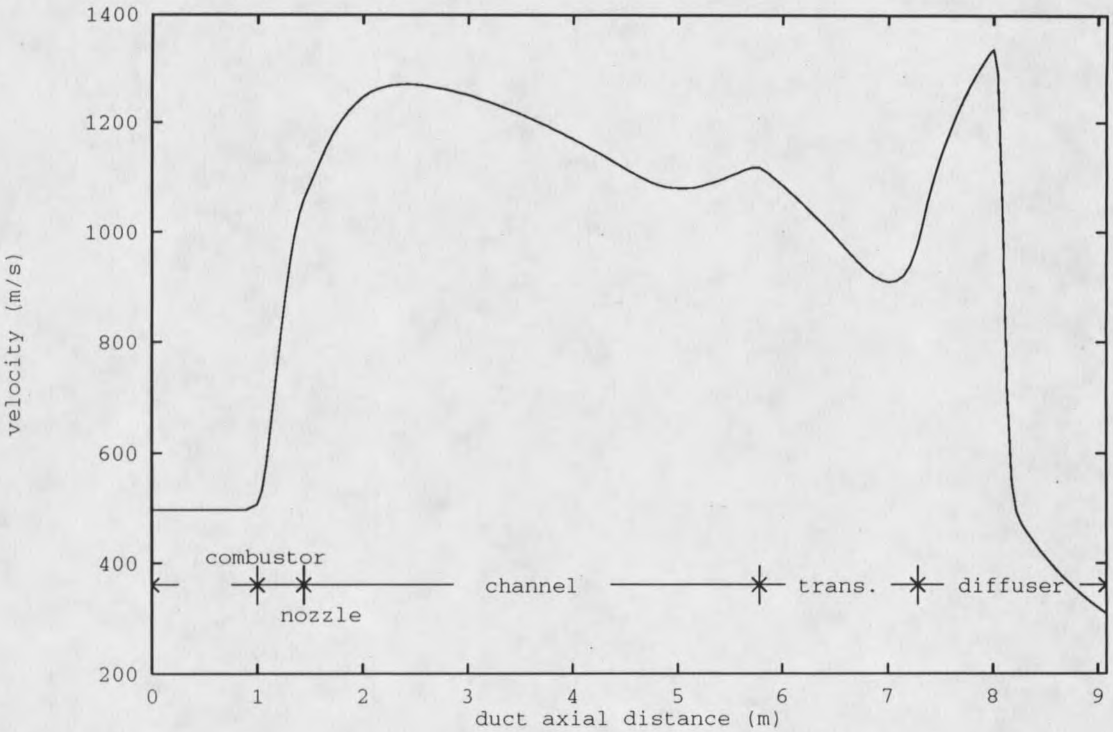

Figure 16: Modeled POC Duct Velocity Profile

Figure 17 shows the corresponding pressure profiles. The upper profile is the stagnation pressure, and the lower is the static pressure. Stagnation pressure should at no time increase down the duct length. Friction, MHD interactions and shock discontinuities can bring about decreases in stagnation pressure. Any increase in stagnation pressure represents a violation of entropy [60, 61]. The minor violations occur at the strong shock and in the nozzle where rapid area variation is occurring and are probably artifacts of the numerical simulation. The points in the channel section of Figure 17 are measured MSE data points taken during a test with similar operating conditions on April 1, 1993. The data lends credibility to the thesis fluid model.

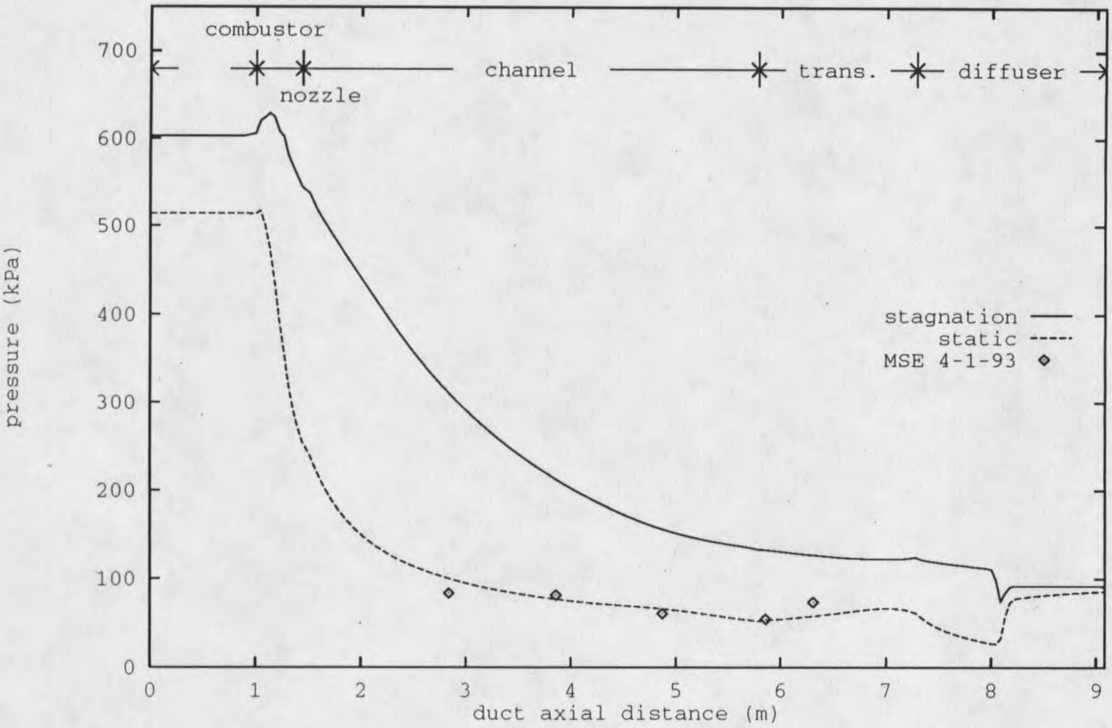

Figure 17: POC Duct Stagnation and Static Pressure Profiles

Some discussion is now offered to assess the gravity and cause of the peculiar Mach profile through the diffusers. It will be helpful to refer to Figure 17 during this discussion. We start by comparing the thesis flow solution method to a conceptually easier flow solution method. Pian [59] presents a well written tutorial on solving MHD flows using shooting techniques. MHD flows are recognized as mixed boundary value problems. Pian points out that MHD design problems are easily solved by specifying input boundary conditions, integrating to the end of the channel, and iterating this procedure as necessary until desired exit boundary conditions are met. Off-nominal operation problems like those studied here are often sensitive and diverge to meaningless, incorrect solutions. Indeed, this recognized shortcoming is among the reasons a discretized model was chosen for the numerous thesis parametric studies. The channel exit boundary condition is most often a channel exit pressure. The pressure is chosen to reflect a predicted stagnation pressure ratio for the diffuser and pressure losses in other downstream components. In the solution of a fully subsonic flow, the solution is obtained by shooting until the exit pressure is matched. For supersonic flow, the choked nozzle fully defines the supersonic channel flow given either known flow rate or combustor pressure. The only constraint is that the channel exit stagnation pressure be at least as great as some minimum exit stagnation pressure. Any stagnation pressure mismatch must be solved through a downstream shock, but the location of the shock may or may not be addressed in a shooting problem solution. If a shocked solution is sought, the researcher must choose the shock location so that the exit pressure is matched. All these solutions are unique, but they are very time intensive.

All the discussion about shock behavior and boundaries for sub-, super- and transonic operating conditions hold for any solution technique. However, shock capturing techniques like that used in the thesis computer model rely on the model to locate shocks and match boundary conditions. Figure 17 shows that there is a mismatch between the stagnation pressure at the channel exit and the quantity of stagnation pressure which can be dumped to friction in the diffusers. Therefore, a shock must occur. While the place at which the model located the shock is questionable, the manner in which the model solved the pressure mismatch is reasonable, and the stagnation pressure mismatch itself is not large. The effect is exaggerated by the expanding diffuser section, which acts like a supersonic nozzle. The flow within the channel—especially supersonic flow—should not be adversely affected by possible shock mislocation in the diffuser.

Figure 18 shows the steady-state stagnation and static temperatures throughout the length of the duct. The separation between the temperatures corresponds to the velocity. As velocity increases, more of the system's energy is transferred to kinetic energy, and the temperature decreases. This figure points out clearly why questionable Mach behavior in the diffuser makes one suspicious of bulk parameters obtained for that section. The supersonic behavior in the diffuser greatly depresses the fluid temperatures. Consequently, one should expect less thermal loss to the wall in the diffuser than would occur with subsonic behavior. Stagnation properties are not so strongly affected.

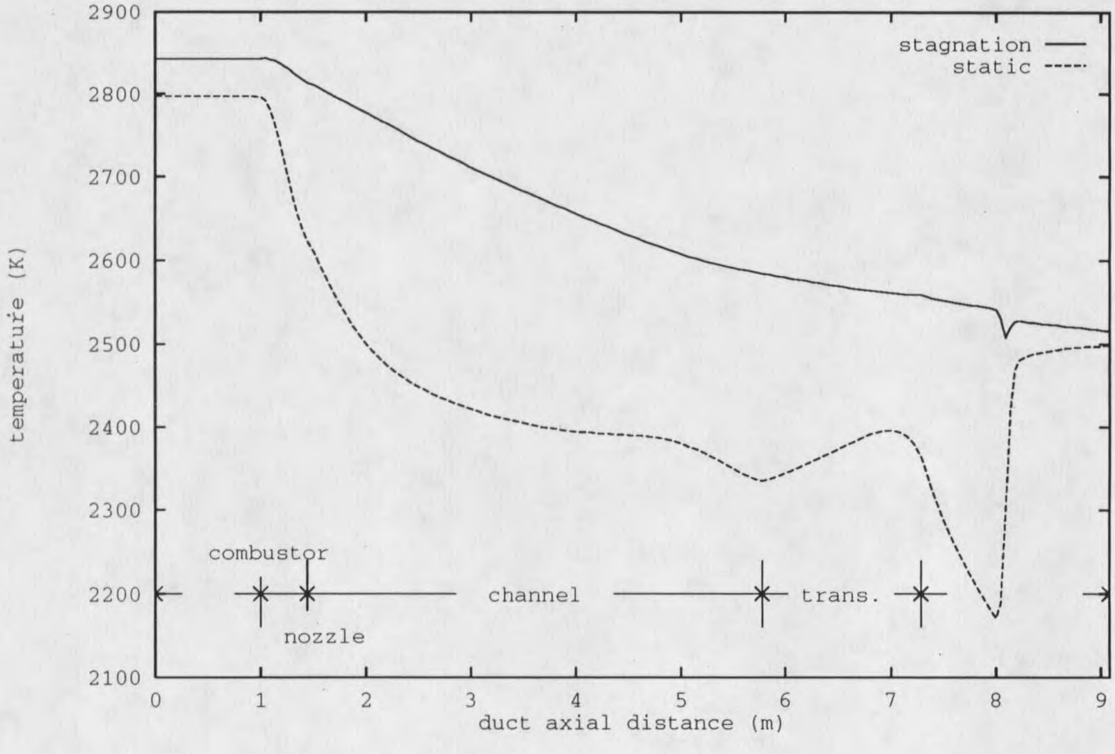

Figure 18: Modeled POC Duct Stagnation and Static Temperature Profiles

As a result of the questionable Mach behavior in the transition section and diffuser, simulation results potentially affected by Mach behavior in these sections must be reported with diminished confidence. As stated in the discussion above, the results obtained for the combustor, nozzle and channel sections should not be greatly affected by the downstream Mach behaviors.

Electrical Property Nominal Profiles

The profiles in this section refer to the modeled nominal behaviors in the electrical channel. Only the channel length will be shown, but the reader should remember the location of the channel section within the MHD duct.

The first profile, Figure 19, demonstrates predicted electrode potentials. The diffuser of the POC is grounded at reference potential zero, and the nozzle potential is allowed to float at a potential approximately equal to the load voltage. The nozzle voltage is negative in respect to ground. The upper curve shows the cathode electrode voltages, and the lower shows anode electrode voltages. The vertical separation of the two curves is the Faraday voltage generated at a channel position. The horizontal separation of the two curves reflects the effect of electrode overlap and should be roughly constant for a constant diagonal overlap channel. A cathode has nearly the same voltage as an anode displaced by the electrode overlap distance, 0.21 meter. The second set of curves on Figure 19 represent MSE data from test #7 on September 28, 1993. While the shapes of the electrode voltage curves are similar, one can see that the thesis model overestimates the total load voltage by about 25%.

There will be minor discrepancies between the Figure 19 profiles and the electrode potentials because the model locates electrodes within the boundary layer voltage drop (chapter 3). The total voltage drop (not shown) was found to be 160 volts near the middle of the channel, 50 volts in the anode PTO region, and 15 volts in

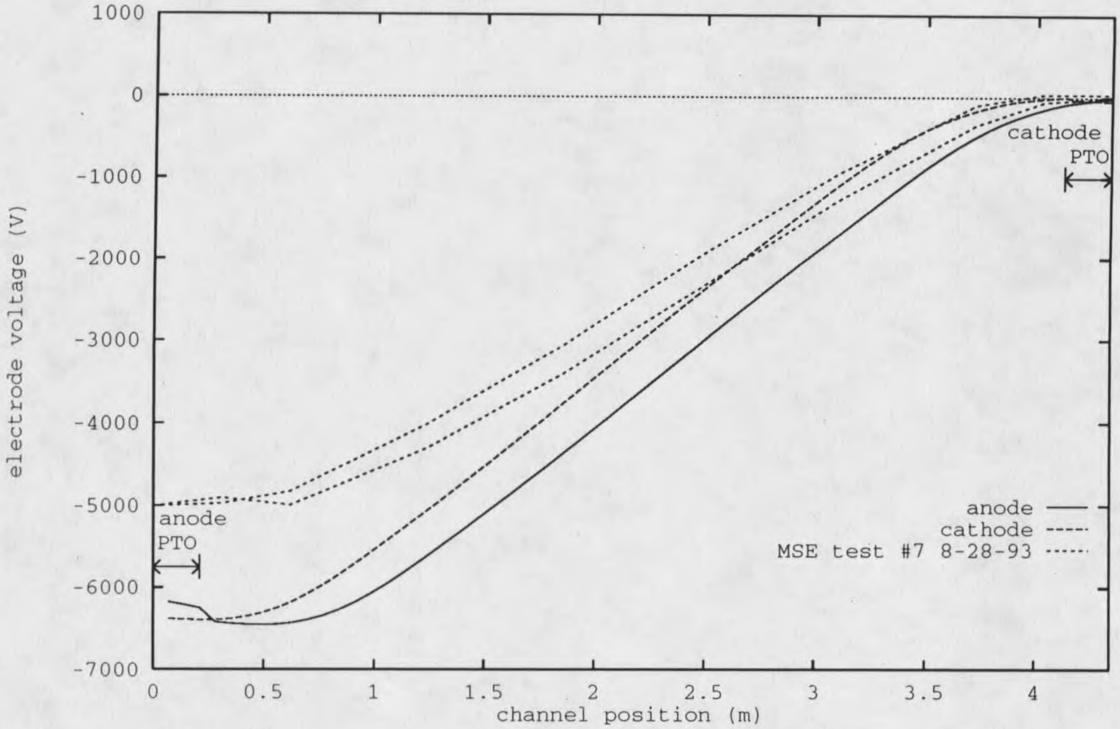

Figure 19: POC Channel Electrode Voltage Profiles

the cathode PTO region. Another small voltage drop occurs in the diagonal connection due to the small resistance ($R_{ccc} = 0.05\Omega$) which models losses in the diagonal connection circuits.

None of these minor discrepancies account for the fact that the electrical model predicts a load voltage which is approximately 25 % too great in magnitude. This error suggests improved electrical modeling may be needed in the areas of leakage currents or nonuniformity effects. Perhaps finer transverse discretization of the electrical model is needed.

The axial and transverse current density profiles are shown in Figure 20. The axial current density is calculated by dividing the axial equivalent circuit current I_x by the local cross sectional area. The transverse current density is calculated by dividing the average electrode currents from the equivalent circuit model by the product of channel width and discretized axial length Δx.

Axial currents in a diagonal generator may be either positive or negative. The transverse currents must be negative. Figure 20 shows that the greatest transverse channel currents occur in the upstream half of the generator. Transverse current densities of greatest magnitude occurred in the anode PTO region for the model. However, there are fewer electrodes in the model anode PTO region than in the actual anode PTO. Therefore, the greatest transverse current densities are likely to occur at about 1.25 meters into the channel. As the current density magnitude exceeds one ampere per square centimeter, the mode of charge transport at electrode surfaces becomes arc mode. The arc mode itself may not be detrimental, but high transverse current density is one warning sign of detrimental interelectrode arcing [62]. Electrode stresses will be great at the channel location having great transverse current density. Transverse current density data from MSE test #7 is included in the figure, and a large discrepancy may be seen. Factors which contribute to the discrepancy include voltage drop magnitudes, current control circuitry, discrepancies between theoretical and measured conductivities and possibly the currents carried in the Z-bar sidewalls.

Both the axial and transverse electrical field profiles in Figure 21 are flat through the high interaction portion of the channel. The profiles approach zero, as expected, near the channel extremes where less MHD interaction occurs. A profile reversal occurs in the anode region, where ohmic effects are greater than MHD effects. Again, this effect is slightly exaggerated because the model used fewer PTO electrodes than the POC generator. The fact that the axial electrical field has a flat profile means that electrical stresses across the insulators separating adjacent electrodes are well distributed in the steady state. Current control circuits are assumed to control any transient cathode shorting and prevent the transfer of any shorts to the anode electrode wall, where interelectrode arcing is more harmful. The effect of excessive

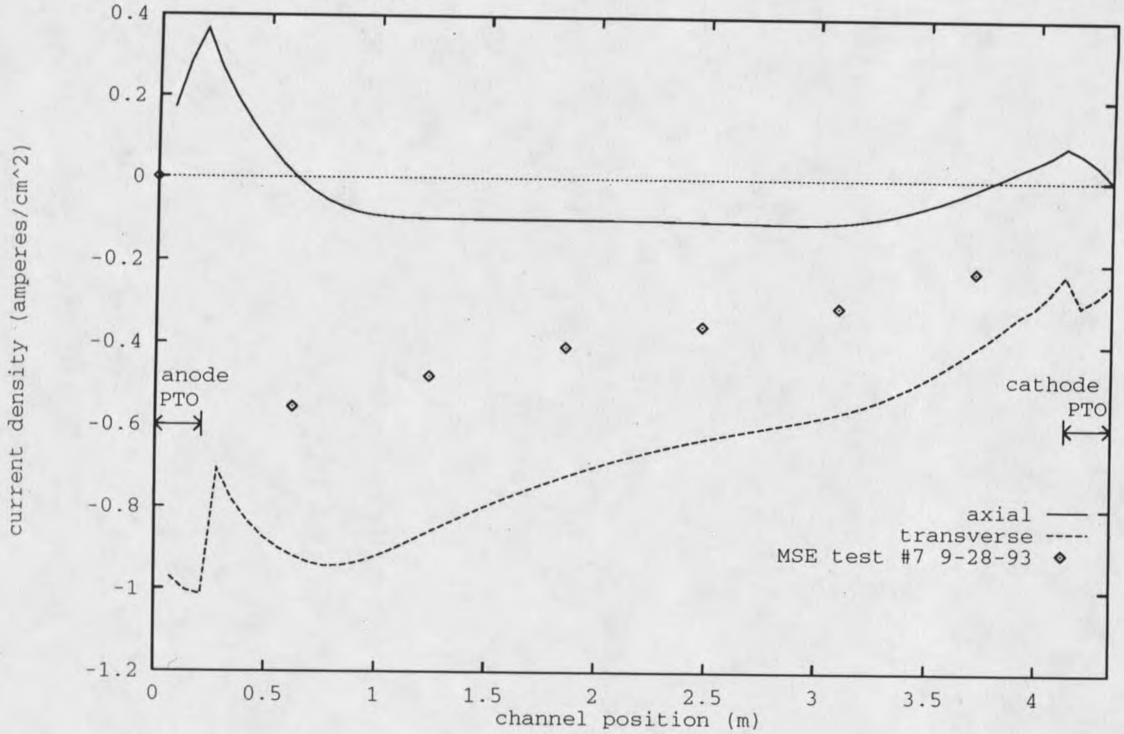

Figure 20: POC Channel Axial and Transverse Current Density Profiles

axial electrical field in promoting interelectrode arcs should not be troublesome unless off nominal operation greatly alters the flat profile or interaction is increased enough to make E_x exceed about 40 volts per centimeter [16, 14].

It is shown in Figure 22 that a reasonable conductivity profile is attained. This conductivity is reduced in the model by the effects of finite electrode segmentation, but it does not reflect any effect of nonuniformities. In practice, POC conductivity data is often reduced by a factor "SIGFAC" [54], which simply reflects the discrepancy between theoretically calculated conductivities and measured conductivities. "SIGFAC" falls in the range of 0.85. Measured conductivities in the POC decreased from about five mho per meter at the channel inlet to about two and one half mho per meter at the channel exit [54]. Since power output is a strong function of conductivity, use of this type of factor in this thesis model may account for much of the discrepancy

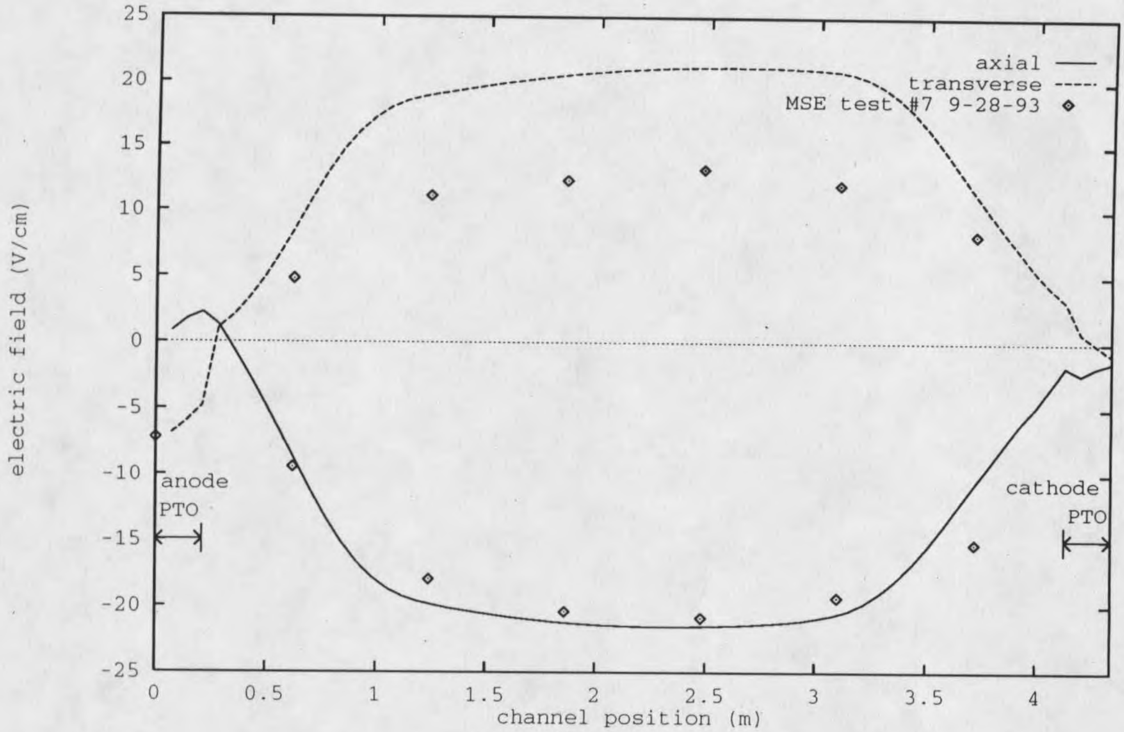

Figure 21: POC Channel Axial and Transverse Electric Field Profiles

in modeled power output.

In Figure 23 the calculated Hall parameter profile is displayed. Hall parameter is a function of magnetic induction and an inverse function of pressure. The Hall parameter increases with increased magnetic induction in the middle of the channel, but it peaks toward the end of the channel where pressure is low. High Hall parameter is one indicator of impending detrimental arcing [63]. Consequently, the location about 3.4 meters into the channel may be a location of significant electrode stress.

Conclusions

The nominal conditions predicted by the thesis computer model show moderate to good agreement with the POC data. A possible modeling problem was illustrated in the modeling of the elliptic flow near the end of the transition section. At this

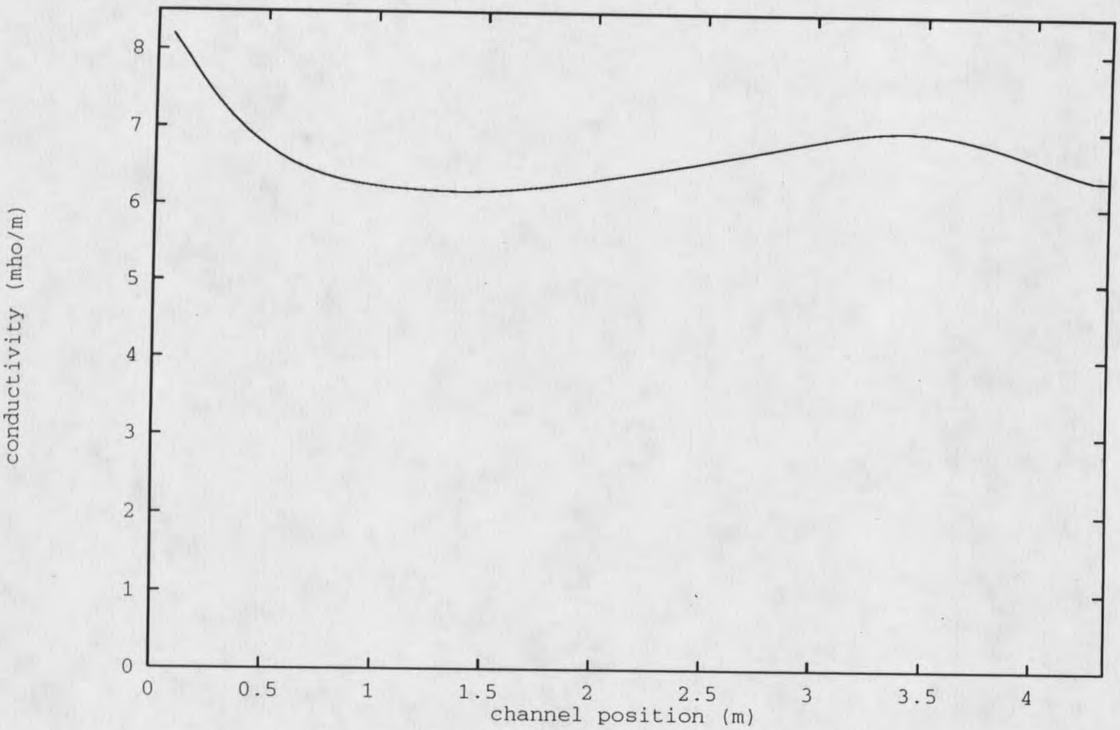

Figure 22: Modeled POC Channel Conductivity Profile

place the Mach behavior either fails to become subsonic, or the behavior once again becomes supersonic near the transition section exit. The questionable Mach profile in the diffuser sections prevents one from making conclusions about occurrences in the transition and diffuser sections with great confidence. The quantities affected include exit temperatures, exit enthalpies, shock location and thermal wall power loss from the transition and diffuser sections.

The model also predicts an available power output which is approximately 30 % too great. One may consider improved modeling of current leakage, inclusion of nonuniformity factors, or corrections to conductivity to better match POC data.

For the most part, the thesis model correctly models duct fluid and MHD interactions. The results are especially noteworthy for the few iterations needed in the numerical algorithm to obtain reasonable results.

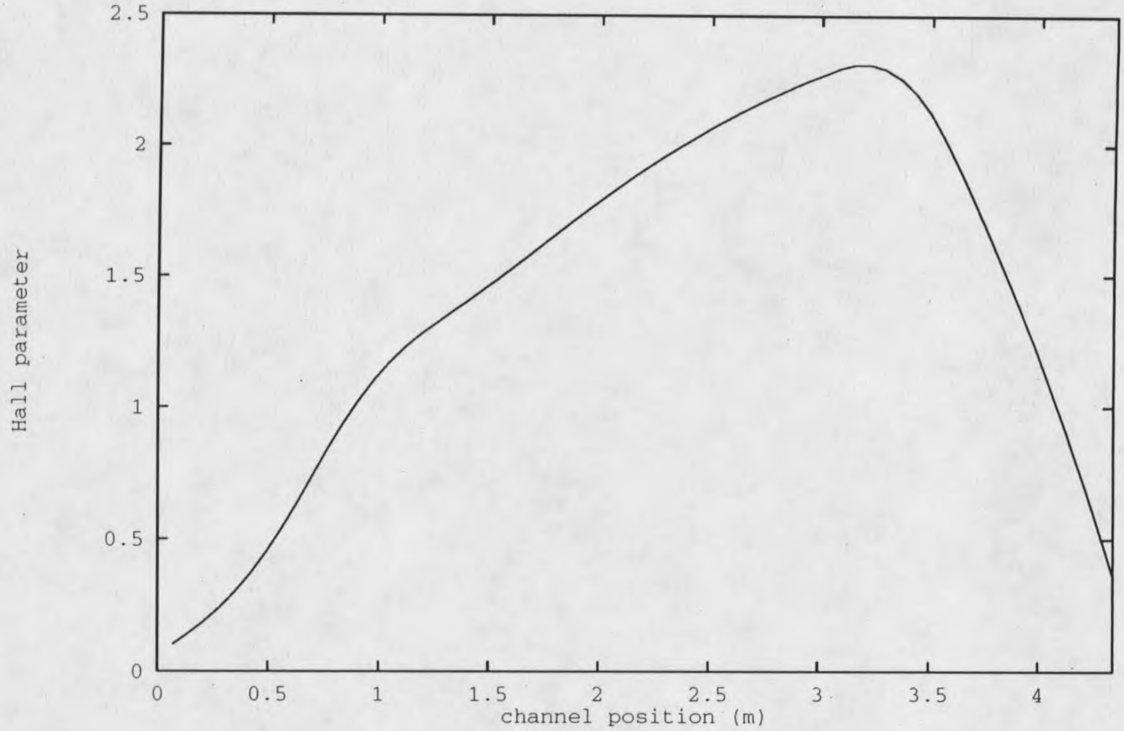

Figure 23: Modeled POC Channel Hall Parameter Profile

Possible electrode stress locations were predicted at about 0.75 meters and 3.4 meters from the beginning of the channel. The first location was attributed to a location of high transverse current density, and the second was attributed to a location with high Hall parameter.

CHAPTER 6

PARAMETRIC STUDIES

The previous chapter demonstrated the accuracy with which the thesis computer model predicts the nominal steady-state operation of the POC generator. Both model strengths and model weaknesses were discussed. In this chapter, eight parametric studies are performed. Off-nominal steady-state behaviors of the POC duct are predicted for variation in coal flow, seed fraction, oxygen enrichment, stoichiometric ratio, diagonal angle, magnetic induction, preheat temperature and load resistance. One parametric independent variable will be defined and investigated in each of the chapter sections.

Results of each parametric study will be interpreted using several criteria: First, a strong shock is not allowed to enter the generator channel. Strong shocks introduce steep pressure and temperature gradients. These mechanical channel stresses are detrimental to channel longevity and are therefore unacceptable. Second, generator efficiency must remain high. Enthalpic extraction efficiency, the fraction of incoming thermal power converted into output electrical power, will be the primary indicator of efficient operation in this study. The POC channel is not very efficient in generating electrical power, but the efficiency trends will be meaningful. Third, the thermal flux to the walls must remain small. This criterion is addressed by observing predicted combustor and channel total cooling requirements. Local thermal fluxes are not monitored. Fourth, the states in the combustor and diffuser exit are observed for possible mechanical stresses. One example of mechanical stress is excessive combustor pressure. Finally, a number of operating conditions identify an increased likelihood for interelectrode arcing. This issue is complicated enough that it warrants more discussion.

High transverse current densities and high axial electric fields increase the likelihood of arcs forming across segmented electrode insulators [64, 65, 63]. Should the product of electrode current and interelectrode voltage exceed one kilowatt, a damaging fault may occur and propagate upstream in the channel [66]. Most arcing occurs on the cathode wall [63]. However, arcs which occur on the anode wall are more damaging because of Lorentz interactions [67, 62]. The Hall effect decreases the critical transverse current density at which arcing begins [63]. Therefore, the Hall parameter must be maintained small in regions of high electrical power extraction. Table 4 summarizes some of the specific criteria cited by other researchers to decrease the likelihood of electrode arcing.

Since the POC generator is a low interaction generator, the extremes of the parametric studies may not violate any of the given criteria. One hopes, however, that the trends observed in the parametric studies on this low interaction generator will be scalable to larger, high interaction channels which may violate the criteria during off-nominal operation.

In any three-dimensional graphs within this chapter, the axis labeled "duct position" gives the axial distance from the combustor section at the beginning of the flow simulation. Only the channel section length of the duct will be shown.

Coal Flow Variation

In the first parametric study, the coal flow introduced into the MHD generator model is varied between 1.5 and 2.2 kg/s. All other parametric independent variables remain constant at their nominal values. As shown in Figure 24, increasing coal flow

$j_y(a/cm^2)$	β	$E_x(V/cm)$	refs.	comments:
> 1			[63]	arcing begins for $T_w < 1500\ K$
> 0.8			[63]	arcing begins for $T_w < 1800\ K$
1			[16]	a sustainable base load
0.8			[62]	at anode for 2 mm separation
1.7				for 5 or 12 mm separation
1.05–1.1			[62]	at cathode for 2 mm separation
> 2				for 5 or 12 mm separation
< 0.6			[14]	
> 0.4	2		[63]	arcing begins with Hall effect
	≤ 4		[14]	allowable Hall parameter
		> 40	[16]	electrode damage begins
		> 20	[16]	axial arc may be sustained
		60 volts	[62, 67]	anode hold off at 2 mm separation
		120 volts		for 5 mm separation
		150 volts		and for 12 mm separation
		350–375 volts	[62]	cathode hold off at 2 mm separation
		> 260 volts		for 5 or 12 mm separation
		< 20	[14]	given a 50 V insulator separation
		70–90 volts	[63]	across a 2.0–2.5 mm insulator

Table 4: Citations Suggesting Allowable Bulk Electrical Parameters

causes increased total flow. The modeled relation is linear. This parametric study therefore investigates solely the effect of total flow variation.

Figure 25 shows that the Mach profile through the parametric domain remains supersonic. However, the channel exit Mach numbers becomes small at low coal flow rate. Very low flow rates are unacceptable because they allow the shock to enter the generator channel. Another subsonic operating region may exist for unchoked flow, but that region will not be investigated here.

Of the three stress related variables—Hall parameter, axial electric field and

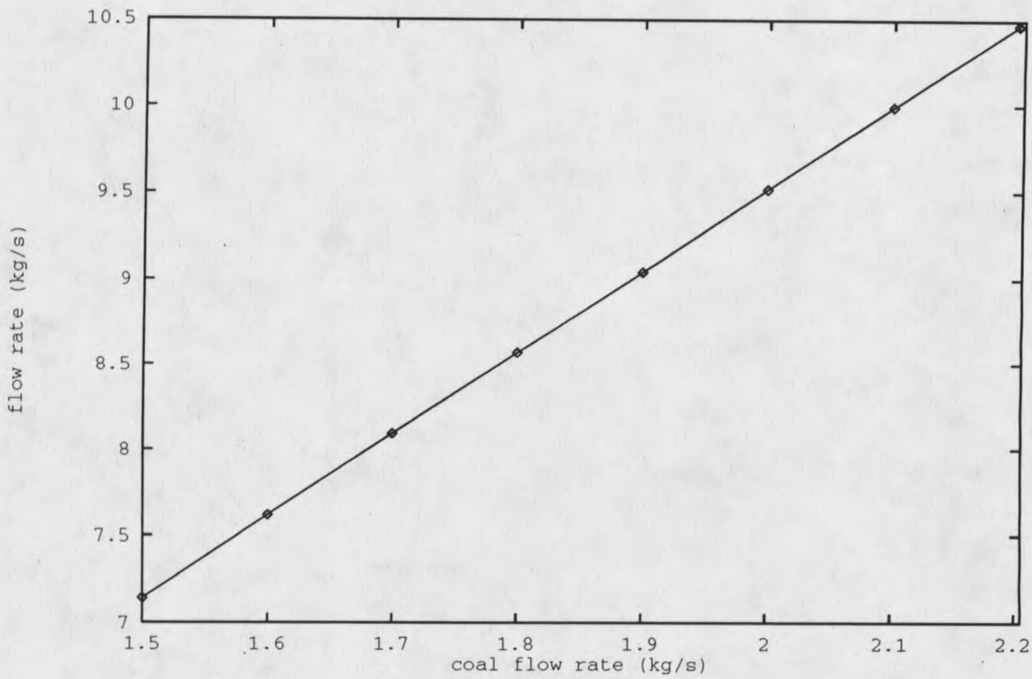

Figure 24: Total Flow Rate Variation with Coal Flow Rate

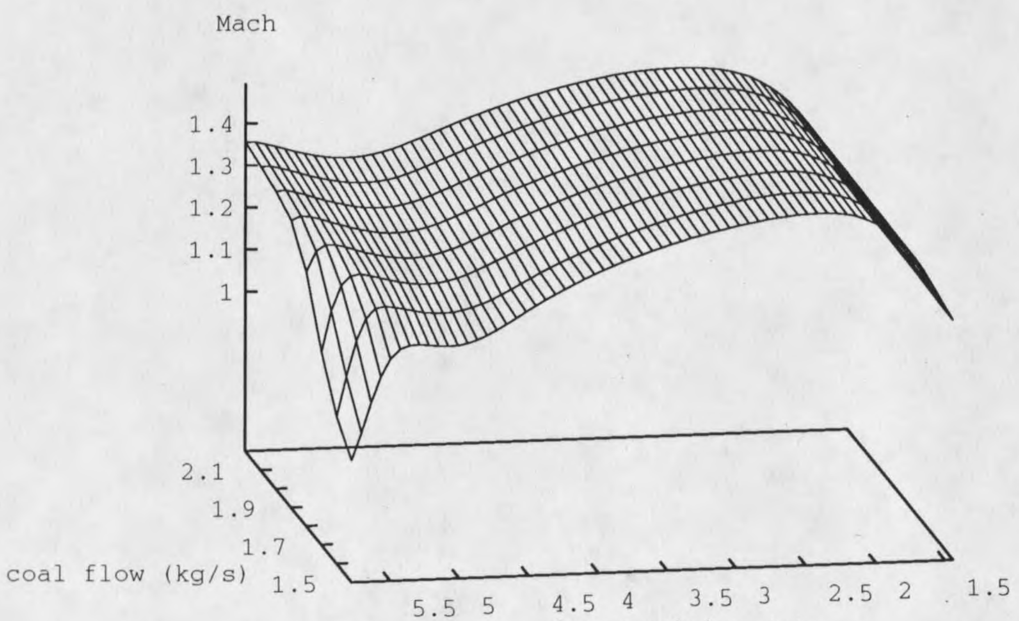

Figure 25: Channel Mach Profile Variation with Coal Flow Rate

transverse current density—only the Hall parameter variation will be presented for this parametric study. Figure 26 shows the variation of Hall parameter along the channel length as coal flow rate is varied. The Hall parameter is greatest for low flow values and at a channel location about 3 meters from the channel entrance. This channel location will be at risk for interelectrode arcing as the flow is decreased.

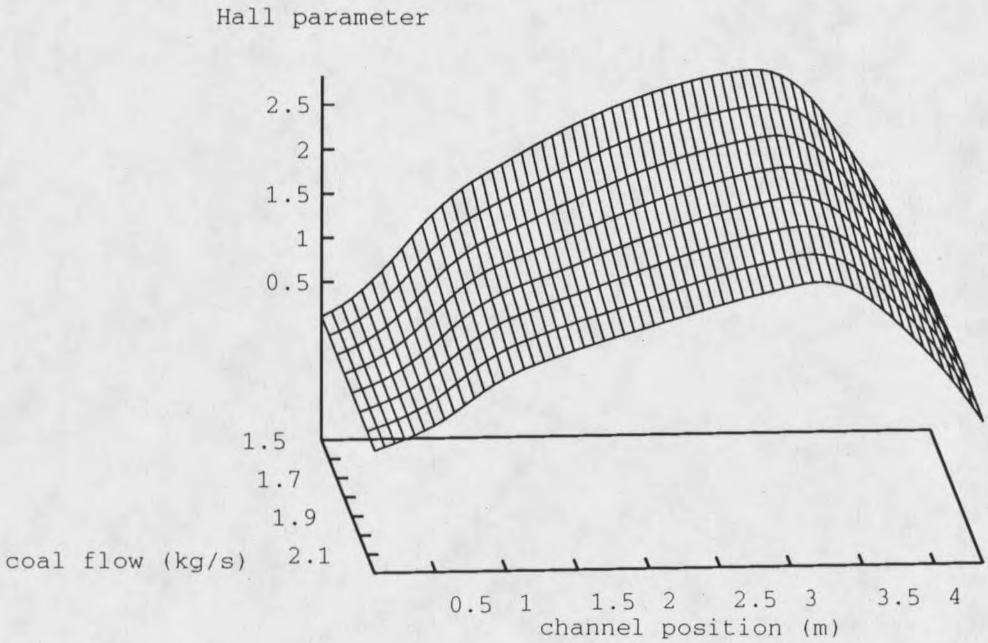

Figure 26: Maximum Hall Parameter Variation with Coal Flow Rate

The axial electric field (not shown) does not vary greatly with change in flow. The maximum axial field magnitude increases gradually from -20.8 V/cm for the lowest flow to -22.0 V/cm at the highest flow. The distribution of axial electric field remains relatively flat throughout the flow range.

Current densities also increase with increasing flow. The highest current densities remain at a channel location about 0.7 meters from the channel inlet. The combined effect of current density and axial field increase the likelihood of sustained arcing for high flow rates.

It should be noted that the Hall parameter promotes electrode stress at low flow while current density and axial electric field magnitudes promote electrode stresses at high flow. This split of stress indicators will prevail throughout the parametric studies in this thesis. Consequently, the simultaneous Hall interaction and high current densities need concern one only during the initial design for nominal operation. If a channel design exhibits acceptable Hall parameters for the nominal current densities, off-nominal operation will not result in both increased Hall parameter and increased current densities.

Enthalpic efficiency decreases steadily with increasing coal flow rate as shown in Figure 27. The POC generator has a significant diminishing return on additional thermal power introduced into the channel. A surprising result of this study is that available electrical power predicted by the computer model is not a strong function of total flow by itself. Therefore, any increase in flow beyond that necessary to maintain a supersonic profile will decrease efficiency.

Furthermore, the thermal loss from the channel section increases with increasing flow as shown in Figure 28. The increase in thermal losses corresponds to the higher temperatures maintained through the length of the channel as flow rate is increased.

Temperature at the exit of the diffuser (not shown) increases as flow increases and as power extraction efficiency decreases. The increase in combustor pressure with increased flow is the primary combustor stress. Figure 29 shows a greater than two atmosphere increase in combustor stagnation pressure with increasing flow over the parametric domain. Once the nozzle has choked, any increase in flow must be accompanied by an increase in combustor pressure. Figure 29 suggests a very linear relation.

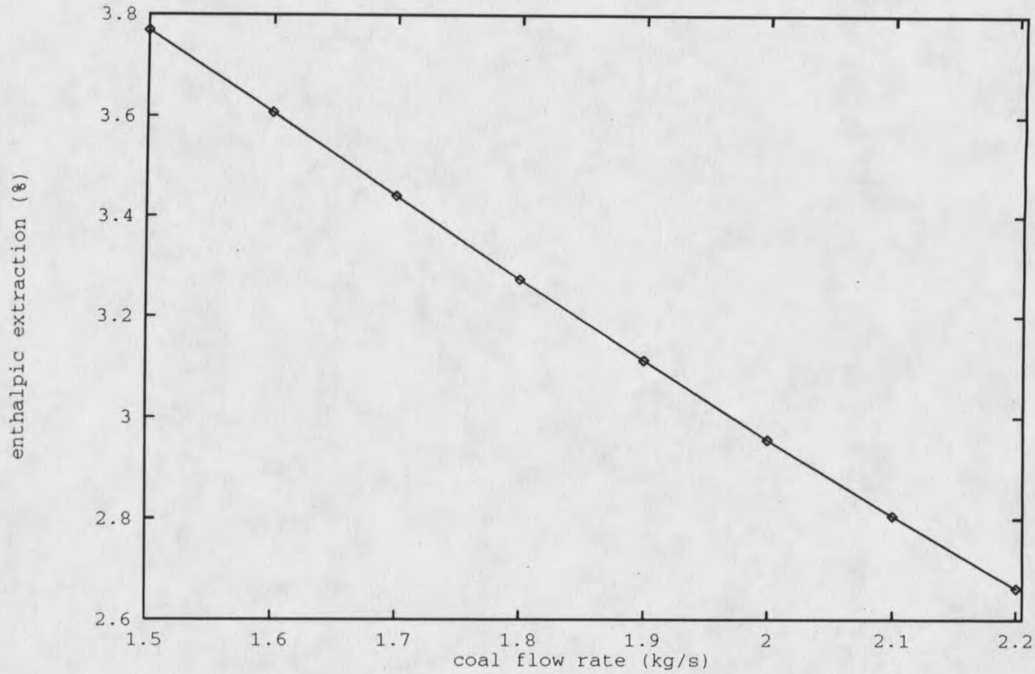

Figure 27: Enthalpic Efficiency Variation with Coal Flow Rate

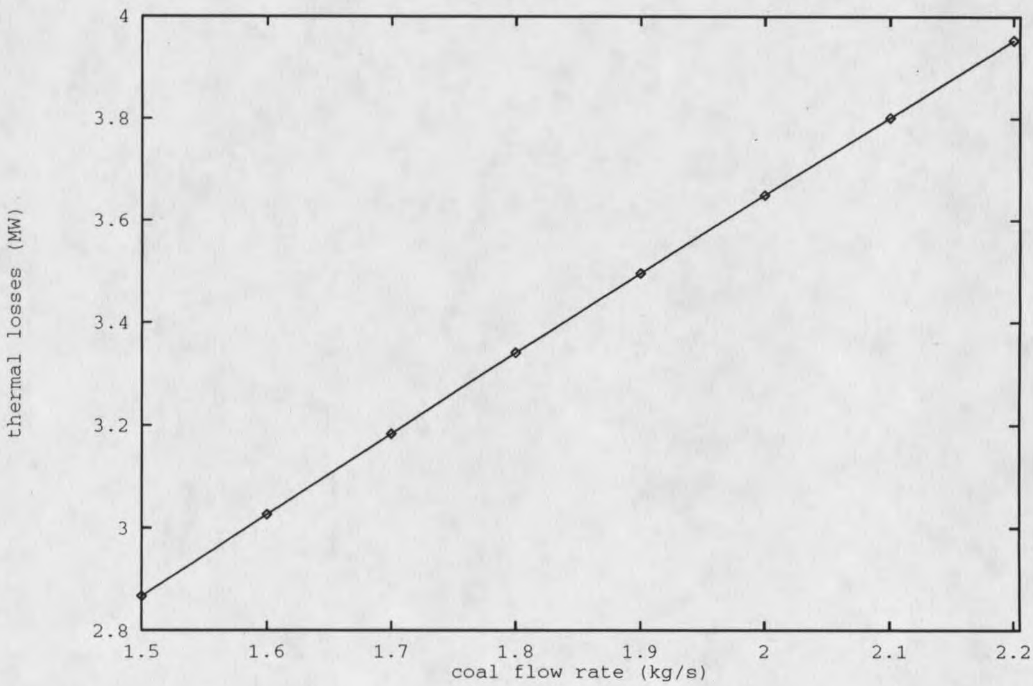

Figure 28: Channel Thermal Loss Variation with Coal Flow Rate

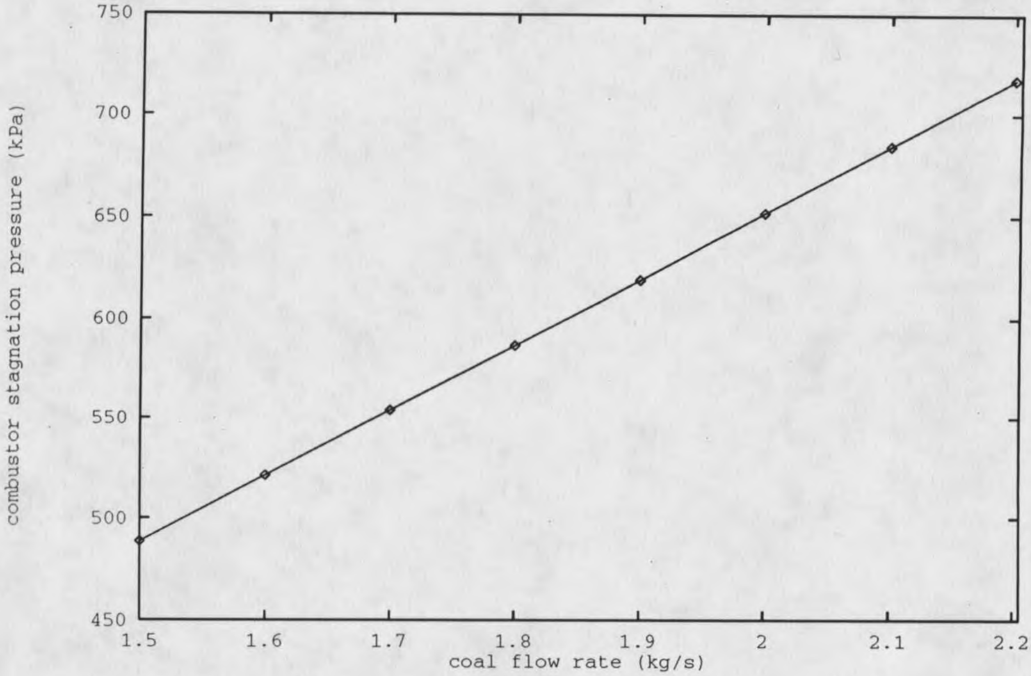

Figure 29: Combustor Stagnation Pressure Variation with Coal Flow Rate

Magnetic Induction Variation

The variation of magnetic induction best shows the unpolluted effect of magnetofluid interactions. The flow composition and flow rate remain constant as the magnitude of the magnetic induction profile is varied. The shape of the magnetic induction profile remains the same. Fringing effects are still modeled. The independent variable in this section is the maximum magnetic induction. The parametric domain varies between 1.5 and 3.5 tesla.

Figure 30 shows that an increase in magnetic induction slows flow. A moderate shock may occur in the middle of the MHD channel where MHD interaction is great. The fluid again accelerates toward the end of the channel, where power extraction is less. The shocks do not appear to be too steep, but one should nonetheless avoid operation in this transonic region.

There is once again a split in the stress variables. Figure 31 shows that Hall

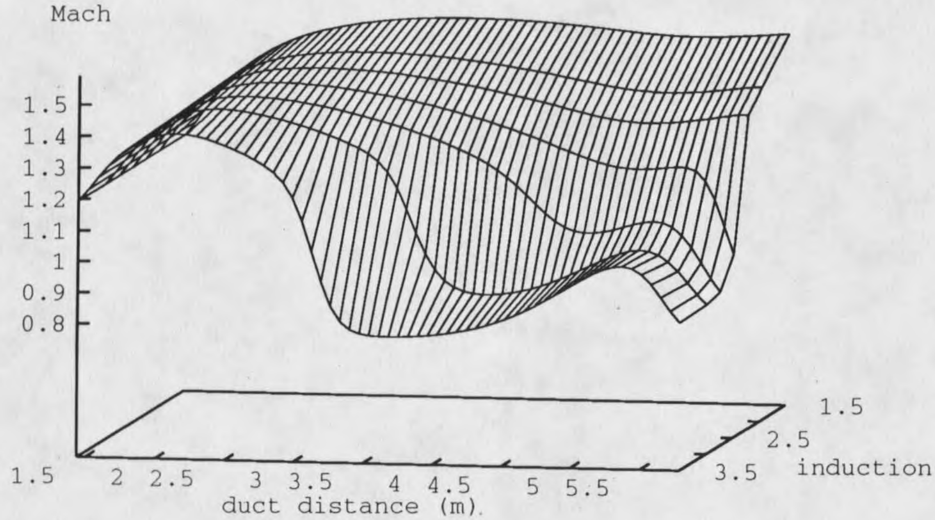

Figure 30: Mach Profile Variation with Magnetic Induction

parameter is greatest for low magnetic induction. The higher Mach numbers at low induction cause lower static pressures. The low static pressures elevate Hall parameter. When the flow becomes subsonic, the pressure again increases and the Hall parameter becomes small. The low Hall parameter in subsonic flow has enticed some designers to choose subsonic channel designs [68].

Axial electric field (Figure 32) and transverse current density (not shown) increase in magnitude as magnetic induction is increased. Great electric field and current stresses will not occur simultaneously with high Hall parameter for the POC design. Figure 32 shows that the Mach behavior of the channel at high magnetic induction distorts the electrical profiles. It is conceivable that the distorted profiles would have loci of high electrode stress in the neighborhood of the shock. However, Ishikawa concluded that shocks do not necessarily cause excessive current densities in the steady state [36].

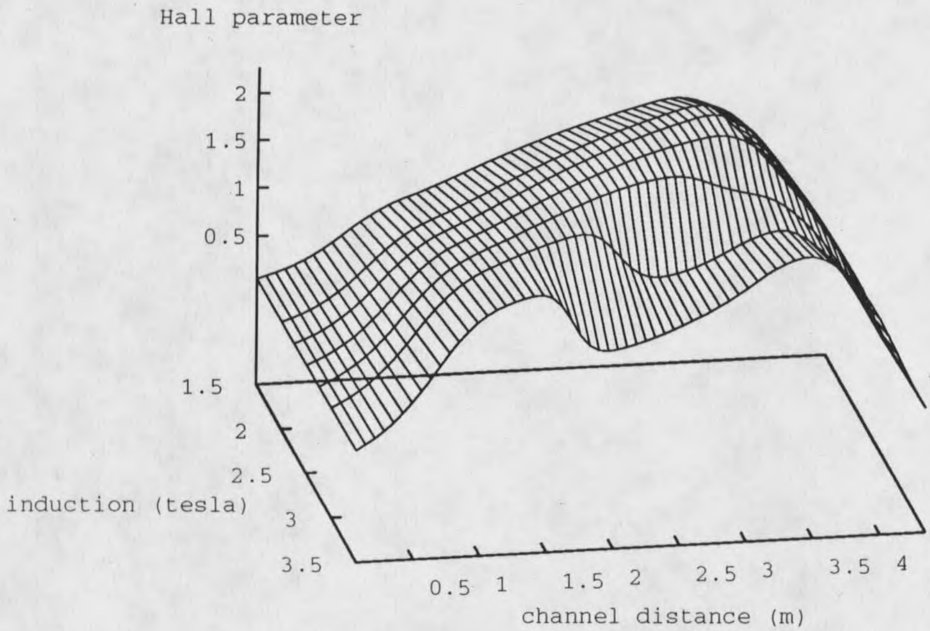

Figure 31: Hall Parameter Profile Variation with Magnetic Induction

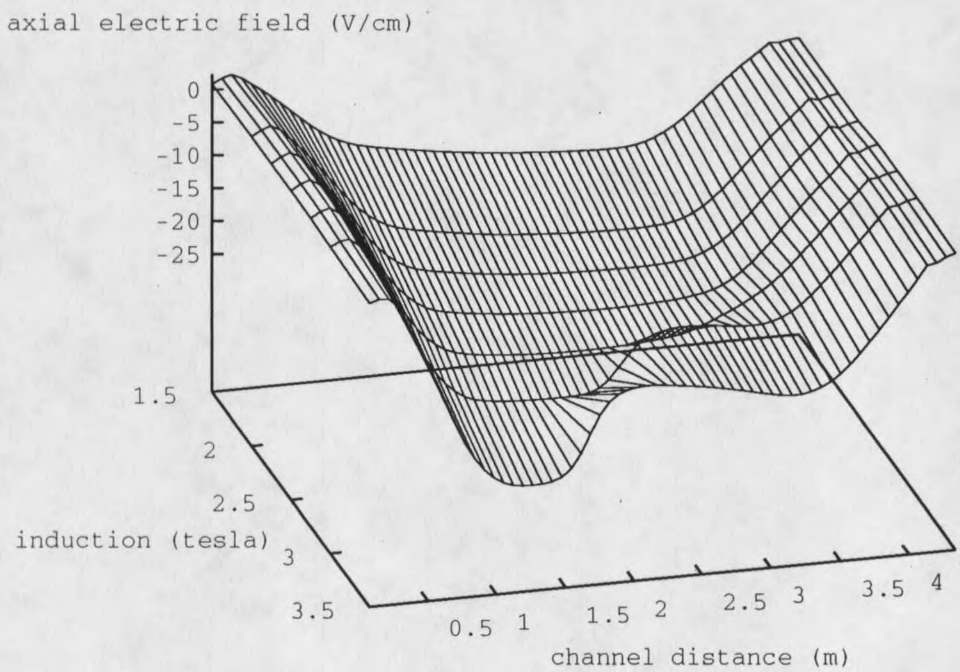

Figure 32: Axial Electric Field Profile Variation with Magnetic Induction

The generated electrical power shown in Figure 33 increases monotonically with increasing magnetic induction. A small wrinkle in the curve appears where some transonic fluid behavior begins. This curve contradicts the notion that power increases with the square of applied induction [3]. However, no attempt was made to optimize power output as induction was varied. MSE data from a September 28, 1993 test analysis under similar operating conditions are included for comparison. It is observed that the thesis model over-predicts generator power by around 0.4 MW. The slope of the curve correlates well to that of the MSE data. Since the flow remains unchanged throughout this parametric study, the shape of the enthalpic efficiency curve will be similar to the power extraction curve over the parametric domain. Enthalpic extraction efficiency ranged from 1.3 to 4.0%.

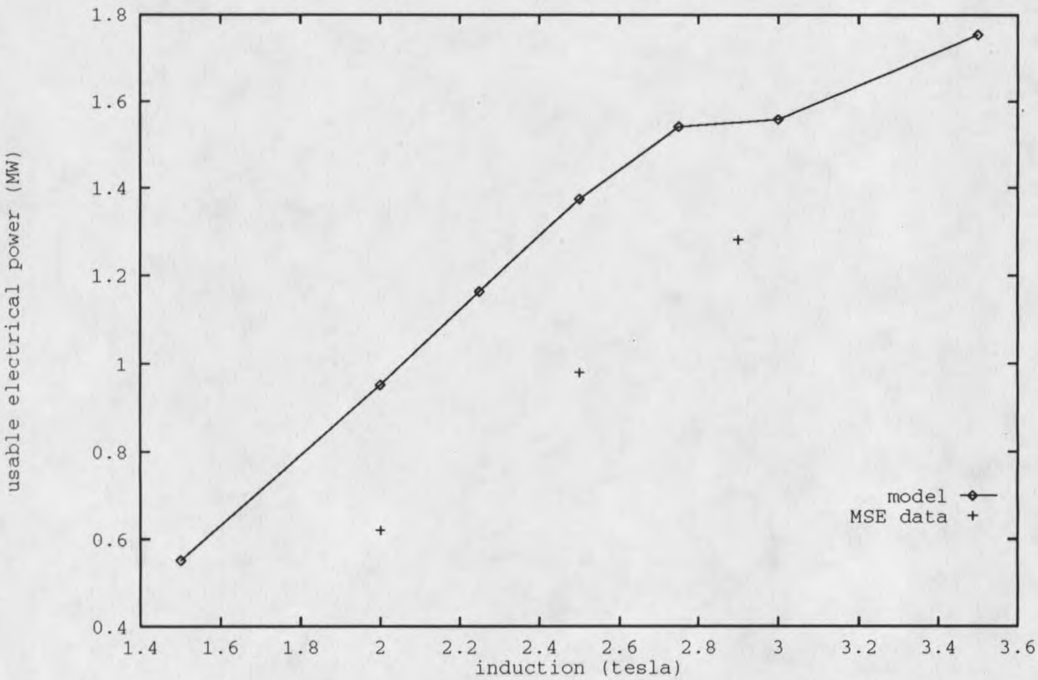

Figure 33: Generated Electrical Power Variation with Magnetic Induction

Conductivity is strongly affected by both pressure and temperature. Therefore, it is strongly affected by the Mach behavior of the fluid as shown in Figure 34. As the fluid shocks and becomes subsonic, the temperature of the fluid increases and conductivity rises.

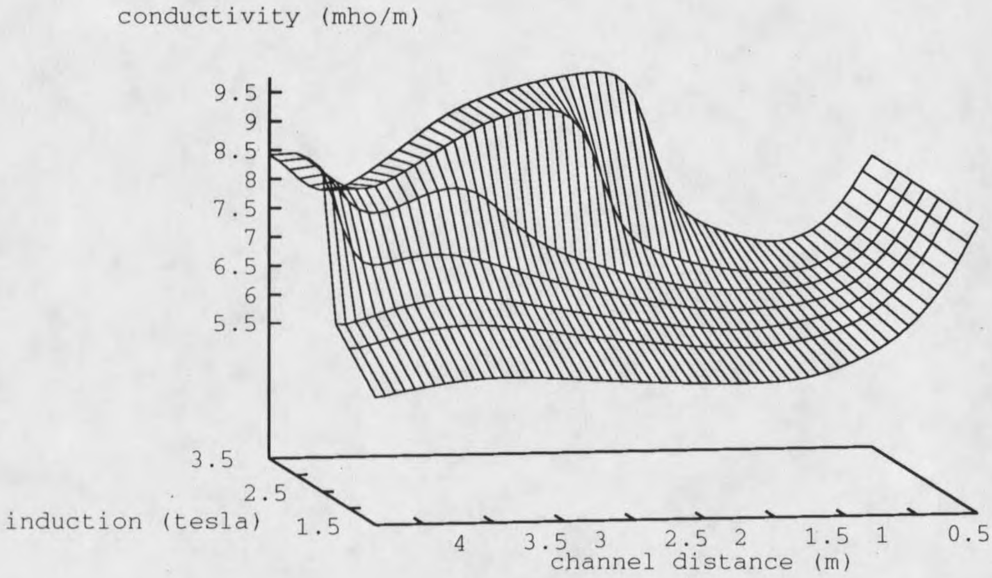

Figure 34: Conductivity Profile Variation with Magnetic Induction

Thermal losses from the combustor and channel are largely unaffected by the variation in magnetic induction. However, there is a small increase in total channel cooling requirement at high magnetic induction. This small increase is probably caused by the elevated temperatures of subsonic flow.

The input and exit thermal power curves (Figure 35) were chosen to demonstrate the effect of varying magnetic induction on the combustor and the diffuser exit states. Flow does not change, so the combustor state will be affected in only a minor way by the increased interactions in the supersonic channel. The two curves diverge. This divergence suggests that increasingly more electrical power extraction or, to a lesser degree, more wall thermal power loss occurs with increasing magnetic induction. Increased magnetic induction should decrease enthalpies and temperatures at the diffuser exit.

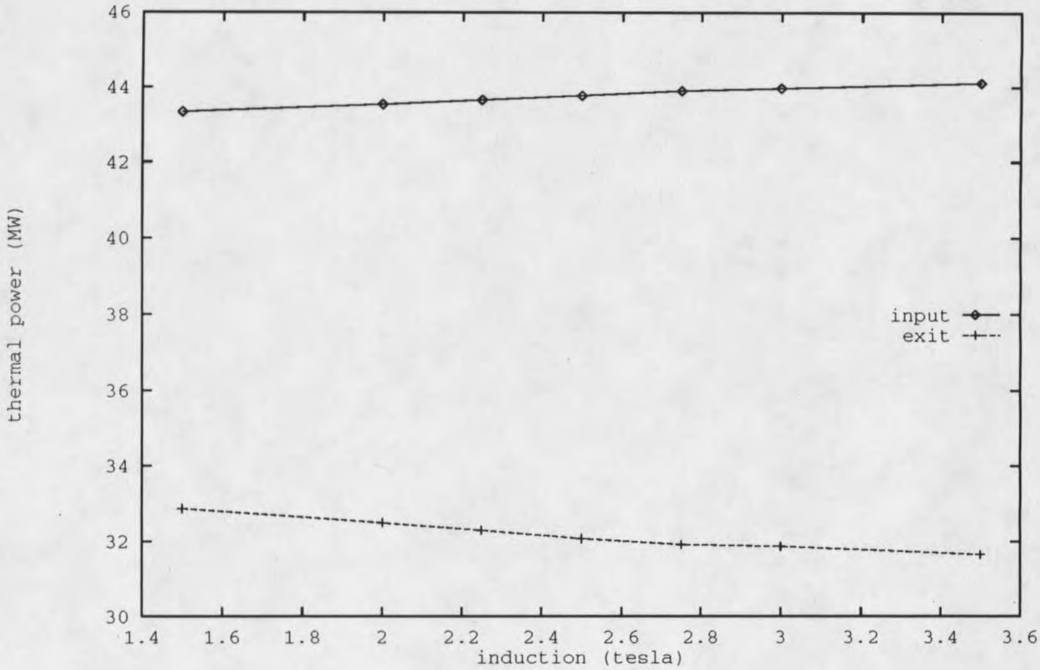

Figure 35: Input and Exit Thermal Power Variation with Magnetic Induction

Diagonal Angle Variation

The diagonal electrode configuration requires that one design for and choose the diagonal angle. A channel may have multiple regions with different diagonal angle for each, but this study shall consider only a single constant diagonal angle throughout the channel. Define the diagonal angle as the angle between the axial fluid flow and an equipotential formed by connecting an anode and cathode electrode pair through an external channel connection. A Faraday channel would have a "diagonal angle" of 90°. The diagonal angle need not be identical to the angle formed by the Z-bar sidewalls [23]. Effects of conducting sidewalls have been ignored for this study.

It has also been assumed that the current controls on the POC channel do not significantly affect steady-state nominal or off-nominal variable profiles. The current control [66] scheme developed by TDS, formerly AVCO, inductively couples small groups of electrodes to prevent transient electrode stresses caused by slag burn-off on the cathode wall [63, 30]. There is a subtle distinction between current controls and power shufflers, which are designed to transfer relatively large amounts of power from one part of the channel to another during off-nominal operation [69, 70]. If indeed the current controls on the POC channel do not significantly affect off-nominal operation, the POC channel may be modeled by simple diagonal loading. Off-nominal operation should result in inefficient axial circulating currents within the channel [69, 70].

Figure 36 shows that large diagonal angles depress the Mach numbers in the channel exit, but none of the tested angles caused any shock mechanical stresses.

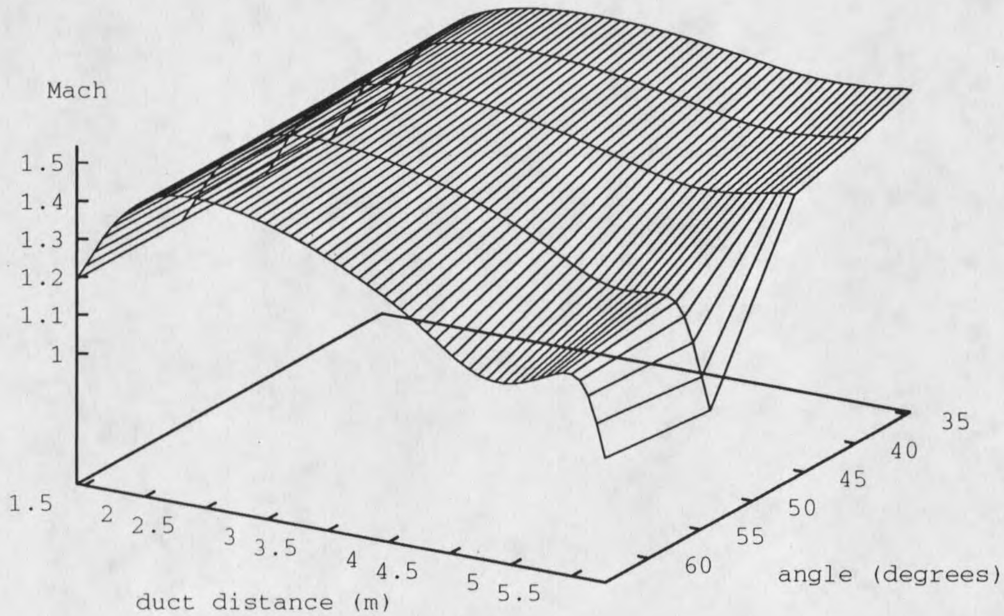

Figure 36: Mach Profile Variation with Diagonal Angle

Electrode stresses are caused by large Hall parameter at small diagonal angles (Figure 37). The high Hall parameters correspond to high Mach number regions toward the end of the channel, where pressures are very low.

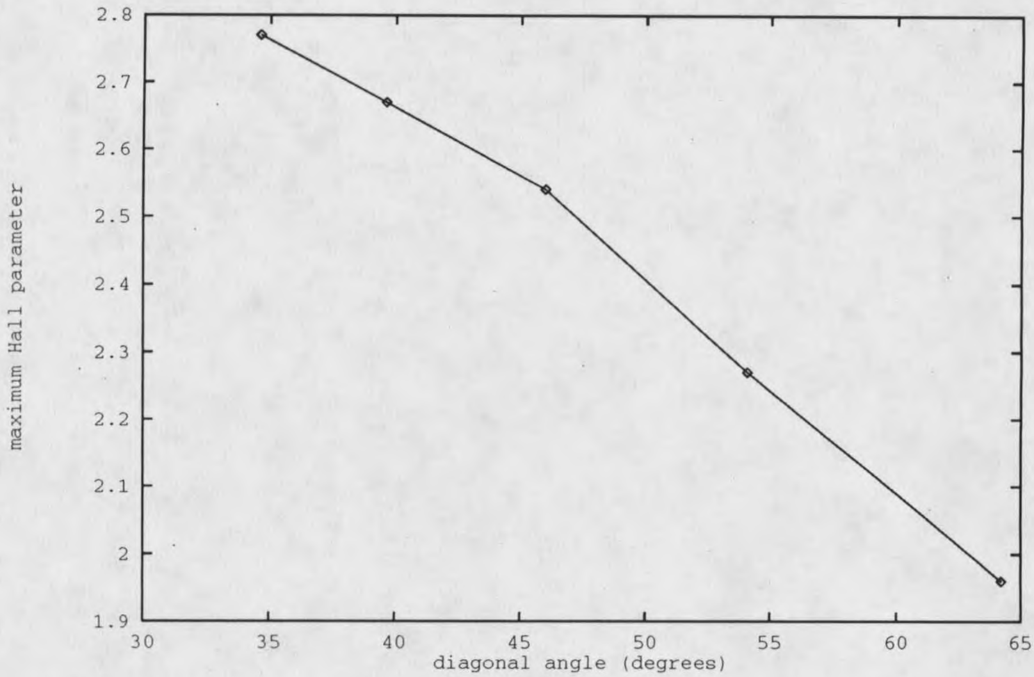

Figure 37: Maximum Hall Parameter Variation with Diagonal Angle

Transverse current densities are strongly affected by the diagonal angle. Figure 38 shows that the electrodes must handle more current at large diagonal angle than at small diagonal angle. This relation makes sense in light of the diagonal approximation equation 19 discussed in chapter 3. Axial currents will flow in the negative direction at small diagonal angle and in the positive direction for large diagonal angle.

The flow of axial currents, either in the positive or in the negative directions, represent channel inefficiencies. Figure 39 shows that an optimum diagonal angle results for reasons discussed above. Maximum electrical power extraction occurs at

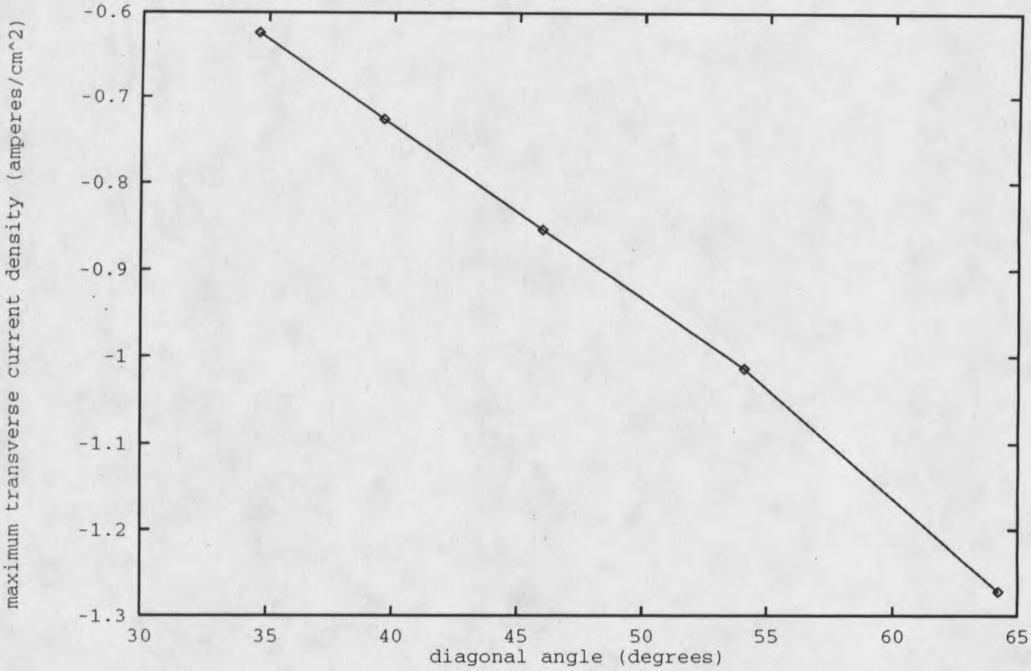

Figure 38: Maximum Transverse Current Density Variation with Diagonal Angle

a diagonal angle of 45°. The Z-bar sidewall angle of the POC channel is 45° and the diagonal angle is about 54°, which is also near the peak on Figure 39. Since the flow composition and flow rate remain unchanged, the shape of the enthalpic efficiency curve (not shown) is very similar to the curve for electrical power extraction. The maximum enthalpic efficiency is about 3.2% at the optimum point on the enthalpic efficiency curve.

The effects of diagonal angle on thermal fluxes, combustor state and diffuser exit state were not large and will not be discussed further.

Stoichiometric Ratio Variation

The stoichiometric ratio defined in this parametric study is the molar ratio of oxygen in the enriched oxidant mixture to carbon in the coal mixture. This definition does not include oxygen and other oxidizing agents present in the coal. Therefore, the

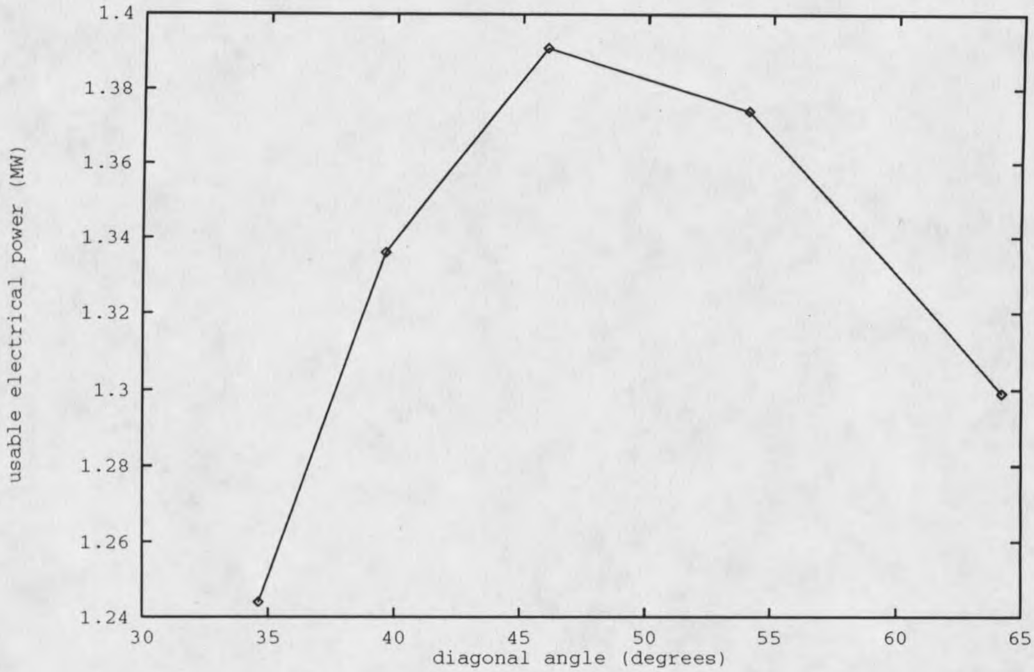

Figure 39: Usable Electrical Power Variation with Diagonal Angle

stoichiometric ratio used as an independent variable in this study will be lower than those stoichiometric ratios used in MSE POC data. This discrepancy was described in the last chapter.

The domain of stoichiometric ratios investigated here range from 0.8 to 1.0. An increase in stoichiometric ratio will be accompanied by a linear increase in total flow rate and an increase in enthalpy. The total flow rate at 0.8 stoichiometric ratio is 8.0 kg/s, and the flow rate is 9.6 kg/s at a stoichiometric ratio of 1.0. The linear variation can be explained by the definition of "stoichiometric ratio" used in this study and the fact that oxidant composition remains constant. Enthalpy increases with increasing stoichiometric ratio because the combustion process nears completion, and more heat of combustion is released.

Thermal power is the product of stagnation enthalpy and total flow rate. Both stagnation enthalpy and total flow rate increase with increasing stoichiometric ratio.

Consequently, Figure 40 shows that thermal power increases rapidly with increasing stoichiometric ratio. The divergence of the input and exit thermal power curves suggests that either thermal power loss or electrical power extraction increases at higher stoichiometric ratios.

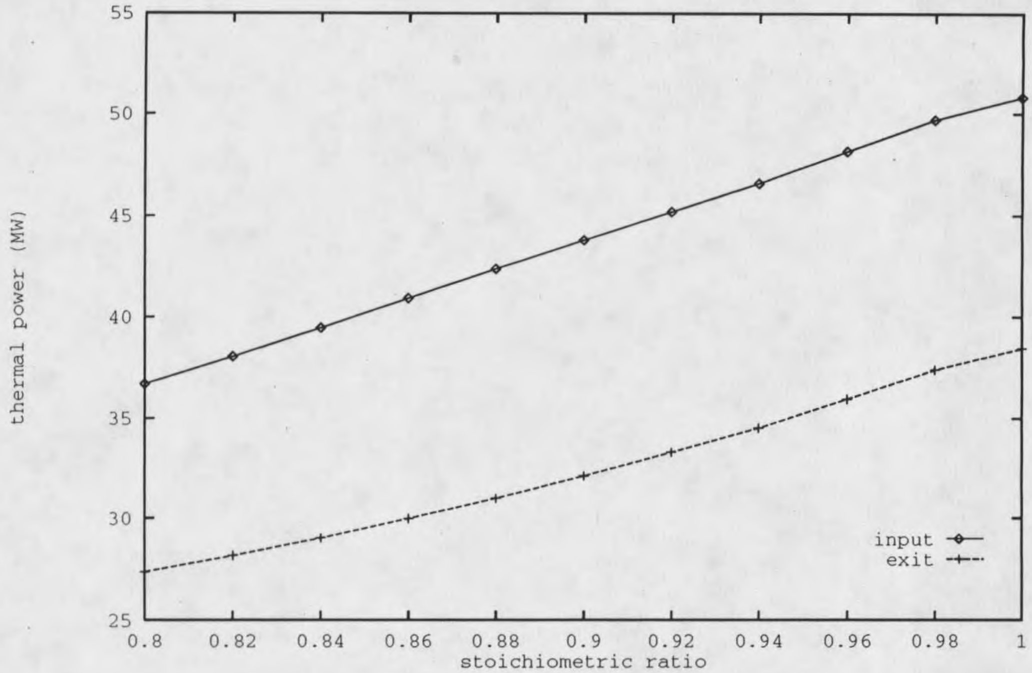

Figure 40: Input and Exit Thermal Power Variation with Stoichiometric Ratio

Figure 41 shows that greater MHD interaction at high stoichiometric ratio depresses the Mach numbers near the channel exit. Flow remains supersonic throughout the tested domain.

Both axial electric field magnitude (not shown) and transverse current density magnitude (Figure 42) increase with increasing stoichiometric ratio. The axial electric field profile remains relatively flat, but the last third of the channel begins to carry more of the interelectrode voltage stress than elsewhere. The location of increased electrode stress due to current density is marked with an arrow. The high current

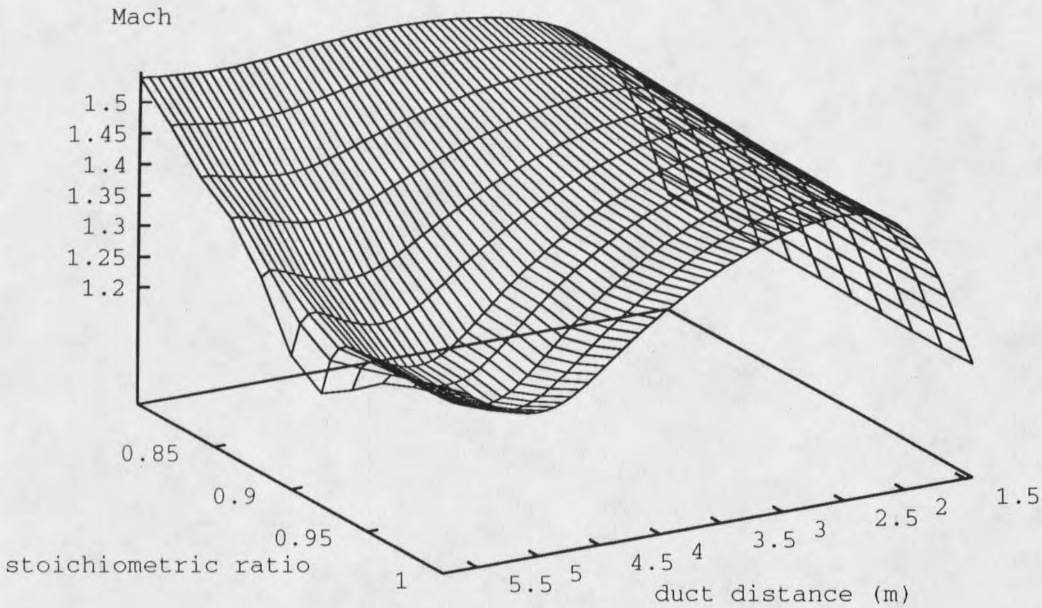

Figure 41: Mach Profile Variation with Stoichiometric Ratio

densities in the anode PTO region will not necessarily be detrimental because the PTO electrode region can be shaped during design to decrease electrode currents, and the anode PTO region occurs in a low MHD interaction portion of the channel.

Hall parameter (Figure 43) shows the opposite trend. High Hall parameters occur at low stoichiometric ratio and toward the exit of the channel (arrow). The Hall parameter is high at this point because supersonic flow has depressed the static pressure. The maximum Hall parameter does not occur at the channel exit because of the fringing effects of the magnetic induction profile.

Figure 44 shows that there is no benefit in operating above a stoichiometric ratio of about 0.9. Above this point, the generated electrical power remains relatively constant. However, Figure 40 showed earlier that thermal power input continues to increase with increasing stoichiometric ratio. As a result, an efficiency optimum must occur at a stoichiometric ratio of 0.9, and efficiency must decrease at greater

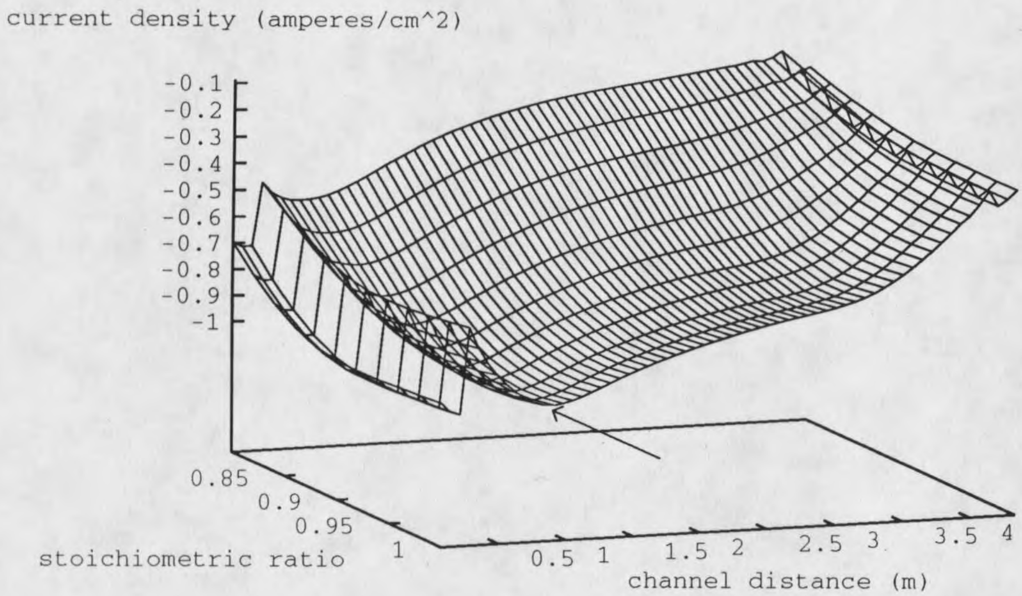

Figure 42: Transverse Current Density Variation with Stoichiometric Ratio

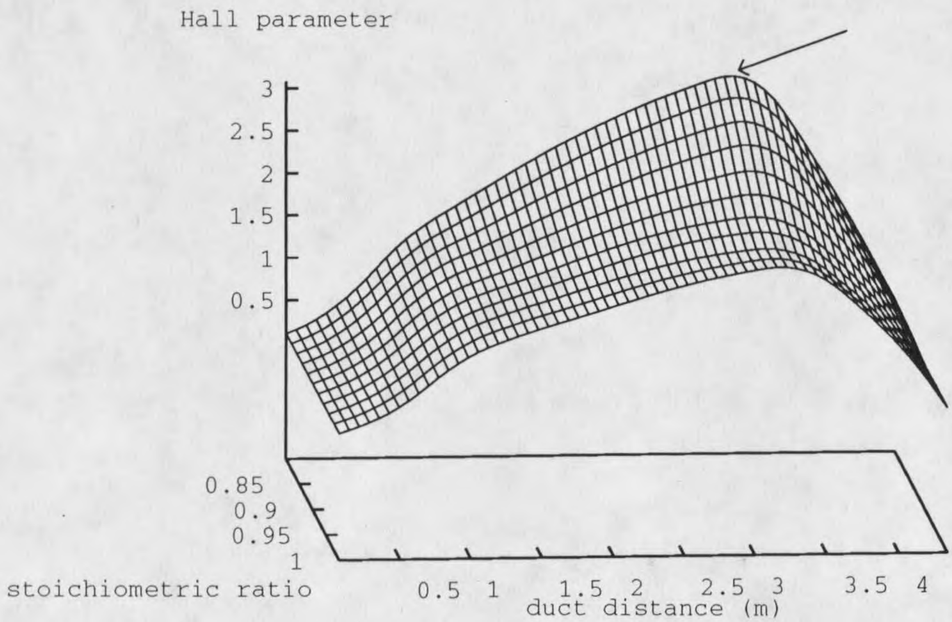

Figure 43: Hall Parameter Variation with Stoichiometric Ratio

stoichiometric ratios. A maximum enthalpic efficiency of 3.2% occurs at a stoichiometric ratio of 0.9.

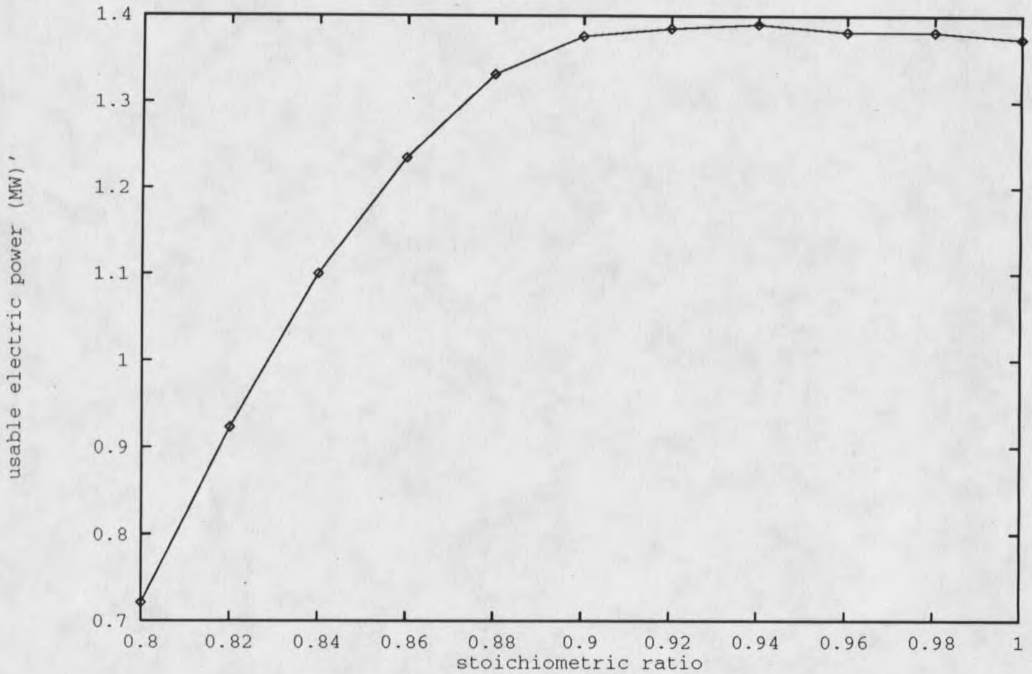

Figure 44: Usable Electrical Power Variation with Stoichiometric Ratio

It is hypothesized that the optimum point described above occurs very close to complete combustion. If a coal oxygen content of 14% is assumed, a 0.9 stoichiometric ratio in this study corresponds to a 0.98 stoichiometric ratio in MSE data. Other oxidizing agents in the reactant mixture could make the equivalent stoichiometric ratio even higher. Therefore, the stoichiometric ratios higher than about 0.92 in this study represent an oxygen rich combustion mixture and would not be used.

The stoichiometric ratio strongly affects channel temperatures. Consequently, the channel conductivity falls off sharply at the lower end of the stoichiometric ratio domain. At 0.8 stoichiometric ratio, most of the channel has conductivities between 3 and 4 mho/m. Closer to complete combustion, conductivities remain above 5.5

mho/m.

Figure 45 shows that both combustor and channel thermal losses increase with increasing stoichiometric ratio. However, the channel wall losses are affected more strongly. The channel losses correspond to higher channel temperatures, but it is unclear why the combustor does not exhibit similar behavior.

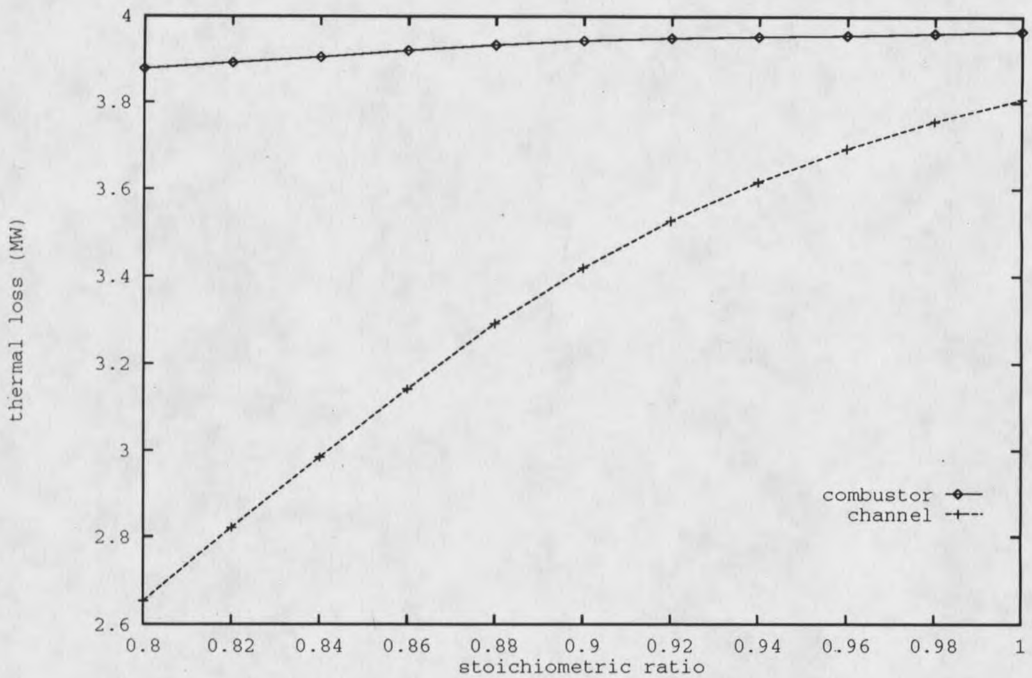

Figure 45: Thermal Wall Power Loss Variation with Stoichiometric Ratio

An increase in stoichiometric ratio will increase temperatures in the combustor and at the diffuser exit. There is a 40 K increase in combustor temperature between a stoichiometric ratio of 0.8 and complete combustion. The diffuser exit temperature increase is only slightly less. These stresses are small and are unlikely to affect operation decisions.

Other factors come into play in the choice of stoichiometric ratio including economic operation and production of nitrogen oxides, but these considerations are not part of this thesis scope.

Oxygen Enrichment Variation

Oxygen enrichment in this study is the molar fraction of oxygen in the enriched oxygen-air mixture. Air, depending upon its moisture content, is 20% oxygen by molar composition. Oxygen ratios greater than about 20% require enrichment with a purer source of oxygen.

As the enriched oxidant mixture becomes purer in oxygen, the quantity of inert mixture components, mostly nitrogen, decreases. Since the combustion process must heat a lesser quantity of inert mixture components at high oxygen enrichment, the combustion mixture enthalpy increases. The combustor specific enthalpy at 0.31 oxygen enrichment is 3.65 MJ/kg; 4.5 MJ/kg at 0.44 oxygen enrichment. By the same reasoning, higher oxygen enrichment is accompanied by a decrease in total flow rate. Total flow rate is 11.6 kg/s at 0.31 oxygen enrichment and 8.6 kg/s at 0.44 oxygen enrichment. The contrary effects of increasing enthalpy and decreasing flow produce a flat input thermal power curve. See Figure 46.

Higher oxygen enrichment numbers depress the Mach numbers near the channel exit as shown in Figure 47. The increased flow rate at low oxygen enrichment numbers supports the supersonic Mach profile at the low oxygen enrichment. The increased channel temperatures which accompany higher enthalpies in the channel support higher MHD interaction for high oxygen enrichment.

The highest maximum Hall parameter (not shown) occurs at an oxygen enrichment of 0.36. The Hall parameter decreases at higher oxygen enrichment numbers because the greater interaction decreases Mach numbers and increases pressures. A pressure increase will also occur at low oxygen enrichment, where more than the design flow is being forced through the channel. This is an interesting result, but

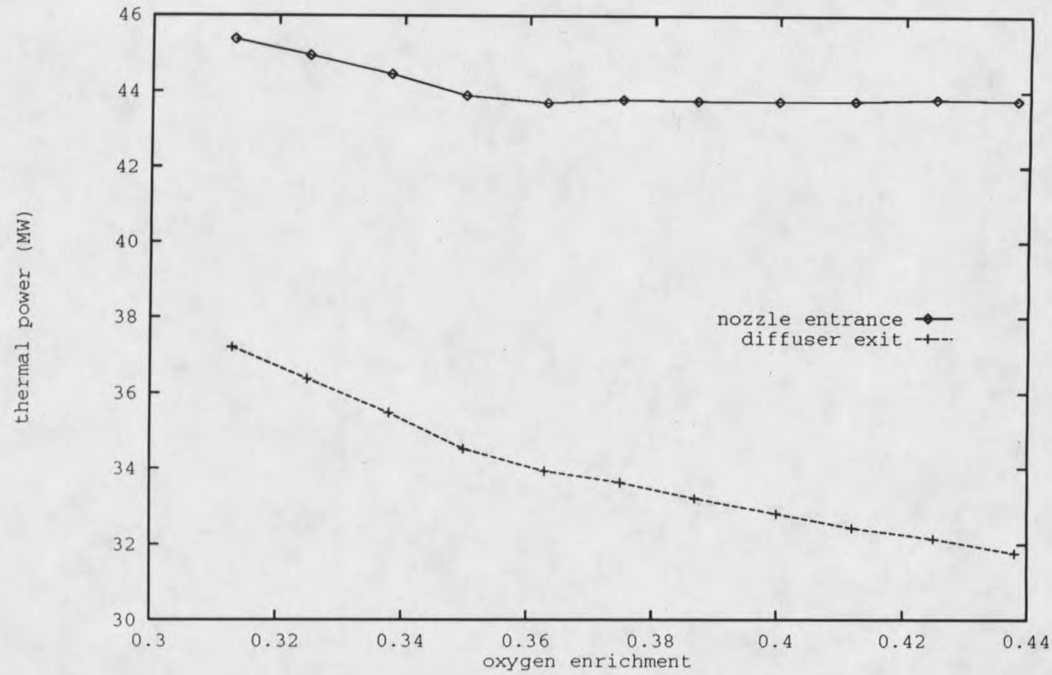

Figure 46: Input and Exit Thermal Power Variation with Oxygen Enrichment

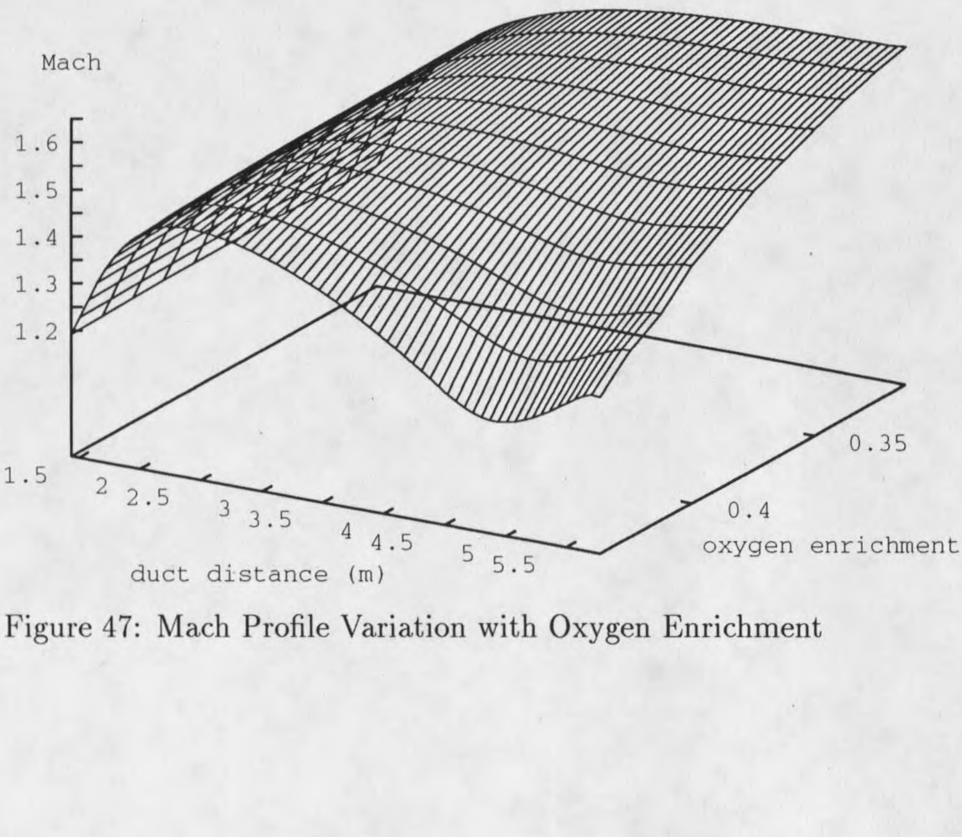

Figure 47: Mach Profile Variation with Oxygen Enrichment

Hall parameter remains between 2.1 and 2.65 throughout the entire parameter domain. The oxygen enrichment parametric study does not decisively show the contrary parameter effects for Hall parameter and current densities. Therefore, variation of oxygen enrichment could simultaneously bring about high Hall parameter and high current density. This condition increases the likelihood of electrode arcing.

Axial electric field (not shown) and transverse current densities (Figure 48) increase with increasing oxygen enrichment. The axial electric field profile remains very flat through the high interaction portion of the channel, but electrode current densities increase most at the location about 0.7 meters into the channel (arrow).

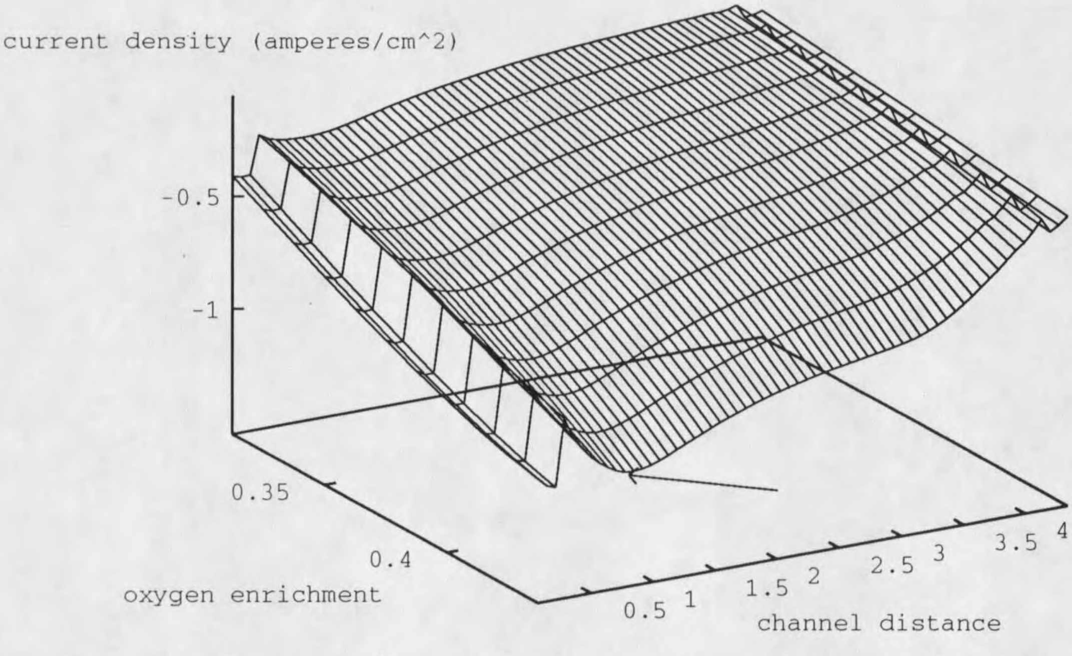

Figure 48: Transverse Current Density Variation with Oxygen Enrichment

Usable electric power increases monotonically with increasing oxygen enrichment as shown in Figure 49. Enthalpic efficiency also increases monotonically from a low of 0.6% at the lowest oxygen enrichment to a high of 3.3% at an oxygen enrichment of 0.44. Clearly, high oxygen enrichment levels are favored, and low oxygen enrichment levels may not result in economic operation.

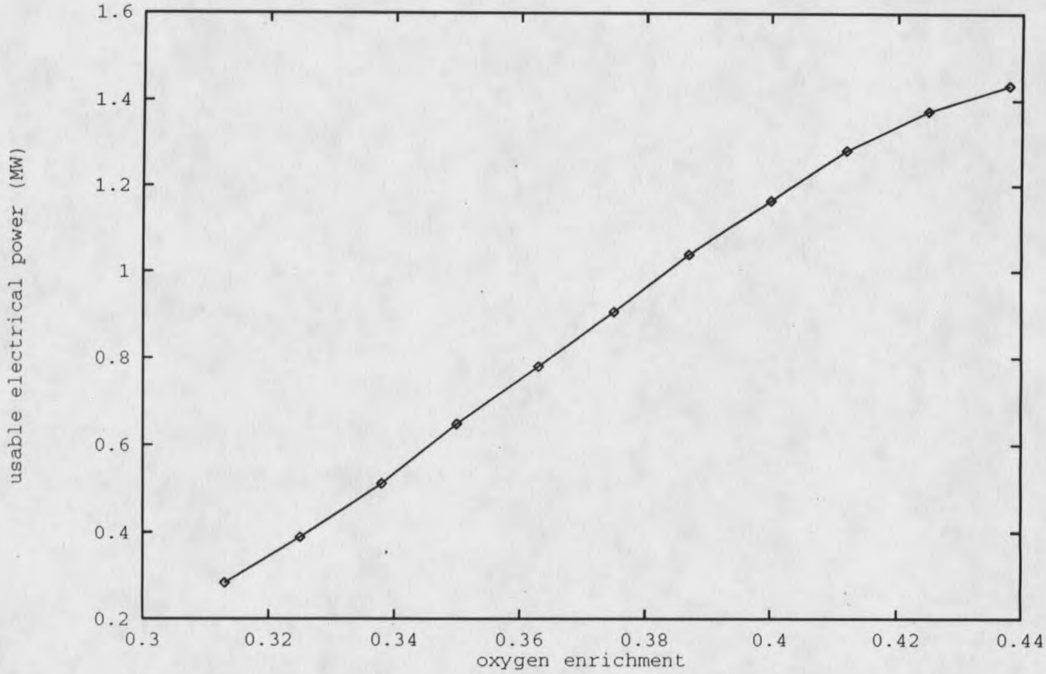

Figure 49: Usable Electric Power Variation with Oxygen Enrichment

The strong influence of oxygen enrichment is demonstrated well by the channel conductivity of Figure 50. The conductivity profile remains very low for low oxygen enrichment.

It was shown in the last section of this chapter that stoichiometric ratio affects channel wall losses more than it affects combustor losses. In contrast, Figure 51 shows that oxygen enrichment strongly increases combustor losses but affects channel wall losses less. The thermal stress on the combustor is likely to be the limitation on maximum allowable oxygen enrichment.

The combustor wall losses are explained by the great increase in combustor temperatures which accompanies increased oxygen enrichment. The combustor

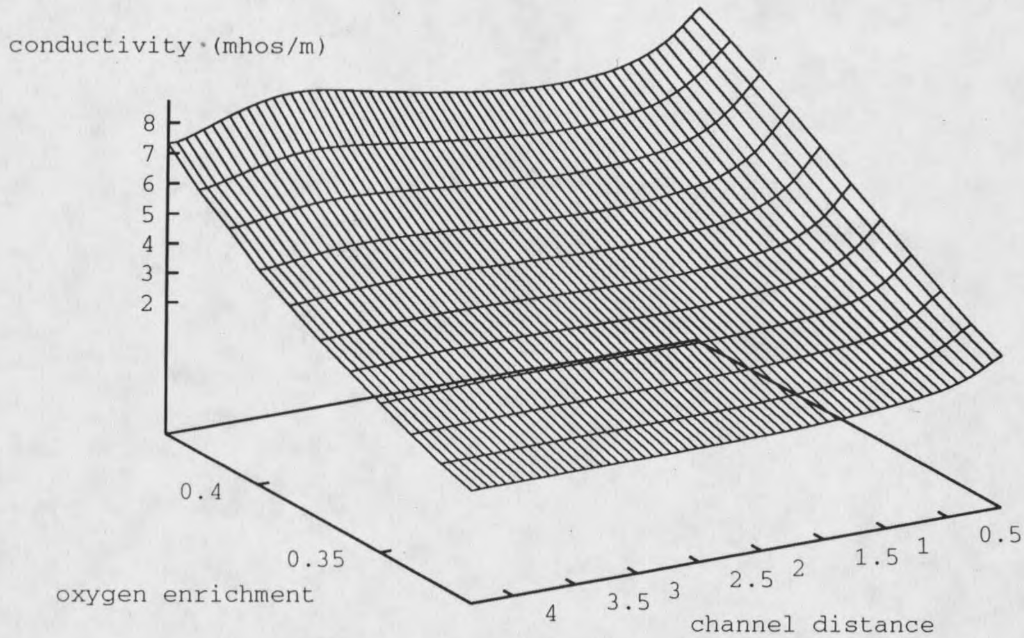

Figure 50: Conductivity Profile Variation with Oxygen Enrichment

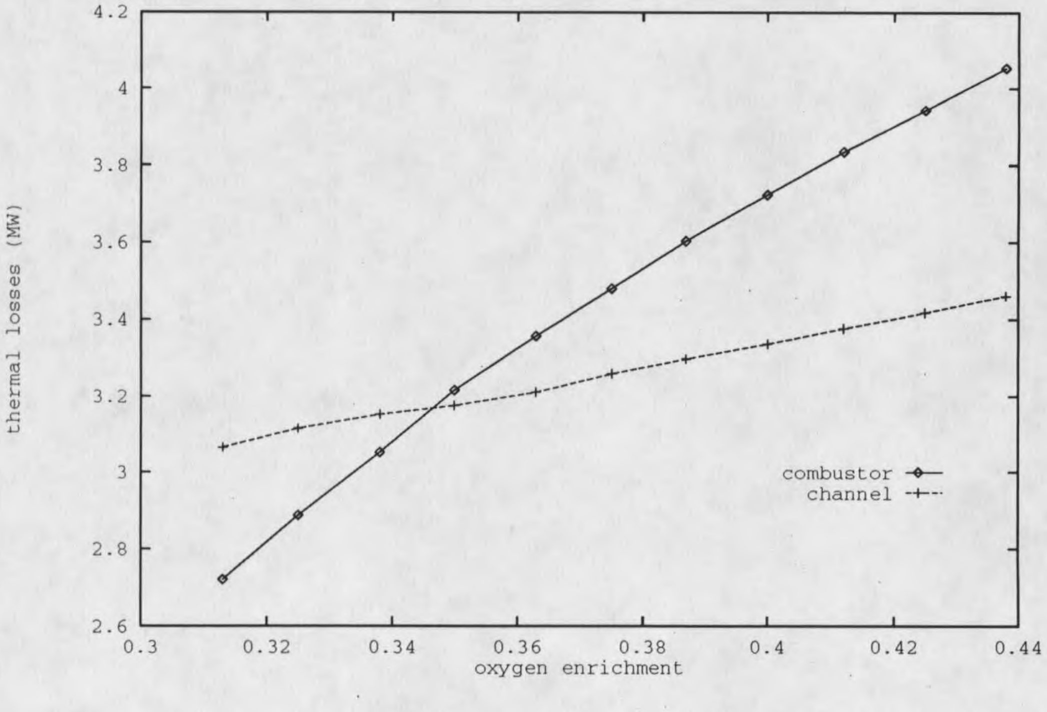

Figure 51: Thermal Wall Loss Variation with Oxygen Enrichment

stagnation temperatures range from 2700 K at an oxygen enrichment of 0.31 to more than 2850 K at an oxygen enrichment of 0.44. The oxygen enrichment domain investigated here also results in more than a 1.6 atmosphere range of combustor pressures. For choked flow, any increase in total flow rate must be accompanied by a significant increase in combustor pressure. High pressure mechanical stresses may limit the lowest allowable oxygen enrichment given constant flow rate and constant stoichiometric ratio.

Seed Variation

Seed fraction is defined as the mass fraction of potassium metal in the total flow. The domain of seed fractions used in this parametric study vary between 0.003 and 0.024. An increase in seed content over this domain increases the total flow rate by only about 4%. The metallic seed and its salt mixture must be heated by the combustion process, so the increase in seed fraction over its domain accounts for about a 6.7% decrease in specific enthalpy in the combustor. The two minor effects reported in this paragraph result in a relatively flat thermal input power over the seed fraction domain in this parametric study. Therefore, the effects observed in this parametric study will be attributable to increased MHD interaction between the seeded fluid and magnetic field only.

The effect of the increase in MHD interaction with increased seeding is evident in Figure 52. The initial additions of seed up to a seed fraction of about 0.015 retards the supersonic flow in the channel. Additional seed contributes a lesser amount to the channel interaction. Refer back to Figure 4 in chapter 2 to gain some insight into this result. Conductivity increases very quickly with the initial quantities of seed. Additional seed increases conductivity at a slower rate.

Hall parameter is greatest for low seed fraction. Figure 53 shows that once

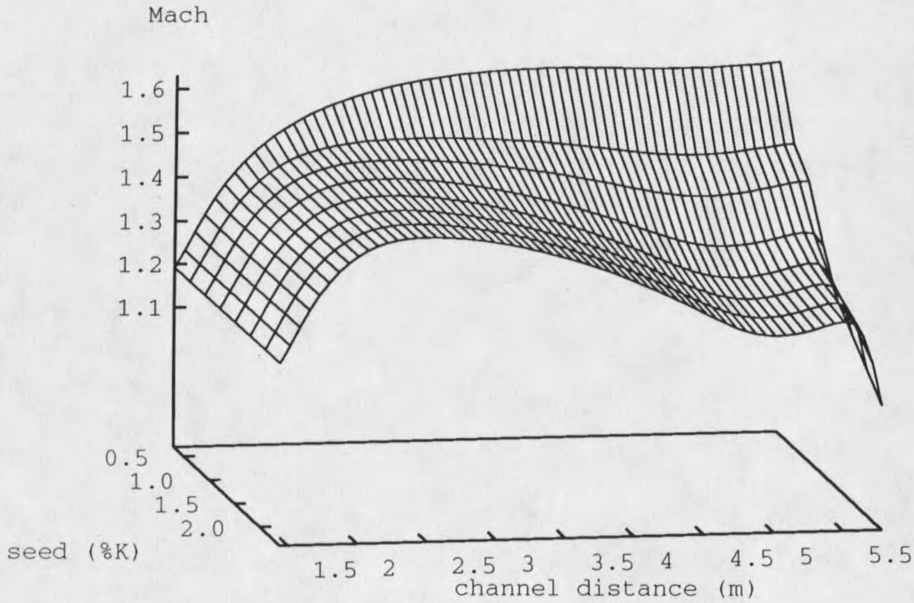

Figure 52: Mach Profile Variation with Seed Fraction

again Hall parameter magnitude follows the Mach behavior. Normally, Hall parameters approaching 3 and greater would be troublesome. In this case, the MHD interaction is so small at low seed fractions that the likelihood of interelectrode shorting is remote.

At high seed fraction, the axial electric field (not shown) and transverse current density magnitudes (Figure 54) increase the risk of interelectrode shorting with increasing seed fraction. Once again, the axial electric field profile remains flat, but the greatest transverse current densities occur in the first third of the channel.

Figure 55 shows that little additional electrical power is extracted when seed fractions greater than 0.015 are utilized. An optimum occurs in the generated electrical power curve near this seed fraction. In practice, higher seed fractions may be needed to remove sulfur from the combustion mixture.

The enthalpic efficiency curve (not shown) exhibits a similar shape. A

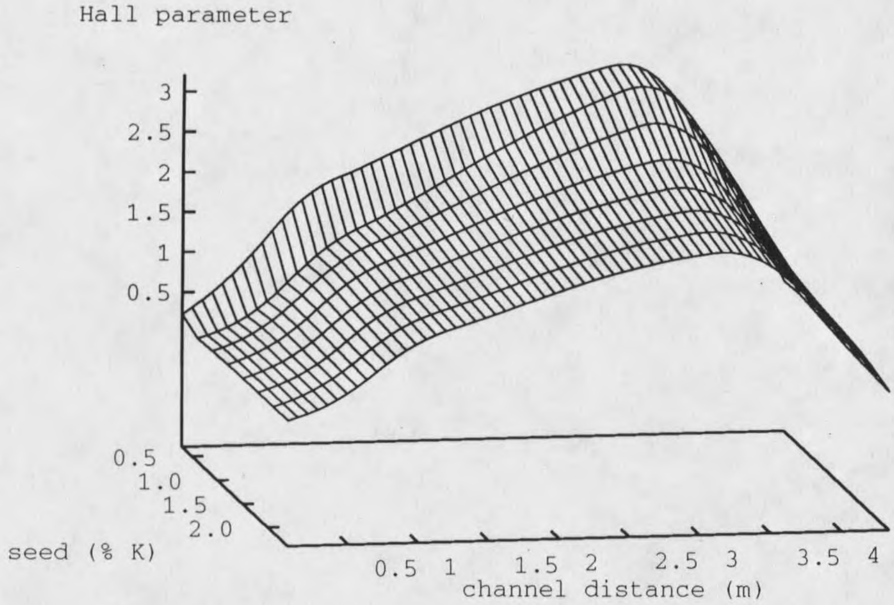

Figure 53: Hall Parameter Profile Variation with Seed Fraction

Figure 54: Transverse Current Density Profile Variation with Seed Fraction

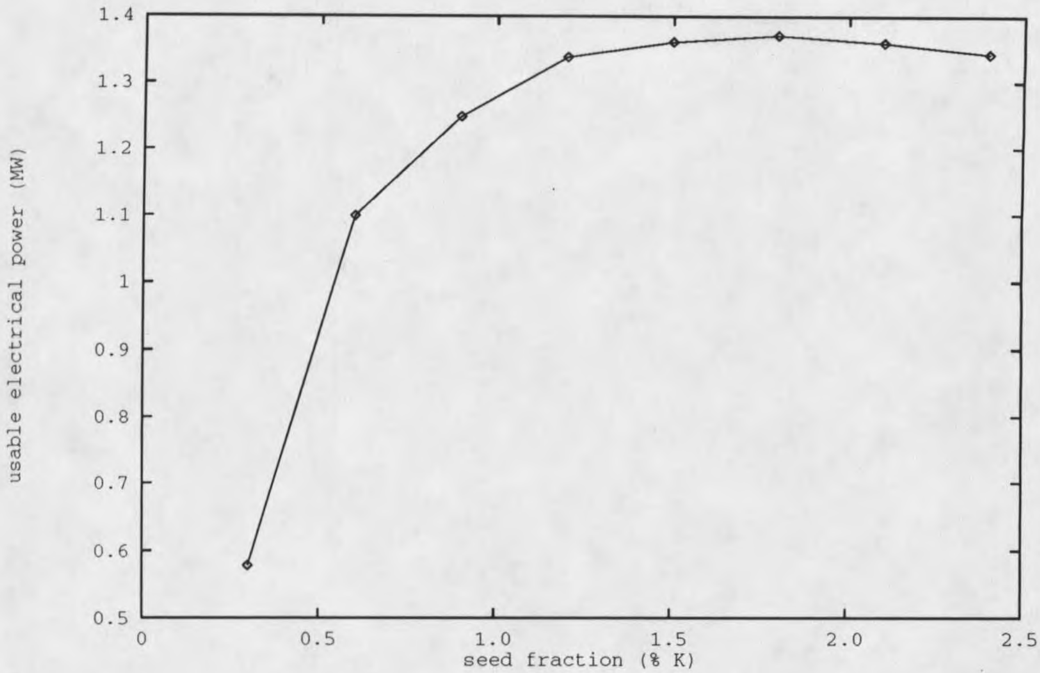

Figure 55: Usable Electric Power Variation with Seed Fraction

maximum enthalpic efficiency of 3.2% is obtained for a 0.018 seed fraction. Enthalpic efficiency falls to 60% of its maximum value at a seed fraction of 0.003. Seeding is clearly necessary, and there is an optimum seed fraction.

An increase in seed fraction results in decreased thermal wall losses in both the combustor and channel. See figure 56. A possible explanation for this is that the power extraction at higher seed fractions reduces channel temperatures and consequently reduces channel losses. The thermal loss in the combustor must be explained entirely by the reduction in specific enthalpy and temperature which accompanies higher seed fractions.

Indeed, combustor stagnation temperature approaches 2900 K when no seed is utilized and drops 80 K when a seed fraction of 0.024 is reached. There is also a decrease in diffuser exit temperature with increasing seed fraction, but some of the decrease can be attributed to the extraction of more electrical power at high seed

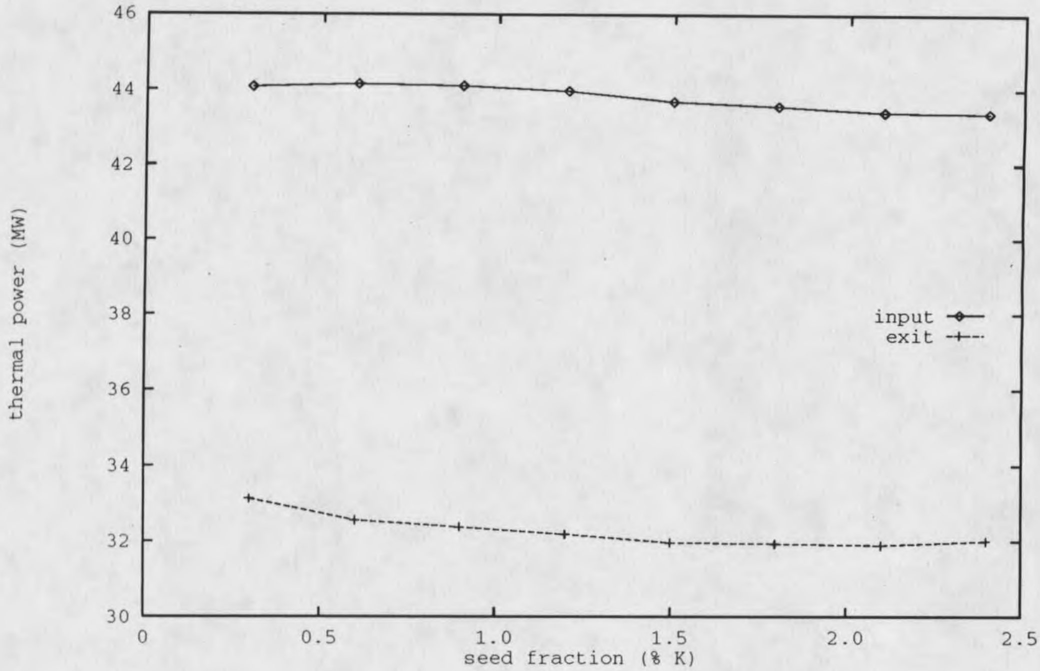

Figure 56: Input and Exit Thermal Power Variation with Seed Fraction

fractions.

Other factors such as economics and sulfur removal must be considered when choosing seed fraction, but these issues are beyond the scope of this thesis.

Preheat Temperature Variation

The preheat temperature is the temperature to which the oxidant mixture is heated before its introduction to the combustor. The parametric domain of preheat temperatures will vary between 900 K and 1080 K.

Flow rate and composition remain unchanged through this parametric study, but the additional heat added to the combustor increases specific stagnation enthalpy and thermal power in the combustor. This effect is demonstrated in Figure 57. The divergence of the two power curves indicates that the combination of thermal power losses to walls and electrical power extraction must increase with increasing preheat temperature.

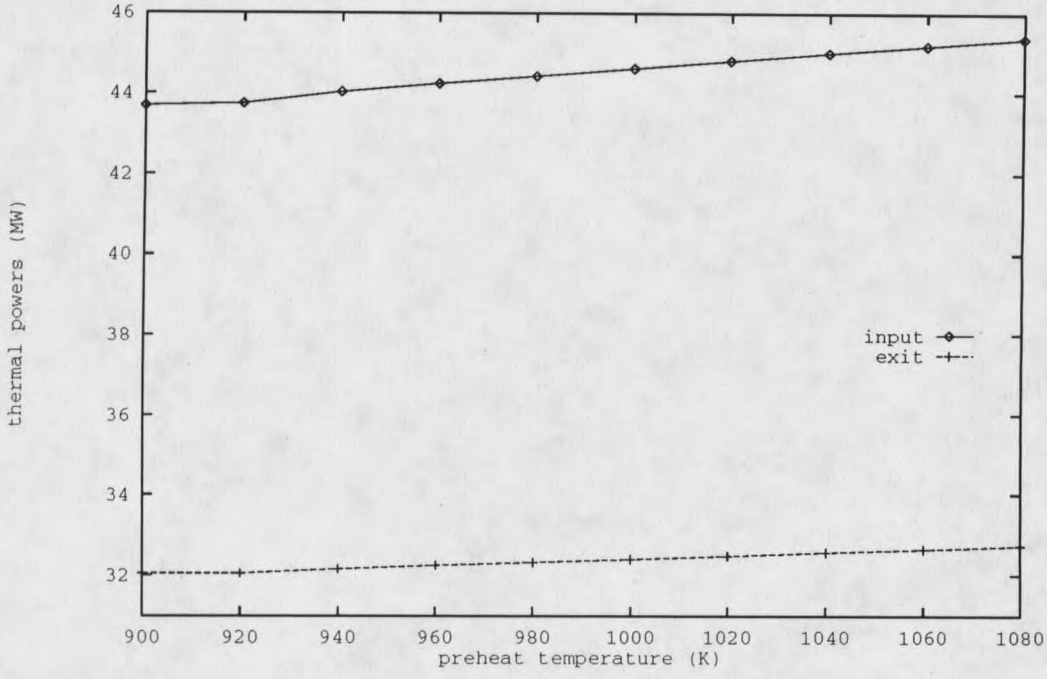

Figure 57: Input and Exit Thermal Power Variation with Preheat Temperature

Figure 58 shows the variation of Mach profile during the parametric study. Greater interaction occurs near the exit of the channel for high preheat temperatures, but this effect is only moderate.

Figure 59 shows that electrodes will carry higher current densities for higher preheat temperature, but this broad range of preheat temperature increases the maximum current densities by only about 13%.

The greatest Hall parameters occur for low preheat temperature (not shown). In this case, there is significant power extraction at low preheat temperatures, so operation at low preheat temperature may be limited by electrode stresses caused by large Hall parameters.

Figure 60 shows that higher electrical power extraction may be expected for

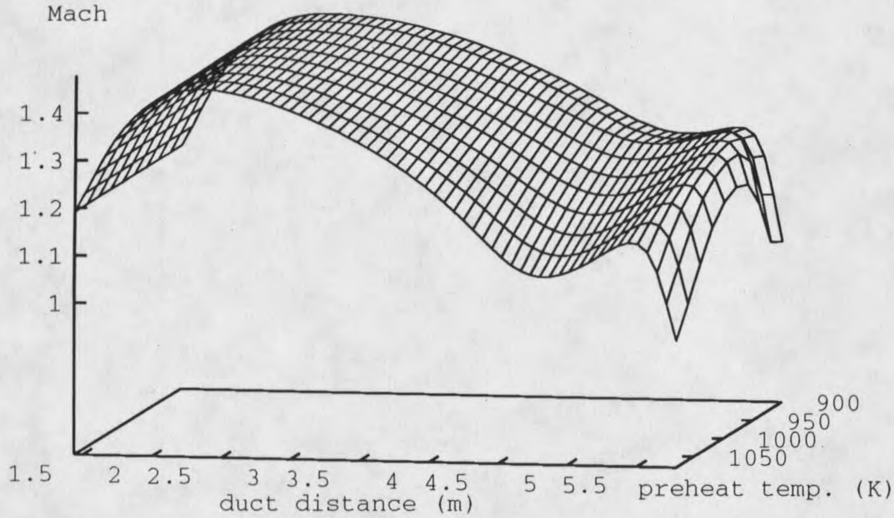

Figure 58: Mach Profile Variation with Preheat Temperature

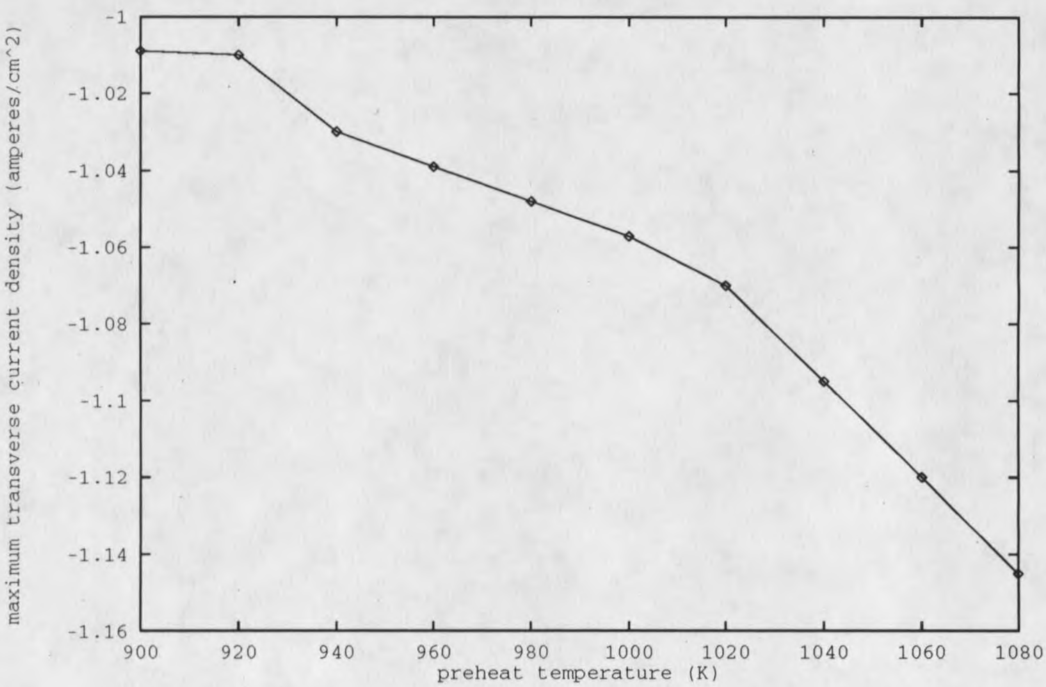

Figure 59: Maximum Current Density Variation with Preheat Temperature

higher preheat temperatures. This figure suggests an optimum near the preheat temperature 1060 K. The increase in electric power represents less than a 6% gain over the parametric domain.

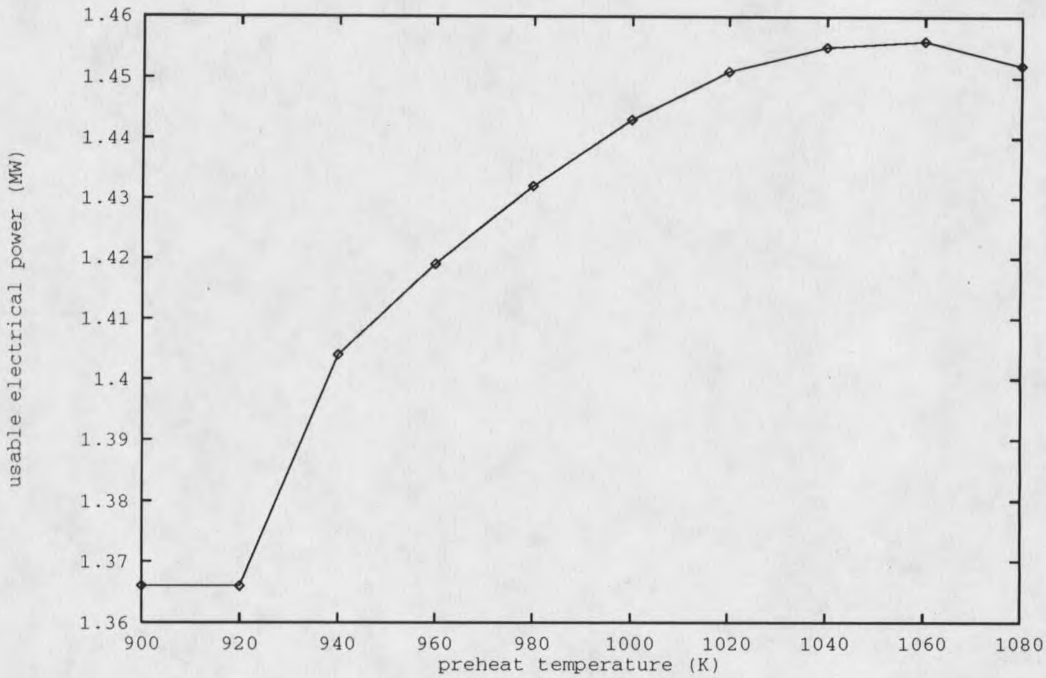

Figure 60: Usable Electric Power Variation with Preheat Temperature

The enthalpic efficiency curve of Figure 61 also shows an optimum, and that maximum enthalpic efficiency of less than 3.3% occurs at a preheat temperature of 1020 K.

It is hypothesized that an optimum occurs in the enthalpic efficiency curve because thermal power loss to the duct walls at high preheat temperature overtakes the initial benefit gained from increasing the combustor thermal power. This hypothesis is backed up by Figure 62. The reason for the apparent outlier data point at preheat temperature 920 K is not known.

Combustor temperatures and diffuser exit temperatures will increase with

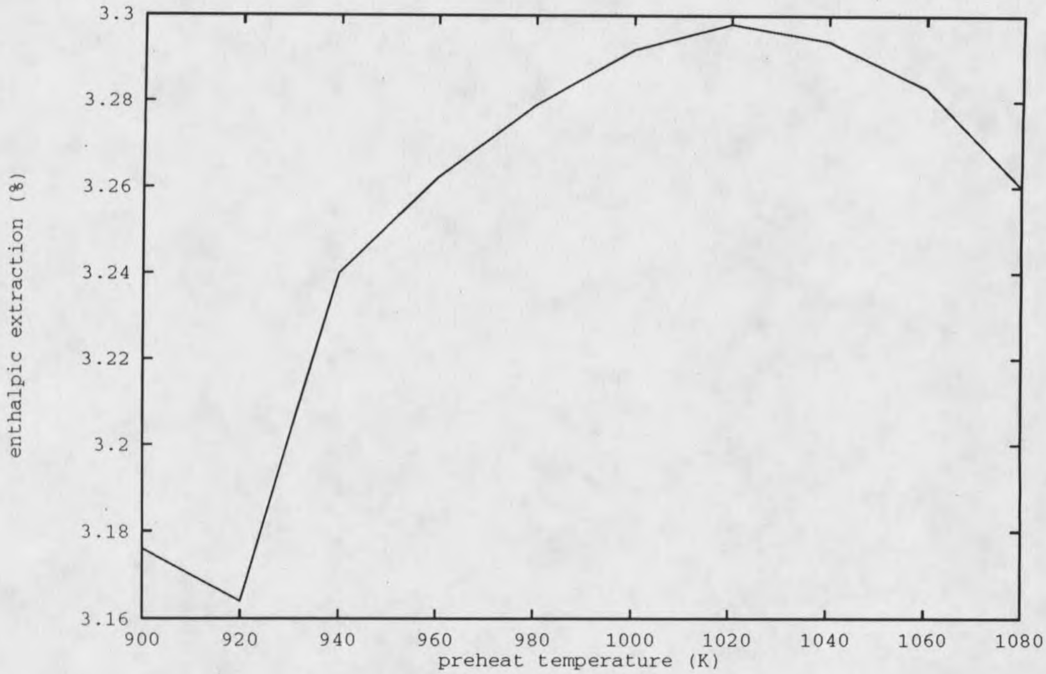

Figure 61: Enthalpic Efficiency Variation with Preheat Temperature

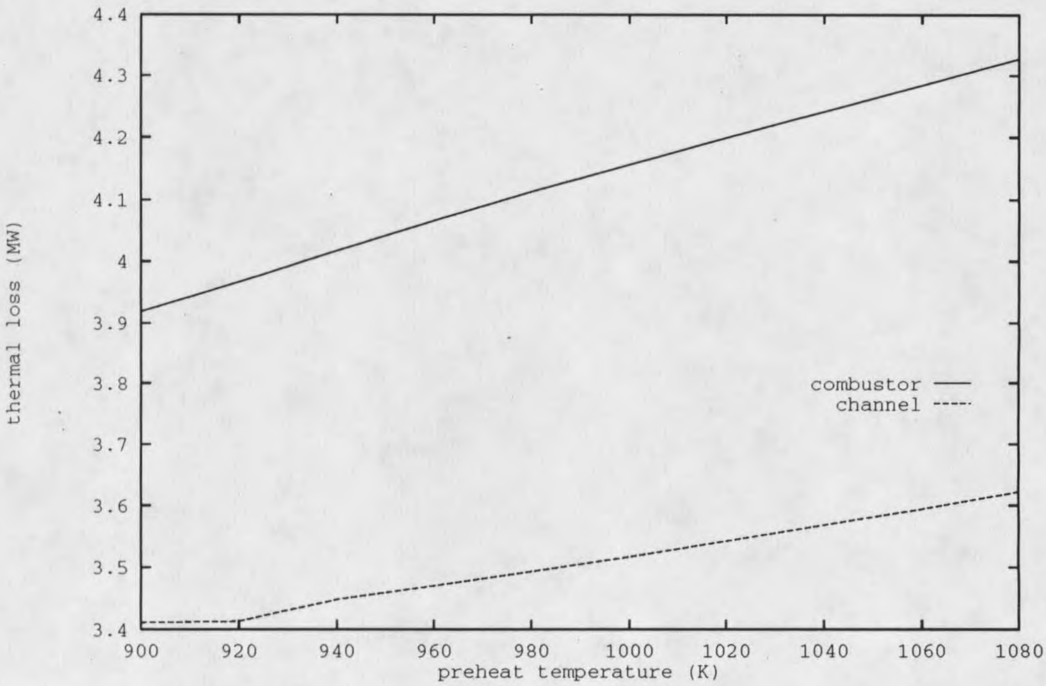

Figure 62: Thermal Wall Loss Variation with Preheat Temperature

increasing preheat temperature. The mechanical stresses imposed by the temperature increases will probably be small.

Load Resistance Variation

This last parametric study investigates the behavior of the thesis POC channel model as load resistance is varied. The result of this type of study is a load line. The extension of a load line to the load current and load voltage axes predicts open and short circuit operating conditions. The slope of a load line is the characteristic conductance of a machine.

A load line was prepared for the thesis POC model. Figure 63 compares the thesis model load line to several load lines compiled in a September 28, 1993 MSE test analysis from the last days of testing on the $1A_4$ POC channel. The comparison data has a number of different combinations of stoichiometric ratio, thermal flow and magnetic induction. These parameter values are given in the figure's key. The variety of operating conditions is included since there is some question about calculation of thermal power and stoichiometric ratio between the model data and the MSE data. It is observed that the thesis model predicts higher electrical powers than those measured in the MSE data. Therefore, the thesis load line is higher than comparable MSE data load lines. The slopes of the MSE $55MW_{th}$ load line and the thesis load line are in good agreement.

Figure 64 shows that the Mach numbers near the channel exit decrease toward the open, high load resistance, condition. The reasons for this behavior will parallel the reasons discussed for the diagonal angle parameter study. A nominal design load resistance should be chosen to minimize axial channel currents, which circulate but do not contribute to power generation. At off-nominal conditions, the loading behavior of a diagonal channel resembles that of a Hall generator. As the loading is moved

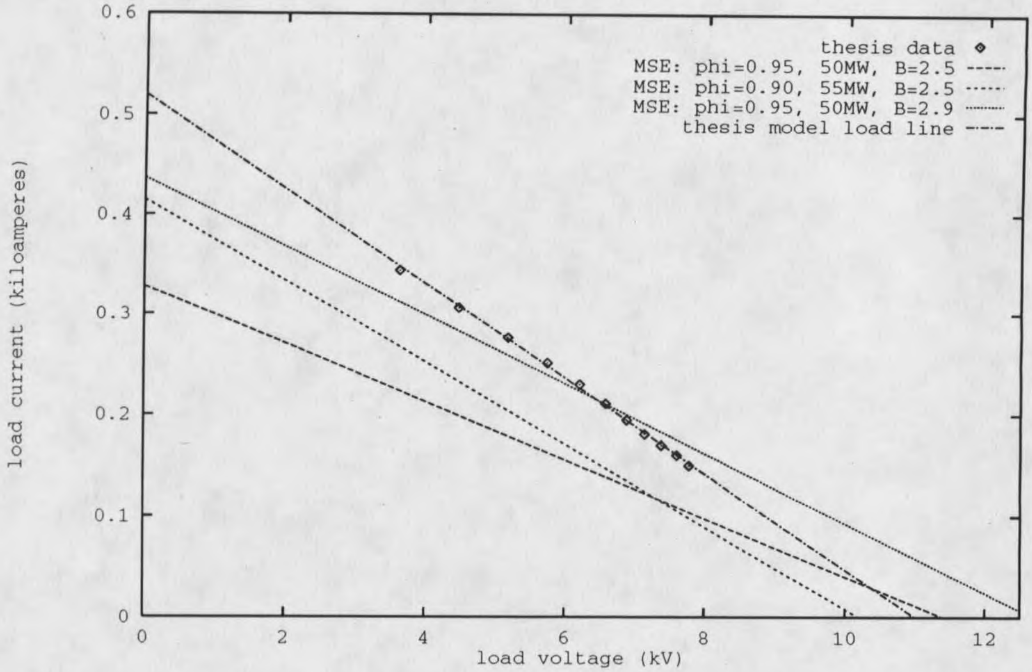

Figure 63: A Comparison of Load Lines

off-nominal toward the open condition, axial currents flow in the negative direction. Conversely, as loading is moved toward the short condition, axial currents will flow in the positive direction.

Figure 65 shows that transverse current densities increase toward the open load condition. While load current is greatest near short circuit conditions (arrow 2), high current density electrode stresses will occur for the open condition (arrow 1). The axial electric field (not shown) is also greatest for the near open loading condition. This observation is understandable given that greatest load voltages occur as one moves toward open loading.

The Hall parameter (not shown) is greatest toward the short loading condition.

Both the generated electrical power (Figure 66) and the enthalpic efficiency curves exhibit maxima near the load resistance of 21 ohms. The value 21 ohms corresponds to the inverse of the slope of the load line in Figure 63.

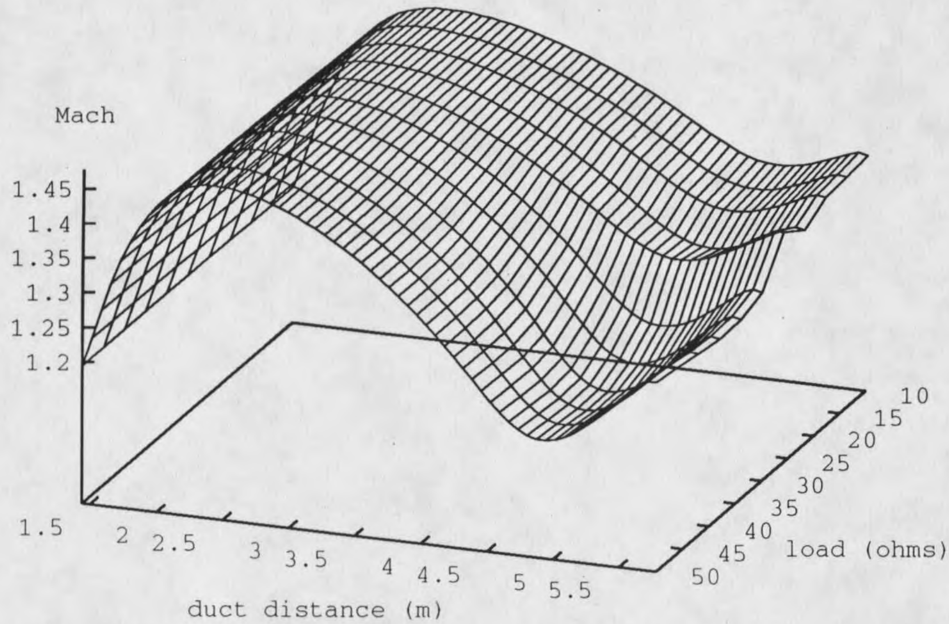

Figure 64: Mach Profile Variation with Load Resistance

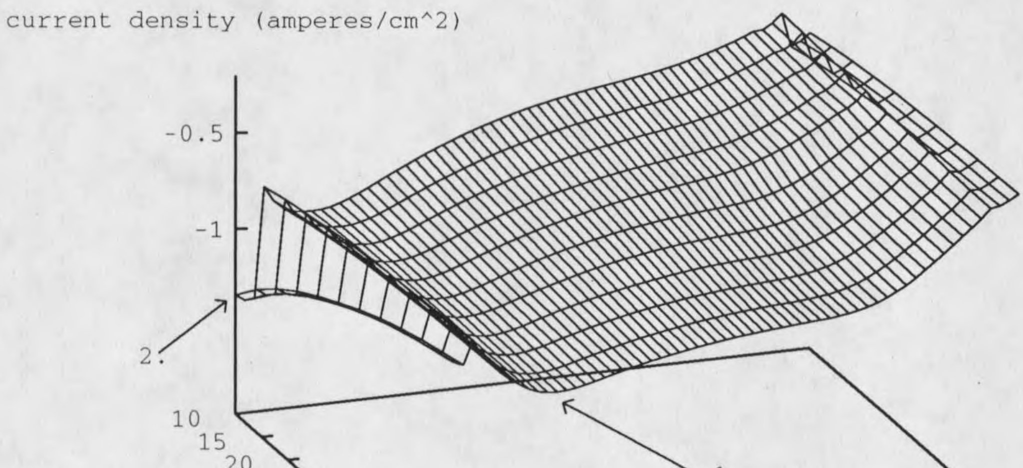

Figure 65: Transverse Current Density Variation with Load Resistance

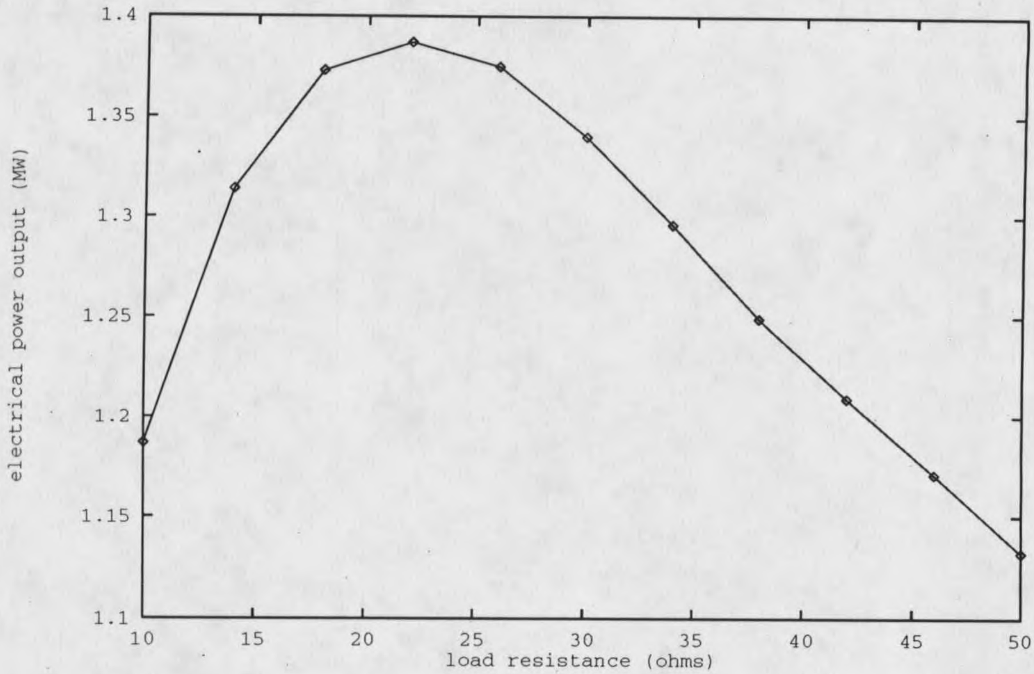

Figure 66: Generated Electric Power Variation with Load Resistance

If possible, this optimum location on the load line should be chosen to optimize generation for any MHD generator operating condition. The load resistance 26 ohm was used as a nominal load resistance throughout this study because the resistance matched data provided by MSE. The value is not far from the identified optimum, but some excess negative axial channel currents should be expected due to the minor mismatch.

Summary of Parametric Results

The results from the parametric studies in this chapter are summarized in Table 5. In this table the first column contains the parametric variable, the second contains the parametric domain, and the remaining columns symbolically represent observed behaviors in each parametric study. The symbols U and L stand for recognized stressful operating conditions at the upper and lower extremes of the domain, respectively. An N means no effect was observed, and an O represents an optimum condition located somewhere between the domain extremes. Those parametric studies having an optimal operating point will have increased stress and reduced efficiencies elsewhere. The small letters u, l and o have the same meanings as their capital counterparts, but the observed relation is either weak or it is less important. Small letters may be used, for example, when the engineer has little control over the parameter or when stressful operation is unlikely.

		shock	arcing	efficiency	thermal	combustor	exit
coal flow rate	1.5–2.2 kg/s	L	h	H	H	H	h
magnetic induction	1.5–3.5 tesla	H	h	L	h	N	l
diagonal angle	35–64°	h	h	O	o	N	o
stoichiometric ratio	0.8–1.0	H	h	l,o	h	h	h
oxygen enrichment	0.31–0.44	H	h	l,o	h	h	h
seed fraction	0.003–0.024	h	H	o	l	l	l
preheat temperature	900–1080 K	h	h	o	h	h	h
load resistance	10–50Ω	h	h	O	o	N	o

Table 5: A Summary of Parametric Study Results

Axial electric field and transverse current density were chosen to represent imminent electrode stresses in the table. However, small letters were used in the "arcing" column whenever the Hall parameter variation might cause arcing elsewhere in the parametric domain.

The symbols in the "efficiency" column reflect parametric locations of unacceptable efficiency. This definition is made for the sake of consistency so that all columns warn of poor or detrimental operation.

CHAPTER 7

DISCUSSION AND CONCLUSIONS

Model Capabilities and Accuracy

The quasi-one-dimensional, Euler MHD equation set was solved to determine steady-state profiles using the state variables pressure P, velocity v_x, and stagnation internal energy $\mathcal{E}_o$. The conservation equation set assures conservation of mass, momentum and energy. Side equations consisting of standard fluid and thermodynamic relations were solved between each update of the state variables. Real gas behavior was modeled by spline interpolation of a number of equilibrium and combustor state tables. Boundary effects were introduced to the equations through a set of empirical equations representing fully developed, turbulent flow.

Limited MSE data was available for fluid state comparison , but a reasonable supersonic velocity profile and an accurate pressure profile were obtained through the channel. The fluid model's placement of a shock in the diffuser rather than in the transition section is questionable, and the questionable Mach behavior in those sections limit the confidence with which study results in the transition and diffuser regions can be reported. It is argued that results from the combustor, nozzle and channel should not be greatly affected by the possible mislocation of the shock, especially for supersonic channel flow.

The comparison of data is complicated somewhat by differences between the definitions of thermal power and stoichiometric ratio used for convenience in the thesis study and those definitions assumed in the MSE POC data. There also may be some disagreement about coal composition. Where possible, adjustments were made to assure that similar quantities were compared.

It was also found that the fully developed, turbulent flow model underestimated the channel thermal wall cooling requirements by 30% at nominal operation. This result agrees with given citations which claim that MHD effects in the channel may increase frictional and thermal losses by as much as 30%. These effects were not included in this thesis model, but they would be worthwhile improvements to thesis model accuracy.

The electrical interactions within the POC MHD channel were separated into an internal equivalent circuit model and an external circuit model. The external circuit modeled the POC diagonal electrode configuration. The internal circuit model is based on Ohm's law and simulates MHD interactions with electrical circuit elements like resistors and dependent voltage sources.

The voltage drop was estimated from an integral type model. The model sums the contributions of slag, thermal boundary layer and electrical sheath voltage drops to approximate the total voltage drop. The model calculates anode and cathode drops in the same way. No data was available for comparison, but typical total electrode voltage drops from the middle of the channel were 80 volts at each electrode surface.

It was found that the electrical model overestimated electrical power extraction by about 0.4 MW. Possible causes of this overestimation include insufficient voltage drop, unmodeled slag leakage [71], insufficient equivalent circuit model discretization, optimistic conductivity values, and nonuniformity effects. Of these, unmodeled slag leakage and nonuniformity effects are most likely causes of the model error.

Patankar's SIMPLER finite volume algorithm was used to integrate the fluid equation set. The method stably and rapidly solves for a steady-state solution without numerically marching along in time.

The internal and external circuits were separated and solved by relaxation. The advantage to this numerical procedure is that the external circuit may be altered to model any electrode configuration. This capability was used in this thesis to investigate the effect of changing electrode overlap. It was found that the stability of the relaxation is improved by including the resistive portion of the electrode drop in the external circuit model.

Allowable MHD Operating Region

After the thesis model nominal operation was checked against nominal MSE data, the thesis model was subjected to eight parametric studies. One of the purposes of the parametric studies was to determine an allowable operating region. Although the POC channel modeled in this thesis has no bottoming cycle for the fluid exiting the diffuser, the allowable operating region for an MHD generator will be of interest for combined cycle MHD-steam plants. The combined cycle plant will certainly be limited by any limitation on the MHD cycle operation.

A set of criteria were chosen to indicate stressful operating conditions. No shock is allowed to enter the MHD channel, the likelihood of interelectrode arcing should be avoided, cooling requirements must remain small, and there must not be large mechanical stresses within the combustor or at the diffuser exit. Axial electric field and transverse current densities are the primary indicators of imminent interelectrode arcing. Hall parameter was also monitored since the Hall parameter decreases the transverse current density magnitude at which arcing begins. Thermal stresses and pressure stresses were assumed to be excessive if they exceed nominal operating values by 20%.

It was found that the allowable operating region of the POC generator is very large. With several exceptions, all tested portions of the parametric domain demonstrated acceptable stress levels. These exceptions and a number of trends will be pointed out below. It must be kept in mind that transverse current density from the MSE data is about 75% of that estimated by the thesis model, and the power extraction for the thesis model is greater than that measured by MSE.

No definitive claims can be made about the combined effects of two or more simultaneous parameter variations. The response of any MHD generator will be nonlinear over the operating region. However, the observations and trends found in this thesis may help one predict the results of simultaneous parameter variations.

The Hall parameter never exceeded 3.3. Furthermore, the gradient of Hall parameter and the gradient of transverse current density almost always point in opposite directions. A nominal design which has an acceptable mix of Hall parameter and current densities will not have both increased Hall parameter and increased current density during off-nominal operation. Therefore, concern about Hall parameter is a design concern only. A minor exception to this statement exists for oxygen enrichment.

Shock stresses occurred at very low total flow (coal flow < 1.5) and at high MHD interaction (induction ≥ 3). In both cases the actual allowable domain is probably larger than predicted because the thesis model overestimates electrical extraction. For all parametric variables except coal flow rate, the Mach profile approaches a channel shock condition as the transverse current density increases. Increased current density increases the $\vec{j} \times \vec{B}$ MHD interaction and reduces Mach numbers. Increased current densities may be caused by increased power extraction as it was for the seed fraction parametric study, or it may be caused by a decrease in efficiency as it was for the load resistance parametric study.

Increased transverse current density and increased axial electric field occur together because the axial field is caused by transverse currents. Neither variable became excessive in any of the parametric studies. This statement is tempered by the fact that both are overpredicted in magnitude by the thesis model. The greatest transverse current densities occurred for the maximum diagonal angle. Interelectrode arc stresses share common causes with Mach stresses, and the likelihood of arcing and of shocking will occur together for the POC channel.

Excessive combustor pressure stress is related nearly linearly to the total flow rate. Therefore, combustor pressure exceeds the nominal combustor pressure by 20% whenever total flow exceeds nominal flow by the same percentage. The coal flow parametric study exceeded this total flow rate toward the upper extreme of its domain. The oxygen enrichment domain also caused a large combustor pressure variation and would exceed 120% of the nominal design pressure for oxygen enrichment less than 0.31. In practice, one would not operate the POC channel in this part of the domain because of poor efficiencies at low oxygen enrichment levels.

Nominal thermal cooling requirements of the combustor and channel were not exceeded in any parametric study by more than 20%, but the channel cooling requirement nearly reached this threshold at the highest coal flow rate (2.2 kg/s). An interesting observation was made. Increase in stoichiometric ratio strongly increases channel thermal stresses without a great change in combustor stress level; increase in oxygen enrichment increases combustor thermal stresses without greatly affecting the channel thermal stress.

The stresses at the diffuser exit are difficult to interpret, but it is observed that temperature will be greater at the diffuser exit for inefficient operation than it will be for efficient operation.

It is not clear how many of these observations and trends are transferable to other and possibly larger MHD generators. Demonstration and commercial MHD generators will nominally operate at high MHD interaction. At high magnetic induction, a channel may be close to allowing a shock to enter the channel. Therefore, the allowable operating region of a larger, high interaction channel may be much smaller than that found for the POC generator.

Potential MHD Contribution to Load Following

In this section the second thesis question is addressed. How might the MHD portion of a combined MHD-steam plant contribute to load following? First, assume that the MHD generator is designed to operate near the top of its machine ratings. Load following will then entail reduction in power output to match a given load. The results from the previous section imply that a great number of options exist for decreasing power output. These options include reducing seed, reducing stoichiometric ratio, reducing oxygen enrichment, reducing flow, reducing the preheat temperature, reducing the magnetic induction, choosing an inefficient load resistance, or any combination of these. If the allowable operating region for the MHD duct is large, as it is for the POC duct, then the combined MHD-steam plant operator has overwhelming freedom in choosing an optimum combined cycle operation. No more can be said of this particular problem until one examines combined cycle operation.

It is more reasonable that bottoming and topping cycle operations would be optimized individually with the constraints that total power generation match the given load and that the interface between topping and bottoming cycle share common pressure, flow rate and stagnation enthalpy. There are two obvious advantages to this simplification. First, the scope of the problem becomes manageable. Second, the MHD channel is well utilized. Thermal and abrasion stresses (not addressed in this thesis) occur whether power is produced or not. Therefore, the time between scheduled shut down and refurbishment of the MHD channel will be determined by thermal flow hours. Because of this and other fixed costs in MHD generator operation, one may decide to shut down the MHD duct altogether when its efficiency becomes lower than that of a bottoming cycle. The results from the parametric studies suggest some strategies which allow efficient operation as load is decreased:

Both oxygen enrichment and stoichiometric ratio should be chosen to be as great in magnitude as possible without causing thermal stresses. It is understood that other factors, such as nitrogen oxide emissions, play a part in this decision. Oxygen enrichment causes thermal stress primarily in the combustor. Stoichiometric ratio causes thermal stress primarily in the channel. Stoichiometric ratios greater than one have no benefit and decrease generator efficiency.

There is an optimal seed fraction at about 0.015. At this level of seeding, fluid conductivity is high. Additional seed contributes little to the generated power, but the combustion process must heat the seed mixture and dissociate the salt. Therefore, excess seed lowers the specific stagnation enthalpy of the fluid mixture. In practice, a greater seed fraction may be chosen to remove most of the coal sulfur pollutant.

An optimum efficiency occurred at the preheat temperature 1020 K for the POC duct. It is hypothesized that the optimum occurs because initial increases in fluid stagnation enthalpy improve electrical extraction efficiency, but at higher oxidant preheat temperatures thermal loss to walls cancels out any gains. For a given oxygen enrichment and stoichiometric ratio, the preheat temperature should be chosen near this optimum.

During the design process, an optimum diagonal angle must be chosen. The most efficient diagonal angle minimizes axial channel currents. For the diagonal MHD generator, the diagonal angle is set during design, and any off-nominal operation results in circulating currents and inefficiency. An interesting control problem would be to describe the steady-state parameter space for which the axial current is always minimal for the choice of diagonal angle. It is more likely that the problem will be addressed by employing shuffle circuits or other electrode current controllers [72, 73, 74, 28] which can prevent axial currents and improve efficiency during off-nominal operation. The POC has no such capability.

The most striking observation is that for efficient operation at a given magnetic induction, the MHD generator flow rate should be just enough to stabilize the supersonic duct flow. As shown in the coal flow rate parametric study, any flow rate above this quantity decreases generator efficiency. It is a significant finding of this study that modeled power output does not increase greatly with increased flow rate. Note that this observation interrelates coal flow rate and magnetic induction. It is likely that coal flow rate will be chosen based on the needs of the bottoming cycle or load, and the induction will be increased until the supersonic flow through the channel is no more than stabilized.

During any channel operation, the ratio of load voltage to load current must be chosen to be equal to the characteristic resistance of the channel. This choice of load resistance optimizes electrical power output.

The above discussion suggests a possible control strategy for using the MHD channel to meet changing loads: Choose diagonal angle, stoichiometric ratio, oxygen enrichment, seed fraction, and preheat temperature optimally as described above. While these optima may change over the operating region, they are a reasonable first guess for off-nominal operation. Coal flow rate is chosen to meet the needs of the load or bottoming cycle, if there is one. The magnetic induction is adjusted to just stabilize the channel supersonic flow. The generator's location on a load curve must be constantly monitored and optimized.

The parametric studies in this thesis have demonstrated a large allowable operating region for the POC channel. It is difficult to extend this result to other or larger MHD channels. If one considers only efficient methods of load following, the efficiency data collected during the parametric studies suggests a general strategy for changing power output to supply varying loads. There is no reason that this strategy could not be adapted to other and larger MHD generators. However, the proposed strategy is only one of many possible strategies, and additional steady-state and transient simulations are needed.

Suggestions for Further Research

As a last section to this thesis, several possible extensions to this body of research shall be suggested. These extensions include electrical model improvements, fluid model improvements, investigation of transient responses, and combined cycle studies. Boundary layers should become less influential for the study of larger MHD generators. Volume increases faster than wall surface area. Therefore, boundary effects will become a lesser and lesser fraction of the total generator output for large MHD generators. The thesis model accuracy may improve for large MHD generators without any further model improvements.

The simplest correction to the electrical model may be the inclusion of leakage currents, currents which flow axially through the conductive slag layer. The slag leakage currents may cause as great as 20% power loss in a 10 MW generator [29]. The slag leakage current might be modeled in the external electrical circuit using resistors between adjacent cathodes, adjacent anodes, or both. The magnitude of the resistors can be approximated by

$$R_s = \frac{\delta_i}{\sigma_s \delta_s w}, \tag{54}$$

where δ_i is the insulator separation between adjacent electrodes, σ_s is the slag conductivity, δ_s is the slag thickness and w is the electrode width. If one assumes a slag thickness of 1 mm and a slag conductivity of $15\mho/m$, a 1.4Ω resistor should be used between adjacent electrodes in the middle of the POC channel model. This resistor would result in a leakage current of about 25 amperes axially along an electrode wall.

Alternatively, the effect of current leakage may be modeled by multiplying the segmentation factor by about 13. Rosa [71] and Petty [75] have suggested this method of leakage current correction. Along the cathode wall, groupings of 10–15 electrodes become essentially shorted together by polarized slag. Transient arcing between these groupings break the slag continuity, and the slag burn-off locations vary with time. For this reason, effective cathode segmentation is decreased, but the continuous path for current leakage to ground along the electrode walls is limited. It is not clear which of the above two methods for modeling leakage current is better.

A nonuniformity factor [3] may be used in the internal circuit model. The nonuniformity factor accounts for the decrease in electrical power output caused by fluid inhomogeneity in the axial direction. The factor is difficult to quantify and justify on a first principles basis. For this reason it was not included in the thesis model.

Gradients of Hall parameter and conductivity can be approximated along the channel length by numerical means. However, these macroscopic parameter gradients do not reflect the periodic gradients caused by electrode segmentation or the time-dependent nonuniformities caused by turbulence and uneven seed or fuel flow. At best, the model nonuniformity factor must be modified until empirical results are matched. This thesis may provide enough data to quantify the nonuniformity factor for the POC generator and improve the accuracy with which the thesis model matches MSE data. A nonuniformity factor of 1.2 is suggested as a starting place.

It has been shown that measured conductivity is only about 0.85 of the theoretical conductivity in an MHD channel [55]. It is not clear how this data might be included in the thesis model. Perhaps the factor is another manifestation of the nonuniformity factor, which is close in magnitude to the reciprocal of "SIGFAC" in the above citation.

Other researchers have used finer equivalent circuit model discretization in the transverse direction. It is questionable whether anything can be gained by fine transverse discretization of the equivalent circuit model when the fluid model is simply quasi-one-dimensional. Nonetheless, this is another area which might be investigated to correct the thesis model's overprediction of electrical power.

The boundary layer interaction may be improved in a quasi-one-dimensional fluid model by separating the viscous and inviscid flow and integrating each simultaneously [76, 24]. These methods better approximate the development of turbulent boundaries, but they require additional computation. If one utilizes higher dimension models, there is no need to separate the boundary and core flows. Finer discretization must be used near the duct walls. Turbulence effects were especially thoroughly modeled in a two-dimensional formulation by Mazzanti and Borghi [35]. Some parts of this method might be used to improve the thesis boundary layer model.

Most higher dimension models assume parabolic flow in the major flow direction. Transverse flow is calculated by a method like SIMPLER, and the results from the transverse flow calculation are used to update the axial pressure profile using the principle of mass conservation [42, 53]. Such models can be used to very accurately model flow in the supersonic channel, but they will fail in the diffusers, where flow is elliptic. The calculation of fully elliptic, three-dimensional flow is very computationally expensive [42]. The discretization dimensions of the electrical model should agree with those of the fluid model, and the electrical model must be of at least as high dimensionality as the fluid model.

The thesis computer model can be easily extended to model transient behaviors within an MHD duct. Only minor modification of the three conservation equations would be necessary. Because the method is fully implicit, the additional time dependence terms may be treated as source terms, and integration proceeds as before. The densities, velocities and stagnation internal energies at a previous time step bias the present calculation of the state. One iterates to a converged solution, records the state at the present time, then again iterates to a converged solution given some finite time step. External electrical circuits which contain energy storage elements like inductors or capacitors would require numerical approximations to time integration or differentiation.

An implicit integration method assumes the future state immediately from the beginning of any integration time step. In contrast, fully explicit methods assume the last calculated state remains constant until a the next time step integration has been completed. Higher order methods interpolate the state between time steps. It may be convenient to use time steps on the same order of magnitude as the electrical and power electronic response times. These response times will be slightly greater than the MHD fluid response times. Consequently, such time-dependent solutions will have meaning from the electrical power generation standpoint, but the MHD fluid high frequency responses will be washed out.

In this thesis, the operational region was investigated through a series of parametric studies in eight independent variables. Each parametric study investigated one vectored domain direction. One independent variable changed while all others remained constant. The research should be extended to investigate the effects of simultaneous parameter variations over the operational domain. If simultaneous parameter variations bring about unacceptable operation, additional limitations on the allowable operating region should be noted. An algebraic function might then be formed to represent steady-state behavior of the MHD generator. This algebraic function could then be used to investigate combined MHD-steam plant operation.

REFERENCES

[1] R. A. Coombe, ed., *Magnetohydrodynamic Generation of Electrical Power.* New York: Reinhold Publishing Corp., 1964.

[2] K. R. Cramer and S. I Pai, *Magnetofluid Dynamics for Engineers and Applied Physicists.* New York, New York: McGraw-Hill Book Company, 1973.

[3] R. J. Rosa, *Magnetohydrodynamic Energy Conversion.* New York, New York: McGraw Hill, 1968.

[4] V. A. Kirillin and A. E. Sheyndin, eds., *MHD Energy Conversion—Physiotechnical Problems.* American Institute of Aeronautics and Astronautics, Inc. and VAAP (the USSR Copyright Agency), 1983. Translation of *Magnitogirdrodinamicheskoe preobrazavanie energii.*

[5] V. R. Malghan, "Towards commercialisation of MHD power plants—a look at the international programmes," *Energy Conversion Management*, vol. 25, no. 2, pp. 225–47, 1985.

[6] M. Petrick and B. Y. Shumyatsky, eds., *Open-Cycle Magnetohydrodynamic Electrical Power Extraction.* Argonne, Illinois: Argonne National Laboratory, 1978.

[7] J. B. Heywood and G. J. Womack, eds., *Open-Cycle MHD Power Generation, (Results of Research Carried out by Members of the British MHD Collaborative Committee).* Oxford: Pergamon Press, 1969.

[8] F. E. Walter, R. J. Labrie, and J. M. Sherick, "Billings magnetohydrodynamics demonstration project viable by year 2000," *Symposium on Engineering Aspects of Magnetohydrodynamics*, vol. 31, June 29–July 1 1993.

[9] M. Ishikawa, H. Yawata, and J. Umoto, "Dynamical behavior of MHD-steam combined system of pilot plant scale," *Energy Conversion Management*, vol. 32, no. 2, pp. 123–31, 1991.

[10] D. T. Trung, *System Analysis of the Integration of a Segmented MHD Generator into an AC Power Network.* PhD thesis, University of Sidney, January 1981.

[11] S. Matair, *Interaction of an MHD Generator with a Line Commutated Inverter System.* PhD thesis, University of Sydney, March 1985.

[12] R. B. Boulay, R. E. Weinstein, and J. C. Cutting, "A simulation of the dynamics of a magnetohydrodynamic/steam power plant," *Symposium on Engineering Aspects of Magnetohydrodynamics*, vol. 19, pp. 14.4–8, June 15–17 1981.

[13] W. D. Jackson, G. R. Seikel, R. J. Harrington, S. A. A. Gawish, and S. S. Rowithal, "Modeling of MHD generators for transient stability analysis," *Symposium on Engineering Aspects of Magnetohydrodynamics*, vol. 24, pp. 251–62, June 24–7 1986.

[14] W. D. Jackson, G. R. Seikel, O. S. Mazzoni, F. E. Bernard, and R. J. Harrington, "Transient modeling and analysis of MHD plants," *Symposium on Engineering Aspects of Magnetohydrodynamics*, vol. 29, pp. VII.1.1–12, June 18–20 1991.

[15] D. A. Rudberg and R. M. Johnson, "A manual of dynamic system modeling for MHD/steam power plants," tech. rep., Montana State University Electronic Research Laboratories, Bozeman, Montana, c. 1980.

[16] J. D. Aspnes and D. A. Pierre, "Dynamic modeling and control of magnetohydrodynamic/steam electrical power generating plants," *Symposium on Engineering Aspects of Magnetohydrodynamics*, pp. X.1.1–7, May 16–18 1977.

[17] R. Johnson and T. Robles, "Transient response of MHD/steam bottoming plants with phased air preheaters and heat capacitor," *Symposium on Engineering Aspects of Magnetohydrodynamics*, vol. 17, pp. I.4.1–5, March 27–9 1978.

[18] D. A. Pierre and D. A. Rudberg, "First-principle component models for control system simulation of MHD-steam plants," *Symposium on Engineering Aspects of Magnetohydrodynamics*, vol. 18, pp. F.4.1–6, June 18–20 1979.

[19] D. Pierre, C. Dudding, and D. Miller, "MHD combustor/nozzle/channel/diffuser simulation and input-output modeling," Tech. Rep. 1276, Montana State University Electronic Research Laboratories, 1976.

[20] A. Chandra, B. S. Bhadoria, U. K. Singh, and S. S. Varma, "Analysis of MHD channel including heat and friction losses," *Symposium on Engineering Aspects of Magnetohydrodynamics*, vol. 30, pp. X.3.1–8, June 29–July 2 1992.

[21] V. M. Faires and C. M. Simmang, *Thermodynamics*. Macmillan Publishing Co., Inc., sixth ed., 1978.

[22] P. M. Prenter, *Splines and Variational Methods*. New York: John Wiley and Sons, 1989.

[23] C. C. P. Pian, S. W. Petty, E. W. Schmitt, D. J. Morrison, and L. C. Farrar, "Electrical characteristics of MHD generator sidewalls with straight-and Z-bar designs," *Symposium on Engineering Aspects of Magnetohydrodynamics*, vol. 29, pp. II.2.1–10, June 18–20 1991.

[24] M. Yoshida and J. Umoto, "A new quasi-two-dimensional analysis of whole electrical and gasdynamical performances of linearly-diverging diagonal type generator," in *International Conference on MHD Electrical Power Generation*, 7, (MIT, Cambridge, Massachusetts), pp. 524–9, June 16–20 1980.

[25] D. J. Hammerstrom, "A computer model of the coupled dynamic fluid and electrical interactions within an MHD duct," Master's thesis, Montana State University, Bozeman, Montana, November 1991.

[26] D. J. Hammerstrom and R. M. Johnson, "A dynamic MHD duct model for study of electrical power extraction," Tech. Rep. 290324-2, Montana State University, September 1991.

[27] D. J. Hammerstrom and R. M. Johnson, "Improvements to a dynamic MHD state model," Tech. Rep. 290324-3, Montana State University, September 1992.

[28] Y. Inui, K. Morimoto, M. Ishikawa, and J. Umoto, "Active and reactive power control of Faraday type MHD generator using new power consolidation-inversion-control system," November 1991. Advanced copy of paper submission.

[29] M. Ishikawa, T. Suemura, M. Fujita, and J. Umoto, "Effects of external control circuit on coal-fired supersonic diagonal MHD generator," *AIAA Fluid Dynamics, Plasma Dynamics and Lasers Conference*, vol. 22, June 24–6 1991.

[30] M. Ishikawa, T. Sugiyama, K. Kishimoto, and J. Umoto, "Preliminary study on control of electrical nonuniformities," *Symposium on Engineering Aspects of Magnetohydrodynamics*, vol. 23, pp. 854–68, 1985.

[31] M. Ishikawa, K. Krishimoto, S. Fukutomi, and J. Umoto, "Simulation of electrical nonuniformities induced in diagonal type generator," *Symposium on Engineering Aspects of Magnetohydrodynamics*, vol. 24, pp. 57–64, June 24–7 1986.

[32] F. Martinez-Tamayo, V. J. Hruby, and B. Pote, "Power management for the integrated topping cycle," *Symposium on Engineering Aspects of Magnetohydrodynamics*, vol. 30, pp. XII.1.1–12, June 29–July 2 1992.

[33] M. Yoshida and J. Umoto, "Influences of coal slag on electrical characteristics of a Faraday MHD generator," *Energy Conversion Management*, vol. 29, no. 3, pp. 217–26, 1989.

[34] L. J. Kovalsky, "Current consolidation systen hardware for the $1A_4$ MHD channel," *Symposium on Engineering Aspects of Magnetohydrodynamics*, vol. 30, pp. XII.2.1–10, June 29–July 2 1992.

[35] G. Mazzanti and C. A. Borghi, "Steady state twodimensional model for linear MHD generator channel analysis," *Symposium on Engineering Aspects of Magnetohydrodynamics*, vol. 29, pp. X.6.1–5, June 18–20 1991.

[36] M. Ishikawa, H. Sugitatsu, and J. Umoto, "Effect of shock-boundary layer interaction in an MHD channel of pilot plant scale," *Symposium on Engineering Aspects of Magnetohydrodynamics*, vol. 30, pp. P.12.1–7, June 29–July 2 1992.

[37] J. Gertz, T. Opar, A. Solbes, and G. Weyl, "Modeling of MHD channel boundary layers using an integral approach," *Symposium on Engineering Aspects of Magnetohydrodynamics*, vol. 18, pp. B.4.1–7, June 18–20 1979.

[38] G. P. Gupta and V. K. Rohatgi, "Comparative study of electrode voltage drops in MHD generators with and without ash in the combustion products," *Energy Conversion Management*, vol. 23, no. 1, pp. 37–41, 1983.

[39] S. W. Petty *et al.*, "Electrode phenomena in slagging MHD channels," *Symposium on Engineering Aspects of Magnetohydrodynamics*, vol. 16, pp. VIII.1.1–12, May 16 1977.

[40] S. W. Petty, A. Dunton, J. Reich, W. Simpson, and L. C. Farrar, "1A_4 channel design and fabrication," *Symposium on Engineering Aspects of Magnetohydrodynamics*, vol. 29, pp. II.1.1–9, June 18–20 1991.

[41] G. A. Sod, *Numerical Methods in Fluid Dynamics.* Cambridge: Cambridge University Press, 1985.

[42] S. V. Patankar, *Numerical Heat Transfer and Fluid Flow.* Hemisphere Publishing Corporation, 1980.

[43] H. K. Messerle, Y. Fang, S. W. Simpson, and S. M. Marty, "Sub-atmospheric disk generators for coal-fired MHD/steam combined power plant," *Energy Conversion Management*, vol. 29, no. 4, pp. 273–8, 1989.

[44] A. Massarini and C. A. Borghi, "Time-dependent quasi-onedimensional flow models for linear MHD generator channels," *Symposium on Engineering Aspects of Magnetohydrodynamics*, vol. 29, pp. X.2.1–6, June 18–20 1991.

[45] P. D. Lax, *Hyperbolic Systems of Conservation Laws and the Mathematical Theory of Shock Waves.* Philadelphia, Pennsylvania: Society for Industrial and Applied Mathematics (SIAM), 1973.

[46] R. Gruber and J. Rappaz, *Finite Element Methods in Linear Ideal Magnetohydrodynamics.* Berlin: Springer-Verlag, 1985.

[47] C. A. Borghi, A. Massarini, G. Mazzanti, and P. L. Riani, "One- and two-dimensional models for a linear MHD generator channel design," *Symposium on Engineering Aspects of Magnetohydrodynamics*, vol. 28, pp. IX.2.1–7, June 26–28 1990.

[48] M.-S. Liou and J. Christopher J. Steffen, "A new flux splitting scheme," *Journal of Computational Physics*, vol. 107, pp. 23–39, 1993.

[49] K. W. Anderson, J. L. Thomas, and B. V. Leer, "A comparison of finite volume flux vector splittings for the Euler equations," *AIAA Journal*, vol. 24, pp. 1453–9, September 1986.

[50] A. J. Chapman, *Heat Transfer.* New York: Macmillan Publishing Co., Inc., third ed., 1974.

[51] W. M. Rohsenow and J. P. Hartnett, eds., *Handbook of Heat Transfer*, pp. 7–4. McGraw Hill Book Company, 1973.

[52] P. Satyamurthy, N. Venkatramani, and V. K. Rohatgi, "Analysis of heat fluxes in the electrode walls of a combustion-driven MHD generator," *Energy Conversion Management*, vol. 25, no. 2, pp. 195–8, 1985.

[53] S. V. Patankar and D. B. Spalding, "A calculation procedure for heat, mass and momentum transfer in three-dimensional parabolic flows," *Journal of Heat and Mass Transfer*, vol. 15, pp. 1787–1806, 1972.

[54] W. H. Press, B. P. Flannery, S. A. Teukilsky, and W. T. Vetterling, *Numerical Recipes, the Art of Scientific Computing (FORTRAN Version).* Cambridge: Cambridge University Press, 1989.

[55] R. Braswell, T. Koyama, M. McAllister, S. Myrick, and B. Pote, "50 MW_{th} prototypical combustor performance," *Symposium on Engineering Aspects of Magnetohydrodynamics*, vol. 31, pp. II.1.1–17, June 29–July 1 1993.

[56] D. A. Rudberg. A number of conversations were carried out during 1993 and 1994 concerning combustor models and the MSE combustor data tables.

[57] D. Lofftus. A number of conversations were carried out during 1992, 1993 and 1994 concerning POC channel testing at the MSE, Inc. facility in Butte, Montana.

[58] S. Kuo, E. Levi, and H. Schlachter, "3-Dimensional current distribution in the nozzle of an MHD channel," *Energy Conversion Management*, vol. 24, pp. 347–52, 1984.

[59] S. Kuo, E. Levi, and H. Schlachter, "Prevention of high current concentrations in the nozzle of MHD generators," *Energy Conversion Management*, vol. 25, no. 1, pp. 101–4, 1985.

[60] C. C. P. Pian and A. W. McClaine, "Techniques for the solution of MHD generator flows," *Computers and Fluids*, vol. 12, no. 4, pp. 319–38, 1984.

[61] F. Cheers, *Elements of Compressible Flow.* John Wiley and Sons, Ltd., 1963.

[62] H. Daneshyar, *One-dimensional Compressible Flow.* Thermodynamics and Fluid Mechanics, Pergamon Press, 1976.

[63] N. N. Baranov, D. K. Burenkov, Y. L. Dolinski, A. D. Izerov, V. V. Kirillov, I. I. Klimovski, V. I. Kovbusiuk, B. Y. Shumiatski, A. S. Tihotski, G. L. Uspenskaia, and V. I. Zalkind, "Axial interelectrode breakdown in MHD channels," *Symposium on Engineering Aspects of Magnetohydrodynamics*, vol. 17, pp. XII.1–10, March 27–29 1978.

[64] A. Chandra, "Hall field break down of seeded walls in MHD channel," *Energy Conversion Management*, vol. 28, no. 4, pp. 275–6, 1988.

[65] A. Chandra and R. Panwar, "Current conduction through hot insulation walls in MHD channel," —*Energy Conversion Management*, vol. 32, no. 3, pp. 263–8, 1991.

[66] V. J. Hruby, "Current control and consolidation circuits development at AERL," *Symposium on Engineering Aspects of Magnetohydrodynamics*, vol. 22, pp. 9.2.1–18, 1984.

[67] V. J. Hruby, "Interanode fault prevention and voltage control," *Symposium on Engineering Aspects of Magnetohydrodynamics*, vol. 29, pp. IX.5.1–12, June 18–20 1991.

[68] J. N. Chapman and N. R. Johanson, "Design considerations for a class of 600 MW_e MHD steam combined cycle power plants," *Proceedings of the* 28^{th} *Intersociety Energy Conversion Engineering Conference*, vol. 1, pp. 1.983–1.888, August 8–13 1993.

[69] C. C. P. Pian and A. M. Demirjian, "Loading schemes for a 50 MW_{th} diagonally connected MHD generator," *Journal of Energy*, vol. 6, pp. 418–424, November-December 1982.

[70] A. M. Demirjian and C. C. P. Pian, "Performance of MHD generators with electrode current control," *Journal of Energy*, vol. 6, pp. 261–5, July-August 1981.

[71] R. J. Rosa, "Leakage current and electrode wear processes," *Symposium on Engineering Aspects of Magnetohydrodynamics*, vol. 29, pp. VII.1.1–4, June 18–20 1991.

[72] R. Johnson and M. Donnelly, "A pulse-amplitude-synthesis-and-control (PASC) inversion system for single source diagonally connected MHD generators," in *IEEE/PES Winter Meeting*, no. 93 WM055-4-EC, 1993.

[73] R. Johnson, M. Donnelly, and K. Marcotte, "Pulse-amplitude-synthesis-and control (PASC) consolidation/inversion system for Faraday connected MHD generators," in *IEEE/PES Summer Meeting*, no. 92 SM520-7 EC, (Seattle, Washington), July 12–16 1992.

[74] R. Johnson and V. Skurdal, "Pulse amplitude synthesis and control (PASC) of MHD commercial power output," *Symposium on Engineering Aspects of Magnetohydrodynamics*, vol. 24, June 24–7 1986.

[75] S. W. Petty, "Effects of cathode slag polarization in MHD generator performance," *Symposium on Engineering Aspects of Magnetohydrodynamics*, vol. 21, pp. 4.5.1–12, 1983.

[76] P. Satyamurthy, N. Venkatramani, and V. K. Rohatgi, "Analysis of combustion MHD generator using a coupled core-boundary layer model," *Energy Conversion Management*, vol. 24, no. 1, pp. 67–74, 1984.

APPENDIX

COMMONER Common Block with Definitions

```
C*******0*********0*********0*********0*********0*********0*********
C COMMON VARIABLE FILE
C*******0*********0*********0*********0*********0*********0*********
      IMPLICIT DOUBLE PRECISION (A-H,O-Z)
      IMPLICIT INTEGER (I-N)
      CHARACTER*1 FLAG,FLAG_T
      INTEGER FLAG_L,FLAG_OP,I,J,L

C NEP == number of electrode pairs
C NNDS_MAX == maximum total number of nodes
C PASCALS == conversion factor [ atm --> Pa ]
C RGAS == gas constant

C*******0*********0*********0*********0*********0*********0*********
C PARAMETERS
C*******0*********0*********0*********0*********0*********0*********
      PARAMETER(                            NEP=62,
     &                                      NNDS_MAX=145,
     &                                      RGAS=8.31432D3,
     &                                      PASCALS=1.01325D5)

C*******0*********0*********0*********0*********0*********0*********
C COMMON BLOCKS
C*******0*********0*********0*********0*********0*********0*********
      COMMON /AREA/                         A(NNDS_MAX),A_MIN(NNDS_MAX)
      COMMON /STIFFNESS/                    ALPHA(NEP)
      COMMON /INDUCTION/                    B(NEP)
      COMMON /HALL_PARAMETER/               BETA(NEP)
      COMMON /FRACTION_OF_INDUCTION/        BFACT
      COMMON /ELECTRODE_CURRENTS/           CANODE(NEP),CCATH(NEP)
      COMMON /SPECIFIC_HEAT/                CP(NNDS_MAX)
      COMMON /LOAD_CURRENT/                 CUR_LOAD
      COMMON /CHANNEL_CURRENTS/             CX(NEP)
      COMMON /BOUNDARY_THICKNESS/           DELTA
      COMMON /COMPRESSIBILITY/              DRHODP(NNDS_MAX)
      common /INTERNAL_STAG_ENERGY/         EIO(NNDS_MAX)
      COMMON /WALL_EMISSIVITY/              EW
      COMMON /ELECTRODE_WALL_FRAC/          EWF
      COMMON /FRICTION_COEFFICIENT/         F(NNDS_MAX)
      COMMON /EVENT_FLAG/                   FLAG
      COMMON /LOAD_FLAG/                    FLAG_L
      COMMON /OUTPUT_FLAG/                  FLAG_OP
```

```
      COMMON /REAL_DYNAMIC_FLAG/       FLAG_DT
      COMMON /FLAG_DYNAMIC_FLAG/       FLAG_T
      COMMON /SPECIFIC_HEAT_RATIO/     GAMMA(NNDS_MAX)
      COMMON /ENTHALPY/                H(NNDS_MAX)
      COMMON /PREV_STAG_INT_ERG/       EIO_OLD(NNDS_MAX)
      COMMON /STAGNATION_ENTHALPY/     HS(NNDS_MAX)
      COMMON /MASTER_ELECTRODES/       MA,MC,NOVRLAP
      COMMON /NODES_COUNTS/            NCOMB,NNOZZ,NCHAN,NTRANS,NDIFF,
     &                                                            NNDS
      COMMON /OXYGEN_ENRICHMENT/       OX
      COMMON /PRESSURE/                P(NNDS_MAX)
      COMMON /OXYGEN_PREHEAT_TEMP/     PHEAT
      COMMON /SECONDARY_STOICH/        PHI
      COMMON /SHEATH_POTENTIAL/        POT
      COMMON /EXIT_STAGNATION_P/       PSEXIT
      COMMON /STAGNATION_PRESSURES/    PSTAG(NNDS_MAX)
      COMMON /THERMAL_COEFFICIENT/     Q(NNDS_MAX)
      COMMON /DIAGONAL_RESISTORS/      RCCC
      COMMON /CONSOLIDATOR_RESISTORS/  RCON
      COMMON /ITERATION_FACTORS/       RELAX,RELAXMIN,RELAXMAX
      COMMON /DENSITY/                 RHO(NNDS_MAX),RHO_MIN(NNDS_MAX)
      COMMON /PREVIOUS_DENSITY/        RHO_OLD(NNDS_MAX)
      COMMON /INVERTER_RESISTANCE/     RINVT
      COMMON /LOAD_RESISTANCE/         RL
      COMMON /SEED_FRACTION/           SEED
      COMMON /SEGMENTATION_RATIO/      SEGR
      COMMON /CONDUCTIVITY/            SIGMA(NEP)
      COMMON /DUCT_LENGTHS/            SCOMB,SNOZZ,SCHAN,STRANS,SDIFF,
     &                                                           SBOIL
      COMMON /DXSTEPS/                 STEP(5),STP_MAJ(NNDS_MAX),
     &                                                STP_MIN(NNDS_MAX)
      COMMON /TEMPERATURE/             T(NNDS_MAX)
      COMMON /INTEGRATION_TIMES/       TIME,TIME_0,TIME_F,DT_MIN,
     &                                                       DT_MAX,DT
      COMMON /SLAG_WALL_T/             TS
      COMMON /STAGNATION_TEMPS/        TSTAG(NNDS_MAX)
      COMMON /ELECTRODE_WALL_T/        TW
      COMMON /VELOCITY/                V(NNDS_MAX),V_MAJ(NNDS_MAX)
      COMMON /PREVIOUS_VELOCITY/       V_OLD(NNDS_MAX)
      COMMON /ELECTRODE_VOLTAGES/      VANODE(NEP),VCATH(NEP)
      COMMON /VOLTAGE_DROPS/           VD(NEP),VDR(NEP)
      COMMON /INVERTER_BACK_EMF/       VINVT
      COMMON /LOAD_VOLTAGE/            VLOAD
      COMMON /MACH_NUMBER/             VMACH(NNDS_MAX)
      COMMON /CHANNEL_VOLTAGES/        VX(NEP),VY(2,NEP)
      COMMON /FLOWRATE/                W(NNDS_MAX)
      COMMON /COAL_FLOWRATE/           WC
      COMMON /MOLECULAR_WEIGHT/        WM(NNDS_MAX)
      COMMON /POSITION/                X(NNDS_MAX)
      COMMON /WALL_HEIGHT/             ZHEIGHT
```

ELEC Subroutine for Electrical Side Equations

```
C*******0*********0*********0*********0*********0*********0*********
C
C     SUBROUTINE: ELEC
C
C     DATE: 1993
C
C     PROGRAMMER:  Donald Hammerstrom, Graduate Student
C                  Department of Electrical Engineering
C                  Montana State University
C                  Bozeman, Montana  59717-0378
C
C     PURPOSE:  This subroutine updates electrical variables.
C
C*******0*********0*********0*********0*********0*********0*********
      SUBROUTINE ELEC

      INCLUDE 'COMMONER.FL'

C*******0*********0*********0*********0*********0*********0*********
C ELECTRICAL VARIABLES
C*******0*********0*********0*********0*********0*********0*********
      DO 10 I = NNOZZ + 1, NCHAN
        L = I - NNOZZ
        SIGMA(L) = SR( 'SIGMA.DAT ', 'Y', OX, PHI, SEED, P(I) /
&                                                 PASCALS, T(I) )
        EMOB = SR( 'EMOB.DAT  ', 'Y', OX, PHI, SEED, P(I) / PASCALS,
     &                                                      T(I) )
        BETA(L) = BFACT * B(L) * EMOB
 10     CONTINUE

      RETURN
      END
```

EXTCIRC External Circuit Subroutine Example

```
C*******0*********0*********0*********0*********0*********0*********
C
C     SUBROUTINE: EXTCIRC
C
C     PROGRAMMER:  Donald Hammerstrom, Graduate Student
C                  Department of Electrical Engineering
C                  Montana State University
C                  Bozeman, Montana  59717-0378
C
C
C     DATE:  1993
C
```

```
C     PURPOSE:
C          This subroutine uses the solved voltage profile within
C     the MHD channel to solve for the electrode currents.  These
C     currents may be time dependent.  The electrode currents
C     calculated in this subroutine are then again used in SOLVEVOLT
C     as boundary conditions in the solution to the discretized field
C     problem.
C          The user must rewrite this subroutine to model new
C     external circuits and circuit interactions.  Do not change
C     SOLVEVOLT.
C
C     INPUTS
C          (1) Electrode voltage profiles VANODE and VCATH
C          (2) Modeled external channel circuit as a function of
C                                                   electrode voltages
C          (3) Time is used only for time dependent circuits
C          (4) NOVRLAP is the diagonal electrode overlap number
C
C     OUTPUTS:
C          (1) Vectors of electrode currents CANODE and CCATH
C
C*******0*********0*********0*********0*********0*********0*********
      SUBROUTINE EXTCIRC

      INCLUDE 'COMMONER.FL'

      FNOVRLAP = FLOAT( NOVRLAP )

C*******0*********0*********0*********0*********0*********0*********
C DETERMINE LOAD VOLTAGE.
C*******0*********0*********0*********0*********0*********0*********
      VLOAD = ( VANODE(MA) - VDR(MA) * CUR_LOAD / FNOVRLAP ) - (
     &               VCATH(MC) + VDR(MC) * CUR_LOAD / FNOVRLAP )

C*******0*********0*********0*********0*********0*********0*********
C DETERMINE THE LOAD CURRENT.
C*******0*********0*********0*********0*********0*********0*********
C Assume 97% inverter and transformer efficiency.  RINVT represents
C those losses.
      RINVT = 0.03 * RL
      CUR_LOAD = 0.25 * VLOAD / ( RL + RINVT ) + 0.75 * CUR_LOAD

C*******0*********0*********0*********0*********0*********0*********
C DETERMINE CURRENTS IN ANODE PTO REGION.
C*******0*********0*********0*********0*********0*********0*********
      DO 20 I = 1, NOVRLAP
 20     CANODE(I) = CUR_LOAD / FNOVRLAP

C*******0*********0*********0*********0*********0*********0*********
C DETERMINE CURRENTS IN CATHODE PTO REGION.
C*******0*********0*********0*********0*********0*********0*********
      DO 30 I = NEP - NOVRLAP + 1, NEP
 30     CCATH(I) = CUR_LOAD / FNOVRLAP
```

```
C********0*********0*********0*********0*********0*********0*********
C  THESE ARE THE STANDARD DIAGONAL CONNECTIONS.
C********0*********0*********0*********0*********0*********0*********
      DO 60 I = 1, NEP - NOVRLAP
         CCATH(I) = ( 1. - ALPHA(I) ) * CCATH(I) + ALPHA(I) * (
     &      VANODE(I+NOVRLAP) - VCATH(I) ) / ( RCCC + VDR(I+NOVRLAP) +
     &                                                          VDR(I) )
 60      CANODE(I+NOVRLAP) = CCATH(I)

C********0*********0*********0*********0*********0*********0*********
C ALL ELECTRODE CURRENTS HAVE BEEN SPECIFIED BY THE EXTERNAL CIRCUIT.
C********0*********0*********0*********0*********0*********0*********
      RETURN
      END
```

FG Model of Boundary Interactions

```
C******* 1 ******* 2 ******* 3 ******* 4 ******* 5 ******* 6 *******
C
C     SUBROUTINE FG
C
C     Originally written by Pierre, Dudding and Miller (1976)
C     Completely rewritten by D. Lofftus (summer 1981)
C     Modified by C. A. Heikes (December 1981)
C     Adopted and modified by Hammerstrom (1992-4)
C
C THIS ROUTINE USES :
C
C  A--------duct cross section area------------------meters**2
C  CONK-----Cp/Cv or gamma---------------------------unitless
C  CONR-----specific gas constant; R-----------------J/kg K
C  CP-------dH/dT OR Cp; specific heat of gas--------J/kg K
C  EW-------emissivity of the walls------------------unitless
C  H--------enthalpy of the core gas-----------------J/kg
C  HW-------enthalpy of the gas along the wall-------J/kg
C  OX-------oxygen enrighment mole fraction----------unitless
C  P--------pressure of the gas----------------------Pa
C  PHI------stoichiometric ratio---------------------unitless
C  RHO------density of the core gas------------------kg/m**3
C  S--------Stefan-Boltzmann number------------------K**4
C  T--------temperature of the gas-------------------K
C  TS-------temperature of the slag walls------------K
C  V--------velocity of the gas----------------------m/s
C  WM-------molecular weight of the gas--------------unitless
C  ZHEIGHT--z-bar wall constant height---------------meters
C
C  OUTPUTS ARE F AND G:
C
C  F--------friction coefficient---------------------Nt/M**3
```

```
C  G--------thermal flux coefficient----------------Watt/M**3
C
C******* 1 ******* 2 ******* 3 ******* 4 ******* 5 ******* 6 *******
      SUBROUTINE FG(I)

      INCLUDE 'COMMONER.FL'

C******* 1 ******* 2 ******* 3 ******* 4 ******* 5 ******* 6 *******
C S--STEFAN-BOLTZMANN CONSTANT
C SEE CRC HANDBOOK, FOR EXAMPLE
      DATA S        / 5.67032E-08 /

C******* 1 ******* 2 ******* 3 ******* 4 ******* 5 ******* 6 *******
C TS--SLAG WALL TEMPERATURE
      TS = DMIN1( DMAX1( 1750.D0 + 0.75D0 * ( TW - 1400.D0 ),
     &                                                1750.D0 ), T(I))

C******* 1 ******* 2 ******* 3 ******* 4 ******* 5 ******* 6 *******
C EMISS----EMISSIVITY OF THE GAS
C SPLINE FIT:  'EMISS.DAT'
C       Gas emissivity function of chemistry and state at assumed
C equilibrium conditions.
C DATA SOURCE: MSE, Ind. gas equilibrium file for Rosebud coal
C ERROR:  (about 1% estimated by worst case match to known data
C points.)
      EMISS = SR( 'EMISS.DAT ', 'Y', OX, PHI, SEED, P(I) / PASCALS,
     &                                                       T(I) )

C******* 1 ******* 2 ******* 3 ******* 4 ******* 5 ******* 6 *******
C TF-------TEMPERATURE OF THE FILM
C [REF 1] PG 413-------------------------K
 10   TF = .55 * T(I) + .45 * TS + .035 * T(I) * VMACH(I)**2

C******* 1 ******* 2 ******* 3 ******* 4 ******* 5 ******* 6 *******
C VISF-----VISCOSITY OF THE FILM
C VISB-----VISCOSITY OF THE BULK OF THE GAS
C VISW-----VISCOSITY OF THE GAS ALONG THE WALLS
C [REF 1] PG 415-------------------------Nt SEC/M**2
      VISF = 1.95E-07 * TF**0.75
      VISB = 1.95E-07 * T(I)**0.75
      VISW = 1.95E-07 * TS**0.75

C******* 1 ******* 2 ******* 3 ******* 4 ******* 5 ******* 6 *******
C THCOND---THERMAL CONDUCTIVITY OF THE GAS
C [REF 1] PG 416-------------------------JOULE/SEC M DEG.K
      THCOND = ( 1.71E-03 * ( 270.0 + TF ) ) / WM(I)

C******* 1 ******* 2 ******* 3 ******* 4 ******* 5 ******* 6 *******
C PR-------PRANDTL NUMBER
C [REF 2] PGS 549 TO 551-----------------UNITLESS
      PR = CP(I) * VISF / THCOND

C******* 1 ******* 2 ******* 3 ******* 4 ******* 5 ******* 6 *******
```

```
C D--HYDRAULIC DIAMETER
C      The hydraulic diameter is necessary for calculations with
C non-circular cross sections.  See BOUNDARY LAYER THEORY by
C Schlichting, p.612, for example. [Hammerstrom 1993]
C      Assume constant sidewall height except in diffuser, where
C dimensions are roughly square.
      D = 4.D0 * A(I) / ( 2.D0 * ( ZHEIGHT + A(I) / ZHEIGHT ) )
      IF ( I .GT. NTRANS ) D = A(I)**0.5

C******* 1 ******* 2 ******* 3 ******* 4 ******* 5 ******* 6 *******
C RE-------REYNOLDS NUMBER
C [REF 2] PGS 549 TO 551-----------------UNITLESS
      RE = RHO(I) * DABS( V_MAJ(I) ) * D / VISF

C******* 1 ******* 2 ******* 3 ******* 4 ******* 5 ******* 6 *******
C QCOEF----HEAT TRANSFER FILM COEFFICIENT
C [REF 3] PG 341------------------------JOULE/M**2 SEC DEG.K
      QCOEF = .027 * RE**0.8 * PR**0.333 * ( VISB / VISW )**0.14 *
     &                                                 THCOND / D

C******* 1 ******* 2 ******* 3 ******* 4 ******* 5 ******* 6 *******
C RECOV----RECOVERY FACTOR
C [REF 4] PG 8-61-----------------------UNITLESS
      RECOV = PR**0.5

C******* 1 ******* 2 ******* 3 ******* 4 ******* 5 ******* 6 *******
C TAW------TEMPERATURE OF AN ADIABATIC WALL;
C "STAGNATION TEMPERATURE"
C [REF 1] PG 413 ; [REF 4] PG 1-3--------DEG.K
      TAW = T(I) + RECOV * V_MAJ(I)**2 / ( 2. * CP(I) )

C******* 1 ******* 2 ******* 3 ******* 4 ******* 5 ******* 6 *******
C QC-------CONVECTIVE HEAT FLUX TO THE WALLS
C [REF 1] PG 410------------------------WATT/M**2
      QC = QCOEF * ( TAW - TS )

C******* 1 ******* 2 ******* 3 ******* 4 ******* 5 ******* 6 *******
C QR-------RADIATIVE HEAT FLUX TO THE WALLS
C [REF 3] PG 447------------------------WATT/M**2
      QR = S * ( T(I)**4 - TS**4 ) / ( 1.0 / EMISS + 1.0 / EW - 1.0)

C******* 1 ******* 2 ******* 3 ******* 4 ******* 5 ******* 6 *******
C FFACT----FRICTION FACTOR
C [REF 4] PGS 7-4 TO 7-6-----------------UNITLESS
      FFACT = 1.0 / ( 1.74 * DLOG( D / 3.D-3 ) + 2.28 )**2

C******* 1 ******* 2 ******* 3 ******* 4 ******* 5 ******* 6 *******
C G--------HEAT TRANSFER PER UNIT VOLUME
C [REF 1] PG 407------------------------WATT/M**3
      Q(I) = 4.0 * ( QC + QR ) / D

C******* 1 ******* 2 ******* 3 ******* 4 ******* 5 ******* 6 *******
C TAUW-----TAUw ; x-DIRECTION WALL SHEAR STRESS
```

```
C [REF 1] PG 410------------------------Nt/M**2
      TAUW = FFACT * RHO(I) * V_MAJ(I)**2 / 2.0

C******* 1 ******* 2 ******* 3 ******* 4 ******* 5 ******* 6 *******
C F--------FRICTION FORCE PER UNIT VOLUME
C [REF 1] PG.407-------------------------Nt/M**3
      F(I) = 4.0 * TAUW / D
C
C
C NOTES :
C
C *** THIS VALUE RETURNED TO THE CALLING PROGRAM
C
C [REF 1] OPEN CYCLE M.H.D. POWER GENERATION
C EDITED BY J.B.Heywood AND G.J.Womack
C PERGAMON PRESS, 1969
C
C [REF 2] THERMODYNAMICS, 6TH EDITION
C V.M.Faires AND C.M.Simmang
C MACMILLIAN PUBLISHING CO., 1978
C
C [REF 3] HEAT TRANSFER, 3RD EDITION
C A.J.Chapman
C MACMILLIAN PUBLISHING CO., 1974
C
C [REF 4] HANDBOOK OF HEAT TRANSFER
C EDITED BY W.M.Rohsenoe AND J.P.Hartnett
C McGRAW-HILL, 1973
C
C      [REF 5] ELEMENTS OF COMPRESSIBLE FLOW
C              F. Cheers, 1963
C
      RETURN
      END
```

MAGNETIC Induction Profile Subroutine

```
C********0*********0*********0*********0*********0*********0*********
C
C     FUNCTION RMAG()
C
C     DATE:     1992
C
C     PROGRAMMER:    Donald Hammerstrom, Graduate Student
C                    Department of Electrical Engineering
C                    Montana State University
C                    Bozeman, Montana  59717-0378
C
C     PURPOSE:
C          This function calculates the magnetic flux density
```

```
C     profile. The user is free to alter this function to obtain a
C     desired flux density profile.  The value B_INIT may be used
C     when the general profile is known, but the strength is
C     available for design.
C
C     INPUTS:
C
C          B_INIT        initial flux density
C          X             node position in meters
C          SIZE          length to beginning of channel
C
C     OUTPUTS:
C
C          RMAG          magnetic flux density
C
C*********0*********0*********0*********0*********0*********0*********
      FUNCTION RMAG( B_INIT, X, SIZE )

      IMPLICIT DOUBLE PRECISION (A-H,O-Z)

C  SCALE IS ADDED TO ACCOUNT FOR CHANGE IN DESIGN CHANNEL LENGTH

      Z = X - SIZE
      SCALE = 4.34 / 9.
      Z = Z / SCALE

      IF ( Z .LE. 0. ) THEN
        RMAG = 0.
      ELSE IF ( Z .LT. 1.45D0 ) THEN
        RMAG = 2.143D0 * Z + .5D0
      ELSE IF ( Z .LT. 2.45D0 ) THEN
        RMAG = 0.3082D0 * Z**3 - 2.90D0 * Z**2 + 8.6086D0 * Z -
     &                                                      3.7166D0
      ELSE IF ( Z .LT. 6.4D0 ) THEN
        RMAG = -.05 * Z + 4.62
      ELSE IF ( Z .LT. 7.4D0 ) THEN
        RMAG = -0.1253D0 * Z**3 + 1.7041D0 * Z**2 - 6.4626D0 * Z +
     &                                                      8.7035D0
      ELSE IF ( Z .LE. 9.01 ) THEN
        RMAG = -1.8293D0 * Z + 16.96D0
      ELSE
        RMAG = 0.
      END IF

      RETURN
      END
```

MHDDJH Driver Program

```
C*******0*********0*********0*********0*********0*********0*********
C
C     PROGRAM: MHDDJH
C
C     DATE: 1994
C
C     PROGRAMMER: Donald Hammerstrom, Graduate Student
C                 Department of Electrical Engineering
C                 Montana State University
C                 Bozeman, Montana  59717-0378
C
C     PURPOSE:
C          This is the driver program for a program set developed at
C     MSU to analyze time dependent or steady-state linear geometry
C     open MHD ducts.
C
C*******0*********0*********0*********0*********0*********0*********

      PROGRAM MHDDJH

      INCLUDE 'COMMONER.FL'
      CHARACTER A_IN_FILE(20), B_IN_FILE(20)
      CHARACTER*10 DS(3)
      REAL*8 SS(3)
      BYTE H_IN_FILE(20), P_IN_FILE(20), H_OUT_FILE(20),
     &  P_OUT_FILE(20), OUT_FILE(20)

C*******0*********0*********0*********0*********0*********0*********
C OPEN AND READ THE MAIN INPUT FILE
C*******0*********0*********0*********0*********0*********0*********
      OPEN( UNIT = 1, FILE = 'MHDDJH.DAT', STATUS = 'OLD', RECL=255 )

C*******0*********0*********0*********0*********0*********0*********
C DUCT SECTION LENGTHS
C*******0*********0*********0*********0*********0*********0*********
C SCOMB  = Combustor length in meters
C SNOZZ  = Nozzle length in meters       => length to end of nozzle
C SCHAN  = channel length in meters      => length to end of channel
C STRANS = transition section length     => length to end of trans.
C SDIFF  = diffuser length in meters     => total duct length
C SBOIL  = length of radiant boiler section included in SDIFF
      READ(1,1010)
      READ(1,1100) SCOMB_IN, SNOZZ_IN, SCHAN_IN, STRANS_IN, SDIFF_IN
      READ(1,1000)
      READ(1,1100) SBOIL_IN

C*******0*********0*********0*********0*********0*********0*********
C NUMBER OF DUCT SECTION CELLS
C*******0*********0*********0*********0*********0*********0*********
C NCOMB  = # of cells in combustor  => # of nodes to end of combustor
```

```
C NNOZZ  = # of cells in nozzle       => # of nodes to end of nozzle
C NCHAN  = # of cells in channel      => # of nodes to end of channel
C NTRANS = # of cell in trans. sect.=> # of nodes to end of trans.
C NDIFF  = # of cells in diffuser     => total number of duct nodes
      READ(1,1020)
      READ(1,1200) NCOMB_IN, NNOZZ_IN, NCHAN_IN, NTRANS_IN, NDIFF_IN

C*******0*********0*********0*********0*********0*********0*********
C INDEPENDENT VARIABLES
C*******0*********0*********0*********0*********0*********0*********
C WC    = coal flow rate (kg/s)
C OX    = oxygen enrichment (unitless)
C PHI   = secondary combustor stoichiometric combustion ratio
C SEED = potassium seed fraction (unitless)
C PSEXIT = diffuser exit stagnation pressure (Pa)
C PHEAT  = oxygen preheat temperature (K)
C BFACT  = fraction of nominal induction profile (unitless)
      READ(1,1020)
      READ(1,1100) WC, OX, PHI, SEED, PSEXIT
      READ(1,1000)
      READ(1,1100) PHEAT, BFACT

C*******0*********0*********0*********0*********0*********0*********
C DUCT GEOMETRY
C*******0*********0*********0*********0*********0*********0*********
C ZHEIGHT = constant Z-bar wall height (m)
C SEGR    = segmentation ratio (unitless)  [See Rosa, for example.]
C EWF     = electrode wall area fraction
C                                (electrode wall area/electrode area)
      READ(1,1020)
      READ(1,1100) ZHEIGHT, SEGR, EWF

C*******0*********0*********0*********0*********0*********0*********
C BOUNDARY LAYER CONSTANTS
C*******0*********0*********0*********0*********0*********0*********
C DELTA = thermal boundary thickness (m)
C POT   = sheath boundary potential drop (V) [See Gupta and Rohatgi.]
C EW    = thermal emissivity of duct walls
C TW    = cold duct wall temperature (K) [Not slag wall temperature.]
      READ(1,1020)
      READ(1,1100) DELTA, POT, EW, TW

C*******0*********0*********0*********0*********0*********0*********
C ELECTRICAL CONSTANTS
C*******0*********0*********0*********0*********0*********0*********
C RINVT = resistance representing inverter losses (ohm)
C RL    = load resistance (ohm) [See flag set.]
C VINVT = inverter back emf (V)
C RCON  = resistor used in PTO region consolidation (ohm)
C RCCC  = resistor representing diagonal shorting angle resistance
C MA,MC = master anode and cathode numbers in PTO regions
      READ(1,1020)
      READ(1,1100) RINVT, RL, VINVT, RCON, RCCC
```

```
      READ(1,1000)
      READ(1,1200) MA, MC, NOVRLAP

C*******0*********0*********0*********0*********0*********0*********
C TIME INTEGRATION CONSTANTS
C*******0*********0*********0*********0*********0*********0*********
C TIME_0 = initial integration time (s)
C TIME_F = final integration time (s)
C DT_MIN = minimum acceptable integration time step (s)
C DT_MAX = maximum acceptable integration time step (s)
      READ(1,1020)
      READ(1,1100) TIME_0, TIME_F, DT_MIN, DT_MAX

C*******0*********0*********0*********0*********0*********0*********
C FLAGS
C*******0*********0*********0*********0*********0*********0*********
C FLAG_T  = (Y,N)  Y <==> experiment is time dependent
C                  N <==> experiment is steady-state
C FLAG_L  = (1,2,3)  1 <==> load should be considered constant
C                    2 <==> load varies
C                    3 <==> load is time dependent
C FLAG_OP = (1,2,3)  1 <==> full output
C                    2 <==> abbreviated output
C                    3 <==> minimal output
      READ(1,1010)
      READ(1,1300) FLAG_T, FLAG_L, FLAG_OP

C*******0*********0*********0*********0*********0*********0*********
C INPUT FILE NAMES
C*******0*********0*********0*********0*********0*********0*********
      READ(1,1010)
      READ(1,1400) NCHAR, ( A_IN_FILE(I), I = 1, NCHAR )
      READ(1,1400) NCHAR, ( H_IN_FILE(I), I = 1, NCHAR )
      H_IN_FILE(NCHAR+1) = 0
      READ(1,1400) NCHAR, ( B_IN_FILE(I), I = 1, NCHAR )
      READ(1,1400) NCHAR, ( P_IN_FILE(I), I = 1, NCHAR )
      P_IN_FILE(NCHAR+1) = 0

C*******0*********0*********0*********0*********0*********0*********
C OUTPUT FILE NAMES
C*******0*********0*********0*********0*********0*********0*********
      READ(1,1000)
      READ(1,1400) NCHAR, ( H_OUT_FILE(I), I = 1, NCHAR )
      H_OUT_FILE(NCHAR+1) = 0
      READ(1,1400) NCHAR, ( P_OUT_FILE(I), I = 1, NCHAR )
      P_OUT_FILE(NCHAR+1) = 0
      READ(1,1400) NCHAR, ( OUT_FILE(I), I = 1, NCHAR )
      OUT_FILE(NCHAR+1) = 0

      CLOSE( UNIT = 1 )

C*******0*********0*********0*********0*********0*********0*********
C DUCT SECTION CUMULATIVE LENGTHS
```

```
C*******0*********0*********0*********0*********0*********0*********
      SCOMB = SCOMB_IN
      SNOZZ = SCOMB + SNOZZ_IN
      SCHAN = SNOZZ + SCHAN_IN
      STRANS = SCHAN + STRANS_IN
      SDIFF = STRANS + SDIFF_IN
      SBOIL = SBOIL_IN

C*******0*********0*********0*********0*********0*********0*********
C DUCT SECTION CUMULATIVE NODE NUMBERS
C*******0*********0*********0*********0*********0*********0*********
      NCOMB = NCOMB_IN + 1
      NNOZZ = NCOMB + NNOZZ_IN
      NCHAN = NNOZZ + NCHAN_IN
      NTRANS = NCHAN + NTRANS_IN
      NDIFF = NTRANS + NDIFF_IN
      NNDS = NDIFF

C*******0*********0*********0*********0*********0*********0*********
C CELL LENGTHS
C*******0*********0*********0*********0*********0*********0*********
C STEP(1) = combustor axial position step
C STEP(2) = nozzle axial position step
C STEP(3) = channel axial position step
C STEP(4) = transition section axial position step
C STEP(5) = diffuser axial position step
C STP_MAJ(I) = major finite volume cell lengths
C STP_MIN(I) = minor finite volume cell lengths
      STEP(1) = SCOMB / DFLOAT( NCOMB_IN )
      STEP(2) = SNOZZ_IN / DFLOAT( NNOZZ_IN )
      STEP(3) = SCHAN_IN / DFLOAT( NCHAN_IN )
      IF ( STRANS_IN .GT. 0.0 .AND. NTRANS_IN .GT. 0 ) THEN
        STEP(4) = STRANS_IN / DFLOAT( NTRANS_IN )
        END IF
      STEP(5) = SDIFF_IN / DFLOAT( NDIFF_IN )

      DO 2 I = 1, NCOMB - 1
        STP_MIN(I) = STEP(1)
 2      STP_MAJ(I) = STEP(1)
      I = NCOMB
        STP_MIN(I) = STEP(2)
        STP_MAJ(I) = 0.5 * ( STEP(1) + STEP(2) )
      DO 3 I = NCOMB + 1, NNOZZ - 1
        STP_MIN(I) = STEP(2)
 3      STP_MAJ(I) = STEP(2)
      I = NNOZZ
        STP_MIN(I) = STEP(3)
        STP_MAJ(I) = 0.5 * ( STEP(2) + STEP(3) )
      DO 4 I = NNOZZ + 1, NCHAN - 1
        STP_MIN(I) = STEP(3)
 4      STP_MAJ(I) = STEP(3)
      I = NCHAN
        STP_MIN(I) = STEP(4)
```

```
          STP_MAJ(I) = 0.5 * ( STEP(3) + STEP(4) )
        DO 5 I = NCHAN + 1, NTRANS - 1
          STP_MIN(I) = STEP(4)
 5        STP_MAJ(I) = STEP(4)
        I = NTRANS
          STP_MIN(I) = STEP(5)
          STP_MAJ(I) = 0.5 * ( STEP(4) + STEP(5) )
        DO 6 I = NTRANS + 1, NNDS
          STP_MIN(I) = STEP(5)
 6        STP_MAJ(I) = STEP(5)

C*******0*********0*********0*********0*********0*********0*********
C IMPORTANT:  Always take first integration as steady-state.
C FLAG_DT = flag used to turn on or off transient analysis.
C DT    = integration time step [Set to 1 for steady-state analysis.]
        FLAG_DT = 0.
        DT = 1.

C*******0*********0*********0*********0*********0*********0*********
C POSITION AND AREA VECTORS
C         X     == position along duct length (m)
C         A     == cross section area at major nodes along duct (m^2)
C         A_MIN == cross section area at minor nodes along duct (m^2)
C SPLINE: 'A.DAT'
C       Gives area profile given duct distance X.
C SOURCE:  Desu=ign predicted for Billings plant by Hammerstrom to
C meet most known design criteria.  Nozzle was designed with DDP to
C meet predicted thermal loss at nominal operation.  Channel assumed
C linear with dimensions suggested by TRW.  Lengths of diffuser
C sections designed to meet boundary and thermal predictions.
C ERROR:  Errors propagate due to unknown final design and numerous
C assumptions made in duct modeling.
C*******0*********0*********0*********0*********0*********0*********
        DO  7 I = 1, NCOMB
          X(I) = DFLOAT(I-1) * STEP(1)
C          A(I) = SR( A_IN_FILE, 'Y', X(I), 0., 0., 0., 0. )
 7        CONTINUE
        DO 10 I = NCOMB + 1, NNOZZ
          X(I) = SCOMB + DFLOAT( I - NCOMB ) * STEP(2)
C          A(I) = SR( A_IN_FILE, 'Y', X(I), 0., 0., 0., 0. )
 10       CONTINUE
        DO 20 I = NNOZZ + 1, NCHAN
          X(I) = SNOZZ + DFLOAT( I - NNOZZ ) * STEP(3)
C          A(I) = SR( A_IN_FILE, 'Y', X(I), 0., 0., 0., 0. )
 20       CONTINUE
        IF ( STRANS_IN .GT. 0.0 .AND. NTRANS_IN .GT. 0) THEN
          DO 30 I = NCHAN + 1, NTRANS
            X(I) = SCHAN + DFLOAT( I - NCHAN ) * STEP(4)
C            A(I) = SR( A_IN_FILE, 'Y', X(I), 0., 0., 0., 0. )
 30         CONTINUE
          DO 40 I = NTRANS + 1, NDIFF
            X(I) = STRANS + DFLOAT( I - NTRANS ) * STEP(5)
C            A(I) = SR( A_IN_FILE, 'Y', X(I), 0., 0., 0., 0. )
```

```
 40        CONTINUE
      ELSE
        DO 50 I = NCHAN + 1, NDIFF
          X(I) = SCHAN + DFLOAT( I - NCHAN ) * STEP(5)
C          A(I) = SR( A_IN_FILE, 'Y', X(I), 0., 0., 0., 0. )
 50       CONTINUE
      END IF

      OPEN( UNIT = 9, FILE = 'AREA_PROF.DAT', STATUS = 'OLD' )
      DO 52 I = 1, NNDS
 52     READ(9,1100) A(I)
      CLOSE( UNIT = 9 )

C*******0*********0*********0*********0*********0*********0*********
C MINOR NODE CROSS SECTION AREAS
C*******0*********0*********0*********0*********0*********0*********
      DO 55 I = 1, NNDS - 1
 55     A_MIN(I) = 0.5 * ( A(I) + A(I+1) )

C*******0*********0*********0*********0*********0*********0*********
C MAGNETIC INDUCTION
C*******0*********0*********0*********0*********0*********0*********
C B = magnetic induction at positions along channel
      DO 60 I = NNOZZ + 1, NCHAN
        L = I - NNOZZ
        B(L) = RMAG( 0., X(I), SNOZZ )
 60     CONTINUE

C*******0*********0*********0*********0*********0*********0*********
C READ INITIAL STATE
C*******0*********0*********0*********0*********0*********0*********
      OPEN( UNIT = 1, FILE = P_IN_FILE, STATUS = 'OLD' )
      OPEN( UNIT = 2, FILE = H_IN_FILE, STATUS = 'OLD' )

      DO 70 I = 1, NNDS, 5
        READ(1,2000) ( P(J), J = I, I + 4 )
        READ(2,2000) ( HS(J), J = I, I + 4 )
 70     CONTINUE

      CLOSE( UNIT = 1 )
      CLOSE( UNIT = 2 )

C*******0*********0*********0*********0*********0*********0*********
C INITIALIZE IMPORTANT VARIABLES
C*******0*********0*********0*********0*********0*********0*********
C INITIAL FLOW RATE AT FIRST NODE.
C This first node requires some iteration.
      I = 1
        PSTAG(I) = P(I)
        T(I) = 2800.
        W(I) = 47.2
 80     TSTAG(I) = SR( 'TEMP.DAT  ', 'Y', OX, PHI, SEED, PSTAG(I) /
     &                                  PASCALS, HS(I) * 1.E-6 )
```

```
     CP(I) = SR( 'CP.DAT    ', 'Y', OX, PHI, SEED, P(I) / PASCALS,
   &                                                    T(I) )
     WM(I) = SR( 'WM.DAT    ', 'Y', OX, PHI, SEED, P(I) / PASCALS,
   &                                                    T(I) )
     A_V = W(I) * RGAS / ( P(I) * WM(I) * A(I) )
     C_V = -A_V * TSTAG(I)
     A_V = A_V / ( 2. * CP(I) )
     V_MAJ(I) = ( -1. + DSQRT( 1. -4. * A_V * C_V) ) / (2. * A_V )
     T(I) = TSTAG(I) - 0.5 * V_MAJ(I)**2 / CP(I)
     CV = CP(I) - RGAS / WM(I)
     GAMMA(I) = CP(I) / CV
     PSTAG(I) = P(I) * ( TSTAG(I) / T(I) )**( GAMMA(I) / (
   &                                             GAMMA(I) - 1. ) )
     W_NEW = WC / 10.0 * SR( 'CF_C10.DAT', 'Y', OX, PHI, SEED,
   &                                  PSTAG(I) / PASCALS, PHEAT )
     IF ( ABS( W_NEW - W(I) ) .GE. 0.1 ) THEN
       W(I) = W_NEW
       GO TO 80
       END IF
     W(I) = W_NEW
     VMACH(I) = V_MAJ(I) / DSQRT( GAMMA(I) * RGAS * T(I) / WM(I) )
     RHO(I) = P(I) *WM(I) / ( RGAS * T(I) )
     H(I) = HS(I) - 0.5 * V_MAJ(I)**2

C FIRST NODE HAS CONVERGED.

C********0*********0*********0*********0*********0*********0*********
C REMAINING NODES . . .
      DO 90 I = 2, NNDS
        W(I) = W(1)
        PSTAG(I) = PSTAG(I-1)
        TSTAG(I) = SR( 'TEMP.DAT  ', 'Y', OX, PHI, SEED, PSTAG(I) /
     &                                  PASCALS, HS(I) * 1.E-6 )
        CP(I) = SR( 'CP.DAT    ', 'Y', OX, PHI, SEED, P(I) / PASCALS,
     &                                                    T(I) )
        WM(I) = SR( 'WM.DAT    ', 'Y', OX, PHI, SEED, P(I) / PASCALS,
     &                                                  T(I-1) )
        A_V = W(I) * RGAS / ( P(I) * WM(I) * A(I) )
        C_V = -A_V * TSTAG(I)
        A_V = A_V / ( 2. * CP(I) )
        V_MAJ(I) = ( -1. + DSQRT( 1. -4. * A_V * C_V ) ) / (2. * A_V)
        T(I) = TSTAG(I) - 0.5 * V_MAJ(I)**2 / CP(I)
        CV = CP(I) - RGAS / WM(I)
        GAMMA(I) = CP(I) / CV
        VMACH(I) = V_MAJ(I) / DSQRT( GAMMA(I) * RGAS * T(I) / WM(I))
        RHO(I) = P(I) * WM(I) / ( RGAS * T(I) )
        H(I) = HS(I) - 0.5 * V_MAJ(I)**2
        IF ( I .GT. NCOMB ) CALL FG(I)
 90     CONTINUE

C********0*********0*********0*********0*********0*********0*********
C INTERPOLATE VELOCITIES AND DENSITIES
C********0*********0*********0*********0*********0*********0*********
```

```
      DO 91 I = 1, NNDS - 1
        RHO_MIN(I) = 0.5 * ( RHO(I) + RHO(I+1) )
 91     V(I) = 0.5 * ( V_MAJ(I) + V_MAJ(I+1) )
      V(NNDS) = V_MAJ(NNDS)

C*******0*********0*********0*********0*********0*********0*********
C INITIALIZE DRHODP()
C*******0*********0*********0*********0*********0*********0*********
      DO 92 I = 1, NNDS
 92     DRHODP(I) = WM(I) / ( RGAS * T(I) )

C*******0*********0*********0*********0*********0*********0*********
C INITIALIZE ELECTRICAL VARIABLES
C*******0*********0*********0*********0*********0*********0*********
      DO 100 I = NNOZZ + 1, NCHAN
        L = I - NNOZZ
        SIGMA(L) = SR ( 'SIGMA.DAT ', 'Y', OX, PHI, SEED, P(I) /
     &                                           PASCALS, T(I) )
        EMOB = SR ( 'EMOB.DAT  ', 'Y', OX, PHI, SEED, P(I) / PASCALS,
     &                                                     T(I) )
 100    BETA(L) = BFACT * B(L) * EMOB

C*******0*********0*********0*********0*********0*********0*********
C INITIALIZE INTEGRATION COUNTERS
C*******0*********0*********0*********0*********0*********0*********
      KOUNT = 0
      KOUNT1 = 0
      KOUNT2 = 0

      C_OLD = 0.

C*******0*********0*********0*********0*********0*********0*********
C CALCULATE ELECTRICAL SOLUTION
C*******0*********0*********0*********0*********0*********0*********
 110  CONTINUE
      CALL SOLVEVOLT
      CALL EXTCIRC
      KOUNT1 = KOUNT1 + 1
      IF ( ABS( CX(NCHAN_IN) ) .GT. 0.01 .OR. ABS( VLOAD-VL_OLD )
     &    .GT. 10.0 .OR. ( KOUNT1 .LT. 3 .AND. KOUNT .EQ. 0 ) ) THEN
          VL_OLD = VLOAD
          GO TO 110
          END IF

C*******0*********0*********0*********0*********0*********0*********
C CALCULATE FLUID SOLUTION
C*******0*********0*********0*********0*********0*********0*********
 120  CALL SIMPLER(RSQRD)
      CALL NONLIN
      KOUNT2 = KOUNT2 + 1
      WRITE(6,1111) RSQRD
      IF ( RSQRD .GT. 80. ) GO TO 120
```

```
C*******0*********0*********0*********0*********0*********0*********
C CHECK FOR CONVERGENCE
C*******0*********0*********0*********0*********0*********0*********
      KOUNT = KOUNT + 1
      CALL ELEC
      IF (KOUNT1 .GT. 2 .OR. KOUNT2 .GT. 1 .OR. RSQRD .GT. 10.0) THEN
        KOUNT1 = 0
        KOUNT2 = 0
        GO TO 110
        END IF

C*******0*********0*********0*********0*********0*********0*********
C SUMMARIZE FINAL DATA
C*******0*********0*********0*********0*********0*********0*********
C SPLINE FIT:  'CL_C10.DAT'
C     Heat loss from the combustor is a function of flow, chemistry,
C and states within a plug flow combustor model.  The "_C10" refers
C to a coal flow rate of 10 Kg/s.
C DATA SOURCE:  MSE, Inc. combustor data
C ERROR:  perfect match to known MSE, Inc. data.  Interpolation
C results may be in error due to variational estimations.
C*******0*********0*********0*********0*********0*********0*********
      I = 1
        QCOMB = 1.D6 * SR( 'CL_C10.DAT', 'Y', OX, PHI, SEED, PSTAG(I)
     &                                             / PASCALS, PHEAT )

C*******0*********0*********0*********0*********0*********0*********
C PRINT OUT RESULTS
C*******0*********0*********0*********0*********0*********0*********
C STATE FILES
C*******0*********0*********0*********0*********0*********0*********
      OPEN( UNIT=1, FILE = P_OUT_FILE, STATUS = 'NEW' )
      OPEN( UNIT=2, FILE = H_OUT_FILE, STATUS = 'NEW' )

      DO 200 I = 1, NNDS, 5
        WRITE(1,2000) ( P(J), J = I, I + 4 )
 200    WRITE(2,2000) ( HS(J), J = I, I + 4 )

      CLOSE( UNIT=1 )
      CLOSE( UNIT=2 )

C*******0*********0*********0*********0*********0*********0*********
C MAIN OUTPUT FILE
C*******0*********0*********0*********0*********0*********0*********
      OPEN( UNIT=1, FILE = OUT_FILE, STATUS = 'NEW', RECL = 255 )

C*******0*********0*********0*********0*********0*********0*********
C RESTATE INPUT DATA
C*******0*********0*********0*********0*********0*********0*********
C NOTE THAT OUTPUT FILE MAY BE USED AS INPUT FILE.
      WRITE(1,3000)
      WRITE(1,5000) SCOMB_IN, SNOZZ_IN, SCHAN_IN, STRANS_IN, SDIFF_IN
      WRITE(1,3001)
```

```
      WRITE(1,5000) SBOIL_IN
      WRITE(1,3010)
      WRITE(1,1200) NCOMB_IN, NNOZZ_IN, NCHAN_IN, NTRANS_IN, NDIFF_IN
      WRITE(1,3020)
      WRITE(1,5000) WC, OX, PHI, SEED, PSEXIT
      WRITE(1,3030)
      WRITE(1,5000) PHEAT, BFACT
      WRITE(1,3040)
      WRITE(1,5000) ZHEIGHT, SEGR, EWF
      WRITE(1,3050)
      WRITE(1,5000) DELTA, POT, EW, TW
      WRITE(1,3060)
      WRITE(1,5000) RINVT, RL, VINVT, RCON, RCCC
      WRITE(1,3070)
      WRITE(1,1200) MA, MC, NOVRLAP
      WRITE(1,3080)
      WRITE(1,5000) TIME_0, TIME_F, DT_MIN, DT_MAX
      WRITE(1,3090)
      WRITE(1,3100) FLAG_T, FLAG_L, FLAG_OP
      WRITE(1,3110)
      WRITE(1,3120) A_IN_FILE, H_IN_FILE, B_IN_FILE, P_IN_FILE
      WRITE(1,3130)
      WRITE(1,3140) H_OUT_FILE, P_OUT_FILE, OUT_FILE

C*******0*********0*********0*********0*********0*********0*********
C MAKE TABLE FOR ALL OUTPUT DATA
C*******0*********0*********0*********0*********0*********0*********

C*******0*********0*********0*********0*********0*********0*********
C INITIALIZE LOSS DATA
C*******0*********0*********0*********0*********0*********0*********
      QCHAN = 0.
      QNOZZ = 0.
      QDIFF = 0.
      QBOIL = 0.
      PELEC = 0.
      PBOUND = 0.

C*******0*********0*********0*********0*********0*********0*********
C PRINT HEADER
C*******0*********0*********0*********0*********0*********0*********
      WRITE(1,1010)
      WRITE(1,1040)
      WRITE(1,4000)
      WRITE(1,1040)

C*******0*********0*********0*********0*********0*********0*********
C FLUID TABLE
C*******0*********0*********0*********0*********0*********0*********
      DO 300 I = 1, NNDS
        L = I - NNOZZ
        PTHERM = HS(I) * W(I)
        IF ( I .EQ. NCOMB ) THEN
```

```
      VOLUME = 0.5 * A(I) * STEP(2)
      QNOZZ = QNOZZ + Q(I) * VOLUME
    ELSE IF ( I .LT. NNOZZ ) THEN
      VOLUME = A(I) * STEP(2)
      QNOZZ = QNOZZ + Q(I) * VOLUME
    ELSE IF ( I .EQ. NNOZZ ) THEN
      VOLUME = A(I) * 0.5 * STEP(2)
      QNOZZ = QNOZZ + Q(I) * VOLUME
      VOLUME = A(I) * 0.5 * STEP(3)
      QCHAN = QCHAN + Q(I) * VOLUME
    ELSE IF ( I .LT. NCHAN ) THEN
      VOLUME = A(I) * STEP(3)
      QCHAN = QCHAN + Q(I) * VOLUME
      PELEC = PELEC + 0.5 * ( VANODE(L) - VCATH(L) ) * (
&                         CANODE(L) + CCATH(L) ) + VX(L) * CX(L)
      PBOUND = PBOUND - CANODE(L) * ( CANODE(L) * VDR(L) + VD(L)
&                 ) - CCATH(L) * ( CCATH(L) * VDR(L) + VD(L) )
    ELSE IF ( I .EQ. NCHAN ) THEN
      VOLUME = 0.5 * A(I) * STEP(3)
      QCHAN = QCHAN + Q(I) * VOLUME
      IF ( STRANS_IN .GT. 0.0 .AND. NTRANS_IN .GT. 0 ) THEN
        VOLUME = 0.5 * A(I) * STEP(4)
        QDIFF = QDIFF + Q(I) * VOLUME
      ELSE
        VOLUME = 0.5 * A(I) * STEP(5)
        QDIFF = QDIFF + Q(I) * VOLUME
      END IF
    ELSE IF ( I .LT. NTRANS ) THEN
      VOLUME = A(I) * STEP(4)
      IF ( X(I) .LT. SDIFF - SBOIL ) THEN
        QDIFF = QDIFF + Q(I) * VOLUME
      ELSE
        QBOIL = QBOIL + Q(I) * VOLUME
      END IF
    ELSE IF ( I .EQ. NTRANS ) THEN
      VOLUME = 0.5 * A(I) * ( STEP(4) + STEP(5) )
      IF ( X(I) .LT. SDIFF - SBOIL ) THEN
        QDIFF = QDIFF + Q(I) * VOLUME
      ELSE
        QBOIL = QBOIL + Q(I) * VOLUME
      END IF
    ELSE IF ( I .LT. NDIFF ) THEN
      VOLUME = A(I) * STEP(5)
      IF ( X(I) .LT. SDIFF - SBOIL ) THEN
        QDIFF = QDIFF + Q(I) * VOLUME
      ELSE
        QBOIL = QBOIL + Q(I) * VOLUME
      END IF
    ELSE IF ( I .EQ. NDIFF ) THEN
      VOLUME = 0.5 * A(I) * STEP(5)
      IF ( X(I) .LT. SDIFF - SBOIL ) THEN
        QDIFF = QDIFF + Q(I) * VOLUME
      ELSE
```

```
            QBOIL = QBOIL + Q(I) * VOLUME
          END IF
        END IF
        PTOT = PTHERM + QCOMB + QNOZZ + QCHAN + QDIFF + QBOIL + PELEC
 300    WRITE(1,4020) X(I), A(I), 1.E-3 * PSTAG(I), 1.E-3 * P(I),
     &    TSTAG(I), T(I), V_MAJ(I), VMACH(I), RHO(I), WM(I), 1.E-6 *
     &    H(I), 1.E-6 * HS(I), 1.E-6 * PTOT, 1.E-6 * PTHERM, 1.E-6 *
     &    PELEC, 1.E-6 * PBOUND

C********0*********0*********0*********0*********0*********0*********
C PRINT FOOTER
C********0*********0*********0*********0*********0*********0*********
      WRITE(1,1040)
      WRITE(1,4000)
      WRITE(1,1040)
      WRITE(1,1010)
      WRITE(1,1010)

C********0*********0*********0*********0*********0*********0*********
C ELECTRICAL STATES AND MORE
C********0*********0*********0*********0*********0*********0*********

C********0*********0*********0*********0*********0*********0*********
C HEADER
C********0*********0*********0*********0*********0*********0*********
      WRITE(1,1010)
      WRITE(1,1040)
      WRITE(1,4010)
      WRITE(1,1040)

C********0*********0*********0*********0*********0*********0*********
C ELECTRICAL TABLE
C********0*********0*********0*********0*********0*********0*********
      DO 400 L = 1, NCHAN_IN
        I = L + NNOZZ
        E_ANGLE = DATAN2D( -( VY(1,L) + VY(2,L) ) / ZHEIGHT, -VX(L) /
     &                                                      STEP(3) )
 400    WRITE(1,4020) X(I) - SNOZZ, VANODE(L), VCATH(L),1.E-4 * CX(L)
     &    / A(I), 0.5E-4 * ( CANODE(L) + CCATH(L) ) / (STEP(3) * A(I)
     &    / ZHEIGHT ), CANODE(L), CCATH(L), -1.E-2 * VX(L) / STEP(3),
     &    -1.E-2 * (VY(1,L) + VY(2,L)) / ZHEIGHT, SIGMA(L), BETA(L),
     &    E_ANGLE, VD(L), -CANODE(L) * VDR(L), VD(L), -CCATH(L) *
     &                                        VDR(L), BFACT * B(L)

      WRITE(1,1040)
      WRITE(1,4010)
      WRITE(1,1040)

C********0*********0*********0*********0*********0*********0*********
C COMBUSTOR ACCOUNTING
C********0*********0*********0*********0*********0*********0*********
      WRITE(1,1010)
      WRITE(1,4040)
```

```
      WRITE(1,1010)
      WRITE(1,4060) W(1), HS(1) / 1.D6, H(1) / 1.D6, TSTAG(1), T(1),
     &                PSTAG(1) / 1.D3, P(1) / 1.D3, V_MAJ(1), VMACH(1)

C*******0*********0*********0*********0*********0*********0*********
C THERMAL LOSS FROM DUCT SECTIONS
C*******0*********0*********0*********0*********0*********0*********
      WRITE(1,1010)
      WRITE(1,4050)
      WRITE(1,1010)
      WRITE(1,4070) QCOMB / 1.D6, QNOZZ / 1.D6, QCHAN / 1.D6, QDIFF /
     &                                           1.D6, QBOIL / 1.D6
      WRITE(1,1010)

C*******0*********0*********0*********0*********0*********0*********
C EXIT STATE ACCOUNTING
C*******0*********0*********0*********0*********0*********0*********
      WRITE(1,4080)
      WRITE(1,1010)
      WRITE(1,4090) HS(NNDS) / 1.D6, H(NNDS) / 1.D6, TSTAG(NNDS),
     &  T(NNDS), PSTAG(NNDS) / 1.D3, P(NNDS) / 1.D3, V_MAJ(NNDS),
     &  VMACH(NNDS)

C*******0*********0*********0*********0*********0*********0*********
C POWER AND PTO ACCOUNTING
C*******0*********0*********0*********0*********0*********0*********
      WRITE(1,1010)
      WRITE(1,4100)
      WRITE(1,1010)
      V_LOAD = VANODE(MA) - VCATH(MC)
C       CUR_LOAD = ( V_LOAD - VINVT ) / ( RL + RINVT )
      PUSE = CUR_LOAD**2 * RL
      CEFF = PUSE / ( PUSE + CUR_LOAD**2 * RINVT )
      EEEF = ( PUSE + CUR_LOAD**2 * RINVT ) / PELEC
      FEE = PUSE / ( HS(1) * W(1) + QCOMB )
      EFFCON = PELEC / ( HS(1) * W(1) + QCOMB - HS(NNDS) * W(1) )
      WRITE(1,4110) 100. * FEE, 100. * CEFF, 100. * EEEF, 100. *
     &  EFFCON, 100. * CEFF * EEEF * EFFCON, PELEC / 1.D6, PTOT /
     &  1.D6, PTHERM / 1.D6, PUSE / 1.D6, -V_LOAD / 1.D3, -CUR_LOAD /
     &  1.D3

C*******0*********0*********0*********0*********0*********0*********
C ADDITIONAL STRESS ACCOUNTING
C*******0*********0*********0*********0*********0*********0*********
      WRITE(1,1010)
      WRITE(1,6200)

C LOCATE SHOCK POSITION(S):
      J = 0
      N = 0
      DO 410 I = NNDS, NCOMB, -1
        IF ( VMACH(I) .GE. 1. .AND. N .EQ. 0 ) THEN
          J = J + 1
```

```
          SS(J) = X(I)
          IF ( I .GT. NTRANS ) THEN
            DS(J) = '  diffuser'
          ELSE IF ( I .GT. NCHAN ) THEN
            DS(J) = 'trans sect'
          ELSE IF ( I .GT. NNOZZ ) THEN
            DS(J) = '   channel'
          ELSE
            DS(J) = '    nozzle'
          END IF
          N = 1
        END IF
        IF ( VMACH(I) .LT. 1. ) N = 0
 410    CONTINUE

      IF ( J .GT. 0 ) THEN
        WRITE(1,1000)
        WRITE(1,6205) J
        DO 420 I = 1, J
 420      WRITE(1,6210) I, SS(I), DS(I)
      END IF

C MAXIMUM ELECTRICAL QUANTITIES:
      BETA_MAX = 0.
      VX_MAX = 0.
      YJ_MAX = 0.
      DO 430 L = 1, NEP
        IF ( BETA(L) .GT. BETA_MAX ) THEN
          BETA_MAX = BETA(L)
          SS(1) = X(L+NNOZZ)
        END IF
        IF ( VX(L) .GT. VX_MAX ) THEN
          VX_MAX = VX(L)
          SS(2) = X(L+NNOZZ)
        END IF
        YJ = 0.5E-4 * ( CANODE(L) + CCATH(L) ) / ( STEP(3) *
     &                                  A(L+NNOZZ) / ZHEIGHT )
        IF ( YJ .LT. YJ_MAX ) THEN
          YJ_MAX = YJ
          SS(3) = X(L+NNOZZ)
        END IF
 430    CONTINUE

      WRITE(1,1000)
      WRITE(1,6300)
      WRITE(1,6310) BETA_MAX, SS(1), -1.E-2 * VX_MAX / STEP(3),
     &                                  SS(2), YJ_MAX, SS(3)

C*******0*********0*********0*********0*********0*********0*********
C FINAL FOOTER
C*******0*********0*********0*********0*********0*********0*********
      WRITE(1,1010)
      WRITE(1,1040)
```

```
      WRITE(1,1040)

      CLOSE( UNIT=1 )

C*********0*********0*********0*********0*********0*********0*********
C ITERATION LOOP FOR DYNAMIC MODELING
C*********0*********0*********0*********0*********0*********0*********
      IF ( FLAG_T .EQ. 'Y' ) THEN
        IF ( TIME .EQ. TIME_0 ) THEN
          DT = DT_MAX
          FLAG_DT = 1.D0
        END IF

C SAVE DYNAMIC VARIABLES OF INTEREST
        OPEN( UNIT=17, FILE = 'DYNAMIC.OUT', STATUS = 'OLD', RECL =
     &                                                          256 )
        WRITE(17,2001) TIME
        DO 500 I = 1, NNOZZ
 500      WRITE(17,2001) V_MAJ(I), P(I), RHO(I), T(I)
        DO 510 I = NNOZZ + 1, NCHAN
          L = I - NNOZZ
 510      WRITE(17,2001) V_MAJ(I), P(I), RHO(I), T(I), VANODE(L),
     &                     VCATH(L), CANODE(L), CCATH(L)
        DO 520 I = NCHAN + 1, NNDS
 520      WRITE(17,2001) V_MAJ(I), P(I), RHO(I), T(I)

C UPDATE TIMER AND LOOP TO COMPLETION
        IF ( TIME .LT. TIME_F ) THEN
          TIME = TIME + DT
          IF ( TIME .GT. TIME_F ) THEN
            DT = DT - ( TIME - TIME_F )
            TIME = TIME_F
          END IF

C OLD STATE VARIABLES ARE SOURCE TERMS IN IMPLICIT FORMULATION
          DO 550 I = 1, NNDS
            V_OLD(I) = V(I)
            EIO_OLD(I) = EIO(I)
            RHO_OLD(I) = RHO(I)
 550        CONTINUE
          GO TO 120
        END IF
      END IF

      CLOSE( UNIT = 17 )

C*********0*********0*********0*********0*********0*********0*********
C INDEPENDENT VARIABLE MODIFICATIONS?
C*********0*********0*********0*********0*********0*********0*********
      IF ( FLAG_T .EQ. 'N' ) THEN
 600    WRITE(6,6000)
        READ(6,6010) N
        IF ( N .LT. 1 .OR. N .GT. 9 ) GO TO 600
```

```
      GO TO ( 610, 620, 630, 640, 650, 660, 670, 680, 690 ) N
C MODIFY VARIABLE OX
 610  WRITE(6,6020) OX
      READ(6,1100)  OX
      GO TO 600

C MODIFY VARIABLE PHI
 620  WRITE(6,6030) PHI
      READ(6,1100)  PHI
      GO TO 600

C MODIFY VARIABLE WC
 630  WRITE(6,6040) RL
      READ(6,1100)  RL
      GO TO 600

C MODIFY VARIABLE PSEXIT
 640  WRITE(6,6050) PSEXIT
      READ(6,1100)  PSEXIT
      GO TO 600

C MODIFY VARIABLE NOVRLAP
 650  WRITE(6,6060) NOVRLAP
      READ(6,1200)  NOVRLAP
      GO TO 600

C MODIFY VARIABLE BFACT
 660  WRITE(6,6070) BFACT
      READ(6,1100)  BFACT
      GO TO 600

C MODIFY VARIABLE PHEAT
 670  WRITE(6,6080) PHEAT
      READ(6,1100)  PHEAT
      GO TO 600

C RETURN FOR NEW COMPUTER EXPERIMENT
 680  WRITE(6,6090,ERR=600) OUT_FILE
      READ(6,6100,ERR=600) NCHAR, ( OUT_FILE(I), I = 1, NCHAR )
      OUT_FILE(NCHAR+1) = 0
      KOUNT = 0
      KOUNT1 = 0
      KOUNT2 = 0
      GO TO 110

C EXIT
 690  CONTINUE

    END IF

C*******0*********0*********0*********0*********0*********0*********
C FORMATS
```

```
C*******0*********0*********0*********0*********0*********0**********
 1000 FORMAT()
 1010 FORMAT(' ',/)
 1020 FORMAT(' ',//)
 1030 FORMAT(' ',///)
 1040 FORMAT(' ',254('*'))
 1100 FORMAT(' ',5F15.0)
 1111 FORMAT(' RESIDUAL IS ',F40.1)
 1200 FORMAT(' ',5I15)
 1300 FORMAT(' ',16X,A1/' ',16X,I1/' ',16X,I1)
 1400 FORMAT(' ',16X,Q,20A1)
 2000 FORMAT(5(' ',E14.4))
 2001 FORMAT(17(' ',E14.4))
 3000 FORMAT(' ','Duct section lengths: (m)'/
     &  ' ',5X,'Combustor:',8X,'Nozzle:',
     &  7X,'Channel:',4X,'Transition:',6X,'Diffuser:')
 3001 FORMAT(' ',3X,'Rad. Boiler:')
 3010 FORMAT(/' ','Number of discrete axial steps in each duct '
     &  ' section:'/' ',5X,'Combustor:',8X,'Nozzle:',7X,'Channel:',
     &  4X,'Transition:',6X,'Diffuser:')
 3020 FORMAT(/' ','Independent input variables:'/' ',
     &  3X,'Coal (kg/s):',4X,'02 enrich.:',1X,'Final stoich.:',
     &  10X,'Seed:',1X,'Ex stg. P(Pa):')
 3030 FORMAT(' ',2X,'02 preheat T:',1X,'Induct. ratio:')
 3040 FORMAT(/' ','Other geometric variables:'/
     &  ' ',1X,'Z-bar ht. (m):',4X,'Seg. Ratio:',1X,'Elect. A rat.:')
 3050 FORMAT(/' ','Boundary layer constants:'/' ',5X,'Delta (m):',
     &  1X,'Pot. Diff.(V):',3X,'Wall emiss.:',3X,'cold wall T:')
 3060 FORMAT(/' ','External electrical circuit constants:'/' ',4X,
     &  'Inverter R:',8X,'Load R:',6X,'Back emf:',5X,'Consol. R:',
     &  5X,'Shuffle R:')
 3070 FORMAT(' ',2X,'Master anode:',2X,'Master cath.:',7X,'Overlap:')
 3080 FORMAT(/' ','Time dependence constants:'/' ',2X,
     &  'Initial time:',4X,'Final time:',2X,'Minimum step:',2X,
     &                                        'Maximum step:')
 3090 FORMAT(/' ','Flags:')
 3100 FORMAT(' ','Time dependent: ',A1/' ',' Constant load: ',I1/
     &  ' ','  Output style: ',I1)
 3110 FORMAT(/' ','Input files:')
 3120 FORMAT(' ','  Area profile: ',20A1/' ',6X,'Enthalpy: ',20A1/
     &  ' ',4X,'Inductance: ',20A1/' ',6X,'Pressure: ',20A1)
 3130 FORMAT(' ','Output files:')
 3140 FORMAT(' ',6X,'Enthalpy: ',20A1/' ',6X,'Pressure: ',20A1/
     &  ' ','Output Summary: ',20A1)
 4000 FORMAT(' ','   POSITION          AREA     STAG. P    PRESSURE',
     &          '     STAG. T         TEMP.    VELOCITY        MACH',
     &          '     DENSITY      MOL.WT.   ENTHALPY     STAG. H',
     &          '  TOTAL POW.     P THERM.    P ELEC.  P BOUNDARY'/
     &     ' ','           M          M**2        kPa         kPa',
     &          '           K             K        M/S            ',
     &          '     KG/M**3    KG/KMOLE       MJ/KG       MJ/KG',
     &          '          MW            MW          MW          MW')
 4010 FORMAT(' ',' CH.  POS.      ANODE V   CATHODE V',
```

```
     &         '           JX            JY      ANODE I   CATHODE I',
     &         '           EX            EY',
     &         '        COND.  HALL PARA.     E ANGLE',
     &         '   ANODE DROP  ANODE DROP  CATH. DROP  CATH. DROP',
     &         '   INDUCTION'/
     &     ' ',' '           M         VOLTS         VOLTS',
     &         '      A/CM**2     A/CM**2     AMPERES      AMPERES',
     &         '     VOLTS/CM    VOLTS/CM',
     &         '        MHO/M                 DEGREES',
     &         '       PURE V     OHMIC V      PURE V      OHMIC V',
     &         '        TESLA')
4020 FORMAT(20(' ',E11.4))
4040 FORMAT(' COMBUSTOR ACCOUNTING INFORMATION:')
4050 FORMAT(' THERMAL LOSSES FROM MHD DUCT SECTIONS:')
4060 FORMAT(10X,'           TOTAL FLUID FLOW RATE: ',F10.6,' KG/S'/
     &       10X,' COMBUSTOR STAGNATION ENTHALPY: ',F10.6,' MJ/KG'/
     &       10X,'       COMBUSTOR EXIT ENTHALPY: ',F10.6,' MJ/KG'/
     &       10X,'        STAGNATION TEMPERATURE: ',F10.2,' K'/
     &       10X,'    COMBUSTOR EXIT TEMPERATURE: ',F10.2,' K'/
     &       10X,' COMBUSTOR STAGNATION PRESSURE: ',F10.5,' KPa'/
     &       10X,'       COMBUSTOR EXIT PRESSURE: ',F10.5,' KPa'/
     &       10X,'       COMBUSTOR EXIT VELOCITY: ',F10.5,' M/S'/
     &       10X,'    COMBUSTOR EXIT MACH NUMBER: ',F10.6)
4070 FORMAT(10X,' COMBUSTOR    NOZZLE    CHANNEL    DIFFUSER',
     &                 '     BOILER'/9X,5F11.4,'   MW')
4080 FORMAT(' AN ACCOUNTING OF DIFFUSER EXIT CONDITIONS:')
4090 FORMAT(10X,'            STAGNATION ENTHALPY: ',F10.6,' MJ/KG'/
     &       10X,'                       ENTHALPY: ',F10.6,' MJ/KG'/
     &       10X,'         STAGNATION TEMPERATURE: ',F10.2,' K'/
     &       10X,'                    TEMPERATURE: ',F10.2,' K'/
     &       10X,'            STAGNATION PRESSURE: ',F10.5,' KPa'/
     &       10X,'                       PRESSURE: ',F10.5,' KPa'/
     &       10X,'         DIFFUSER EXIT VELOCITY: ',F10.5,' M/S'/
     &       10X,'      DIFFUSER EXIT MACH NUMBER: ',F10.6)
4100 FORMAT(' SOME POWER AND PTO SYSTEM ACCOUNTING:')
4110 FORMAT(10X,' PERCENT TOTAL ENTHALPY EXTRACTION: ',F10.6,' %'/
     &       10X,'               INVERTER EFFICIENCY: ',F10.6,' %'/
     &       10X,'             ELECTRICAL EFFICIENCY: ',F10.6,' %'/
     &       10X,'             CONVERSION EFFICIENCY: ',F10.6,' %'/
     &       10X,'       TOTAL ELECTRICAL EFFICIENCY: ',F10.6,' %'/
     &       10X,'            TOTAL ELECTRICAL POWER: ',F10.6,' MW'/
     &       10X,'         TOTAL THERMAL INPUT POWER: ',F10.6,' MW'/
     &       10X,'          THERMAL POWER INTO HRSR: ',F10.6,' MW'/
     &       10X,'        AVAILABLE ELECTRICAL POWER: ',F10.6,' MW'/
     &       10X,'             INVERTER LOAD VOLTAGE: ',F10.6,' KV'/
     &       10X,'             INVERTER LOAD CURRENT: ',F10.6,' KA')
5000 FORMAT(' ',5F15.5)
6000 FORMAT(' '/////' ',10X,'Choose an option:'/
     &       ' ',20X,'(1) Modify oxygen enrichment'/
     &       ' ',20X,'(2) Modify stoichiometric ratio'/
     &       ' ',20X,'(3) Modify load'/
     &       ' ',20X,'(4) Modify exit stagnation pressure'/
     &       ' ',20X,'(5) Modify electrode overlap'/
```

```
&         ' ',20X,'(6) Modify fraction applied induction'/
&         ' ',20X,'(7) Modify preheat temperature'/
&         ' ',20X,'(8) Begin computer experiment'/
&         ' ',20X,'(9) Exit program')
 6010 FORMAT(I1)
 6020 FORMAT(' ','OX = ',F10.7,' Set OX = _______.')
 6030 FORMAT(' ','PHI = ',F10.7,' Set PHI = _______.')
 6040 FORMAT(' ','RL = ',F10.5,' Set RL = _______.')
 6050 FORMAT(' ','PSEXIT = ',F10.1,' Set PSEXIT = _______.')
 6060 FORMAT(' ','NOVRLAP = ',I3,' Set NOVRLAP = _______.')
 6070 FORMAT(' ','BFACT = ',F10.7,' Set BFACT = _______.')
 6080 FORMAT(' ','PHEAT = ',F10.2,' Set PHEAT = _______.')
 6090 FORMAT(' ','     Present output file name = ',20A1/
    &  ' ','     New output file name = _____________.')
 6100 FORMAT(' ',Q,20A1)
 6200 FORMAT(' ',' DUCT STRESS INFORMATION:')
 6205 FORMAT(' ',10X,'Number of shocks which occurred: ',I1)
 6210 FORMAT(' ',15X,'Shock #',I1,' occurred at location ',F5.2,
    &  ' meters in the ',A10,'.')
 6300 FORMAT(' ',10X,'These electrical stresses were noted:')
 6310 FORMAT(' ',15x,'Maximum Hall parameter was ',F4.2,' at ',F5.2,
    &   ' meters.'/' ',15X,'Maximum Ex field was ',F6.2,' V/cm at ',
    &   F5.2,' meters.'/' ',15X,'Maximum Jy was ',F6.3,' a/cm^2 at '
    &   ,F5.2,' meters.')

      END
```

NONLIN Subroutine for Fluid Side Equations

```
C********0*********0*********0*********0*********0*********0*********0*********
C
C     SUBROUTINE: NONLIN
C
C     DATE: 1993
C
C     PROGRAMMER: Donald Hammerstrom, Graduate Student
C                 Department of Electrical Engineering
C                 Montana State University
C                 Bozeman, Montana  59717-0378
C
C     PURPOSE:
C          This subroutine updates the algebraic variables after
C     complete iterations of the fluid state calculations.
C
C********0*********0*********0*********0*********0*********0*********0*********
      SUBROUTINE NONLIN

      INCLUDE 'COMMONER.FL'

      DO 10 I = 1, NNDS
```

```
C********0*********0*********0*********0*********0*********0*********
C MAJOR NODE VELOCITY INTERPOLATION:
C********0*********0*********0*********0*********0*********0*********
      IF ( I .EQ. 1 ) THEN
        V_MAJ(I) = 1.5 * V(I) - 0.5 * V(I+1)
      ELSE IF ( I .EQ. NNDS ) THEN
        V_MAJ(I) = 1.5 * V(I-1) - 0.5 * V(I-2)
      ELSE
        V_MAJ(I) = 0.5 * ( STP_MIN(I) * V(I-1) + STP_MIN(I-1) *
     &                                  V(I) ) / STP_MAJ(I)
      END IF

C********0*********0*********0*********0*********0*********0*********
C STAGNATION ENTHALPY:
C                                 Hs = e + P/rho
C********0*********0*********0*********0*********0*********0*********
      HS(I) = EIO(I) + P(I) / RHO(I)

C********0*********0*********0*********0*********0*********0*********
C ENTHALPY, LESS KINETIC ENERGY:
C********0*********0*********0*********0*********0*********0*********
      H(I) = HS(I) - 0.5 * V_MAJ(I)**2

C********0*********0*********0*********0*********0*********0*********
C STAGNATION AND STATIC TEMPERATURES:
C SPLINE FIT:  'TEMP.DAT'
C      Stagnation temperature function of state at assumed
C equilibrium conditions.  This file was prepared from an N-R fit on
C data giving H = f( T ).  The stagnation and static temperatures are
C calculated in the stationary and moving reference frames,
C respectively.
C SOURCE:  MSE, Inc. equilibrium data.
C********0*********0*********0*********0*********0*********0*********
      TSTAG(I) = SR( 'TEMP.DAT  ', 'Y', OX, PHI, SEED, PSTAG(I) /
     &                                   PASCALS, HS(I) * 1.E-6 )

      T(I) = SR( 'TEMP.DAT  ', 'Y', OX, PHI, SEED, P(I) / PASCALS,
     &                                         H(I) * 1.E-6 )

C********0*********0*********0*********0*********0*********0*********
C SPECIFIC HEATS AND SPECIFIC HEAT RATIO:
C                    Cp = v^2 / ( 2. * ( Ts - T ) )
C                           Cv = Cp - R
C                         Gamma = Cp / Cv
C********0*********0*********0*********0*********0*********0*********
      CP(I) = 0.5 * V_MAJ(I)**2 / ( TSTAG(I) - T(I) )
      CV = CP(I) - RGAS / WM(I)
      GAMMA(I) = CP(I) / CV


C********0*********0*********0*********0*********0*********0*********
C AVERAGE MOLECULAR WEIGHT:
```

```
C SPLINE FIT:  'WM.DAT'
C      Average molecular weight function of chemistry and state at
C assumed equilibrium conditions.
C SOURCE:  MSE, Inc. equilibrium data.
C ERROR:  (About 1% estimated from worst fit on known data points.)
C********0*********0*********0*********0*********0*********0*********
        WM(I) = SR( 'WM.DAT    ', 'Y', OX, PHI, SEED, P(I) / PASCALS,
     &                                                       T(I) )

C********0*********0*********0*********0*********0*********0*********
C STAGNATION PRESSURE:
C                   Ps = P * ( Ts/T )^[ gamma / (gamma - 1) ]
C********0*********0*********0*********0*********0*********0*********
        PSTAG(I) = P(I) * ( TSTAG(I) / T(I) )**( GAMMA(I) / (
     &                                              GAMMA(I) - 1. ) )

C********0*********0*********0*********0*********0*********0*********
C DENSITY AT MAJOR AND MINOR NODES:
C                          rho = P / ( R * T )
C********0*********0*********0*********0*********0*********0*********
        RHO(I) = P(I) * WM(I) / ( RGAS * T(I) )

        IF ( I .GT. 1 ) RHO_MIN(I-1) = 0.5 * ( RHO(I-1) + RHO(I) )

C********0*********0*********0*********0*********0*********0*********
C FLOW RATE:
C********0*********0*********0*********0*********0*********0*********
        IF ( FLAG_T .EQ. 'Y' ) W(I) = RHO(I) * V_MAJ(I) * A(I)

C********0*********0*********0*********0*********0*********0*********
C MACH NUMBER:
C********0*********0*********0*********0*********0*********0*********
        VMACH(I) = DABS( V_MAJ(I) ) / DSQRT( GAMMA(I) * RGAS * T(I) /
     &                                                        WM(I) )

C********0*********0*********0*********0*********0*********0*********
C COMPRESSIBILITY PARTIAL:
C********0*********0*********0*********0*********0*********0*********
        DRHODP(I) = WM(I) / ( RGAS * T(I) )

C********0*********0*********0*********0*********0*********0*********
C FRICTION AND THERMAL COEFFICIENTS:
C********0*********0*********0*********0*********0*********0*********
        IF ( I .GT. NCOMB ) THEN
          CALL FG(I)
        ELSE
          F(I) = 0.
          Q(I) = 0.
        END IF

 10     CONTINUE

C********0*********0*********0*********0*********0*********0*********
```

```
C INPUT FLOW RATE:
C*******0*********0*********0*********0*********0*********0*********
      I = 1
        W(I) = WC / 10.0 * SR( 'CF_C10.DAT', 'Y', OX, PHI, SEED,
     *                                 PSTAG(I) / PASCALS, PHEAT )

      IF ( FLAG_T .EQ. 'N' ) THEN
        DO 20 I = 1, NNDS
 20       W(I) = W(1)
      END IF

      RETURN
      END
```

SIMPLER Numerical Integration Subroutine

```
C*******0*********0*********0*********0*********0*********0*********
C
C     SUBROUTINE: SIMPLER
C
C     PROGRAMMER:  Donald J. Hammerstrom, Graduate Student
C                  Department of Electrical Engineering
C                  Montana State University
C                  Bozeman, Montana  59717-0378
C
C     DATE:  1994
C
C     PURPOSE:
C          This program carries out integration of the MHD equation
C     set using the SIMPLER (Semi-Implicit Method for Pressure-Linked
C     Equations, Revised) algorithm of Patankar (1980).  The momentum
C     equation also incorporates Van Leer flux splitting to better
C     represent the partially elliptic nature of the problem.
C     Patankar's suggestion for incorporating compressibility effects
C     (Patankar, 1980 prob. 6-6) is used to stabilize both the
C     pressure and pressure correction equations.
C          The subroutine is written to be fully implicit in time.
C     Both steady and unsteady behaviors may be obtained.
C     The unsteady solution is like a succession of converged steady
C     solutions.
C
C*******0*********0*********0*********0*********0*********0*********
      SUBROUTINE SIMPLER(RES)

      INCLUDE 'COMMONER.FL'

      DIMENSION  V_STAR(NNDS_MAX), P_PRIME(NNDS_MAX), FLUX(NNDS_MAX),
     &  V_HAT(NNDS_MAX), ZP(NNDS_MAX), ZA(NNDS_MAX), ZB(NNDS_MAX),
     &  ZC(NNDS_MAX), BB(NNDS_MAX), ZETAA(NNDS_MAX), ZETAB(NNDS_MAX),
     &  ZETAC(NNDS_MAX), BBB(NNDS_MAX), FSU(NNDS_MAX), FSD(NNDS_MAX),
```

```
     &  VS(NNDS_MAX)

C*******0*********0*********0*********0*********0*********0*********
C  FIND V_HAT FROM THE MOMENTUM EQUATION:
C
C              X,X-, and X+ == major node positions on staggered grid
C              x,x-, and x+ == minor node positions on staggered grid
C              Z()          == coefficients
C              b            == source terms
C              D()          == diffusion
C              F()          == flux
C
C Note that the grid is staggered as shown below:
C
C  cell i-1        |        cell i         |        cell i+1       |
C     |            |            |          |            |          |
C     0 -------- o -------- 0 -------- o -------- 0 -------- o ----
C     X-           x-           X          x            X+         x+
C     |            |            |          |            |          |
C                  |                       |                       |
C
C     Z(x)*v(x) = Z(x+)*v(x+) + Z(x-)*v(x-) + b + Zp(x)*(P(X+)-P(X))
C
C                               Z(x+) = D(X+) - F(X+)
C                               Z(x-) = D(X-) + F(X-)
C                             Z(x) = Z(x+) + Z(x-) + . . .
C                                b = source terms
C                                 Zp(x) = -A(x)*dt
C
C                    v(x) = v_hat(x) + Zp/Z(x)*(P(X+)-P(X)),     where
C                     v_hat(x) = (Z(x+)*v(x+) + Z(x-)*v(x-) + b)/Z(x)
C
C BEGIN FLUX SPLITTING:
C     Flux splitting is a method of reflecting the acoustic
C propagation of states.  Increasingly more upstream state is used
C in the bias until Mach one, at which only upstream states affect
C the local node.  This differencing is a monotone upwind
C differencing scheme.  It has some advantage over simple upwind
C differencing promoted by Patankar because it utilizes both adjacent
C neighbors even when there is no true diffusion term.  Upstream
C influence is particularly necessary in partially eliptic problems
C where downstream states affect upstream states.
C*******0*********0*********0*********0*********0*********0*********

C*******0*********0*********0*********0*********0*********0*********
C LOCAL VELOCITY OF SOUND:
C
C              VS()     == local velocity of sound
C
C     Some interpolation is necessary because of staggered grid.
C
C                        v(sound) = sqrt( gamma * R * T )
C
```

```
C*******0*********0*********0*********0*********0*********0*********
      DO 10 I = 1, NNDS - 1
        T_AVE = 0.5 * ( T(I) + T(I+1) )
        WM_AVE = 0.5 * ( WM(I) + WM(I+1) )
        GAMMA_AVE = 0.5 * ( GAMMA(I) + GAMMA(I+1) )
 10     VS(I) = DSQRT( GAMMA_AVE * RGAS * T_AVE / WM_AVE )

      I = NNDS
        VS(I) = DSQRT( GAMMA(I) * RGAS*T(I) / WM(I) )

C*******0*********0*********0*********0*********0*********0*********
C VAN LEER ADVECTED FLUX:
C
C          FSD()    == upstream advected flux (Van Leer's F-)
C          FSU()    == downstream advected flux (Van Leer's F+)
C          VMACH()  == local Mach number
C
C Van Leer's scheme of flux splitting:
C
C                       fs+ =  0.25 * VS * (M + 1)**2,     |M|<1.0
C                              0.50 * VS * (M + |M|) ,     otherwise
C
C                       fs- = -0.25 * VS * (M - 1)**2,     |M|<1.0
C                              0.50 * VS * (M - |M|) ,     otherwise
C*******0*********0*********0*********0*********0*********0*********
      DO 20 I = 1, NNDS - 1
        VMACH(I) = V(I) / VS(I)
        IF ( DABS( VMACH(I) ) .LT. 1.D0 ) THEN
          FSU(I) =  0.25D0 * VS(I) * ( VMACH(I) + 1.D0 )**2
          FSD(I) = -0.25D0 * VS(I) * ( VMACH(I) - 1.D0 )**2
        ELSE
          FSU(I) =  0.50D0 * VS(I) * ( VMACH(I) + DABS( VMACH(I) ) )
          FSD(I) =  0.50D0 * VS(I) * ( VMACH(I) - DABS( VMACH(I) ) )
        END IF
        FSU(I) = FSU(I) * RHO_MIN(I)
        FSD(I) = FSD(I) * RHO_MIN(I)
 20     CONTINUE

      I=NNDS
        VMACH(I) = V(I)/VS(I)
        FSD(I) = -0.25D0 * VS(I) * ( VMACH(I) - 1.D0 )**2
        FSD(I) = FSD(I) * RHO(I)

C*******0*********0*********0*********0*********0*********0*********
C MOMENTUM EQUATION:
C
C          ZA(),ZB(),ZC()  == velocity coefficients
C          ZP()            == coefficient of pressure difference
C          BBB()           == source terms
C
C     The solution of the momentum equation is centered on the cell
C interfaces.  Solution is fully implicit in time.  Most quantities
C are interpolated by a linear interpolation.  All quantities except
```

```
C velocity are defined at major node points.  Velocity is defined at
C cell interfaces located half way between the major node centers.
C
C           d(rho*v*A)/dt + d(rho*v^2*A)/dx = -A*F - A*dP/dx + A*jB
C
C*******0*********0*********0*********0*********0*********0*********
      DO 30 I = 2, NNDS - 2
C INTERPOLATIONS:
        RHO_MINOR_OLD = 0.5 * ( RHO_OLD(I) + RHO_OLD(I+1) )
        F_MINOR = ( F(I) * F(I+1) )**0.5
C COEFFICIENT ASSIGNMENTS:
        ZA(I) =  FSU(I-1) / STP_MAJ(I) * STP_MIN(I) * DT
        ZC(I) = -FSD(I+1) / STP_MAJ(I+1) * STP_MIN(I) * DT
        ZB(I) = FSU(I) / STP_MAJ(I) * STP_MIN(I) * DT
     &         - FSD(I) / STP_MAJ(I+1) * STP_MIN(I) * DT
     &         + STP_MIN(I) * RHO_MIN(I) * FLAG_DT
     &         + 2.0 * F_MINOR * STP_MIN(I) * DT / V(I)
     &         + 2.0 * RHO_MIN(I) * V(I) / A_MIN(I) * (A(I+1) - A(I))
     &                                                            * DT
        ZP(I) = -DT
        BBB(I) = STP_MIN(I) * RHO_MINOR_OLD * V_OLD(I) * FLAG_DT
     &          + F_MINOR * STP_MIN(I) * DT
     &          + RHO_MIN(I) * V(I)**2 / A_MIN(I) * (A(I+1) - A(I))
     &                                                            * DT
 30     CONTINUE

C*******0*********0*********0*********0*********0*********0*********
C EXCEPTIONS TO THE ABOVE GENERAL EQUATIONS:
C*******0*********0*********0*********0*********0*********0*********

C*******0*********0*********0*********0*********0*********0*********
C FIRST NODE:
C
C     The first node momentum equation assumes that the gradient of
C the momentum flux is zero at the input boundary.  This is an
C infinite volume combustor assumption.  It is further assumed that
C there are no friction or thermal losses in the combustor since
C these losses are handled elsewhere.
C*******0*********0*********0*********0*********0*********0*********
      I = 1
        RHO_MINOR_OLD = 0.5 * ( RHO_OLD(I) + RHO_OLD(I+1) )
        ZA(I) = 0.
        ZC(I) = -FSD(I+1) * DT
        ZB(I) = -FSD(I) * DT
     &         + FSU(I) * DT
     &         + STP_MIN(I) * RHO_MIN(I) * FLAG_DT
        ZP(I) = -DT
        BBB(I) = STP_MIN(I) * RHO_MINOR_OLD * V_OLD(I) * FLAG_DT
     &          + FSU(I) * V(I) * DT

C*******0*********0*********0*********0*********0*********0*********
C CHANNEL NODE LORENTZ FORCE TERMS:
C*******0*********0*********0*********0*********0*********0*********
```

```
      I = NNOZZ
        L = I - NNOZZ
        ECURAV = 0.5 * ( CANODE(L+1) + CCATH(L+1) )
        WIDTH = A(I+1) / ZHEIGHT
        EAREA = STP_MAJ(I+1) * WIDTH
        FJ1 = ECURAV / EAREA
        BBB(I) = BBB(I)
     &           + 0.5 * FJ1 * BFACT * B(L+1) * DT * STP_MIN(I)

      DO 40 I = NNOZZ + 1, NCHAN - 1
        L = I - NNOZZ
        WIDTH = A(I) / ZHEIGHT
        EAREA = STP_MAJ(I) * WIDTH
        ECURAV = 0.5 * ( CANODE(L) + CCATH(L) )
        FJ1 = ECURAV / EAREA
        WIDTH = A(I+1) / ZHEIGHT
        EAREA = STP_MAJ(I+1) * WIDTH
        ECURAV = 0.5 * ( CANODE(L+1) + CCATH(L+1) )
        FJ2 = ECURAV / EAREA
 40     BBB(I) = BBB(I)
     &           + 0.5 * BFACT * ( FJ1 * B(L) + FJ2 * B(L+1) ) * DT *
     &                                                         STP_MIN(I)

      I = NCHAN
        L = I - NNOZZ
        ECURAV = 0.5 * ( CANODE(L) + CCATH(L) )
        WIDTH = A(I) / ZHEIGHT
        EAREA = STP_MAJ(I) * WIDTH
        FJ1 = ECURAV / EAREA
        BBB(I) = BBB(I)
     &           + 0.5 * STP_MIN(I) * FJ1 * BFACT * B(L) * DT

C*******0*********0*********0*********0*********0*********0*********
C LAST NODE:
C     Use simple backward differencing at exit nodes.
C*******0*********0*********0*********0*********0*********0*********
      I = NNDS - 1
        RHO_MINOR_OLD = 0.5 * ( RHO_OLD(I) + RHO_OLD(I+1) )
        F_MINOR = ( F(I) * F(I+1) )**0.5
        FLUXM = RHO(I) * V_MAJ(I) * DT
        FLUXP = RHO(I+1) * V(I+1) * DT
        ZA(I) = DMAX1( 0.D0, FLUXM )
        ZC(I) = DMAX1( 0.D0, -FLUXP )
        ZB(I) = ZA(I)
     &          + ZC(I)
     &          + STP_MIN(I) * RHO_MIN(I) * FLAG_DT
     &          + 2.0 * F_MINOR * STP_MIN(I) * DT / V(I)
     &          + 2.0 * RHO_MIN(I) * V(I) / A_MIN(I) * (A(I+1) - A(I))
     &                                                              * DT
        ZP(I) = -DT
        BBB(I) = STP_MIN(I) * RHO_MINOR_OLD * V_OLD(I) * FLAG_DT
     &           + F_MINOR * STP_MIN(I) * DT
     &           + RHO_MIN(I) * V(I)**2 / A_MIN(I) * ( A(I+1) - A(I) )
```

```
     &                                                                 * DT

C NORMALIZATION:
      DO 50 I = 1, NNDS - 1
        ZA(I) = ZA(I) / ZB(I)
        ZC(I) = ZC(I) / ZB(I)
        ZP(I) = ZP(I) / ZB(I)
        BBB(I) = BBB(I) / ZB(I)
 50     ZB(I) = 1.

C*******0*********0*********0*********0*********0*********0*********
C  V_HAT:
C      This is an approximation of velocity without pressure effects.
C Note that there is one less minor node than major node in this
C solution.
C*******0*********0*********0*********0*********0*********0*********
      I = 1
        V_HAT(I) = ZC(I) * V(I+1)
     &             + BBB(I)

      DO 60 I = 2, NNDS - 2
 60     V_HAT(I) = ZA(I) * V(I-1)
     &             + ZC(I) * V(I+1)
     &             + BBB(I)

      I = NNDS - 1
        V_HAT(I) = ZA(I) * V(I-1)
     &              + BBB(I)

      I = NNDS
        V_HAT(I) = 1.5 * V_HAT(I-1) - 0.5 * V_HAT(I-2)

C*******0*********0*********0*********0*********0*********0*********
C  CONTINUITY EQUATION:
C
C                    K(X)P(X) = K(X+)P(X+) + K(X-)P(X-) + r
C
C                       K(X+) = -Zp(x+)*A(x+)*rho(x+)*dt
C                       K(X-) = -Zp(x-)*A(x-)*rho(x-)*dt
C                           K(0)  = K(X+) + K(X-)
C                         r = {-equation of continuity}
C
C  (Flux uses V_HAT for pressure eqn.; V_STAR for pressure correction
C eqn.)
C
C  (Remember that ZP is defined to be negative.)
C*******0*********0*********0*********0*********0*********0*********
      DO 100 I = 1, NNDS - 1
        ZETAC(I)   = -DT * ZP(I) * RHO_MIN(I)
        ZETAA(I+1) = ZETAC(I)
 100    CONTINUE

C FIRST MAJOR NODE: (Separated due to source term.)
```

```
        I = 1
          ZETAB(I) = ZETAC(I)
     &               + DRHODP(I) * STP_MAJ(I) * FLAG_DT
     &               + DMAX1( 0.D0, 0.5 * DRHODP(I) * V_HAT(I) * DT )
          ZETAA(I) = 0.
          ZETAC(I) = -ZETAC(I)
     &               + DMIN1( 0.D0, 0.5 * DRHODP(I+1) * V_HAT(I) * DT )
          BB(I) = STP_MAJ(I) * RHO_OLD(I) * FLAG_DT
     &            + DMAX1(0.D0, -0.5 * DRHODP(I) * V_HAT(I) * P(I) * DT)
     &            + DMIN1(0.D0, -0.5 * DRHODP(I+1) * V_HAT(I) * P(I+1) *
     &                                                             DT )
     &            + W(I) * DT / A(I)

C REMAINING MAJOR DUCT NODES:
        DO 120 I = 2, NNDS - 1

C COMPLETE COEFFICIENT ASSIGNMENTS AT ALL MAJOR NODES:
          ZETAB(I) = ZETAA(I)
     &               + ZETAC(I)
     &               + DRHODP(I) * STP_MAJ(I) * FLAG_DT
     &               + DMAX1( 0.D0, 0.5 * DRHODP(I) * V_HAT(I) * DT )
     &               + DMAX1( 0.D0, -0.5 * DRHODP(I) * V_HAT(I-1) * DT )
     &               + DRHODP(I) * V_MAJ(I) / A(I) * ( A_MIN(I) -
     &                                            A_MIN(I-1) ) * DT
          ZETAA(I) = -ZETAA(I)
     &               + DMIN1(0.D0, -0.5 * DRHODP(I-1) * V_HAT(I-1) * DT)
          ZETAC(I) = -ZETAC(I)
     &               + DMIN1( 0.D0, 0.5 * DRHODP(I+1) * V_HAT(I) * DT )
          BB(I) = STP_MAJ(I) * RHO_OLD(I) * FLAG_DT
     &               + DMAX1( 0.D0, -0.5 * DRHODP(I) * V_HAT(I) * P(I) *
     &                                                             DT )
     &               + DMAX1( 0.D0, 0.5 * DRHODP(I) * V_HAT(I-1) * P(I) *
     &                                                             DT )
     &               + DMIN1(0.D0, 0.5 * DRHODP(I-1) * V_HAT(I-1) *
     &                                                    P(I-1) * DT )
     &               + DMIN1(0.D0, -0.5 * DRHODP(I+1) * V_HAT(I) * P(I+1)
     &                                                           * DT )
 120      CONTINUE

C*******0*********0*********0*********0*********0*********0*********
C  THE LAST NODE: (Dir. boundary condition.)
C*******0*********0*********0*********0*********0*********0*********
        I = NNDS
          ZETAA(I) = 0.
          ZETAB(I) = 1.
          ZETAC(I) = 0.
          BB(I) = PSEXIT * ( T(I) / TSTAG(I) )**( GAMMA(I) / ( GAMMA(I)
     &                                                         - 1. ) )

C*******0*********0*********0*********0*********0*********0*********
C  TDMA ALGORITHM:
C  SOURCE:  FORTRAN NUMERICAL RECIPIES (1989)
C        The outlet pressure is the boundary condition.
```

```
C  Underrelaxation of the calculation using 0.8 underrelaxation
C  factor is suggested by Patankar.
C********0*********0*********0*********0*********0*********0*********
      CALL TRIDIAG( ZETAA, ZETAB, ZETAC, BB, P_PRIME, NNDS )

      DO 130 I = 1, NNDS
 130    P(I) = 0.2 * P(I) + 0.8 * DMAX1( 0.D0, P_PRIME(I) )

C********0*********0*********0*********0*********0*********0*********
C  V_STAR:
C       Underrelaxation factor of 0.5 is suggested by Patankar.
C       The coefficients require only minor modification.  Some of
C  these modifications account for changes in density assumed in
C  pressure equation result.
C********0*********0*********0*********0*********0*********0*********
      DO 200 I = 1, NNDS - 1
        ZA(I) = -ZA(I)
        ZB(I) = ZB(I) - 0.2 * ZP(I) * P(I+1) / V(I)
        ZC(I) = -ZC(I)
        BBB(I) = BBB(I)
     &           - ZP(I) * P(I)
     &           + 0.8 * ZP(I) * P(I+1)
 200    CONTINUE

C********0*********0*********0*********0*********0*********0*********
C  TDMA ALGORITHM:
C       Do not calculate the last velocity node, which is beyond
C  boundaries.
C********0*********0*********0*********0*********0*********0*********
      CALL TRIDIAG( ZA, ZB, ZC, BBB, V_HAT, NNDS - 1 )

      DO 210 I = 1, NNDS - 1
 210    V_STAR(I) = 0.5 * V(I) + 0.5 * DMAX1( 0.D0, V_HAT(I) )

      I = NNDS
        V_STAR(I) = 1.5 * V_STAR(I-1) - 0.5 * V_STAR(I-2)

C********0*********0*********0*********0*********0*********0*********
C CORRECT DENSITY AS IMPLIED IN PRESSURE CALCULATION
C********0*********0*********0*********0*********0*********0*********
      DO 140 I = 1, NNDS
 140    RHO(I) = DRHODP(I) * P(I)

      DO 150 I = 1, NNDS-1
 150    RHO_MIN(I) = 0.5 * ( RHO(I) + RHO(I+1) )

C********0*********0*********0*********0*********0*********0*********
C  PRESSURE CORRECTION EQUATION:
C  The pressure correction equations are used to correct the velocity
C  profile.  The calculation is almost the same as for the pressure
C  equation, but the source term becomes the continuity error.
C       A correction has been incorporated to account for
C  compressibility.
```

```
C       Note that the evaluation of BB is useful for convergence
C  criterion since it is simply a statement of continuity.
C       Negative signs are used for off diagonals because of
C  tridiagonal form of solution.
C       FLAG_DT is used to toggle on or off the transient response.
C*******0*********0*********0*********0*********0*********0*********

C CALCULATE FLUX AT MINOR NODES:
      DO 300 I = 1, NNDS - 1
        ZETAC(I) = -DT * ZP(I) * RHO_MIN(I)
        ZETAA(I+1) = ZETAC(I)
        FLUX(I) = DT * V_STAR(I) * RHO_MIN(I)
 300    CONTINUE
      I = NNDS
        FLUX(I) = DT * V_STAR(I) * RHO(I)

C FIRST MAJOR NODE: (Separated due to source term.)
      I = 1
        ZETAB(I) =  ZETAC(I)
     &             + DRHODP(I) * STP_MAJ(I) * FLAG_DT
     &             + DMAX1( 0.D0, 0.5 * DRHODP(I) * V_STAR(I) * DT )
        ZETAC(I) = -ZETAC(I)
     &             + DMIN1( 0.D0, 0.5 * DRHODP(I+1) * V_STAR(I) * DT )
        ZETAA(I) = 0.
        BB(I) = STP_MAJ(I) * ( RHO_OLD(I) - RHO(I) ) * FLAG_DT
     &          + W(I) / A(I) * DT - FLUX(I)

C REMAINING MAJOR DUCT NODES:
      DO 320 I = 2, NNDS - 1

C COEFFICIENTS:
        ZETAB(I) = ZETAA(I)
     &             + ZETAC(I)
     &             + DRHODP(I) * STP_MAJ(I) * FLAG_DT
     &             + DMAX1( 0.D0, 0.5 * DRHODP(I) * V_STAR(I) * DT )
     &             + DMAX1( 0.D0, -0.5 * DRHODP(I) * V_STAR(I-1) * DT)
        ZETAA(I) = -ZETAA(I)
     &             + DMIN1(0.D0,-0.5 * DRHODP(I-1) * V_STAR(I-1) * DT)
        ZETAC(I) = -ZETAC(I)
     &             + DMIN1( 0.D0, 0.5 * DRHODP(I+1) * V_STAR(I) * DT )
        BB(I) = STP_MAJ(I) * ( RHO_OLD(I) - RHO(I) ) * FLAG_DT
     &          - FLUX(I)
     &          + FLUX(I-1)
     &          - RHO(I) * V_MAJ(I) / A(I) * ( A_MIN(I) - A_MIN(I-1) )
     &                                                             * DT
 320    CONTINUE

C*******0*********0*********0*********0*********0*********0*********
C LAST NODE.
C*******0*********0*********0*********0*********0*********0*********
      I = NNDS
      ZETAA(I) = 0.
      ZETAB(I) = 1.
```

```
      ZETAC(I) = 0.
      BB(I) = 0.

C********0*********0*********0*********0*********0*********0*********0*********
C  TDMA ALGORITHM:
C       The outlet pressure is the boundary condition.
C********0*********0*********0*********0*********0*********0*********0*********
      CALL TRIDIAG( ZETAA, ZETAB, ZETAC, BB, P_PRIME, NNDS )

C********0*********0*********0*********0*********0*********0*********0*********
C  CORRECT THE VELOCITY FIELD:
C       It is suggested by Patankar that no relaxation be used in
C  this calculation to assure a velocity profile which adheres to
C  continuity.  **[Patankar (1980) eq. (6.17)]:
C                    V(x) = V_star(x) + Zp(x)*(P'(X+) - P'(X))
C********0*********0*********0*********0*********0*********0*********0*********
      DO 400 I = 1, NNDS - 1
        DVMAX = ZP(I) * ( P_PRIME(I+1) - P_PRIME(I) )
        V(I) = V_STAR(I) + DVMAX
 400    CONTINUE
      I = NNDS
        V(I) = V(I-1) + 0.5 * ( V(I-1) - V(I-2) )

      DO 410 I = 1, NNDS
        P(I) = P(I) + 0.8 * P_PRIME(I)
        RHO(I) = DRHODP(I) * P(I)
 410    IF ( I .GT. 1 ) RHO_MIN(I-1) = 0.5 * ( RHO(I-1) + RHO(I) )

C********0*********0*********0*********0*********0*********0*********0*********
C  STAGNATION ENTHALPY EQUATION:
C       The first node is specified from combustor data provided by
C  MSE, Inc.  The result of previous calculations should be a flat
c  flux profile.  The stagnation enthalpy is used to calculate the
C  temperature profile, which affects the fluid density.
C
C                   a(X)*h(X) = a(X+)*h(X+) + a(X-)*h(X+) + n
C
C                          a(X+) = [[ 0 , -F(x+) ]]
C                          a(X-) = [[ 0 ,  F(x-) ]]
C          a(X)  = rho(X)*A(X)*dx + [[ 0 , F(x+) ]] + [[ 0 , -F(x-) ]]
C n = rho(X,old)*A(X)*dx*h(X,old) + [(Jx*Ex + Jy*Ey)-Q(X)]*A(0)*dx*dt
C
C                          F(y) = rho(y)*v(y)*A(y)*dt
C********0*********0*********0*********0*********0*********0*********0*********

C FIRST MAJOR NODE: (Dir. boundary condition.)
      I = 1
        ZA(I) = 0.
        ZB(I) = 1.
        ZC(I) = 0.
        HS(I) = SR( 'CE_C10.DAT', 'Y', OX, PHI, SEED, PSTAG(I) /
     &                                                  PASCALS, PHEAT )
        BBB(I) = HS(I) - P(I) / RHO(I)
```

```
C REMAINING MAJOR DUCT NODES:
      DO 600 I = 2, NNDS - 1

        IF ( EIO(I) .EQ. 0. ) EIO(I) = HS(I) - P(I) / RHO(I)

C CALCULATE MAJOR NODE COEFFICIENTS:
        L = I - NNOZZ
        P_MINORP = 0.5 * ( P(I) + P(I+1) )
        P_MINORM = 0.5 * ( P(I) + P(I-1) )
        FLOW = RHO(I) * V_MAJ(I) * DT
        ZA(I) = DMAX1( 0.D0,  FLOW ) / STP_MIN(I-1) * STP_MAJ(I)
        ZC(I) = DMAX1( 0.D0, -FLOW ) / STP_MIN(I) * STP_MAJ(I)
        ZB(I) = RHO(I) * STP_MAJ(I) * FLAG_DT
     &         + ZA(I)
     &         + ZC(I)
     &         + 0.5 * FLOW * P_MINORP / RHO_MIN(I) * DT / EIO(I)
     &         + 0.5 * Q(I) * STP_MAJ(I) * DT / EIO(I)
        BBB(I) = RHO(I) * STP_MAJ(I) * EIO_OLD(I) * FLAG_DT
     &          - 0.5 * Q(I) * STP_MAJ(I) * DT
     &          + FLOW * P_MINORM / RHO_MIN(I-1) * DT
     &          - 0.5 * FLOW * P_MINORP / RHO_MIN(I) * DT

        IF ( I .GT. NNOZZ .AND. I .LE. NCHAN ) THEN
          ECURAV = 0.5 * ( CANODE(L) + CCATH(L) )
          WIDTH = A(I) / ZHEIGHT
          EAREA = STP_MAJ(I) * WIDTH
          FY1 = ECURAV / EAREA
          FX1 = CX(L) / A(I)
          EY1 = -( VY(1,L) - VDR(L) * CANODE(L) + VY(2,L) - VDR(L) *
     &                                      CCATH(L) ) / ZHEIGHT
          EX1 = -VX(L) / STP_MAJ(I)
          BBB(I) = BBB(I)
     &            + ( FY1 * EY1 + FX1 * EX1 ) * STP_MAJ(I) * DT
        END IF
        ZA(I) = -ZA(I)
        ZC(I) = -ZC(I)
 600    CONTINUE

C LAST MAJOR NODE: (Half-cell method.)
      I = NNDS
        IF ( EIO(I) .EQ. 0. ) EIO(I) = HS(I) - P(I) / RHO(I)
        P_MINORM = 0.5 * ( P(I) + P(I-1) )
        FLOW = RHO(I) * V(I) * DT
        ZA(I) = DMAX1( 0.D0,  FLOW )
        ZC(I) = DMAX1( 0.D0, -FLOW )
        ZB(I) = RHO(I) * 0.5 * STP_MAJ(I) * FLAG_DT
     &         + ZA(I)
     &         + ZC(I)
     &         + 0.25 * Q(I) * STP_MAJ(I) * DT / EIO(I)
     &         +  0.25 * FLOW * P(I) / RHO(I) * DT / EIO(I) *
     &                                              STP_MAJ(I)
        ZA(I) = -ZA(I)
```

```
      BBB(I) = RHO(I) * 0.5 * STP_MAJ(I) * EIO_OLD(I) * FLAG_DT
     &          - 0.25 * Q(I) * STP_MAJ(I) * DT
     &          + 0.5 * FLOW * P_MINORM / RHO_MIN(I-1) * DT *
     &                                                  STP_MAJ(I)
     &          - 0.25 * FLOW * P(I) / RHO(I) * DT * STP_MAJ(I)
     &          + ZC(I) * EIO(I)
      ZC(I) = 0.

C*******0*********0*********0*********0*********0*********0*********
C  TDMA SOLUTION:
C*******0*********0*********0*********0*********0*********0*********
      CALL TRIDIAG( ZA, ZB, ZC, BBB, EIO, NNDS )

C*******0*********0*********0*********0*********0*********0*********
C  CHECK FOR CONVERGENCE:
C*******0*********0*********0*********0*********0*********0*********
      RES = 0.

      DO 700 I = 2, NNDS - 1
 700    RES = RES + ABS( BB(I) )

C*******0*********0*********0*********0*********0*********0*********
C STATE HAS BEEN CALCULATED.
C*******0*********0*********0*********0*********0*********0*********
      RETURN
      END
```

SOLVEVOLT Channel Electrical Interaction Subroutine

```
C*******0*********0*********0*********0*********0*********0*********
C
C     SUBROUTINE: SOLVEVOLT
C
C     PROGRAMMER:  Donald Hammerstrom, Graduate Student
C                  Department of Electrical Engineering
C                  Montana State University
C                  Bozeman, Montana  59717-0378
C
C     DATE:  1993
C
C     PURPOSE:
C          This subroutine solves the voltage profile of the internal
C     MHD circuit model.  It is assumed that the external circuit has
C     been called in another routine to determine boundary currents
C     of this solution as functions of electrode voltages.  The
C     internal circuit model includes parts of the Gupta and Rohatgi
C     voltage drop layer which are not proportional to current.
C     Those parts proportional to current are included in the
C     external circuit model.
C
```

```
C
C  Cx(i-1)          o  | Canode(i)
C     -->           |
C                o--o--o              Cx(i)=Ccath(i)-Canode(i)+Cx(i-1)
C                   |
C                   o  ^
C                      | Ccath(i)
C
C
c
C                   --             -     -   --      - -
C                  |Vx|           |Rxx Rxy||Ix|     | 0 |
C                  |  |     =     |        ||  | -  |   |
C                  |Vy|           |Ryx Ryy||Iy|     |hvB|
C                   --             -     -   --      - -
C
C     INPUTS:
C          (1) Boundary electrode current profile determined by
C              external circuit
C          (2) Fluid conductivity at each node
C          (3) Cell dimensions
C          (4) A parameter alpha to ease convergence
C          (5) The non-"resistive" portion of the G & R voltage
C              drop model
C
C     OUTPUTS:
C          (1) Internal circuit voltage profile
C          (2) x - direction current profile
C          (3) Electrode voltage profile
C
C********0*********0*********0*********0*********0*********0*********
      SUBROUTINE SOLVEVOLT

      INCLUDE 'COMMONER.FL'

C********0*********0*********0*********0*********0*********0*********
C CALCULATE THE HALL CURRENT PROFILE BY CURRENT CONSERVATION AT NODES
C********0*********0*********0*********0*********0*********0*********
      CX(1) = CCATH(1) - CANODE(1)
      DO 10 I = 2, NEP
 10     CX(I) = CCATH(I) - CANODE(I) + CX(I-1)

C********0*********0*********0*********0*********0*********0*********
C USE CURRENT DISTRIBUTION TO OBTAIN VOLTAGE PROFILE.
C RXX,RXY,RYX AND RYY ARE MATRIX ELEMENTS AS SHOWN IN HEADER.
C E_Y IS THE LONE SOURCE TERM.
C ALPHA IS THE MATRIX OF RELAXATION FACTORS.
C********0*********0*********0*********0*********0*********0*********
      DO 20 I = 1, NEP
        L = NNOZZ + I
        WIDTH = A(L) / ZHEIGHT
        REDUCER = 1. + SEGR * ( BETA(I) - 0.44 )
        RXX = -REDUCER * STP_MAJ(L) / ( SIGMA(I) * A(L) )
        RXY = -BETA(I) / ( SIGMA(I) * WIDTH )
```

```
      RYX = -RXY
      RYY = -REDUCER * ZHEIGHT / ( SIGMA(I) * STP_MAJ(L) * WIDTH )
      E_Y = V_MAJ(L) * BFACT * B(I) * ZHEIGHT
      ALPHA(I) = -0.25 * ( 2. * VDR(I) + RCCC ) / RYY
      IF ( ALPHA(I) .GT. 0.5 ) ALPHA(I) = 0.5
        VX(I) = RXX * CX(I) + 0.5 * RXY * ( CANODE(I) + CCATH(I) )
        VY(2,I) = 0.5 * RYX * CX(I) + .5 * RYY * CANODE(I) - 0.5 *
     &                                                            E_Y
        VY(1,I) = 0.5 * RYX * CX(I) + 0.5 * RYY * CCATH(I) - 0.5 *
     &                                                            E_Y
 20   CONTINUE

C********0*********0*********0*********0*********0*********0*********
C VOLTAGE DROPS:
C    VD  non-ohmic voltage drop at both anode and cathode (V)
C   VDR  ohmic resistance to current at this electrode (R)
C      Use pure voltage drop in internal circuit and equivalent
C resistance on the external circuit.  This division allows
C convergence even for external short circuits.  Do not change this
C code section.
C REFERENCE: Gupta and Rohatgi
C********0*********0*********0*********0*********0*********0*********
      DO 30 I = NNOZZ + 1, NCHAN
        L = I - NNOZZ
        EX = -VX(L) / STP_MAJ(I)
        VD(L) = VDROPP( TW, TS, T(I), POT, DELTA, BETA(L), V_MAJ(I),
     &                                  BFACT * B(L), -EX, SEGR )
        VDR(L) = VDROPR(TW, TS, T(I), DELTA, BETA(L), SIGMA(L), SEGR)
          VDR(L) = EWF * VDR(L) / ( STP_MAJ(I) * A(I) / ZHEIGHT )
 30   CONTINUE

C********0*********0*********0*********0*********0*********0*********
C ELECTRODE VOLTAGES:
C           VANODE == anode voltages
C            VCATH == cathode voltages
C********0*********0*********0*********0*********0*********0*********
      SUM = 0.
      DO 40 I = NEP, 1, -1
        SUM = SUM - VX(I)
      VANODE(I) = SUM + VY(2,I) + VD(I)
 40   VCATH(I) = SUM - VY(1,I) - VD(I)

      RETURN
      END
```

SPLINER Spline Function Creation Program

```
C********0*********0*********0*********0*********0*********0*********
C
C     PROGRAM SPLINER
```

```
C
C     DATE:  1992
C
C     PROGRAMMER:  Donald Hammerstrom, Graduate Student
C                  Department of Electrical Engineering
C                  Montana State University
C                  Bozeman, Montana  59717
C
C     PURPOSE:
C          This program creates a file from an existing function or a
C     set of data points.  The file contains information to carry
C     out a cubic Hermite spline interpolation of dimension one to
C     five.
C
C     INPUTS:
C
C          Function F1(V1,V2,...) must be available to give function
C               evaluation or to interpret a data file.
C
C          The user inputs some information interactively.
C
C     OUTPUTS:
C
C          Program terminates with a summary of spline file
C               information.  The spline file contains all
C               information necessary for cubic spline fit in
C               dimensions up to five.
C
C     OUTPUT FILE FORMAT:
C
C          RECORD ONE:
C               Spline name, number of independent variables, number
C                    of nodes in each independent variable.
C          RECORD TWO:
C               List of variable values at spline nodes.
C          RECORDS THREE . . . :
C               Variable values at one node, evaluation at the node,
C                    first varaiations, second variations, . . .,
C                    fifth variation.
C
C*******0*********0*********0*********0*********0*********0*********
      PROGRAM SPLINER

      IMPLICIT DOUBLE PRECISION (A-H,P-Z)

      CHARACTER*10 OUTFILE

      DIMENSION NMPS(24),DOMAIN(5,2),VV(5,24),V0(4000),V1(5,4000),
     &  V2(10,4000),V3(10,4000),V4(5,4000),V5(4000),SP(5,24),SM(5,24)

C*******0*********0*********0*********0*********0*********0*********
C                    INPUT NUMBER OF INDEPENDENT VARIABLES
C                  "NIVS" = NUMBER OF INDEPENDENT VARIABLES
```

```
C*******0*********0*********0*********0*********0*********0*********
      WRITE(*,1040)
      READ*, NIVS

C*******0*********0*********0*********0*********0*********0*********
C                    PROVIDE A USER OPTION FOR INPUT FORMAT
C             "OPT1" = 1 ==> SPLINE DEVELOPED FROM EXISTING FUNCTION
C                      2 ==> SPLINE DEVELOPED FROM DISCRETE DATA
C             "OPT2" = 1 ==> USE ONE-SIDED DIFFERENCES AT BOUNDARIES
C                      2 ==> USE TWO-SIDED DIFFERENCES AT BOUNDARIES
C             "OPT3" = 1 ==> USE AUTOMATIC EVEN NODE SPLACING
C                      2 ==> INPUT ALL NODE VARIABLES
C*******0*********0*********0*********0*********0*********0*********

 13   WRITE(*,1045)
      READ*, OPT1
      IF(OPT1.EQ.2) THEN
        OPT2=1
        OPT3=2
      ELSE IF(OPT1.EQ.1) THEN
        WRITE(*,1085)
        READ*, OPT2
        WRITE(*,1087)
        READ*, OPT3
      ELSE
        WRITE(*,991)
        GO TO 13
      END IF

C*******0*********0*********0*********0*********0*********0*********
C           INPUT THE TOTAL NUMBER OF MESH POINTS FOR EACH VARIABLE
C             "NMPS(J)" = NUMBER OF MESH POINTS FOR THE VARIABLE J
C*******0*********0*********0*********0*********0*********0*********

      DO I=1,NIVS
        WRITE(*,1060) I
        READ*, NMPS(I)
      END DO

C*******0*********0*********0*********0*********0*********0*********
C                    INPUT THE DOMAINS ON THE VARIABLES
C              "DOMAIN(I,1)" = LOW DOMAIN BOUNDARY FOR VARIABLE I
C              "DOMAIN(I,2)" = HIGH  "       "      "       "
C           "SP(I,J)" = DISTANCE BETWEEN NODES J AND J+1 IN VARIABLE I
C           "SM(I,J)" =     "       "       "   J-1 AND J  "    "    "
C             "VV(I,J) = VARIABLE VALUES FOR JTH NODE OF VARIABLE I
C*******0*********0*********0*********0*********0*********0*********

      DO I=1,NIVS
        IF(OPT3.EQ.1) THEN
 19       WRITE(*,1080) I
          READ*, DOMAIN(I,1),DOMAIN(I,2)
          IF(DOMAIN(I,2).LE.DOMAIN(I,1)) THEN
```

```
            WRITE(*,3333)
            GO TO 19
          END IF
          DO J=1,NMPS(I)
            SP(I,J)=(DOMAIN(I,2)-DOMAIN(I,1))/(NMPS(I)-1)
            SM(I,J)=SP(I,J)
            VV(I,J)=DOMAIN(I,1)+SP(I,J)*(J-1)
          END DO
        ELSE IF(OPT3.EQ.2) THEN
 15       WRITE(*,1081) I
          READ*, (VV(I,J),J=1,NMPS(I))
          DO J=2,NMPS(I)
            IF(VV(I,J).LE.VV(I,J-1)) THEN
              WRITE(*,3333)
              GO TO 15
            END IF
          END DO
          DO J=1,NMPS(I)-1
            SP(I,J)=VV(I,J+1)-VV(I,J)
            SM(I,J+1)=VV(I,J+1)-VV(I,J)
          END DO
 17       WRITE(*,8888)
          DO J=1,NMPS(I)
            WRITE(*,1082) J,VV(I,J)
          END DO
            WRITE(*,1083)
            READ*, J
            IF(J.NE.0) THEN
              DO K=J,NMPS(I)-1
                VV(I,K)=VV(I,K+1)
                SP(I,K)=SP(I,K+1)
                SM(I,K)=SM(I,K+1)
              END DO
              VV(I,K)=0.
              NMPS(I)=NMPS(I)-1
              GO TO 17
            END IF
        ELSE
          WRITE(*,990)
          GO TO 13
        END IF
      END DO

C********0*********0*********0*********0*********0*********0*********
C    SELECT EITHER ONE- OR TWO- SIDED DIFFERENCE SCHEME AT BOUNDARIES
C********0*********0*********0*********0*********0*********0*********

      DO I=1,NIVS
        IF(OPT2.EQ.1) THEN
          SP(I,NMPS(I))=0.
          SM(I,1)=0.
        ELSE IF(OPT2.EQ.2) THEN
          SP(I,NMPS(I))=SM(I,NMPS(I))
```

```
        SM(I,1)=SP(I,1)
      ELSE
        WRITE(*,992)
        GO TO 13
      END IF
    END DO

C********0*********0*********0*********0*********0*********0*********
C              ESTABLISH VARIABLE FOR DIFFERENTIAL APPROXIMATIONS
C             "D" = DISTANCE OF VARIATION AS FRACTION OF NODE SPACING
C           IF INPUT IS DISCRETE POINTS, USE D=1; OTHERWISE MAKE D<<1.
C********0*********0*********0*********0*********0*********0*********

      IF(OPT1.EQ.2) THEN
        D=1.D0
      ELSE
        WRITE(*,1200)
        READ*, D
      END IF

C********0*********0*********0*********0*********0*********0*********
C                             APPROXIMATE THE VARIATIONS
C          "F1(V(1),V(2),...,V(5))" = FUNCTION EVALUATION INPUT FOR
C                              THE GIVEN VARIABLE VALUES
C          "V1(J,K)" = FIRST VARIATION IN VARIABLE J AT POINT K
C          "V2(J,K)" = SECOND   "      "      "    "  "    "    "
C                            OPEN A FILE TO THROW DATA
C********0*********0*********0*********0*********0*********0*********

      WRITE(*,1234)
      READ(*,1235) OUTFILE

      OPEN(UNIT=3,FILE=OUTFILE,ACCESS='DIRECT',RECL=352,
     2  STATUS='NEW',FORM='FORMATTED')

C********0*********0*********0*********0*********0*********0*********
C                        THE FIRST TWO RECORDS CONTAIN GENERAL DATA
C********0*********0*********0*********0*********0*********0*********

      WRITE(3,1110,REC=1) OUTFILE,NIVS,(NMPS(I),I=1,NIVS)
      WRITE(3,1111,REC=2) ((VV(I,J),J=1,NMPS(I)),I=1,NIVS)

C********0*********0*********0*********0*********0*********0*********
C                             FIRST DIMENSION
C********0*********0*********0*********0*********0*********0*********

      DO I1=1,NMPS(1),1

       V1P=VV(1,I1)+D*SP(1,I1)
       V1M=VV(1,I1)-D*SM(1,I1)
       D1=D*(SP(1,I1)+SM(1,I1))

       IF(NIVS.EQ.1) THEN
```

```
      INDEX=I1

      V0(INDEX)=F1(VV(1,I1))

      V1(1,INDEX)=(F1(V1P)-F1(V1M))/D1

      WRITE(3,1111,REC=INDEX+2) V0(INDEX),V1(1,INDEX)

     END IF

C********0*********0*********0*********0*********0*********0*********
C                             SECOND DIMENSION
C********0*********0*********0*********0*********0*********0*********

     DO I2=1,NMPS(2),1

      V2P=VV(2,I2)+D*SP(2,I2)
      V2M=VV(2,I2)-D*SM(2,I2)
      D2=D*(SP(2,I2)+SM(2,I2))

      IF(NIVS.EQ.2) THEN

       INDEX=(I1-1)*NMPS(2)+I2

       V0(INDEX)=F1(VV(1,I1),VV(2,I2))

       V1(1,INDEX)=(F1(V1P,VV(2,I2))-F1(V1M,VV(2,I2)))/D1
       V1(2,INDEX)=(F1(VV(1,I1),V2P)-F1(VV(1,I1),V2M))/D2

       V2(1,INDEX)=((F1(V1P,V2P)-F1(V1P,V2M))/D2
    &   -(F1(V1M,V2P)-F1(V1M,V2M))/D2)/D1

       WRITE(3,1111,REC=INDEX+2) V0(INDEX),
    &   (V1(J,INDEX),J=1,2),V2(1,INDEX)
      END IF

C********0*********0*********0*********0*********0*********0*********
C                          THIRD DIMENSION
C********0*********0*********0*********0*********0*********0*********

      DO I3=1,NMPS(3),1

       V3P=VV(3,I3)+D*SP(3,I3)
       V3M=VV(3,I3)-D*SM(3,I3)
       D3=D*(SP(3,I3)+SM(3,I3))

       IF(NIVS.EQ.3) THEN

        INDEX=((I1-1)*NMPS(2)+(I2-1))*NMPS(3)+I3

        V0(INDEX)=F1(VV(1,I1),VV(2,I2),VV(3,I3))
```

```
      V1(1,INDEX)=(F1(V1P,VV(2,I2),VV(3,I3))
     &   -F1(V1M,VV(2,I2),VV(3,I3)))/D1
      V1(2,INDEX)=(F1(VV(1,I1),V2P,VV(3,I3))
     &   -F1(VV(1,I1),V2M,VV(3,I3)))/D2
      V1(3,INDEX)=(F1(VV(1,I1),VV(2,I2),V3P)
     &   -F1(VV(1,I1),VV(2,I2),V3M))/D3

      V2(1,INDEX)=((F1(V1P,V2P,VV(3,I3))-F1(V1P,V2M,VV(3,I3)))/D2
     &   -(F1(V1M,V2P,VV(3,I3))-F1(V1M,V2M,VV(3,I3)))/D2)/D1
      V2(2,INDEX)=((F1(V1P,VV(2,I2),V3P)-F1(V1P,VV(2,I2),V3M))/D3
     &   -(F1(V1M,VV(2,I2),V3P)-F1(V1M,VV(2,I2),V3M))/D3)/D1
      V2(3,INDEX)=((F1(VV(1,I1),V2P,V3P)-F1(VV(1,I1),V2P,V3M))/D3
     &   -(F1(VV(1,I1),V2M,V3P)-F1(VV(1,I1),V2M,V3M))/D3)/D2

      V3(1,INDEX)=(((F1(V1P,V2P,V3P)-F1(V1P,V2P,V3M))/D3
     &   -(F1(V1P,V2M,V3P)-F1(V1P,V2M,V3M))/D3)/D2
     &   -((F1(V1M,V2P,V3P)-F1(V1M,V2P,V3M))/D3
     &   -(F1(V1M,V2M,V3P)-F1(V1M,V2M,V3M))/D3)/D2)/D1

      WRITE(3,1111,REC=INDEX+2) V0(INDEX),(V1(J,INDEX),J=1,3),
     &   (V2(J,INDEX),J=1,3),V3(1,INDEX)

     END IF

C*******0*********0*********0*********0*********0*********0*********
C                                  FOURTH DIMENSION
C*******0*********0*********0*********0*********0*********0*********

     DO I4=1,NMPS(4),1

      V4P=VV(4,I4)+D*SP(4,I4)
      V4M=VV(4,I4)-D*SM(4,I4)
      D4=D*(SP(4,I4)+SM(4,I4))

      IF(NIVS.EQ.4) THEN

       INDEX=(((I1-1)*NMPS(2)+(I2-1))*NMPS(3)+(I3-1))*NMPS(4)+I4

       V0(INDEX)=F1(VV(1,I1),VV(2,I2),VV(3,I3),VV(4,I4))

       V1(1,INDEX)=(F1(V1P,VV(2,I2),VV(3,I3),VV(4,I4))
     &   -F1(V1M,VV(2,I2),VV(3,I3),VV(4,I4)))/D1
       V1(2,INDEX)=(F1(VV(1,I1),V2P,VV(3,I3),VV(4,I4))
     &   -F1(VV(1,I1),V2M,VV(3,I3),VV(4,I4)))/D2
       V1(3,INDEX)=(F1(VV(1,I1),VV(2,I2),V3P,VV(4,I4))
     &   -F1(VV(1,I1),VV(2,I2),V3M,VV(4,I4)))/D3
       V1(4,INDEX)=(F1(VV(1,I1),VV(2,I2),VV(3,I3),V4P)
     &   -F1(VV(1,I1),VV(2,I2),VV(3,I3),V4M))/D4

       V2(1,INDEX)=((F1(V1P,V2P,VV(3,I3),VV(4,I4))
     &   -F1(V1P,V2M,VV(3,I3),VV(4,I4)))/D2
     &   -(F1(V1M,V2P,VV(3,I3),VV(4,I4))
     &   -F1(V1M,V2M,VV(3,I3),VV(4,I4)))/D2)/D1
```

```
      V2(2,INDEX)=((F1(V1P,VV(2,I2),V3P,VV(4,I4))
&      -F1(V1P,VV(2,I2),V3M,VV(4,I4)))/D3
&      -(F1(V1M,VV(2,I2),V3P,VV(4,I4))
&      -F1(V1M,VV(2,I2),V3M,VV(4,I4)))/D3)/D1
      V2(3,INDEX)=((F1(V1P,VV(2,I2),VV(3,I3),V4P)
&      -F1(V1P,VV(2,I2),VV(3,I3),V4M))/D4
&      -(F1(V1M,VV(2,I2),VV(3,I3),V4P)
&      -F1(V1M,VV(2,I2),VV(3,I3),V4M))/D4)/D1
      V2(4,INDEX)=((F1(VV(1,I1),V2P,V3P,VV(4,I4))
&      -F1(VV(1,I1),V2P,V3M,VV(4,I4)))/D3
&      -(F1(VV(1,I1),V2M,V3P,VV(4,I4))
&      -F1(VV(1,I1),V2M,V3M,VV(4,I4)))/D3)/D2
      V2(5,INDEX)=((F1(VV(1,I1),V2P,VV(3,I3),V4P)
&      -F1(VV(1,I1),V2P,VV(3,I3),V4M))/D4
&      -(F1(VV(1,I1),V2M,VV(3,I3),V4P)
&      -F1(VV(1,I1),V2M,VV(3,I3),V4M))/D4)/D2
      V2(6,INDEX)=((F1(VV(1,I1),VV(2,I2),V3P,V4P)
&      -F1(VV(1,I1),VV(2,I2),V3P,V4M))/D4
&      -(F1(VV(1,I1),VV(2,I2),V3M,V4P)
&      -F1(VV(1,I1),VV(2,I2),V3M,V4M))/D4)/D3

      V3(1,INDEX)=(((F1(V1P,V2P,V3P,VV(4,I4))
&      -F1(V1P,V2P,V3M,VV(4,I4)))/D3
&      -(F1(V1P,V2M,V3P,VV(4,I4))
&      -F1(V1P,V2M,V3M,VV(4,I4)))/D3)/D2
&      -((F1(V1M,V2P,V3P,VV(4,I4))
&      -F1(V1M,V2P,V3M,VV(4,I4)))/D3
&      -(F1(V1M,V2M,V3P,VV(4,I4))
&      -F1(V1M,V2M,V3M,VV(4,I4)))/D3)/D2)/D1
      V3(2,INDEX)=(((F1(V1P,V2P,VV(3,I3),V4P)
&      -F1(V1P,V2P,VV(3,I3),V4M))/D4
&      -(F1(V1P,V2M,VV(3,I3),V4P)
&      -F1(V1P,V2M,VV(3,I3),V4M))/D4)/D2
&      -((F1(V1M,V2P,VV(3,I3),V4P)
&      -F1(V1M,V2P,VV(3,I3),V4M))/D4
&      -(F1(V1M,V2M,VV(3,I3),V4P)
&      -F1(V1M,V2M,VV(3,I3),V4M))/D4)/D2)/D1
      V3(3,INDEX)=(((F1(V1P,VV(2,I2),V3P,V4P)
&      -F1(V1P,VV(2,I2),V3P,V4M))/D4
&      -(F1(V1P,VV(2,I2),V3M,V4P)
&      -F1(V1P,VV(2,I2),V3M,V4M))/D4)/D3
&      -((F1(V1M,VV(2,I2),V3P,V4P)
&      -F1(V1M,VV(2,I2),V3P,V4M))/D4
&      -(F1(V1M,VV(2,I2),V3M,V4P)
&      -F1(V1M,VV(2,I2),V3M,V4M))/D4)/D3)/D1
      V3(4,INDEX)=(((F1(VV(1,I1),V2P,V3P,V4P)
&      -F1(VV(1,I1),V2P,V3P,V4M))/D4
&      -(F1(VV(1,I1),V2P,V3M,V4P)
&      -F1(VV(1,I1),V2P,V3M,V4M))/D4)/D3
&      -((F1(VV(1,I1),V2M,V3P,V4P)
&      -F1(VV(1,I1),V2M,V3P,V4M))/D4
&      -(F1(VV(1,I1),V2M,V3M,V4P)
&      -F1(VV(1,I1),V2M,V3M,V4M))/D4)/D3)/D2
```

```
      V4(1,INDEX)=((((F1(V1P,V2P,V3P,V4P)-F1(V1P,V2P,V3P,V4M))
&                                                          /D4
&       -(F1(V1P,V2P,V3M,V4P)-F1(V1P,V2P,V3M,V4M))/D4)/D3
&       -((F1(V1P,V2M,V3P,V4P)-F1(V1P,V2M,V3P,V4M))/D4
&       -(F1(V1P,V2M,V3M,V4P)-F1(V1P,V2M,V3M,V4M))/D4)/D3)/D2
&       -(((F1(V1M,V2P,V3P,V4P)-F1(V1M,V2P,V3P,V4M))/D4
&       -(F1(V1M,V2P,V3M,V4P)-F1(V1M,V2P,V3M,V4M))/D4)/D3
&       -((F1(V1M,V2M,V3P,V4P)-F1(V1M,V2M,V3P,V4M))/D4
&       -(F1(V1M,V2M,V3M,V4P)-F1(V1M,V2M,V3M,V4M))/D4)/D3)/D2)/D1

      WRITE(3,1111,REC=INDEX+2) V0(INDEX),(V1(J,INDEX),J=1,4),
&      (V2(J,INDEX),J=1,6),(V3(J,INDEX),J=1,4),V4(1,INDEX)

     END IF

C********0*********0*********0*********0*********0*********0*********
C                                 FIFTH DIMENSION
C********0*********0*********0*********0*********0*********0*********

     DO I5=1,NMPS(5),1

      V5P=VV(5,I5)+D*SP(5,I5)
      V5M=VV(5,I5)-D*SM(5,I5)
      D5=D*(SP(5,I5)+SM(5,I5))

      IF(NIVS.EQ.5) THEN

       INDEX=((((I1-1)*NMPS(2)+(I2-1))*NMPS(3)+(I3-1))*NMPS(4)
&       +(I4-1))*NMPS(5)+I5

       V0(INDEX)=F1(VV(1,I1),VV(2,I2),VV(3,I3),VV(4,I4),VV(5,I5
&                                                          ))

       V1(1,INDEX)=(F1(V1P,VV(2,I2),VV(3,I3),VV(4,I4),VV(5,I5))
&       -F1(V1M,VV(2,I2),VV(3,I3),VV(4,I4),VV(5,I5)))/D1
       V1(2,INDEX)=(F1(VV(1,I1),V2P,VV(3,I3),VV(4,I4),VV(5,I5))
&       -F1(VV(1,I1),V2M,VV(3,I3),VV(4,I4),VV(5,I5)))/D2
       V1(3,INDEX)=(F1(VV(1,I1),VV(2,I2),V3P,VV(4,I4),VV(5,I5))
&       -F1(VV(1,I1),VV(2,I2),V3M,VV(4,I4),VV(5,I5)))/D3
       V1(4,INDEX)=(F1(VV(1,I1),VV(2,I2),VV(3,I3),V4P,VV(5,I5))
&       -F1(VV(1,I1),VV(2,I2),VV(3,I3),V4M,VV(5,I5)))/D4
       V1(5,INDEX)=(F1(VV(1,I1),VV(2,I2),VV(3,I3),VV(4,I4),V5P)
&       -F1(VV(1,I1),VV(2,I2),VV(3,I3),VV(4,I4),V5M))/D5

       V2(1,INDEX)=((F1(V1P,V2P,VV(3,I3),VV(4,I4),VV(5,I5))
&       -F1(V1P,V2M,VV(3,I3),VV(4,I4),VV(5,I5)))/D2
&       -(F1(V1M,V2P,VV(3,I3),VV(4,I4),VV(5,I5))
&       -F1(V1M,V2M,VV(3,I3),VV(4,I4),VV(5,I5)))/D2)/D1
       V2(2,INDEX)=((F1(V1P,VV(2,I2),V3P,VV(4,I4),VV(5,I5))
&       -F1(V1P,VV(2,I2),V3M,VV(4,I4),VV(5,I5)))/D3
&       -(F1(V1M,VV(2,I2),V3P,VV(4,I4),VV(5,I5))
&       -F1(V1M,VV(2,I2),V3M,VV(4,I4),VV(5,I5)))/D3)/D1
```

```
      V2(3,INDEX)=((F1(V1P,VV(2,I2),VV(3,I3),V4P,VV(5,I5))
&      -F1(V1P,VV(2,I2),VV(3,I3),V4M,VV(5,I5)))/D4
&      -(F1(V1M,VV(2,I2),VV(3,I3),V4P,VV(5,I5))
&      -F1(V1M,VV(2,I2),VV(3,I3),V4M,VV(5,I5)))/D4)/D1
      V2(4,INDEX)=((F1(V1P,VV(2,I2),VV(3,I3),VV(4,I4),V5P)
&      -F1(V1P,VV(2,I2),VV(3,I3),VV(4,I4),V5M))/D5
&      -(F1(V1M,VV(2,I2),VV(3,I3),VV(4,I4),V5P)
&      -F1(V1M,VV(2,I2),VV(3,I3),VV(4,I4),V5M))/D5)/D1
      V2(5,INDEX)=((F1(VV(1,I1),V2P,V3P,VV(4,I4),VV(5,I5))
&      -F1(VV(1,I1),V2P,V3M,VV(4,I4),VV(5,I5)))/D3
&      -(F1(VV(1,I1),V2M,V3P,VV(4,I4),VV(5,I5))
&      -F1(VV(1,I1),V2M,V3M,VV(4,I4),VV(5,I5)))/D3)/D2
      V2(6,INDEX)=((F1(VV(1,I1),V2P,VV(3,I3),V4P,VV(5,I5))
&      -F1(VV(1,I1),V2P,VV(3,I3),V4M,VV(5,I5)))/D4
&      -(F1(VV(1,I1),V2M,VV(3,I3),V4P,VV(5,I5))
&      -F1(VV(1,I1),V2M,VV(3,I3),V4M,VV(5,I5)))/D4)/D2
      V2(7,INDEX)=((F1(VV(1,I1),V2P,VV(3,I3),VV(4,I4),V5P)
&      -F1(VV(1,I1),V2P,VV(3,I3),VV(4,I4),V5M))/D5
&      -(F1(VV(1,I1),V2M,VV(3,I3),VV(4,I4),V5P)
&      -F1(VV(1,I1),V2M,VV(3,I3),VV(4,I4),V5M))/D5)/D2
      V2(8,INDEX)=((F1(VV(1,I1),VV(2,I2),V3P,V4P,VV(5,I5))
&      -F1(VV(1,I1),VV(2,I2),V3P,V4M,VV(5,I5)))/D4
&      -(F1(VV(1,I1),VV(2,I2),V3M,V4P,VV(5,I5))
&      -F1(VV(1,I1),VV(2,I2),V3M,V4M,VV(5,I5)))/D4)/D3
      V2(9,INDEX)=((F1(VV(1,I1),VV(2,I2),V3P,VV(4,I4),V5P)
&      -F1(VV(1,I1),VV(2,I2),V3P,VV(4,I4),V5M))/D5
&      -(F1(VV(1,I1),VV(2,I2),V3M,VV(4,I4),V5P)
&      -F1(VV(1,I1),VV(2,I2),V3M,VV(4,I4),V5M))/D5)/D3
      V2(10,INDEX)=((F1(VV(1,I1),VV(2,I2),VV(3,I3),V4P,V5P)
&      -F1(VV(1,I1),VV(2,I2),VV(3,I3),V4P,V5M))/D5
&      -(F1(VV(1,I1),VV(2,I2),VV(3,I3),V4M,V5P)
&      -F1(VV(1,I1),VV(2,I2),VV(3,I3),V4M,V5M))/D5)/D4

      V3(1,INDEX)=(((F1(V1P,V2P,V3P,VV(4,I4),VV(5,I5))
&      -F1(V1P,V2P,V3M,VV(4,I4),VV(5,I5)))/D3
&      -(F1(V1P,V2M,V3P,VV(4,I4),VV(5,I5))
&      -F1(V1P,V2M,V3M,VV(4,I4),VV(5,I5)))/D3)/D2
&      -((F1(V1M,V2P,V3P,VV(4,I4),VV(5,I5))
&      -F1(V1M,V2P,V3M,VV(4,I4),VV(5,I5)))/D3
&      -(F1(V1M,V2M,V3P,VV(4,I4),VV(5,I5))
&      -F1(V1M,V2M,V3M,VV(4,I4),VV(5,I5)))/D3)/D2)/D1
      V3(2,INDEX)=(((F1(V1P,V2P,VV(3,I3),V4P,VV(5,I5))
&      -F1(V1P,V2P,VV(3,I3),V4M,VV(5,I5)))/D4
&      -(F1(V1P,V2M,VV(3,I3),V4P,VV(5,I5))
&      -F1(V1P,V2M,VV(3,I3),V4M,VV(5,I5)))/D4)/D2
&      -((F1(V1M,V2P,VV(3,I3),V4P,VV(5,I5))
&      -F1(V1M,V2P,VV(3,I3),V4M,VV(5,I5)))/D4
&      -(F1(V1M,V2M,VV(3,I3),V4P,VV(5,I5))
&      -F1(V1M,V2M,VV(3,I3),V4M,VV(5,I5)))/D4)/D2)/D1
      V3(3,INDEX)=(((F1(V1P,V2P,VV(3,I3),VV(4,I4),V5P)
&      -F1(V1P,V2P,VV(3,I3),VV(4,I4),V5M))/D5
&      -(F1(V1P,V2M,VV(3,I3),VV(4,I4),V5P)
&      -F1(V1P,V2M,VV(3,I3),VV(4,I4),V5M))/D5)/D2
```

```
&          -((F1(V1M,V2P,VV(3,I3),VV(4,I4),V5P)
&          -F1(V1M,V2P,VV(3,I3),VV(4,I4),V5M))/D5
&          -(F1(V1M,V2M,VV(3,I3),VV(4,I4),V5P)
&          -F1(V1M,V2M,VV(3,I3),VV(4,I4),V5M))/D5)/D2)/D1
         V3(4,INDEX)=(((F1(V1P,VV(2,I2),V3P,V4P,VV(5,I5))
&         -F1(V1P,VV(2,I2),V3P,V4M,VV(5,I5)))/D4
&         -(F1(V1P,VV(2,I2),V3M,V4P,VV(5,I5))
&         -F1(V1P,VV(2,I2),V3M,V4M,VV(5,I5)))/D4)/D3
&         -((F1(V1M,VV(2,I2),V3P,V4P,VV(5,I5))
&         -F1(V1M,VV(2,I2),V3P,V4M,VV(5,I5)))/D4
&         -(F1(V1M,VV(2,I2),V3M,V4P,VV(5,I5))
&         -F1(V1M,VV(2,I2),V3M,V4M,VV(5,I5)))/D4)/D3)/D1
         V3(5,INDEX)=(((F1(V1P,VV(2,I2),V3P,VV(4,I4),V5P)
&          -F1(V1P,VV(2,I2),V3P,VV(4,I4),V5M))/D5
&          -(F1(V1P,VV(2,I2),V3M,VV(4,I4),V5P)
&          -F1(V1P,VV(2,I2),V3M,VV(4,I4),V5M))/D5)/D3
&          -((F1(V1M,VV(2,I2),V3P,VV(4,I4),V5P)
&          -F1(V1M,VV(2,I2),V3P,VV(4,I4),V5M))/D5
&          -(F1(V1M,VV(2,I2),V3M,VV(4,I4),V5P)
&          -F1(V1M,VV(2,I2),V3M,VV(4,I4),V5M))/D5)/D3)/D1
         V3(6,INDEX)=(((F1(V1P,VV(2,I2),VV(3,I3),V4P,V5P)
&          -F1(V1P,VV(2,I2),VV(3,I3),V4P,V5M))/D5
&          -(F1(V1P,VV(2,I2),VV(3,I3),V4M,V5P)
&          -F1(V1P,VV(2,I2),VV(3,I3),V4M,V5M))/D5)/D4
&          -((F1(V1M,VV(2,I2),VV(3,I3),V4P,V5P)
&          -F1(V1M,VV(2,I2),VV(3,I3),V4P,V5M))/D5
&          -(F1(V1M,VV(2,I2),VV(3,I3),V4M,V5P)
&          -F1(V1M,VV(2,I2),VV(3,I3),V4M,V5M))/D5)/D4)/D1
         V3(7,INDEX)=(((F1(VV(1,I1),V2P,V3P,V4P,VV(5,I5))
&          -F1(VV(1,I1),V2P,V3P,V4M,VV(5,I5)))/D4
&          -(F1(VV(1,I1),V2P,V3M,V4P,VV(5,I5))
&          -F1(VV(1,I1),V2P,V3M,V4M,VV(5,I5)))/D4)/D3
&          -((F1(VV(1,I1),V2M,V3P,V4P,VV(5,I5))
&          -F1(VV(1,I1),V2M,V3P,V4M,VV(5,I5)))/D4
&          -(F1(VV(1,I1),V2M,V3M,V4P,VV(5,I5))
&          -F1(VV(1,I1),V2M,V3M,V4M,VV(5,I5)))/D4)/D3)/D2
         V3(8,INDEX)=(((F1(VV(1,I1),V2P,V3P,VV(4,I4),V5P)
&          -F1(VV(1,I1),V2P,V3P,VV(4,I4),V5M))/D5
&          -(F1(VV(1,I1),V2P,V3M,VV(4,I4),V5P)
&          -F1(VV(1,I1),V2P,V3M,VV(4,I4),V5M))/D5)/D3
&          -((F1(VV(1,I1),V2M,V3P,VV(4,I4),V5P)
&          -F1(VV(1,I1),V2M,V3P,VV(4,I4),V5M))/D5
&          -(F1(VV(1,I1),V2M,V3M,VV(4,I4),V5P)
&          -F1(VV(1,I1),V2M,V3M,VV(4,I4),V5M))/D5)/D3)/D2
         V3(9,INDEX)=(((F1(VV(1,I1),V2P,VV(3,I3),V4P,V5P)
&          -F1(VV(1,I1),V2P,VV(3,I3),V4P,V5M))/D5
&          -(F1(VV(1,I1),V2P,VV(3,I3),V4M,V5P)
&          -F1(VV(1,I1),V2P,VV(3,I3),V4M,V5M))/D5)/D4
*          -((F1(VV(1,I1),V2M,VV(3,I3),V4P,V5P)
&          -F1(VV(1,I1),V2M,VV(3,I3),V4P,V5M))/D5
&          -(F1(VV(1,I1),V2M,VV(3,I3),V4M,V5P)
&          -F1(VV(1,I1),V2M,VV(3,I3),V4M,V5M))/D5)/D4)/D2
         V3(10,INDEX)=(((F1(VV(1,I1),VV(2,I2),V3P,V4P,V5P)
```

```
&        -F1(VV(1,I1),VV(2,I2),V3P,V4P,V5M))/D5
&        -(F1(VV(1,I1),VV(2,I2),V3P,V4M,V5P)
&        -F1(VV(1,I1),VV(2,I2),V3P,V4M,V5M))/D5)/D4
&        -((F1(VV(1,I1),VV(2,I2),V3M,V4P,V5P)
&        -F1(VV(1,I1),VV(2,I2),V3M,V4P,V5M))/D5
&        -(F1(VV(1,I1),VV(2,I2),V3M,V4M,V5P)
&        -F1(VV(1,I1),VV(2,I2),V3M,V4M,V5M))/D5)/D4)/D3

        V4(1,INDEX)=((((F1(V1P,V2P,V3P,V4P,VV(5,I5))
&        -F1(V1P,V2P,V3P,V4M,VV(5,I5)))/D4
&        -(F1(V1P,V2P,V3M,V4P,VV(5,I5))
&        -F1(V1P,V2P,V3M,V4M,VV(5,I5)))/D4)/D3
&        -((F1(V1P,V2M,V3P,V4P,VV(5,I5))
&        -F1(V1P,V2M,V3P,V4M,VV(5,I5)))/D4
&        -(F1(V1P,V2M,V3M,V4P,VV(5,I5))
&        -F1(V1P,V2M,V3M,V4M,VV(5,I5)))/D4)/D3)/D2
&        -(((F1(V1M,V2P,V3P,V4P,VV(5,I5))
&        -F1(V1M,V2P,V3P,V4M,VV(5,I5)))/D4
&        -(F1(V1M,V2P,V3M,V4P,VV(5,I5))
&        -F1(V1M,V2P,V3M,V4M,VV(5,I5)))/D4)/D3
&        -((F1(V1M,V2M,V3P,V4P,VV(5,I5))
&        -F1(V1M,V2M,V3P,V4M,VV(5,I5)))/D4
&        -(F1(V1M,V2M,V3M,V4P,VV(5,I5))
&        -F1(V1M,V2M,V3M,V4M,VV(5,I5)))/D4)/D3)/D2)/D1
        V4(2,INDEX)=((((F1(V1P,V2P,V3P,VV(4,I4),V5P)
&        -F1(V1P,V2P,V3P,VV(4,I4),V5M))/D5
&        -(F1(V1P,V2P,V3M,VV(4,I4),V5P)
&        -F1(V1P,V2P,V3M,VV(4,I4),V5M))/D5)/D3
&        -((F1(V1P,V2M,V3P,VV(4,I4),V5P)
&        -F1(V1P,V2M,V3P,VV(4,I4),V5M))/D5
&        -(F1(V1P,V2M,V3M,VV(4,I4),V5P)
&        -F1(V1P,V2M,V3M,VV(4,I4),V5M))/D5)/D3)/D2
&        -(((F1(V1M,V2P,V3P,VV(4,I4),V5P)
&        -F1(V1M,V2P,V3P,VV(4,I4),V5M))/D5
&        -(F1(V1M,V2P,V3M,VV(4,I4),V5P)
&        -F1(V1M,V2P,V3M,VV(4,I4),V5M))/D5)/D3
&        -((F1(V1M,V2M,V3P,VV(4,I4),V5P)
&        -F1(V1M,V2M,V3P,VV(4,I4),V5M))/D5
&        -(F1(V1M,V2M,V3M,VV(4,I4),V5P)
&        -F1(V1M,V2M,V3M,VV(4,I4),V5M))/D5)/D3)/D2)/D1
        V4(3,INDEX)=((((F1(V1P,V2P,VV(3,I3),V4P,V5P)
&        -F1(V1P,V2P,VV(3,I3),V4P,V5M))/D5
&        -(F1(V1P,V2P,VV(3,I3),V4M,V5P)
&        -F1(V1P,V2P,VV(3,I3),V4M,V5M))/D5)/D4
&        -((F1(V1P,V2M,VV(3,I3),V4P,V5P)
&        -F1(V1P,V2M,VV(3,I3),V4P,V5M))/D5
&        -(F1(V1P,V2M,VV(3,I3),V4M,V5P)
&        -F1(V1P,V2M,VV(3,I3),V4M,V5M))/D5)/D4)/D2
&        -(((F1(V1M,V2P,VV(3,I3),V4P,V5P)
&        -F1(V1M,V2P,VV(3,I3),V4P,V5M))/D5
&        -(F1(V1M,V2P,VV(3,I3),V4M,V5P)
&        -F1(V1M,V2P,VV(3,I3),V4M,V5M))/D5)/D4
&        -((F1(V1M,V2M,VV(3,I3),V4P,V5P)
```

```
&        -F1(V1M,V2M,VV(3,I3),V4P,V5M))/D5
&        -(F1(V1M,V2M,VV(3,I3),V4M,V5P)
&        -F1(V1M,V2M,VV(3,I3),V4M,V5M))/D5)/D4)/D2)/D1
        V4(4,INDEX)=((((F1(V1P,VV(2,I2),V3P,V4P,V5P)
&        -F1(V1P,VV(2,I2),V3P,V4P,V5M))/D5
&        -(F1(V1P,VV(2,I2),V3P,V4M,V5P)
&        -F1(V1P,VV(2,I2),V3P,V4M,V5M))/D5)/D4
&        -((F1(V1P,VV(2,I2),V3M,V4P,V5P)
&        -F1(V1P,VV(2,I2),V3M,V4P,V5M))/D5
&        -(F1(V1P,VV(2,I2),V3M,V4M,V5P)
&        -F1(V1P,VV(2,I2),V3M,V4M,V5M))/D5)/D4)/D3
&        -(((F1(V1M,VV(2,I2),V3P,V4P,V5P)
&        -F1(V1M,VV(2,I2),V3P,V4P,V5M))/D5
&        -(F1(V1M,VV(2,I2),V3P,V4M,V5P)
&        -F1(V1M,VV(2,I2),V3P,V4M,V5M))/D5)/D4
&        -((F1(V1M,VV(2,I2),V3M,V4P,V5P)
&        -F1(V1M,VV(2,I2),V3M,V4P,V5M))/D5
&        -(F1(V1M,VV(2,I2),V3M,V4M,V5P)
&        -F1(V1M,VV(2,I2),V3M,V4M,V5M))/D5)/D4)/D3)/D1
        V4(5,INDEX)=((((F1(VV(1,I1),V2P,V3P,V4P,V5P)
&        -F1(VV(1,I1),V2P,V3P,V4P,V5M))/D5
&        -(F1(VV(1,I1),V2P,V3P,V4M,V5P)
&        -F1(VV(1,I1),V2P,V3P,V4M,V5M))/D5)/D4
&        -((F1(VV(1,I1),V2P,V3M,V4P,V5P)
&        -F1(VV(1,I1),V2P,V3M,V4P,V5M))/D5
&        -(F1(VV(1,I1),V2P,V3M,V4M,V5P)
&        -F1(VV(1,I1),V2P,V3M,V4M,V5M))/D5)/D4)/D3
&        -(((F1(VV(1,I1),V2M,V3P,V4P,V5P)
&        -F1(VV(1,I1),V2M,V3P,V4P,V5M))/D5
&        -(F1(VV(1,I1),V2M,V3P,V4M,V5P)
&        -F1(VV(1,I1),V2M,V3P,V4M,V5M))/D5)/D4
&        -((F1(VV(1,I1),V2M,V3M,V4P,V5P)
&        -F1(VV(1,I1),V2M,V3M,V4P,V5M))/D5
&        -(F1(VV(1,I1),V2M,V3M,V4M,V5P)
&        -F1(VV(1,I1),V2M,V3M,V4M,V5M))/D5)/D4)/D3)/D2

        V5(INDEX)=(((((F1(V1P,V2P,V3P,V4P,V5P)
&        -F1(V1P,V2P,V3P,V4P,V5M))/D5
&        -(F1(V1P,V2P,V3P,V4M,V5P)
&        -F1(V1P,V2P,V3P,V4M,V5M))/D5)/D4
&        -((F1(V1P,V2P,V3M,V4P,V5P)
&        -F1(V1P,V2P,V3M,V4P,V5M))/D5
&        -(F1(V1P,V2P,V3M,V4M,V5P)
&        -F1(V1P,V2P,V3M,V4M,V5M))/D5)/D4)/D3
&        -(((F1(V1P,V2M,V3P,V4P,V5P)
&        -F1(V1P,V2M,V3P,V4P,V5M))/D5
&        -(F1(V1P,V2M,V3P,V4M,V5P)
&        -F1(V1P,V2M,V3P,V4M,V5M))/D5)/D4
&        -((F1(V1P,V2M,V3M,V4P,V5P)
&        -F1(V1P,V2M,V3M,V4P,V5M))/D5
&        -(F1(V1P,V2M,V3M,V4M,V5P)
&        -F1(V1P,V2M,V3M,V4M,V5M))/D5)/D4)/D3)/D2
&        -((((F1(V1M,V2P,V3P,V4P,V5P)
```

```
     &        -F1(V1M,V2P,V3P,V4P,V5M))/D5
     &        -(F1(V1M,V2P,V3P,V4M,V5P)
     &        -F1(V1M,V2P,V3P,V4M,V5M))/D5)/D4
     &        -((F1(V1M,V2P,V3M,V4P,V5P)
     &        -F1(V1M,V2P,V3M,V4P,V5M))/D5
     &        -(F1(V1M,V2P,V3M,V4M,V5P)
     &        -F1(V1M,V2P,V3M,V4M,V5M))/D5)/D4)/D3
     &        -(((F1(V1M,V2M,V3P,V4P,V5P)
     &        -F1(V1M,V2M,V3P,V4P,V5M))/D5
     &        -(F1(V1M,V2M,V3P,V4M,V5P)
     &        -F1(V1M,V2M,V3P,V4M,V5M))/D5)/D4
     &        -((F1(V1M,V2M,V3M,V4P,V5P)
     &        -F1(V1M,V2M,V3M,V4P,V5M))/D5
     &        -(F1(V1M,V2M,V3M,V4M,V5P)
     &        -F1(V1M,V2M,V3M,V4M,V5M))/D5)/D4)/D3)/D2)/D1

             WRITE(3,1111,REC=INDEX+2) V0(INDEX),(V1(J,INDEX),J=1,5),
     &        (V2(J,INDEX),J=1,10),(V3(J,INDEX),J=1,10),(V4(J,INDEX),
     &        J=1,5),V5(INDEX)

            END IF

           END DO
          END DO
         END DO
        END DO
       END DO

       CLOSE(UNIT=3)

C********0*********0*********0*********0*********0*********0*********0*********
C                                SUMMARIZE FILE DATA
C********0*********0*********0*********0*********0*********0*********0*********

       WRITE(*,2000)
       WRITE(*,2000)
       WRITE(*,2010)
       WRITE(*,2020) OUTFILE
       WRITE(*,2030) NIVS
       WRITE(*,2040) (J,J=1,NIVS)
       DO J=1,JMAX0(NMPS(1),NMPS(2),NMPS(3),NMPS(4),NMPS(5))
         WRITE(*,2050) (VV(I,J),I=1,NIVS)
       END DO
       NRECS=1
       DO I=1,NIVS
         NRECS=NRECS*NMPS(I)
       END DO
       WRITE(*,2060) NRECS+2
       IF(OPT1.EQ.1) THEN
         WRITE(*,2080)
       ELSE IF(OPT1.EQ.2) THEN
         WRITE(*,2085)
       END IF
```

```
      IF(OPT2.EQ.1) THEN
        WRITE(*,2070)
      ELSE IF(OPT2.EQ.2) THEN
        WRITE(*,2086)
      END IF
      IF(OPT3.EQ.1) THEN
        WRITE(*,2087)
      ELSE IF(OPT3.EQ.2) THEN
        WRITE(*,2088)
      END IF
      WRITE(*,8888)
      WRITE(*,2000)
      WRITE(*,2000)

      STOP

C********0*********0*********0*********0*********0*********0*********
C                                   FORMATS
C********0*********0*********0*********0*********0*********0*********
 990  FORMAT(' !!!! AN ERROR HAS OCCURRED IN SELECTING OPTION #3 !!')
 991  FORMAT(' !!!! AN ERROR HAS OCCURRED IN SELECTING OPTION #1 !!')
 992  FORMAT(' !!!! AN ERROR HAS OCCURRED IN SELECTING OPTION #2 !!')
 1040 FORMAT(//' HOW MANY INDEPENDENT VARIABLES? (I1) ')
 1045 FORMAT(//' CHOOSE ONE OF THE OPTIONS:'//
     &       '      (1) CREATE SPLINE FIT FROM EXISTING FUNCTION'/
     &       '      (2) CREATE SPLINE FROM SET OF DISCRETE POINTS')
 1060 FORMAT(//' HOW MANY MESH POINTS IN INDEPENDENT '
     2  'VARIABLE ',I2,'? (I2) ')
 1080 FORMAT(//' GIVE THE RANGE OF INDEPENDENT VARIABLE ',I1,
     & '(2F10.0): ')
 1081 FORMAT(//' GIVE ALL NODE VARIABLE VALUES IN ORDER FOR VARIABLE'
     &  ,I1,'.'/)
 1082 FORMAT(' ',30X,'#',I2,'  ',F12.6)
 1083 FORMAT(//' INDICATE BY NUMBER ANY OF THESE YOU WISH TO USE FOR'
     &  'VARIATIONAL DATA ONLY: (I2)'/
     &  62X,'TYPE "0" FOR NONE')
 1085 FORMAT(//' CHOOSE AN OPTION FOR DETERMINING VARIATION AT '
     &          'BOUNDARIES:'//
     &       '      (1) ONE-SIDED DIFFERENCE SCHEME'/
     &       '      (2) TWO-SIDED DIFFERENCE SCHEME')
 1087 FORMAT(//' CHOOSE AN OPTION FOR NODE SPACING:'//
     &       '      (1) EVEN NODE SPACING'/
     &       '      (2) INPUT ALL NODES')
 1110 FORMAT(A10,31I10)
 1111 FORMAT(32E11.4)
 1200 FORMAT(//' INPUT THE FRACTION OF NODE SPACING TO BE '
     &  'USED IN EVALUATING VARIATIONS. (F4.3)')
 1234 FORMAT(//' NAME THE SPLINE FILE YOU WISH TO CREATE (A10): ')
 1235 FORMAT(A10)
 2000 FORMAT(' ',79('*'))
 2010 FORMAT(//' ',30X,' SPLINE FILE SUMMARY ')
 2020 FORMAT(/' ',20X,' SPLINE FILE NAME: ',A10)
 2030 FORMAT(' ',20X,' THERE ARE ',I1,' INDEPENDENT VARIABLES.')
```

```
2040 FORMAT(/' ',10X,5(I2,' VARIABLE '))
2050 FORMAT(' ',10X,5(' ',E10.4,' '))
2060 FORMAT(/' ',20X,' THE TOTAL NUMBER OF FILE RECORDS IS',I4,'.'/)
2070 FORMAT(' **AN OPTION WAS CHOSEN TO USE NON-CENTERED '
   &        'DIFFERENCES AT DOMAIN BOUNDARIES.')
2080 FORMAT(' **AN OPTION WAS CHOSEN TO EXPECT DISCRETE DATA ONLY.')
2085 FORMAT(' *DATA COMES FROM ANOTHER FUNCTION OF SAME DIMENSION.')
2086 FORMAT(' **A TWO-SIDED DIFFERENCE SCHEME WAS USED AT DOMAIN '
   &  'BOUNDARIES.')
2087 FORMAT(' **EVEN NODE SPACING WAS ASSUMED.')
2088 FORMAT(' **THE USER INPUT ALL NODE VARIABLE VALUES.')
3333 FORMAT(/' AN ERROR HAS OCCURRED IN DATA INPUT.  ENTER POINTS ',
   &  'IN INCREASING ORDER!**'/)
8888 FORMAT(/)

     END
```

SR Spline Function Interpolation Subroutine

```
C*******0*********0*********0*********0*********0*********0*********
C
C     SUBROUTINE: SR
C
C     PROGRAMMER: Donald Hammerstrom, Graduate Student
C                 Department of Electrical Engineering
C                 Montana State University
C                 Bozeman, Montana  59717-0378
C
C     DATE: 1992
C
C     PURPOSE:
C          This subroutine interprets and interpolates a cubic
C     Hermite spline file which was created by program SPLINER.FOR.
C
C*******0*********0*********0*********0*********0*********0*********
      FUNCTION SR(NMFL,OPT,VAR1,VAR2,VAR3,VAR4,VAR5)

      IMPLICIT DOUBLE PRECISION (A-H,P-Z)

      IMPLICIT INTEGER (I-O)

      DIMENSION V(5),NMPS(5),VNV(5,25),ND(5,2),P(5,4),V1(5),
     &  V2(10),V3(10),V4(5)

      CHARACTER*10 NMFL,NMFL2
      CHARACTER*1 OPT

      OPEN(UNIT=1,FILE=NMFL,FORM='FORMATTED',STATUS='OLD',RECL=352,
     &  ACCESS='DIRECT')
```

```
      V(1)=VAR1
      V(2)=VAR2
      V(3)=VAR3
      V(4)=VAR4
      V(5)=VAR5

C********0*********0*********0*********0*********0*********0*********
C                GET INDEXING INFORMATION FROM FIRST TWO FILE RECORDS
C               "NMFL2" = FILE NAME
C                "NIVS" = NUMBER OF INDEPENDENT VARIABLES
C             "NMPS(I)" = NUMBER OF MESH POINTS IN VARIABLE I
C            "VNV(I,J)" = VARIABLE NODE VALUE FOR NODE J, VARIABLE I
C********0*********0*********0*********0*********0*********0*********
      READ(1,1000,REC=1) NMFL2,NIVS,(NMPS(I),I=1,NIVS)
      READ(1,1010,REC=2) ((VNV(I,J),J=1,NMPS(I)),I=1,NIVS)

C********0*********0*********0*********0*********0*********0*********
C                                 LOCATE POINT
C                    "ND(I,1)" = LOW NODE INDEX FOR VARIABLE I
C                    "ND(I,2)" = HIGH NODE INDEX FOR VARIABLE I
C********0*********0*********0*********0*********0*********0*********

      DO I=1,NIVS
        ND(I,1)=0
        DO J=1,NMPS(I)
          IF(V(I).LT.VNV(I,J)) THEN
            ND(I,1)=J-1
            ND(I,2)=J
            GO TO 5
          END IF
        END DO
 5      CONTINUE
        IF(ND(I,1).EQ.0) THEN
          IF(V(I).GE.VNV(I,NMPS(I))) THEN
            ND(I,1)=NMPS(I)
            ND(I,2)=NMPS(I)
          ELSE IF(V(I).LT.VNV(I,1)) THEN
            ND(I,1)=1
            ND(I,2)=1
          END IF
C          WRITE(*,999) I,V(I)
        END IF
      END DO

C********0*********0*********0*********0*********0*********0*********
C                           ESTABLISH THE BASIS FUNCTIONS
C         "W" = DISTANCE OF VARIABLE I FROM LOW NODE
C       "WBS" = FRACTIONAL DISTANCE OF VARIABLE I BETWEEN NEAR NODES
C    "P(I,J)" = Jth BASIS CUBIC WEIGHTING FOR VARIABLE I
C   "OPT" = 'Y' QUADRATIC BASIS FUNCTION IS DESIRED AT BOUNDARIES
C NOTE:  USE THIS OPT. WHEN VARIATIONAL DATA AT BOUNDARIES IS SUSPECT
C********0*********0*********0*********0*********0*********0*********
```

```
      DO I=1,NIVS
        IF(ND(I,2).EQ.1) THEN
          W=V(I)-VNV(I,1)
          P(I,1)=0.
          P(I,2)=1.
          P(I,3)=0.
          P(I,4)=W
        ELSE IF(ND(I,1).EQ.NMPS(I)) THEN
          W=V(I)-VNV(I,NMPS(I))
          P(I,1)=1.
          P(I,2)=0.
          P(I,3)=W
          P(I,4)=0.
        ELSE IF(ND(I,1).EQ.1.AND.OPT.EQ.'Y') THEN
          W=V(I)-VNV(I,ND(I,1))
          WBS=W/(VNV(I,ND(I,2))-VNV(I,ND(I,1)))
          P(I,1)=WBS*(WBS-2.D0)+1.D0
          P(I,2)=-P(I,1)+1.D0
          P(I,3)=0.D0
          P(I,4)=W*(WBS-1.D0)
        ELSE IF(ND(I,2).EQ.NMPS(I).AND.OPT.EQ.'Y') THEN
          W=V(I)-VNV(I,ND(I,1))
          WBS=W/(VNV(I,ND(I,2))-VNV(I,ND(I,1)))
          P(I,1)=-WBS*WBS+1.D0
          P(I,2)=-P(I,1)+1.D0
          P(I,3)=W*(1.D0-WBS)
          P(I,4)=0.D0
        ELSE
          W=V(I)-VNV(I,ND(I,1))
          WBS=W/(VNV(I,ND(I,2))-VNV(I,ND(I,1)))
          P(I,1)=WBS*WBS*(2.D0*WBS-3.0)+1.D0
          P(I,2)=-P(I,1)+1.D0
          P(I,3)=W*(WBS*(WBS-2.D0)+1.D0)
          P(I,4)=P(I,3)+W*(WBS-1.D0)
        END IF
      END DO

C********0*********0*********0*********0*********0*********0*********
C                            INTERPOLATE USING SPLINE FILE
C********0*********0*********0*********0*********0*********0*********

      SR=0.

      DO 10,I1=1,2
       I1P=I1+2
       IF(NIVS.EQ.1) THEN
        INDEX=INDX(NIVS,NMPS,ND(1,I1),0,0,0,0)
        READ(1,1010,REC=INDEX) V0,V1(1)
        SR=SR+V0*P(1,I1)
     &    +V1(1)*P(1,I1P)
        GO TO 10
       END IF
       DO 20,I2=1,2
```

```
      I2P=I2+2
      IF(NIVS.EQ.2) THEN
       INDEX=INDX(NIVS,NMPS,ND(1,I1),ND(2,I2),0,0,0)
       READ(1,1010,REC=INDEX) V0,(V1(J),J=1,2),V2(1)
       SR=SR+V0*P(1,I1)*P(2,I2)
     &   +V1(1)*P(1,I1P)*P(2,I2)
     &   +V1(2)*P(1,I1)*P(2,I2P)
     &   +V2(1)*P(1,I1P)*P(2,I2P)
       GO TO 20
      END IF
      DO 30,I3=1,2
       I3P=I3+2
       IF(NIVS.EQ.3) THEN
        INDEX=INDX(NIVS,NMPS,ND(1,I1),ND(2,I2),ND(3,I3),0,0)
        READ(1,1010,REC=INDEX) V0,(V1(J),J=1,3),(V2(J),J=1,3),V3(1)
        SR=SR+V0*P(1,I1)*P(2,I2)*P(3,I3)
     &    +V1(1)*P(1,I1P)*P(2,I2)*P(3,I3)
     &    +V1(2)*P(1,I1)*P(2,I2P)*P(3,I3)
     &    +V1(3)*P(1,I1)*P(2,I2)*P(3,I3P)
     &    +V2(1)*P(1,I1P)*P(2,I2P)*P(3,I3)
     &    +V2(2)*P(1,I1P)*P(2,I2)*P(3,I3P)
     &    +V2(3)*P(1,I1)*P(2,I2P)*P(3,I3P)
     &    +V3(1)*P(1,I1P)*P(2,I2P)*P(3,I3P)
       GO TO 30
       END IF
       DO 40,I4=1,2
        I4P=I4+2
        IF(NIVS.EQ.4) THEN
         INDEX=INDX(NIVS,NMPS,ND(1,I1),ND(2,I2),ND(3,I3),ND(4,I4),
     &                                                              0)
         READ(1,1010,REC=INDEX) V0,(V1(J),J=1,4),(V2(J),J=1,6),
     &     (V3(J),J=1,4),V4(1)
         SR=SR+V0*P(1,I1)*P(2,I2)*P(3,I3)*P(4,I4)
     &     +V1(1)*P(1,I1P)*P(2,I2)*P(3,I3)*P(4,I4)
     &     +V1(2)*P(1,I1)*P(2,I2P)*P(3,I3)*P(4,I4)
     &     +V1(3)*P(1,I1)*P(2,I2)*P(3,I3P)*P(4,I4)
     &     +V1(4)*P(1,I1)*P(2,I2)*P(3,I3)*P(4,I4P)
     &     +V2(1)*P(1,I1P)*P(2,I2P)*P(3,I3)*P(4,I4)
     &     +V2(2)*P(1,I1P)*P(2,I2)*P(3,I3P)*P(4,I4)
     &     +V2(3)*P(1,I1P)*P(2,I2)*P(3,I3)*P(4,I4P)
     &     +V2(4)*P(1,I1)*P(2,I2P)*P(3,I3P)*P(4,I4)
     &     +V2(5)*P(1,I1)*P(2,I2P)*P(3,I3)*P(4,I4P)
     &     +V2(6)*P(1,I1)*P(2,I2)*P(3,I3P)*P(4,I4P)
     &     +V3(1)*P(1,I1P)*P(2,I2P)*P(3,I3P)*P(4,I4)
     &     +V3(2)*P(1,I1P)*P(2,I2P)*P(3,I3)*P(4,I4P)
     &     +V3(3)*P(1,I1P)*P(2,I2)*P(3,I3P)*P(4,I4P)
     &     +V3(4)*P(1,I1)*P(2,I2P)*P(3,I3P)*P(4,I4P)
     &     +V4(1)*P(1,I1P)*P(2,I2P)*P(3,I3P)*P(4,I4P)
         GO TO 40
        END IF
        DO 50,I5=1,2
         I5P=I5+2
         IF(NIVS.EQ.5) THEN
```

```
            INDEX=INDX(NIVS,NMPS,ND(1,I1),ND(2,I2),ND(3,I3),ND(4,I4),
     &        ND(5,I5))
            READ(1,1010,REC=INDEX) V0,(V1(J),J=1,5),(V2(J),J=1,10),
     &         (V3(J),J=1,10),(V4(J),J=1,5),V5
            SR=SR+V0*P(1,I1)*P(2,I2)*P(3,I3)*P(4,I4)*P(5,I5)
     &        +V1(1)*P(1,I1P)*P(2,I2)*P(3,I3)*P(4,I4)*P(5,I5)
     &        +V1(2)*P(1,I1)*P(2,I2P)*P(3,I3)*P(4,I4)*P(5,I5)
     &        +V1(3)*P(1,I1)*P(2,I2)*P(3,I3P)*P(4,I4)*P(5,I5)
     &        +V1(4)*P(1,I1)*P(2,I2)*P(3,I3)*P(4,I4P)*P(5,I5)
     &        +V1(5)*P(1,I1)*P(2,I2)*P(3,I3)*P(4,I4)*P(5,I5P)
     &        +V2(1)*P(1,I1P)*P(2,I2P)*P(3,I3)*P(4,I4)*P(5,I5)
     &        +V2(2)*P(1,I1P)*P(2,I2)*P(3,I3P)*P(4,I4)*P(5,I5)
     &        +V2(3)*P(1,I1P)*P(2,I2)*P(3,I3)*P(4,I4P)*P(5,I5)
     &        +V2(4)*P(1,I1P)*P(2,I2)*P(3,I3)*P(4,I4)*P(5,I5P)
     &        +V2(5)*P(1,I1)*P(2,I2P)*P(3,I3P)*P(4,I4)*P(5,I5)
     &        +V2(6)*P(1,I1)*P(2,I2P)*P(3,I3)*P(4,I4P)*P(5,I5)
     &        +V2(7)*P(1,I1)*P(2,I2P)*P(3,I3)*P(4,I4)*P(5,I5P)
     &        +V2(8)*P(1,I1)*P(2,I2)*P(3,I3P)*P(4,I4P)*P(5,I5)
     &        +V2(9)*P(1,I1)*P(2,I2)*P(3,I3P)*P(4,I4)*P(5,I5P)
     &        +V2(10)*P(1,I1)*P(2,I2)*P(3,I3)*P(4,I4P)*P(5,I5P)
     &        +V3(1)*P(1,I1P)*P(2,I2P)*P(3,I3P)*P(4,I4)*P(5,I5)
     &        +V3(2)*P(1,I1P)*P(2,I2P)*P(3,I3)*P(4,I4P)*P(5,I5)
     &        +V3(3)*P(1,I1P)*P(2,I2P)*P(3,I3)*P(4,I4)*P(5,I5P)
     &        +V3(4)*P(1,I1P)*P(2,I2)*P(3,I3P)*P(4,I4P)*P(5,I5)
     &        +V3(5)*P(1,I1P)*P(2,I2)*P(3,I3P)*P(4,I4)*P(5,I5P)
     &        +V3(6)*P(1,I1P)*P(2,I2)*P(3,I3)*P(4,I4P)*P(5,I5P)
     &        +V3(7)*P(1,I1)*P(2,I2P)*P(3,I3P)*P(4,I4P)*P(5,I5)
     &        +V3(8)*P(1,I1)*P(2,I2P)*P(3,I3P)*P(4,I4)*P(5,I5P)
     &        +V3(9)*P(1,I1)*P(2,I2P)*P(3,I3)*P(4,I4P)*P(5,I5P)
     &        +V3(10)*P(1,I1)*P(2,I2)*P(3,I3P)*P(4,I4P)*P(5,I5P)
     &        +V4(1)*P(1,I1P)*P(2,I2P)*P(3,I3P)*P(4,I4P)*P(5,I5)
     &        +V4(2)*P(1,I1P)*P(2,I2P)*P(3,I3P)*P(4,I4)*P(5,I5P)
     &        +V4(3)*P(1,I1P)*P(2,I2P)*P(3,I3)*P(4,I4P)*P(5,I5P)
     &        +V4(4)*P(1,I1P)*P(2,I2)*P(3,I3P)*P(4,I4P)*P(5,I5P)
     &        +V4(5)*P(1,I1)*P(2,I2P)*P(3,I3P)*P(4,I4P)*P(5,I5P)
     &        +V5*P(1,I1P)*P(2,I2P)*P(3,I3P)*P(4,I4P)*P(5,I5P)
          END IF

 50         CONTINUE
 40        CONTINUE
 30       CONTINUE
 20      CONTINUE
 10     CONTINUE

        RETURN

C********0*********0*********0*********0*********0*********0*********
C                                 FORMATS
C********0*********0*********0*********0*********0*********0*********

 999   FORMAT(' WARNING: VARIABLE ',I1,' HAS EXCEEDED DOMAIN. '/
     &  ' EXTRAPOLATING TO VALUE ',F20.10)
 1000 FORMAT(A10,36I10)
```

```
 1010 FORMAT(37E11.4)
      END

C*******0*********0*********0*********0*********0*********0*********
C                                  FUNCTION INDX
C                             LOCATE NODE POINT FILE RECORD
C*******0*********0*********0*********0*********0*********0*********

      INTEGER FUNCTION INDX(NIVS,NMPS,K1,K2,K3,K4,K5)

      DIMENSION NMPS(5),K(5)

      INDX=0
      K(1)=K1
      K(2)=K2
      K(3)=K3
      K(4)=K4
      K(5)=K5

      DO J=1,NIVS-1,1
        INDX=(INDX+(K(J)-1))*NMPS(J+1)
      END DO
      INDX=INDX+K(NIVS)+2

      RETURN
      END
```

TRIDIAG Tridiagonal Matrix Solver

```
C*******0*********0*********0*********0*********0*********0*********
C TRIDIAG
C      This subroutine comes from the FORTRAN numerical recipies
C book.  It solves tridiagonal matrix form for input vectors A, B and
C C and source vector R.  The result is vector U.
C*******0*********0*********0*********0*********0*********0*********
      SUBROUTINE TRIDIAG( A, B, C, R, U, N )

      IMPLICIT DOUBLE PRECISION (A-H,O-Z)

      PARAMETER( NMAX = 300 )

      DIMENSION GAM(NMAX), A(N), B(N), C(N), R(N), U(N)

C*******0*********0*********0*********0*********0*********0*********
C  DO NOT ALLOW USER TO EXCEED PARAMETER.
C*******0*********0*********0*********0*********0*********0*********
      IF ( N .GT. NMAX ) THEN
        WRITE(*,998)
        WRITE(*,1000)
```

```
      STOP
      END IF

C********0*********0*********0*********0*********0*********0*********
C ERROR CONDITIONS APPLY WHENEVER SINGULARITY OCCURS.
C********0*********0*********0*********0*********0*********0*********
      IF ( B(1) .EQ. 0. ) THEN
        WRITE(*,999) 1
        WRITE(*,1000)
        STOP
        END IF

C********0*********0*********0*********0*********0*********0*********
C BEGIN ALGORITHM.
C FORWARD PORTION OF ALGORITHM.
C********0*********0*********0*********0*********0*********0*********
      BET = B(1)
      U(1) = R(1) / BET
      DO 10 J = 2, N
        GAM(J) = C(J-1) / BET
        BET = B(J) - A(J) * GAM(J)
        IF ( BET .EQ. 0. )  THEN
          WRITE(*,999) J
          WRITE(*,1000)
          RETURN
          END IF
        U(J) = ( R(J) - A(J) * U(J-1) ) / BET
 10     CONTINUE

C********0*********0*********0*********0*********0*********0*********
C BACKWARD PORTION OF ALGORITHM.
C********0*********0*********0*********0*********0*********0*********
      DO 11 J = N - 1, 1, -1
        U(J) = U(J) - GAM(J+1) * U(J+1)
 11     CONTINUE

C********0*********0*********0*********0*********0*********0*********
C FORMATS
C********0*********0*********0*********0*********0*********0*********
 998  FORMAT(' **ERROR: VARIABLE "N" EXCEEDS VARIABLE "NMAX".')
 999  FORMAT(' **ERROR: VARIABLE "BET(',I3,')" CANNOT BE ZERO.')
 1000 FORMAT(' PROGRAM IS TERMINATED IN MODULE "TRIDIAG".')

C********0*********0*********0*********0*********0*********0*********
C TRIDIAGONAL MATRIX HAS BEEN SOLVED.
C********0*********0*********0*********0*********0*********0*********
      RETURN
      END
```

VDROP Voltage Drop Model Subroutine

```
C********0*********0*********0*********0*********0*********0*********
C
C     FUNCTION VDROPP()
C
C     DATE:       1994
C
C     PROGRAMMER:  Donald Hammerstrom, Graduate Student
C                  Department of Electrical Engineering
C                  Montana State University
C                  Bozeman, Montana  59717
C
C     PURPOSE:
C         This function calculates an electrode voltage drop based
C     on theoretical and empiracal functions described in Gupta and
C     Rohatgi, 1982.  This particular function is for a non-ohmic
C     voltage drop, which is included as part of the internal MHD
C     circuit model.
C
C     VARIABLES:
C
C     B          magnetic flux density                              tesla
C     BETA       Hall parameter in core flow
C     DELTA      boundary layer thickness                           meter
C     -EFF       suffix meaning "effective'
C     EX         local Hall electric field                          V/m
C     POT        electrode potential w.r.t. undisturbed plasma V
C     SEGR       electrode segmentation ratio
C     T          core flow temperature                              K
C     THETAWS    temperature ratio used in referenced paper
C     TS         slag wall temperature                              K
C     TW         electrode wall temperature                         K
C     V          velocity in core flow                              meter/s
C     VDROPP     voltage drop returned by function                  V
C
C********0*********0*********0*********0*********0*********0*********

      REAL*8 FUNCTION VDROPP( TW, TS, T, POT, DELTA, BETA, V, B, EX,
     &                                                         SEGR )

      IMPLICIT DOUBLE PRECISION (A-H,O-Z)
      IMPLICIT INTEGER (I-N)

      TS = DMIN1( DMAX1( 1750.D0 + 0.75D0 * ( TW - 1400.D0 ), 1750.D0
     &                                                        ), T )

      VDROPP = 0.0D0

C********0*********0*********0*********0*********0*********0*********
C ELECTRICAL SHEATH VOLTAGE DROP
C********0*********0*********0*********0*********0*********0*********
```

```
      VDROPP = VDROPP + DSQRT( POT * T ) * 9.283D-3

C*******0*********0*********0*********0*********0*********0*********
C GASDYNAMIC VOLTAGE DROP
C*******0*********0*********0*********0*********0*********0*********

      IF ( TS .LT. T ) THEN
        DENOM = 1. + SEGR * ( BETA - 0.4D0 )
        BETAEFF = BETA / DENOM
        THETAW = TS / T

        VDROPP = VDROPP - V * DELTA * B / 8.D0 + BETAEFF * DELTA *
     &    EX * ( 1.D0 - 7.D0 / ( ( 1.D0 - THETAW )**7 ) * FIT2(
     &                                                   THETAW ) )
      END IF

      RETURN

      END

C*******0*********0*********0*********0*********0*********0*********
C FUNCTION FIT2()
C FIT2 carries out a crude numerical integration
C*******0*********0*********0*********0*********0*********0*********

      REAL*8 FUNCTION FIT2( THETAW )

      IMPLICIT DOUBLE PRECISION (A-H,O-Z)
      IMPLICIT INTEGER (I-N)

      FIT2 = 0.D0

      DO I = JIDINT( THETAW * 1000.D0 ), 1000
        RI = DFLOAT( I ) / 1000.D0
        FIT2 = FIT2 + RI**0.5 * ( RI - THETAW )**6 * 1.D-3
      END DO

      RETURN
      END

C*******0*********0*********0*********0*********0*********0*********
C
C     FUNCTION VDROPR()
C
C     DATE:     1993
C
C     PROGRAMMER:  Donald Hammerstom, Graduate Student
C                  Department of Electrical Engineering
C                  Montana State University
C                  Bozeman, Montana  59717
C
C     PURPOSE:
```

```
C        This function calculates an electrical voltage drop
C     resistance based on theoretical and empiracal functions
C     described in Gupta and Rohatgi, 1982.  This particular function
C     calculates the ohmic resistivity to be used in the external
C     electrical circuit.
C
C     VARIABLES:
C
C     BETA       Hall parameter in core flow
C     DELTA      boundary layer thickness                        meter
C     -EFF       suffix meaning "effective"
C     FACTOR     factor defined for clean code
C     GAMMA      ratio from referenced paper
C     S          slag thickness                                  meter
C     SEGR       electrode segmentation ratio
C     SIGMA      conductivity in core flfow                      mho/meter
C     SLAGSIG    conductivity of slag wall                       mho/meter
C     T          core flow temperature                           K
C     THETAWS    temperature ratio used in referenced paper
C     TS         slag wall temperature                           K
C     TW         electrode wall temperature                      K
C     VDROPR     voltage drop returned by function               V
C
C*******0*********0*********0*********0*********0*********0*********
      REAL*8 FUNCTION VDROPR( TW, TS, T, DELTA, BETA, SIGMA, SEGR )

      IMPLICIT DOUBLE PRECISION (A-H,O-Z)
      IMPLICIT INTEGER (I-N)

      PARAMETER( RK = 1.380662D-23, EPS = 6.952D-19 )

      TS = DMIN1( DMAX1( 1750.D0 + 0.75D0 * ( TW - 1400.D0 ), 1750.D0
     &                                                         ), T )
      VDROPR = 0.0D0

C*******0*********0*********0*********0*********0*********0*********
C SLAG VOLTAGE DROP
C*******0*********0*********0*********0*********0*********0*********
C SLAG THICKNESS:
      IF ( TW .LE. TS ) THEN
        S = 4.86D-3 - 2.78D-6 * TW
      ELSE
        S = 0.D0
      END IF

      GAMMA = 1.256D4 / TS
      SLAGSIG = 4.04D4 * DEXP( -GAMMA )
      THETAWS = TW / TS
      FACTOR = S / ( SLAGSIG * ( 1.D0 - THETAWS ) )

      DO I = JIDINT( THETAWS * 1000 ), 1000
        RI = DFLOAT( I ) / 1000.D0
        VDROPR = VDROPR + FACTOR * DEXP( GAMMA * ( 1.D0 / RI - 1.D0 )
```

```
     &                                                            ) * 1.D-3
      END DO

C*******0*********0*********0*********0*********0*********0*********
C GASDYNAMIC VOLTAGE DROP
C*******0*********0*********0*********0*********0*********0*********

      IF ( TS .LT. T ) THEN
        DENOM = 1. + SEGR * ( BETA - 0.4D0 )
        BETAEFF = BETA / DENOM
        SIGMAEFF = SIGMA / DENOM
        THETAW = TS / T

        VDROPR = VDROPR + DELTA * ( 1.D0 + BETAEFF**2 ) / SIGMAEFF *
     &    ( 7.D0 / ( ( 1.D0 - THETAW )**7 ) * BETAEFF**2 / ( 1.D0 +
     &    BETAEFF**2 ) * FIT1( THETAW, BETAEFF, T ) - 1.D0 )
      END IF

      RETURN

      END

C*******0*********0*********0*********0*********0*********0*********
C FUNCTION FIT1()
C FIT1() carries out a crude numerical integration
C*******0*********0*********0*********0*********0*********0*********

      REAL*8 FUNCTION FIT1( THETAW, BETAEFF, T )

      IMPLICIT DOUBLE PRECISION (A-H,O-Z)
      IMPLICIT INTEGER (I-N)

      PARAMETER( EPS = 6.952D-19, RK = 1.380662D-23 )

      FIT1 = 0.D0

      DO I = JIDINT( THETAW * 1000.D0 ), 1000
        RI = DFLOAT(I) / 1000.D0
        FIT1 = FIT1 + RI**( -0.75 ) * ( 1. / BETAEFF**2 + RI ) * ( (
     &    RI - THETAW )**6 ) * DEXP( EPS / ( 2.D0 * RK * T ) * ( 1.D0
     &                                        / RI - 1.D0 ) ) * 1.D-3
      END DO

      RETURN
      END
```